Advances in Mathematical Physics

Fractals and Fractional Calculus in Mathematical Physics

Lead Guest Editor: Muhammad Nadeem
Guest Editors: Qura Tul Ain and T. Sathiyaraj

Fractals and Fractional Calculus in Mathematical Physics

Advances in Mathematical Physics

Fractals and Fractional Calculus in Mathematical Physics

Lead Guest Editor: Muhammad Nadeem
Guest Editors: Qura Tul Ain and T. Sathiyaraj

Contents

Hindawi
Advances in Mathematical Physics
Volume 2024, Article ID 9306915, 13 pages
https://doi.org/10.1155/2024/9306915

Research Article

Application of Constant Proportional Caputo Fractional Derivative to Thermodiffusion Flow of MHD Radiative Maxwell Fluid under Slip Effect over a Moving Flat Surface with Heat and Mass Diffusion

Adnan Ahmad,[1] M. Nazar,[1] M. Ahmad,[1,2] Sayed M. Eldin,[3] Zaib Un Nisa,[2] Hassan Waqas,[4] and M. Imran[5]

[1]*Centre for Advanced Studies in Pure and Applied Mathematics, Bahauddin Zakariya University, Multan, Pakistan*
[2]*Department of Mathematics and Statistics, Institute of Southern Punjab, Multan, Pakistan*
[3]*Center of Research, Faculty of Engineering, Future University in Egypt, New Cairo 11835, Egypt*
[4]*School of Energy and Power Engineering, Jiangsu University, Zhenjiang 212013, China*
[5]*Department of Mathematics, Government College University, Faisalabad, Pakistan*

Correspondence should be addressed to Hassan Waqas; syedhasanwaqas@hotmail.com and M. Imran; drmimranchaudhry@gcuf.edu.pk

Received 20 October 2022; Revised 23 July 2023; Accepted 31 July 2023; Published 22 January 2024

Academic Editor: Mohammad W. Alomari

Thermal diffusion is a phenomenon where the concentration gradient or diffusive flux is created due to the temperature gradient. Thermal diffusion is induced because of the higher temperature and uneven distribution of the mixture. Formally, thermal diffusion is called the Soret effect, and it is a crucial factor in a number of natural occurrences like the separation of isotopes technique of purification. In this research paper, Maxwell fluid's flow in the vicinage of a flat plate is discussed by considering the effect of the thermodiffusion subject to the first-order slip at the boundary with the application of a constant proportional Caputo (CPC) fractional derivative. The effect of heat generation and radiation is also taken into consideration, as well as the effect of a magnetic field of constant magnitude. The generalized heat and mass fluxes are considered, and this generalization of heat and mass fluxes is done by utilizing the CPC fractional derivative. After converting the current model's governing equations into a dimensionless form, the temperature, concentration, and velocity fields' analytical solutions are found. By drawing graphs of the temperature, concentration, and velocity fields for the parametric modifications, the results are graphically illustrated. It becomes clear from the results discussion that the outcomes produced by the constant proportional derivative are more decaying than those obtained with the classical differential operator of order one.

1. Introduction

Thermodiffusion is a physical phenomenon that occurs in the mixture of different moving particles with an adverse response to the temperature gradient. In this phenomenon, the particles of smaller inertia tend to move in the region of higher temperature, while the particles with the greater inertia try to move in the area of lower temperature. Formally, this phenomenon is called the Soret effect and has many industrial and biological applications like isotope separation [1, 2].

Slippage of the flowing fluid over a flat surface is important in many complex flows of non-Newtonian fluids. Slip of the fluid occurs at the boundary when there is relative motion between fluid and boundary. This mechanical situation is addressed properly by the Robin-type boundary condition and specifically, it is known as the slip boundary condition. The slip effect is formulated by many theorists to address the different geometric situations for the boundary layer flows. Vieru et al. [3] explained the aspect of slip for second-grade fluid flow. Tahir et al. [4] considered Maxwell

fluid motion over an oscillation surface. Jameel and Khan [5] discussed an impulsive flow over the flat plate. Hayat et al. [6] studied the Stokes flow for the slip condition. Imran et al. [7] applied the first order slip for the motion of the non-Newtonian fluid. Sajid et al. [8] explained the slippage motion of the rate-type fluid. Hayat et al. [9] studied the flow of Maxwell fluid between the plates under the influence of MHD and radiation. Ramesh et al. [10] studied the Maxwell fluid over a stretching sheet and discussed the impact of radiation on the motion of the fluid. Khan et al. [11] reported the flow of Maxwell fluid by taking into account the influence of radiation. Chen et al. [12] utilized the fractional derivatives boundary layer flow of Maxwell fluid on an unsteady stretching surface and obtained the results for the velocity. Over a vertical plate, Imran et al. [13] considered a slippage flow of a radiative fluid.

Opangua et al. [14] explained the effect of slip on the flow of coupled stressed fluid. Hayat and Asghar [15] and Hayat et al. [16, 17] considered the impact of heat transfer over the slippage flow of peristaltic fluid. Shakeel et al. [18] employed the slip effect to rate-type fluid over an accelerating plate. Shah et al. [19] applied the fractional calculus to get the generalized results for the unidirectional velocity for Maxwell fluid. Shah et al. [20] used the slip conditions at the boundary for MHD Carreau fluid through a porous regime. Freidoonimehr and Jafari [21] also employed slip conditions at the boundary for MHD nanofluid flow. Schneider [22] considered the motion of electrorheological suspensions and laid out the impact of wall slip on the rheological behavior of the suspension. Raza [23] stagnation point flow of Casson fluid by considering the impact of slip. Norouzi et al. [24] investigated the flow of Oldroyd-B fluid in the cylindrical domain by studying the effect of slip at the boundary. Fetecau et al. [25] discussed the flow of Newtonian fluid by taking into account the effect of slip at the edge of the flow. Khan et al. [26] applied the slip attribute to the viscous nanofluid flow and obtained the velocity field.

Khan et al. [27] discussed the impact of the transfer of heat on the flow of Maxwell fluid. Chu et al. [28] studied nanofluid flow with four different types of nanoparticles, which are subject to the nonhomogenous source of heat, and applied the numerical technique to obtain the approximated solutions. Alqahtani et al. [29] did a detailed analysis of the impact of radiation on the flow of nanofluid. Puneeth et al. [30] explained the effect of convection on nanofluid's flow over a sheet. Alharbi et al. [31] illustrated the effect of the bioconvective hydromagnetic flow of Oldroyd-B nanofluid over a stretching surface having pores. Khan et al. [32] took under consideration the unsteady flow of hybrid nanofluid on a radiated porous surface subject to the magnetic field. Qaiser et al. [33] investigated the effects of active energy and entropy for nanofluid flow subject to viscous dissipation and cross-diffusion. Some other investigations related to nanofluid flow in different physical situations have been done [33–39].

The Maxwell fluid model is suitable for momentum, heat, and mass transfer phenomena as it captures relaxation time effects. Khan et al. [40] discussed the generalized conclusions for the flow of Maxwell fluid by taking into consideration the modified Fick's and Fourier laws for mass and heat transfer, respectively. Khan et al. [41] utilized the Cattaneo–Christov mechanism for the heat transfer of Maxwell fluid through a closed path. Tang et al. [42] discussed the flow of Maxwell fluid subject to uniform heat flux and thermal radiation by applying the fractional derivative. Mansoor et al. [43] also considered the Maxwell fluid's flow, and the effect of chemical reaction over the velocity field is explained.

The fractional derivatives are flexible and nonlocal because the order of the fractional derivatives can be any real number. Due to nonlocality and flexibility, the fractional derivatives are suitable for approximating real data values with more reliability than classical derivatives for the effect of global interactions (nonlocality of space) and memory (nonlocality of time). Nowadays, fractional calculus is applied efficiently to explain the complex flow phenomenon. There are different approaches to the fractional derivative used by mathematicians [44–47], and a recent development in the fractional is the constant proportional Caputo (CPC) derivative proposed by Baleanu et al. [48].

The thermodiffusion, formally known as the Soret effect, occurs when a concentration gradient is generated due to a temperature gradient. This effect is significant for complex mixtures containing different species of diverse sizes and polarities, for example, in the petroleum system. The principal interest of this article is to widen the research work done in [25] by taking the flow of Maxwell fluid, and the flow modeling is done with a fractional derivative of the recent approach, namely the constant Caputo fractional derivative. The graphical illustration of field variables is done by using MATHCAD software. In addition to this, the slip at the boundary is analyzed with other parameters. Such work addressing the thermodiffusion effect for Maxwell fluid's flow with CPC fractional derivative is yet to be reported in the literature.

2. Mathematical Description

Considered Maxwell fluid flowing over a vertical plate. The vertical plate is situated in the xz-plane in a way that the y-axis becomes normal to the place of the plate, as indicated in Figure 1. At first, the plate with the fluid is not moving; after the time $t > 0$, the plate starts moving with the velocity $V_0 f(t)$, and by considering the slip effect over the plate fluid also move. Under the assumption, the Maxwell fluid flow model in mathematical form is as follows [25, 27]:

$$\rho\left(\lambda_1\frac{\partial}{\partial t}+1\right)\frac{\partial u}{\partial t}=\mu\frac{\partial^2 u}{\partial y^2}+g(\rho\beta_T)\left(1+\lambda_1\frac{\partial}{\partial t}\right)[T-T_\infty]+g(\rho\beta_C)\left(1+\lambda_1\frac{\partial}{\partial t}\right)[C-C_\infty]-\left(1+\lambda_1\frac{\partial}{\partial t}\right)B_0^2\sigma u, \tag{1}$$

$$k\frac{\partial^2 T}{\partial y^2}-\frac{\partial q_r}{\partial y}-Q_0[T-T_\infty]-\left(\rho c_p\right)\frac{\partial T}{\partial t}=0, \tag{2}$$

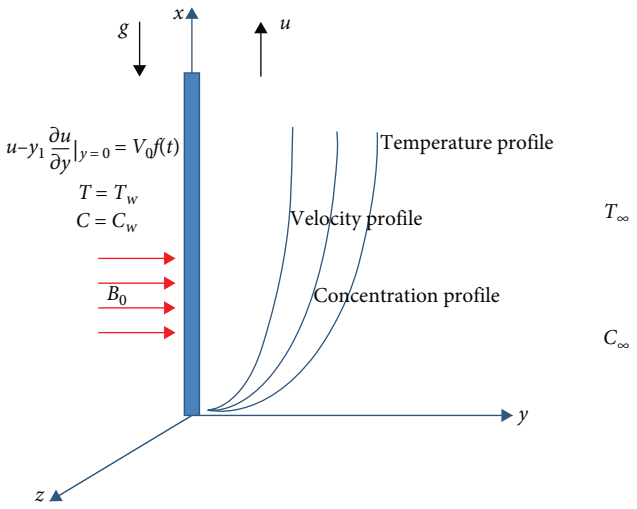

FIGURE 1: Flow geometry.

$$D_m\frac{\partial^2 C}{\partial y^2}+\frac{D_m k_T}{T_m}\frac{\partial^2 T}{\partial y^2}-\frac{\partial C}{\partial t}=0, \tag{3}$$

and related conditions

$$\text{for } t=0\Rightarrow u=0, T=T_\infty, \quad C=C_\infty, \tag{4}$$

$$u-\gamma_1\frac{\partial u}{\partial y}|_{y=0}=V_0f(t), \quad T=T_w, \quad C=C_w, \quad y=0, \tag{5}$$

$$u\to 0, T\to T_\infty, \quad C\to C_\infty, \quad y\to\infty. \tag{6}$$

The radiated flux from Equation (2) is approximated by using the Roseland approach [49, 50] for the minor temperature difference between the temperature of the fluid and the free stream temperature [51, 52].

$$k[N_r+1]\left(\frac{\partial^2}{\partial y^2}-(\rho c_p)\frac{\partial}{\partial t}\right)T(y,t)=Q_0[T(y,t)-T_\infty], \tag{7}$$

where $N_r=\frac{16\sigma_1 T_\infty^3}{3kk_1}$ is the radiation parameter.

Nondimensional relations [25]

$$u^*=\frac{u}{V_0}, \quad y^*=\frac{yV_0}{\nu}, \quad t^*=\frac{V_0^2}{\nu}t, \quad C^*=\frac{C-C_\infty}{C_w-C_\infty}, \quad T^*=\frac{T-T_\infty}{T_w-T_\infty},$$
$$Q^*=\frac{\nu Q_0}{(\rho c_p)V_0^2}, \quad \gamma_1^*=\frac{V_0}{\nu}\gamma_1, \quad f^*(t^*)=f\left(\frac{\nu}{V_0^2}t^*\right), \quad \lambda=\frac{V_0^2}{\nu}\lambda_1, \tag{8}$$

with $V_0=[\nu g\beta_T(T_w-T_\infty)]^{1/3}$ is specific velocity, and after using Equations (1)–(7) and Equation (8) dimensionless model takes the following form:

$$\left(\lambda\frac{\partial}{\partial t}+1\right)\frac{\partial u}{\partial t}=\frac{\partial^2 u}{\partial y^2}+\left(1+\lambda\frac{\partial}{\partial t}\right)[T-Mu+NC], \tag{9}$$

$$\frac{\partial T}{\partial t}=\frac{1}{\mathrm{Pr}_{\mathrm{eff}}}\frac{\partial^2 T}{\partial y^2}-QT, \tag{10}$$

$$\mathrm{ScSr}\frac{\partial^2 T}{\partial y^2}=\mathrm{Sc}\frac{\partial C}{\partial t}-\frac{\partial^2 C}{\partial y^2}, \tag{11}$$

and corresponding dimensionless initial conditions and boundary conditions

$$u=0, T=0, C=0, t=0, \tag{12}$$

$$f(t)=u-\gamma_1\tfrac{\partial u}{\partial y}|_{y=0}, \quad T=1, C=1, y=0, \tag{13}$$

$$u\to 0, T\to 0, C\to 0, y\to\infty, \tag{14}$$

$$N=\frac{\rho\beta_C[C_w-C_\infty]}{\rho\beta_T[T_w-T_\infty]}, \quad \mathrm{Pr}_{\mathrm{eff}}=\frac{\mathrm{Pr}}{Nr+1}, \quad M=\frac{\nu\sigma B_0^2}{\rho V_0^2},$$
$$\mathrm{Sc}=\frac{\nu}{D_m}, \quad \mathrm{Sr}=\frac{D_m k_T[T_w-T_\infty]}{\nu T_m[C_w-C_\infty]}, Q=\frac{\nu Q_0}{\rho c_p V_0^2}, \tag{15}$$

where N is the ratio of the thermal Grashof number to the mass Grashof number, $\mathrm{Pr}_{\mathrm{eff}}$ effective Prandtl number, M is a nondimensional magnetic parameter, Sc is the Schmidt number, Q is the nondimensional heat generation parameter, and Sr is the Soret effect parameter.

3. Classical Solution of the Model

3.1. Temperature. Equation (10) is reduced to an ordinary differential equation as follows:

$$Pr_{\mathrm{eff}}q\overline{T}(y,q)+Q\overline{T}(y,q)=\frac{\partial^2\overline{T}(y,q)}{\partial y^2}. \tag{16}$$

Equation (16) is solved by conditions given below:

$$T(\infty,q)=0, \overline{T}(0,q)=q^{-1}, \tag{17}$$

and solution transformed for temperature is as follows:

$$\overline{T}(y,q)=\frac{1}{q}e^{\left[-y\sqrt{Pr_{\mathrm{eff}}}\sqrt{Q+q}\right]}. \tag{18}$$

3.2. Concentration. Equation (11), by using the Laplace transform, is reduced to an ODE as follows:

$$\mathrm{Sc}q\overline{C}(y,q)=\frac{\partial^2\overline{C}(y,q)}{\partial y^2}+\mathrm{Sr}\frac{\partial^2\overline{T}(y,q)}{\partial y^2}. \tag{19}$$

Equation (19) is solved by the conditions as follows:

$$C(\infty,q)=0,\overline{C}(0,q)=q^{-1}. \tag{20}$$

The solutions are given below:

$$\begin{aligned}\overline{C}(y,q)=&\frac{1}{q}\exp\left(-y\sqrt{\mathrm{Sc}q}\right)\\&+\frac{\mathrm{ScSrPr_{eff}}(Q+q)}{[(Pr_{\mathrm{eff}}-\mathrm{Sc})q+QPr_{\mathrm{eff}}]q}\exp\left[-y\sqrt{\mathrm{Sc}q}\right]\\&-\frac{\mathrm{ScSrPr_{eff}}(Q+q)\exp\left[-y\sqrt{Pr}_{\mathrm{eff}}(Q+q)\right]}{q[q(Pr_{\mathrm{eff}}-\mathrm{Sc})+Pr_{\mathrm{eff}}Q]}\end{aligned} \tag{21}$$

3.3. Velocity Field. Equation (9), by using the Laplace transform, is reduced to the following:

$$\begin{aligned}\left[1+\lambda\left(\frac{k_1(\alpha)}{q}+k_0(\alpha)\right)q^{\alpha}\right]q\overline{u}(y,q)=&\frac{\partial^2\overline{u}(y,q)}{\partial y^2}\\&+\left[1+\lambda\left(\frac{k_1(\alpha)}{q}+k_0(\alpha)\right)q^{\alpha}\right]\\&\times\left[\overline{T}(q,y)-M\overline{u}(q,y)+N\overline{C}(q,y)\right].\end{aligned} \tag{22}$$

Equation (22) is solved by the following transformed condition:

$$\overline{u}(\infty,q)=0,\overline{u}(0,q)-\gamma\frac{\partial\overline{u}(y,q)}{\partial y}\bigg|_{y=0}=f(q), \tag{23}$$

and its solution is as follows:

$$\begin{aligned}\overline{u}(y,q)=&\frac{F(q)\mathrm{e}^{-y\sqrt{[1+\lambda q][M+q]}}}{1+\gamma_1\sqrt{[1+\lambda q][M+q]}}+\frac{[1+\lambda q]\left[1+\gamma_1\sqrt{Pr}_{\mathrm{eff}}(Q+q)\right]}{[Pr_{\mathrm{eff}}(Q+q)-(M+q)(1+\lambda q)]q}\\&\times\left[1-\frac{N\mathrm{ScSrPr_{eff}}(Q+q)}{[Pr_{\mathrm{eff}}-\mathrm{Sc}]q+QPr_{\mathrm{eff}}}\right]\left[\frac{\mathrm{e}^{-y\sqrt{[1+\lambda q][M+q]}}}{1+\gamma_1\sqrt{[1+\lambda q][M+q]}}-\frac{\mathrm{e}^{-y\sqrt{Pr}_{\mathrm{eff}}(Q+q)}}{1+\gamma_1\sqrt{Pr}_{\mathrm{eff}}[Q+q]}\right]\\&+\frac{N(\lambda q+1)[1+\gamma_1\sqrt{\mathrm{Sc}q}]}{[\mathrm{Sc}q-(q+M)[\lambda q+1]]q}\left[1+\frac{\mathrm{ScPr_{eff}Sr}[Q+q]}{q(Pr_{\mathrm{eff}}-\mathrm{Sc})+QPr_{\mathrm{eff}}}\right]\\&\times\left[\frac{\mathrm{e}^{-y\sqrt{[\lambda q+][M+q]}}}{1+\gamma_1\sqrt{[\lambda q+1][M+q]}}-\frac{\mathrm{e}^{-y\sqrt{\mathrm{Sc}q}}}{1+\gamma_1\sqrt{\mathrm{Sc}q}}\right].\end{aligned} \tag{24}$$

4. Generalization with CPC

In this section, the flow model is generalized by introducing the generalized constitutive relations for momentum, heat, and mass fluxes. The generalization is made by newly developed fractional derivative, known as CPC fractional derivative denoted by ${}^{\mathrm{CPC}}D_t^{\alpha}$ and defined as follows [48]:

$${}^{\mathrm{CPC}}D_t^{\alpha}f(t)=\frac{1}{\Gamma(1-\alpha)}\int_0^t[k_1(\alpha)f(s)+k_0(\alpha)f'(\tau)](t-s)^{-\alpha}ds\ , \tag{25}$$

and its Laplace transform is defined as follows [48]:

$$\pounds\{{}^{\mathrm{CPC}}D_t^{\alpha}f(t)\}=\left(\frac{k_1(\alpha)}{q}+k_0(\alpha)\right)q^{\alpha}\overline{f}(q)-k_0(\alpha)q^{\alpha-1}f(0). \tag{26}$$

The momentum equation

$$\left(\lambda\frac{\partial}{\partial t}+1\right)\frac{\partial u}{\partial t}=\frac{\partial\tau_{\alpha}(y,t)}{\partial y}+\left(\lambda\frac{\partial}{\partial t}+1\right)[T-Mu+NC], \tag{27}$$

where $\tau_{\alpha}(y,t)$ is the shared stress is given by the following generalized constitutive relation

$$\tau_{\alpha}(y,t)={}^{\mathrm{CPC}}D_t^{\alpha}\frac{\partial u(y,t)}{\partial y}. \tag{28}$$

The equation for the temperature profile in generalized form is as follows:

$$Pr_{\mathrm{eff}}\frac{\partial T(y,t)}{\partial t}=-\frac{\partial q_{\beta}(y,t)}{\partial y}-Pr_{\mathrm{eff}}QT(y,t), \tag{29}$$

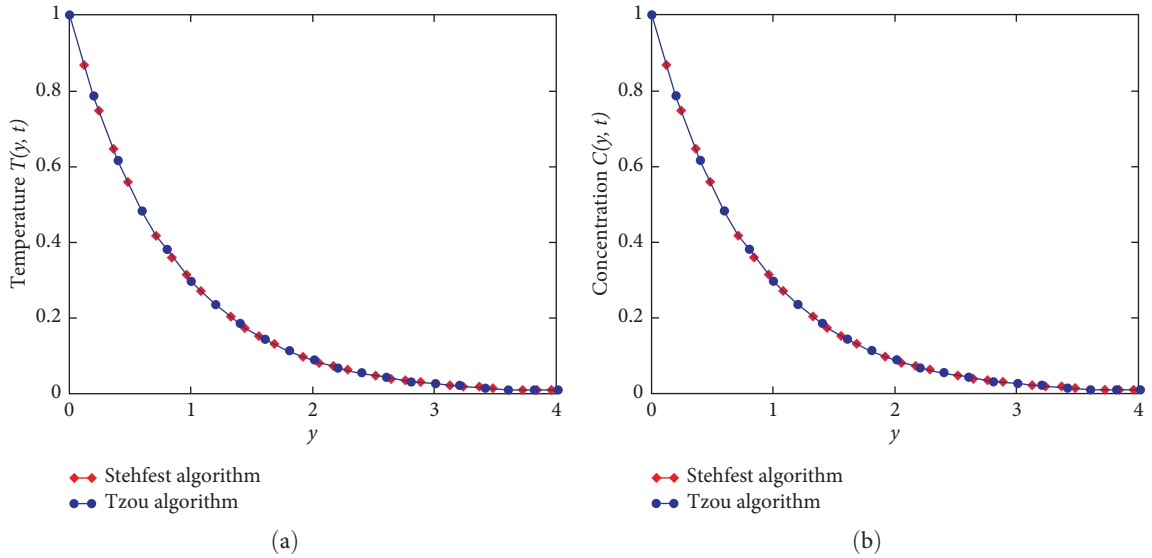

FIGURE 2: Inverse of temperature (a) and concentration (b) fields.

and $q_\beta(y,t)$ is given in the equation below:

$$q_\beta(y,t) = -{}^{\mathrm{CPC}}D_t^\beta \frac{\partial T(y,t)}{\partial y}. \tag{30}$$

The diffusion balance in terms of generalized mass flux is as follows:

$$\mathrm{Sc}\frac{\partial C(y,t)}{\partial t} = -\frac{\partial q_\gamma(y,t)}{\partial y} + \mathrm{ScSr}\frac{\partial^2 T(y,t)}{\partial y^2}, \tag{31}$$

where the generalized mass flux is as follows:

$$q_\gamma(y,t) = -{}^{\mathrm{CPC}}D_t^\gamma \frac{\partial C(y,t)}{\partial y}. \tag{32}$$

Using the generalized constitutive relations for stress, heat flux, and mass flux from Equations (28), (30), and (32) into Equations (27), (29), and (31), respectively

$$\left(\lambda\frac{\partial}{\partial t}+1\right)\frac{\partial u}{\partial t} = \frac{\partial\left[{}^{\mathrm{CPC}}D_t^\alpha \frac{\partial u(y,t)}{\partial y}\right]}{\partial y} + \left(\lambda\frac{\partial}{\partial t}+1\right)[T(y,t) - Mu(y,t) + NC(y,t)], \tag{33}$$

$$\frac{\partial T(y,t)}{\partial t} = -\frac{1}{Pr_{\mathrm{eff}}}\frac{\partial\left[-{}^{\mathrm{CPC}}D_t^\beta \frac{\partial T(y,t)}{\partial y}\right]}{\partial y} - QT(y,t), \tag{34}$$

and

$$\mathrm{Sc}\frac{\partial C}{\partial t} = -\frac{\partial\left[-{}^{\mathrm{CPC}}D_t^\gamma \frac{\partial C(y,t)}{\partial y}\right]}{\partial y} + \mathrm{ScSr}\frac{\partial^2 T}{\partial y^2}. \tag{35}$$

5. Generalized Solution to the Problem

5.1. Generalized Temperature Field. Equation (34) is transformed as below:

$$q\overline{T}(y,q) = \frac{1}{Pr_{\mathrm{eff}}}\left(\frac{k_1(\beta)}{q}+k_0(\beta)\right)q^\beta\frac{\partial^2\overline{T}(y,q)}{\partial y^2} - Q\overline{T}(y,q), \quad y>0. \tag{36}$$

Equation (36) is solved under the conditions in Equation (17) is as follows:

$$\overline{T}(y,q) = \frac{1}{q}\exp\left[-y\sqrt{\frac{Pr_{\mathrm{eff}}q^{1-\beta}(q+Q)}{[k_1(\beta)+k_0(\beta)q]}}\right]. \tag{37}$$

In Equation (37), the expressions under the root are complicated, and it is not an easy task to invert the Laplace transform. Therefore, the inversion of the Laplace is obtained by executing Stehfest's algorithm [53] and Tzou's [54], and the outcomes of the algorithms are presented in Figure 2(a).

5.2. Generalized Concentration Field. From Equation (35)

$$\mathrm{Sc}q\overline{C}(y,q)=\left(\frac{k_1(\gamma)}{q}+k_0(\gamma)\right)q^{\gamma}\frac{\partial^2\overline{C}(y,q)}{\partial y^2}+\mathrm{ScSr}\frac{\partial^2\overline{T}(y,q)}{\partial y^2},\quad y>0. \tag{38}$$

Equation (38) is solved under the transformed boundary conditions in Equation (20) as follows:

$$\begin{aligned}\overline{C}(y,q)=&\frac{1}{q}\exp\left[-y\sqrt{\frac{\mathrm{Sc}q^{2-\gamma}}{[k_1(\gamma)+k_0(\gamma)q]}}\right]\\&+\frac{\mathrm{ScSrPr_{eff}}(Q+q)q^{1-\gamma}}{[(Pr_{\mathrm{eff}}-\mathrm{Sc})q+Q\,Pr_{\mathrm{eff}}][k_1(\gamma)+k_0(\gamma)q]q}\exp\left[-y\sqrt{\frac{\mathrm{Sc}q^{2-\gamma}}{[k_1(\gamma)+k_0(\gamma)q]}}\right]\\&-\frac{\mathrm{ScSrPr_{eff}}(Q+q)q^{1-\gamma}}{[(Pr_{\mathrm{eff}}-\mathrm{Sc})q+Q\,Pr_{\mathrm{eff}}][k_1(\gamma)+k_0(\gamma)q]q}\exp\left[-y\sqrt{\frac{Pr_{\mathrm{eff}}q^{1-\gamma}(q+Q)}{[k_1(\gamma)+k_0(\gamma)q]}}\right].\end{aligned} \tag{39}$$

Equation (39) is inverted by algorithms and shown in Figure 2(b) [53, 54].

5.3. Generalized Velocity Field. Equation (33) is reduced to an ODE by using Laplace transform as follows:

$$(1+\lambda q)q\overline{u}=\left(\frac{k_1(\alpha)}{q}+k_0(\alpha)\right)q^{\alpha}\frac{\partial^2\overline{u}}{\partial y^2}+[\lambda q+1]\left[\overline{T}-M\overline{u}+N\overline{C}\right], \tag{40}$$

$$\begin{aligned}&\frac{\partial^2\overline{u}(y,q)}{\partial y^2}-\frac{(1+\lambda q)(q^{2-\alpha}+M)}{[k_1(\alpha)+k_0(\alpha)q]}\overline{u}(y,q)\\&\quad=-\frac{(1+\lambda q)q^{1-\alpha}}{[k_1(\alpha)+k_0(\alpha)q]}\left[\overline{T}(y,t)+N\overline{C}(y,q)(y,q)\right].\end{aligned} \tag{41}$$

Equation (41) is solved subject to the condition in Equation (23) as follows:

$$\begin{aligned}\overline{u}(y,q)=&\frac{F(q)\exp\left[-y\sqrt{\frac{[\lambda q+1](q^{2-\alpha}+M)}{[k_1(\alpha)+k_0(\alpha)q]}}\right]}{1+\gamma_1\sqrt{\frac{(1+\lambda q)(q^{2-\alpha}+M)}{[k_1(\alpha)+k_0(\alpha)q]}}}+\frac{(1+\lambda q)\left(1+\gamma_1\sqrt{\frac{Pr_{\mathrm{eff}}q^{1-\beta}(q+Q)}{[k_1(\beta)+k_0(\beta)q]}}\right)}{[(q+Q)\,Pr_{\mathrm{eff}}-(M+q^{2-\beta})(1+\lambda q)]q}\\&\times\left[1-\frac{N\mathrm{ScSrPr_{eff}}(Q+q)q^{-\beta}}{[(Pr_{\mathrm{eff}}-Sc)q+Q\,Pr_{\mathrm{eff}}][k_1(\beta)+k_0(\beta)q]}\right]\\&\times\left[\frac{\exp\left(-y\sqrt{\frac{(1+\lambda q)(q^{2-\alpha}+M)}{[k_1(\alpha)+k_0(\alpha)q]}}\right)}{1+\gamma_1\sqrt{\frac{(1+\lambda q)(q^{2-\alpha}+M)}{[k_1(\alpha)+k_0(\alpha)q]}}}-\frac{\exp\left(-y\sqrt{\frac{Pr_{\mathrm{eff}}q^{1-\beta}(q+Q)}{[k_1(\beta)+k_0(\beta)q]}}\right)}{1+\gamma_1\sqrt{\frac{Pr_{\mathrm{eff}}q^{1-\beta}(q+Q)}{[k_1(\beta)+k_0(\beta)q]}}}\right]\\&+\frac{N[\lambda q+1]\left[1+\gamma_1\sqrt{\frac{\mathrm{Sc}q^{2-\alpha}}{[k_1(\alpha)+k_0(\alpha)q]}}\right]}{q[\mathrm{Sc}q-(q+M)(\lambda q+)]}\left[1+\frac{\mathrm{ScPr_{eff}Sr}(Q+q)q^{-\gamma}}{[q[Pr_{\mathrm{eff}}-\mathrm{Sc}]+Q\,Pr_{\mathrm{eff}}][k_1(\gamma)+k_0(\gamma)q]}\right]\\&\times\left[\frac{\exp\left(-y\sqrt{\frac{(1+\lambda q)(q^{2-\alpha}+M)}{[k_1(\alpha)+k_0(\alpha)q]}}\right)}{1+\gamma_1\sqrt{\frac{[\lambda q+1](q^{2-\alpha}+M)}{[k_1(\alpha)+k_0(\alpha)q]}}}-\frac{\exp\left(-y\sqrt{\frac{\mathrm{Sc}q^{2-\gamma}}{[k_1(\gamma)+k_0(\gamma)q]}}\right)}{1+\gamma_1\sqrt{\frac{\mathrm{Sc}q^{2-\gamma}}{[k_1(\gamma)+k_0(\gamma)q]}}}\right].\end{aligned} \tag{42}$$

Equation (42) in its present form cannot invert in the domain, so its inverse is obtained numerically by the suitable algorithm known as Stehfest's algorithm [53] and Tzou's [54], and the outcomes of this process are presented in and presented in Figures 3(a) and 3(b) for no-slip condition and slip conditions.

6. Results and Discussion

The motion of Maxwell fluid on a flat surface is discussed by considering the effect of the thermodiffusion subject to the first-order slip at the boundary. The effect of heat generation and radiation is also considered with the effect of the

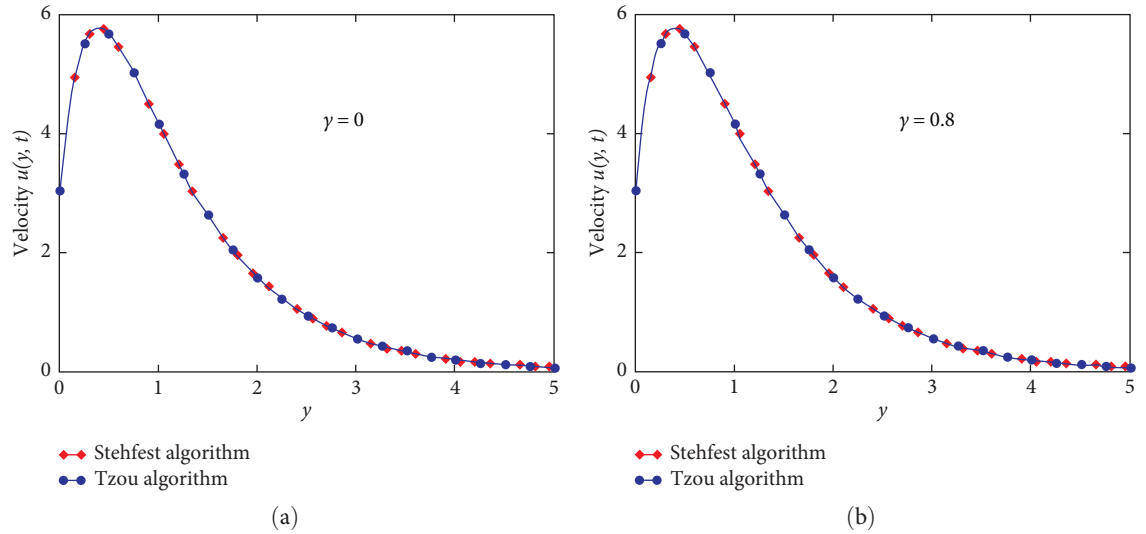

FIGURE 3: Inverse of the velocity field for (a) for no slip and (b) for slip.

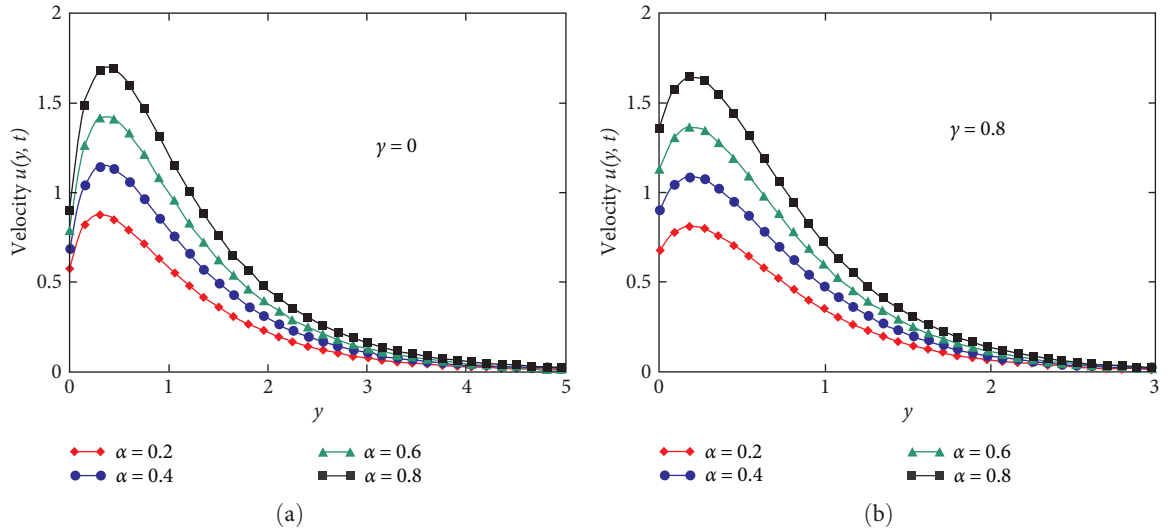

FIGURE 4: Velocity for variation of α (a) for no slip and (b) for slip $N = 0.5, Pr = 1.5, \mathrm{Sc} = 0.5, \mathrm{Sr} = 1.5, M = 0.5, \lambda = 2.5$.

magnetic field of constant magnitude. The generalized heat and mass fluxes are considered, and generalization is made by considering the new hybrid fractional derivative. The graphical illustrations for different parametric values are done using the same graphics of velocity against y.

The primary goal of this research is to study the objectivity of the fractional parameter over the velocity field. For this purpose, Figures 4(a) and 4(b) are plotted, and the impact of a fractional parameter over the flow is explained for slip and no slip. The outlines of profiles present an elevating trend for enhancing values of fractional parameters, and this peak in the velocity profiles is seen because of the power law kernel of fractional derivative. In the case of the CPC fractional derivative, the kernel of the operator obeys the power law. Moreover, the subjectivity of velocity for the variation of the other parameter is also explained graphically. The parameter is referred to the relative effect of bouncy forces. Figures 5 and 6 show the effect on the velocity of Maxwell fluid for both positive and negative values. The positive value of N means there is a supporting bouncy for the fluid flow, and the negative value means there is an opposing bouncy to the fluid flow. The results of positive values over fluid velocity is addressed in Figure 7. As $Q>0$ refers to the heat absorption and more energy in the flow domain due to this fluid motion increases for the growing values of Q as shown in Figure 7. The negative value of Q refers to the heat generation in the flow domain, and some energy is lost due to this fluid velocity decreases, which is revealed in Figure 8.

In Figure 9, the influence of Sc is discussed, and a decreasing trend is seen against the elevating value of Sc because for the elevating value of Sc, momentum diffusivity is dominant; therefore, the velocity field decreases for the increasing values of Sc. The Soret effect Sr over the velocity field is seen in Figure 10, and from the outline of Figure 10, it

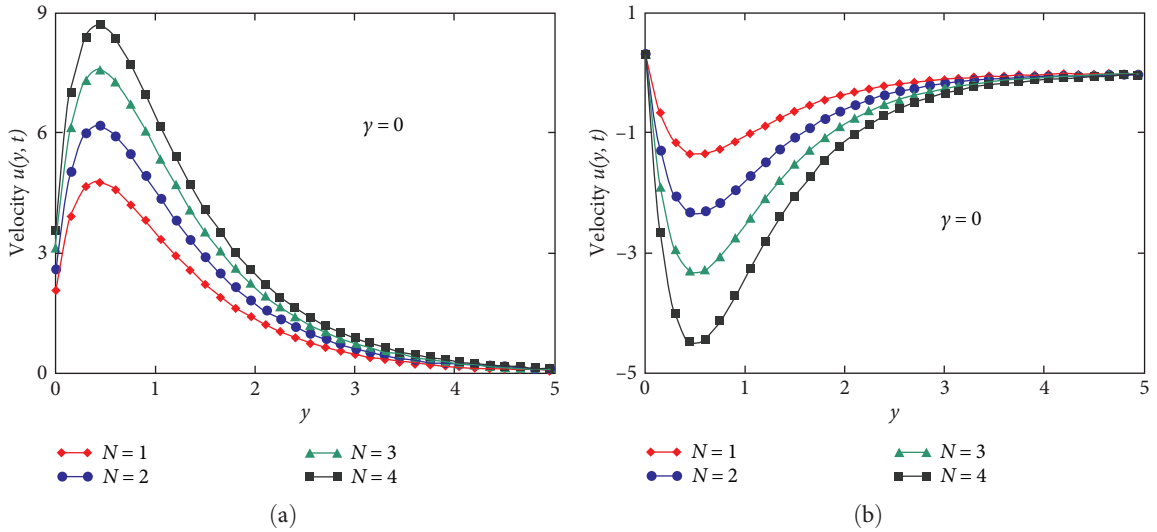

FIGURE 5: Effect of N positive (a) and negative (b) over velocity with no slip $\alpha = 0.5, Pr = 1.5, \mathrm{Sc} = 0.5, \mathrm{Sr} = 1.5, M = 0.5, \lambda = 2.5$.

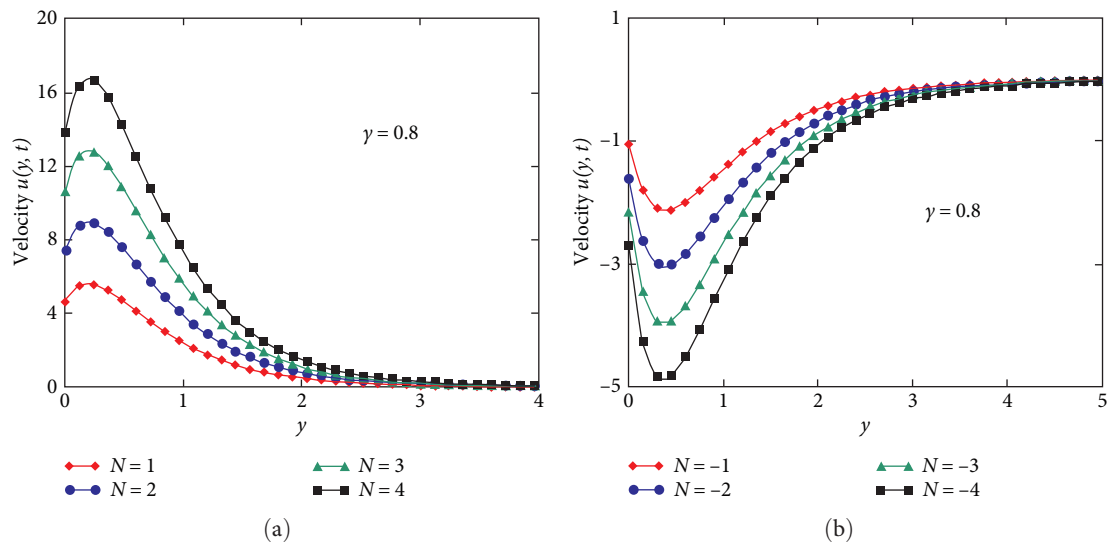

FIGURE 6: Effect of N positive (a) and negative (b) over velocity in the presence of slip, $\alpha = 0.5, Pr = 1.5, \mathrm{Sc} = 0.5, \mathrm{Sr} = 1.5, M = 0.5, \lambda = 2.5$.

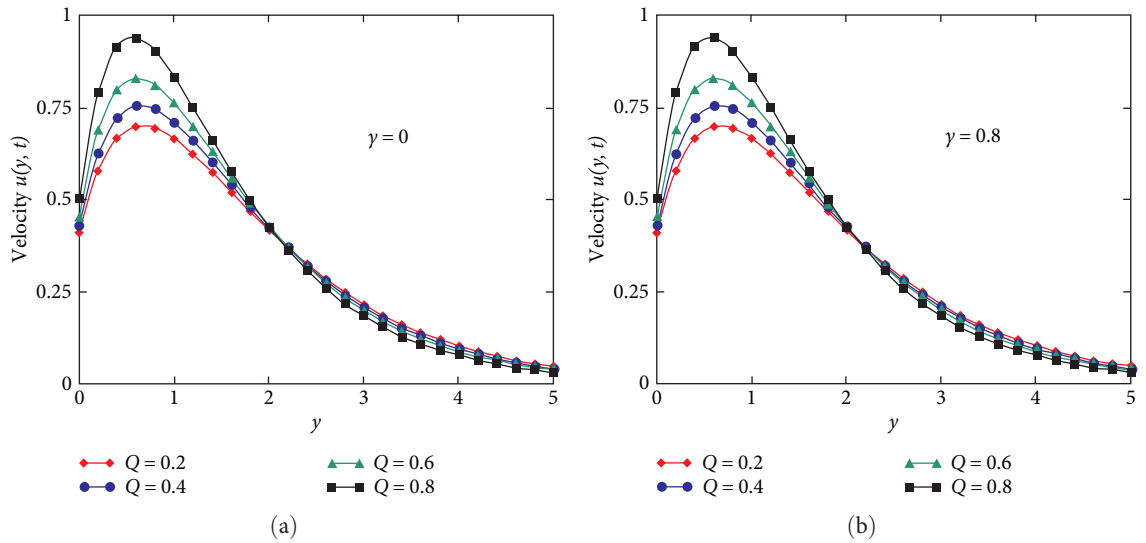

FIGURE 7: Effect of positive Q over velocity (a) for no slip and (b) for slip $\alpha = 0.5, Pr = 1.5, \mathrm{Sc} = 0.5, \mathrm{Sr} = 1.5, M = 0.5, \lambda = 2.5$.

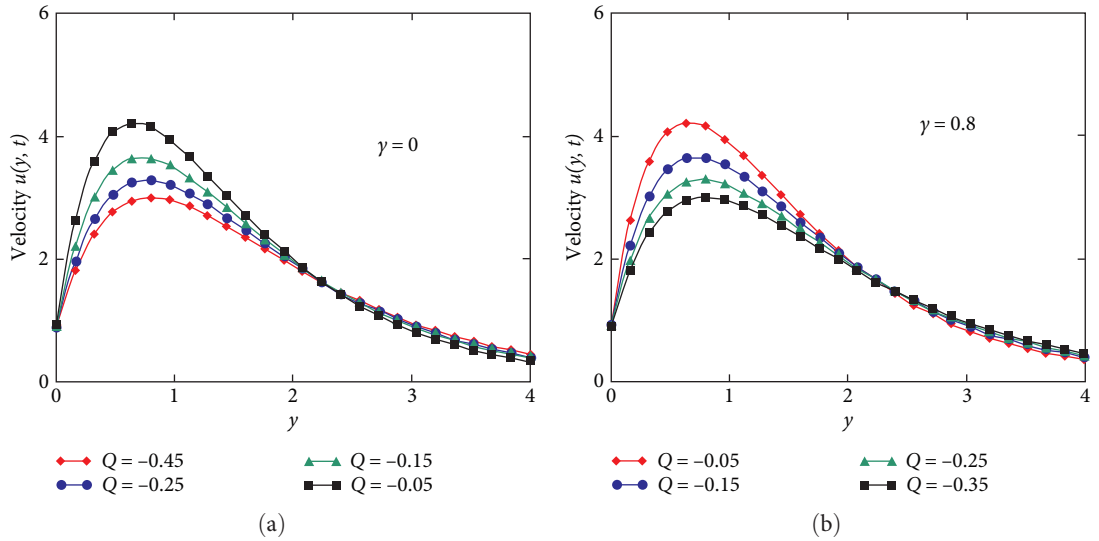

Figure 8: Effect of negative Q over velocity (a) for no slip and (b) for slip $\alpha = 0.5, Pr = 1.5, \mathrm{Sc} = 0.5, \mathrm{Sr} = 1.5, M = 0.5, \lambda = 2.5$.

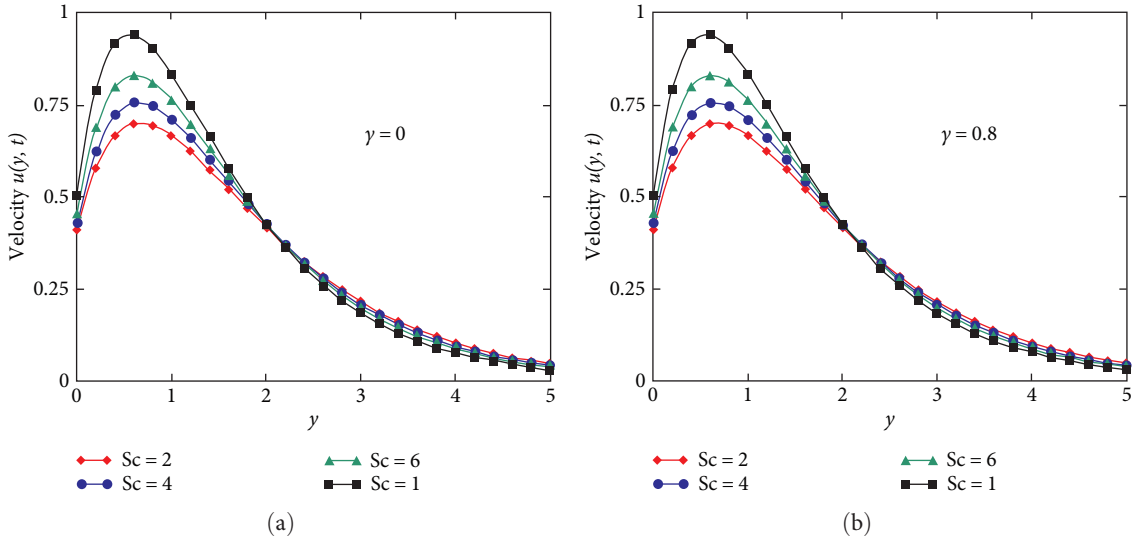

Figure 9: Effect of Sc over velocity (a) for no slip and (b) for slip $N = 0.5, Pr = 1.5, Q = 0.5, \mathrm{Sr} = 1.5, M = 0.5, \lambda = 2.5, \alpha = 0.5$.

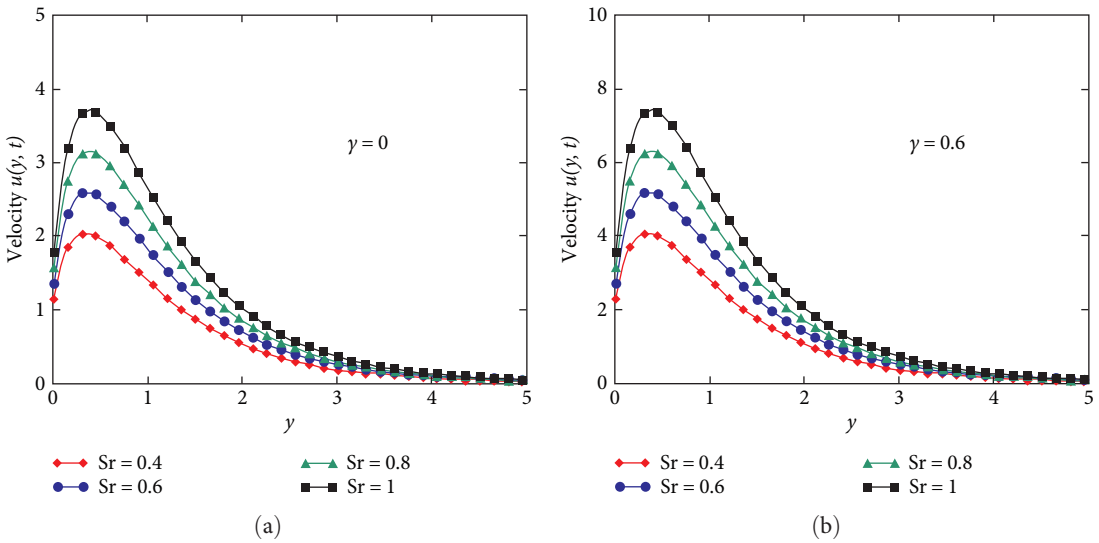

Figure 10: Effect of Sr over velocity (a) for no slip and (b) for slip $N = 0.5, Pr = 1.5, \mathrm{Sc} = 0.5, Q = 0.5, M = 0.5, \lambda = 2.5, \alpha = 0.5$.

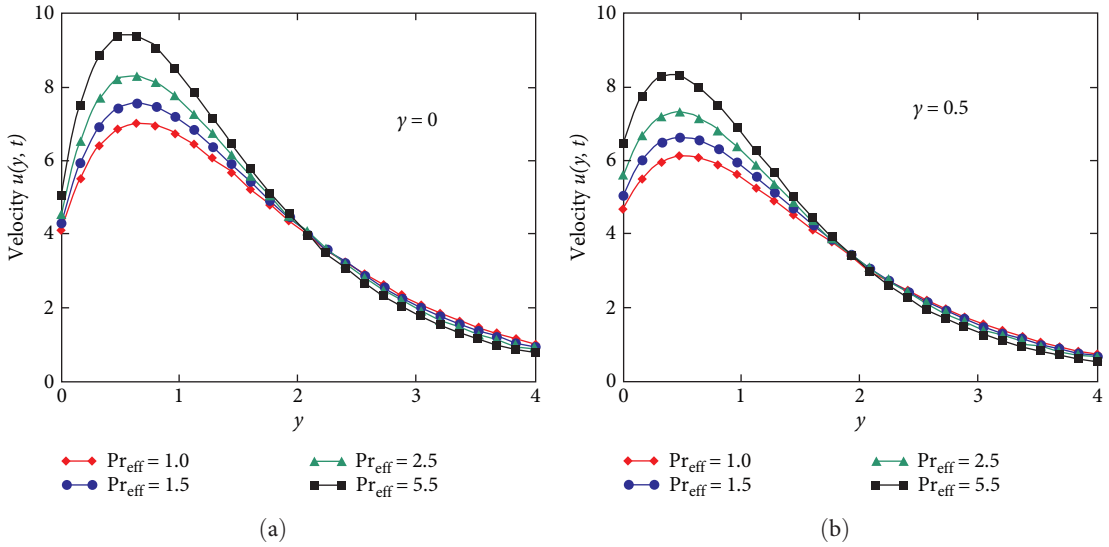

FIGURE 11: Effect of Pr_{eff} over velocity (a) for no slip and (b) for slip $N = 0.5, Q = 0.5, \text{Sc} = 0.5, \text{Sr} = 1.5, M = 0.5, \lambda = 2.5, \alpha = 0.5$.

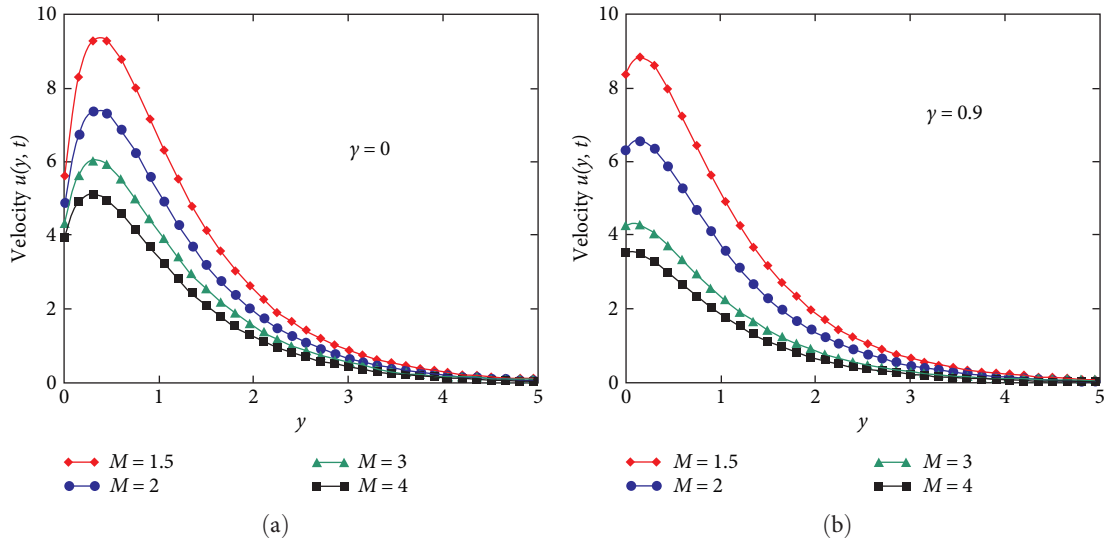

FIGURE 12: Velocity for Sr variation (a) for no slip and (b) for slip $N = 0.5, Q = 0.5, \text{Sc} = 0.5, \text{Sr} = 1.5, Pr = 1.5, \lambda = 2.5, \alpha = 0.5$.

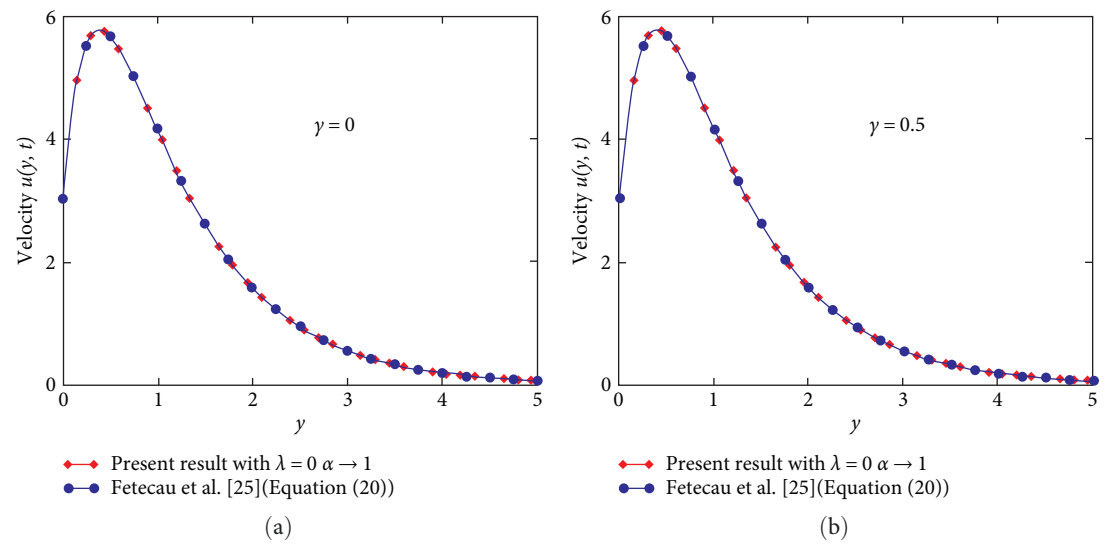

FIGURE 13: Velocity comparison with Fetecau et al. [25] (a) for no slip and (b) for slip $N = 0.5, Q = 0.5, \text{Sc} = 0.5, \text{Sr} = 1.5, M = 0.5, Pr = 1.5$.

is revealed that elevating Sr accelerates the fluid flow. In Figure 11, the subjectivity of effective Pr_{eff} is illustrated, and from Figure 11, it is evident that the flow velocity falls for ascending values Pr_{eff}. A larger value of Pr_{eff} refers to the more momentum diffusivity in the flow domain, which slows down the velocity of the fluid. Figure 12 is sketched to observe the potentness of magnetic parameter M. The pattern of Figure 12 reveals the decreasing trend for the elevating value of M. The effects of a magnetic field in the flow creates some resistive force that opposes the fluid flow that is why fluid velocity decreases for the increasing values of a magnetic parameter.

As it is stated, our prime motive was to make advancements in the research work done by Fetecau et al. [25] for a bigger class of fluid, namely Maxwell fluid. Moreover, it also includes an additional aspect of fractional instead of ordinary derivative. Therefore, the obtained result for velocity is also compared with the result of velocity obtained in [25] graphically. For this purpose, the velocity profiles are sketched in Figure 13 by letting the Maxwell parameter $\lambda = 0$ and fractional parameter $\alpha = 1$ for both slip and nonslip. The overlapping graphic profiles show the validation of our obtained result for velocity.

7. Conclusions

Thermodiffusion is a physical phenomenon that occurs because of the higher temperature and slanting distribution of the mixture. Thermodiffusion results in the isotope separation. In the present study, analytical results for mass and heat transfer flow of Maxwell fluid over a flat plate are considered by taking the effect of the first order slip at the boundary with the fractional derivative, which is known as the CPC fractional derivative. The impacts of radiation and generation of heat are also taken into consideration, along with the effect of a magnetic field of constant magnitude. The pearlized results for velocity, concentration, and temperature are obtained. The graphical illustrations are done using the same graphics of velocity for both cases, slip and no-slip effects. Moreover, this research work may extend to more complex fluids like Oldroyd-B fluid. The conclusions given below are drawn for the present research study.

(1) The fluid flows with an increasing velocity for the variation of α, β, γ, and Sr.

(2) Velocity for Sc, and slip parameter γ_1 is a decreasing function.

(3) For positive N velocity exhibits an enhancing posture the decerned trend for a negative value of N.

(4) For positive Q fluid speeds up, and the negative fluid flow slows down.

(5) The application of the CPC fractional derivative is a far better choice to obtain the generalized solution of the velocity field.

(6) The advantage of the fractional model is nonlocality and flexibility, which is why one can fit the data according to desired results by the variation of the order of fractional derivatives.

Nomenclature

u: Velocity component along x-axis
t: Time
ρ: Density of the fluid
μ: Viscosity of the fluid
g: Gravity
β_T, β_C: Coefficients of volumetric expansion
B_0: Magnitude of the magnetic field
λ_1: Maxwell fluid parameter
σ_1: Stefan–Boltzmann
k: Thermal conductivity
M: Magnetic parameter,
Sc: Schmidt number,
Sr: Soret effect parameter
Q: Nondimensional heat generation parameter
${}^{\text{CPC}}D_t^{\alpha}$: Constant proportional Caputo fractional derivative (CPC)
q_r: Radiation flux
Q_0: Heat generation
c_p: Specific heat at constant pressure
D_m: Molecular diffusivity,
C_w: Concentration near the wall.
γ_1: Slip parameter
C: Concentration
q: Laplace transform variable
T_w: Wall temperature
T_∞: Ambient temperature
N_r: Radiation parameter
α, β, γ: Fractional parameter
N: Ratio of mass Grashof number to thermal Grashof number
Pr, Pr_{eff}: Prandtl number and effective Prandtl number
σ: Current density.

Data Availability

The data used to support the findings of this study are available from the corresponding author upon request.

Conflicts of Interest

The authors declare that there are no conflicts of interest regarding the publication of this paper.

References

[1] A. J. Chamkha and A. Ben-Nakhi, "MHD mixed convection–radiation interaction along a permeable surface immersed in a porous medium in the presence of Soret and Dufour's Effects," *Heat and Mass Transfer*, vol. 44, pp. 845–856, 2008.

[2] O. D. Makinde, "On MHD mixed convection with Soret and Dufour effects past a vertical plate embedded in a porous medium," *Latin American Applied Research*, vol. 41, pp. 63–68, 2011.

[3] D. Vieru, M. A. Imran, and A. Rauf, "Slip effect on free convection flow of second grade fluids with ramped wall temperature," *Heat Transfer Research*, vol. 46, no. 8, pp. 713–724, 2015.

[4] M. Tahir, M. A. Imran, N. Raza, M. Abdullah, and M. Aleem, "Wall slip and non-integer order derivative effects on the heat transfer flow of Maxwell fluid over an oscillating vertical plate with new definition of fractional Caputo–Fabrizio derivatives," *Results in Physics*, vol. 7, no. 3, pp. 1887–1898, 2017.

[5] M. Jamil and N. A. Khan, "Slip effects on fractional viscoelastic fluids," *International Journal of Differential Equations*, vol. 2011, Article ID 193813, 19 pages, 2011.

[6] T. Hayat, M. F. Afzaal, C. Fetecau, and A. A. Hendi, "Slip effects on the oscillatory flow in a porous medium," *Journal of Porous Media*, vol. 14, no. 6, pp. 481–493, 2011.

[7] M. A. Imran, N. A. Shah, K. Rafique, A. Sohail, and S. Ejaz, "General solutions of convective flows of MHD Casson fluid with slip and Radiative heat transfer at the boundary," *Computational Thermal Sciences*, vol. 9, no. 1, pp. 1–11, 2011.

[8] M. Sajid, Z. Abbas, N. Ali, T. Javaid, and I. Ahmad, "Slip flow of a Maxwell fluid past a stretching sheet," *Walailak Journal of Science and Technology*, vol. 11, no. 12, pp. 1093–1103, 2014.

[9] T. Hayat, R. Sajjad, Z. Abbas, M. Sajid, and A. A. Hendi, "Radiation effects on MHD flow of Maxwell fluid in a channel with porous medium," *International Journal of Heat and Mass Transfer*, vol. 54, no. 4, pp. 854–862, 2011.

[10] G. K. Ramesh, B. J. Gireesha, T. Hayat, and A. Alsaedi, "MHD flow of Maxwell fluid over a stretching sheet in the presence of nanoparticles, thermal radiation and chemical reaction: a numerical study," *Journal of Nanofluids*, vol. 4, no. 1, pp. 100–107, 2015.

[11] I. Khan, N. A. Shah, and L. C. C. Dennis, "A scientific report on heat transfer analysis in mixed convection flow of Maxwell fluid over an oscillating vertical plate," *Scientific Report*, vol. 8, Article ID 46975, 2018.

[12] S. Chen, L. Zheng, B. Shen, and X. Chen, "Time–space dependent fractional boundary layer flow of Maxwell fluid over an unsteady stretching surface," *Theoretical and Applied Mechanics Letters*, vol. 5, no. 6, pp. 262–266, 2015.

[13] M. A. Imran, S. Sarwar, M. Imran, and M. Aleem, "Combined effect of slip and radiation on MHD flow past a constantly moving vertical plate with variable temperature," *Journal of Prime Research in Mathematics*, vol. 12, pp. 130–144, 2016.

[14] A. A. Opanuga, H. I. Okagbue, O. O. Agboola, and S. A. Bishop, "Second law analysis of ion slip effect on MHD couple stress fluid," *International Journal of Mechanics*, vol. 12, pp. 96–101, 2018.

[15] T. Hayat and Z. Asghar, "Heat transfer analysis on the peristaltic motion with slip effects," *Zeitschrift für Naturforschung A*, vol. 65, no. 8-9, pp. 697–704, 2010.

[16] T. Hayat, S. Hina, and A. A. Hendi, "Slip effects on peristaltic transport of a Maxwell fluid with heat and mass transfer," *Journal of Mechanics in Medicine and Biology*, vol. 12, no. 1, Article ID 1250001, 2012.

[17] T. Hayat, M. Imtiaz, and A. Alsaedi, "Partial slip effects in flow over nonlinear stretching surface," *Applied Mathematics and Mechanics*, vol. 36, pp. 1513–1526, 2015.

[18] A. Shakeel, S. Ahmad, H. Khan, N. A. Shah, and S. Haq, "Flows with slip of Oldroyd-B fluids over a moving plate," *Advances in Mathematical Physics*, vol. 2016, Article ID 8619634, 9 pages, 2016.

[19] N. A. Shah, C. Fetecau, and D. Vieru, "First general solutions for unsteady unidirectional motions of rate type fluids in cylindrical domains," *Alexandria Engineering Journal*, vol. 57, no. 3, pp. 1185–1196, 2018.

[20] R. A. Shah, T. Abbas, M. Idrees, and M. Ullah, "MHD Carreau fluid slip flow over a porous stretching sheet with viscous dissipation and variable thermal conductivity," *Boundary Value Problems*, vol. 2017, Article ID 94, 2017.

[21] N. Freidoonimehr and S. S. Jafari, "Second law of thermodynamics analysis of hydro-magnetic nano-fluid slip flow over a stretching permeable surface," *Journal of the Brazilian Society of Mechanical Sciences and Engineering*, vol. 37, pp. 1245–1256, 2015.

[22] S. Schneider, "Wall slip effects measuring the rheological behavior of electrorheological (ER) suspensions," *International Journal of Modern Physics B*, vol. 26, no. 1, Article ID 1250006, 2012.

[23] J. Raza, "Thermal radiation and slip effects on magnetohydrodynamic (MHD) stagnation point flow of Casson fluid over a convective stretching sheet," *Propulsion and Power Research*, vol. 8, no. 2, pp. 138–146, 2019.

[24] M. Norouzi, M. Davoodi, O. Anwar Bég, and M. D. Shamshuddin, "Theoretical study of Oldroyd-B visco-elastic fluid flow through curved pipes with slip effects in polymer flow processing," *International Journal of Applied and Computational Mathematics*, vol. 4, Article ID 108, 2018.

[25] C. Fetecau, D. Vieru, C. Fetecau, and I. Pop, "Slip effects on the unsteady radiative MHD free convection flow over a moving plate with mass diffusion and heat source," *The European Physical Journal Plus*, vol. 130, Article ID 6, 2015.

[26] S. A. Khan, Y. Nie, and B. Ali, "Multiple slip effects on MHD unsteady viscoelastic nano-fluid flow over a permeable stretching sheet with radiation using the finite element method," *SN Applied Sciences*, vol. 2, Article ID 66, 2020.

[27] I. Khan, N. A. Shah, Y. Mahsud, and D. Vieru, "Heat transfer analysis in a Maxwell fluid over an oscillating vertical plate using fractional Caputo–Fabrizio derivatives," *The European Physical Journal Plus*, vol. 132, Article ID 194, 2017.

[28] Y.-M. Chu, M. Ijaz Khan, T. Abbas et al., "Radiative thermal analysis for four types of hybrid nanoparticles subject to non-uniform heat source: keller box numerical approach," *Case Studies in Thermal Engineering*, vol. 40, Article ID 102474, 2022.

[29] A. M. Alqahtani, M. Riaz Khan, N. Akkurt, V. Puneeth, A. Alhowaity, and H. Hamam, "Thermal analysis of a radiative nanofluid over a stretching/shrinking cylinder with viscous dissipation," *Chemical Physics Letters*, vol. 808, Article ID 140133, 2022.

[30] V. Puneeth, F. Ali, M. R. Khan, M. S. Anwar, and N. A. Ahammad, "Theoretical analysis of the thermal characteristics of Ree–Eyring nanofluid flowing past a stretching sheet due to bioconvection," *Biomass Conversion and Biorefinery*, 2022.

[31] K. A. M. Alharbi, M. R. Khan, M. Ould Sidi, A. M. Algelany, S. Elattar, and N. A. Ahammad, "Investigation of hydromagnetic bioconvection flow of Oldroyd-B nanofluid past a porous stretching surface," *Biomass Conversion and Biorefinery*, vol. 13, pp. 4331–4342, 2023.

[32] M. R. Khan, S. Algarni, T. Alqahtani, S. A. M. Alsallami, T. Saeed, and A. M. Galal, "Numerical analysis of a time-dependent aligned MHD boundary layer flow of a hybrid nanofluid over a porous radiated stretching/shrinking surface," *Waves in Random and Complex Media*, 2022.

[33] D. Qaiser, Z. Zheng, M. Riaz Khan, and A. M. Galal, "Significance of activation energy and entropy optimization in radiative stagnation point flow of nanofluid with cross-diffusion and viscous dissipation," *Waves in Random and Complex Media*, 2022.

[34] V. Puneeth, M. Shoaib Anwar, and M. Riaz Khan, "Bioconvective Darcy–Frochherimer flow of the Ree–Eyring nanofluid through a

stretching sheet with velocity and thermal slips," *Waves in Random and Complex Media*, pp. 1–14, 2022.

[35] M. R. Khan, A. M. Alqahtani, S. E. Alhazmi et al., "Numerical investigation of Darcy–Forchheimer hybrid nanofluid flow with energy transfer over a spinning fluctuating disk under the influence of chemical reaction and heat source," *Micromachines*, vol. 14, no. 1, Article ID 48, 2023.

[36] L. Kolsi, A. Raza, K. Al-Khaled, K. Ghachem, S. U. Khan, and A. U. Haq, "Thermal applications of copper oxide, silver, and titanium dioxide nanoparticles via fractional derivative approach," *Waves in Random and Complex Media*, vol. 33, no. 3, pp. 794–807, 2023.

[37] Z. Jie, M. Ijaz Khan, K. Al-Khaled et al., "Thermal transport model for Brinkman type nanofluid containing carbon nanotubes with sinusoidal oscillations conditions: a fractional derivative concept," *Waves in Random and Complex Media*, 2022.

[38] A. Raza, S. Ullah Khan, K. Al-Khaled et al., "A fractional model for the kerosene oil and water-based Casson nanofluid with inclined magnetic force," *Chemical Physics Letters*, vol. 787, Article ID 139277, 2022.

[39] A. Raza, A. Ghaffari, S. U. Khan, A. U. Haq, M. I. Khan, and M. R. Khan, "Non-singular fractional computations for the radiative heat and mass transfer phenomenon subject to mixed convection and slip boundary effects," *Chaos, Solitons & Fractals*, vol. 155, Article ID 111708, 2022.

[40] S. U. Khan, S. A. Shehzad, N. Ali, and M. N. Bashir, "Some generalized results for Maxwell fluid flow over porous oscillatory surface with modified Fourier and Fick's theories," *Journal of the Brazilian Society of Mechanical Sciences and Engineering*, vol. 40, Article ID 474, 2018.

[41] S. U. Khan, N. Ali, M. Sajid, and T. Hayat, "Heat transfer characteristics in oscillatory hydromagnetic channel flow of Maxwell fluid using Cattaneo–Christov model," *Proceedings of the National Academy of Sciences, India Section A: Physical Sciences*, vol. 89, pp. 377–385, 2019.

[42] R. Tang, S. Rehman, A. Farooq et al., "Comparative study of natural convection flow of fractional Maxwell fluid with uniform heat flux and radiation," *Complexity*, vol. 2021, Article ID 9401655, 16 pages, 2021.

[43] M. Mansoor, Y. Nawaz, B. Ahmad, and M. Irfan, "Chemically reactive flow and energy transport phenomenon considering variable conductivity on Maxwell fluid: a numerical simulation," *Mathematical Problems in Engineering*, vol. 2022, Article ID 8461613, 9 pages, 2022.

[44] M. A. Imran, M. Aleem, M. B. Riaz, R. Ali, and I. Khan, "A comprehensive report on the convective flow of fractional (ABC) and (CF) MHD viscous fluid subject to generalized boundary conditions," *Chaos, Solitons & Fractals*, vol. 118, pp. 274–289, 2019.

[45] D. Baleanu and A. Fernandez, "On fractional operators and their classifications," *Mathematics*, vol. 7, no. 9, Article ID 830, 2019.

[46] F. Jarad, T. Abdeljawad, S. Rashid, and Z. Hammouch, "More properties of the proportional fractional integrals and derivatives of a function with respect to another function," *Advances in Difference Equations*, vol. 2020, Article ID 303, 2020.

[47] M. Ahmad, M. A. Imran, M. Aleem, and I. Khan, "A comparative study and analysis of natural convection flow of MHD non-Newtonian fluid in the presence of heat source and first-order chemical reaction," *Journal of Thermal Analysis and Calorimetry*, vol. 137, pp. 1783–1796, 2019.

[48] D. Baleanu, A. Fernandez, and A. Akgül, "On a fractional operator combining proportional and classical differ integrals," *Mathematics*, vol. 8, no. 3, Article ID 360, 2020.

[49] J. R. Howell and R. Siegel, *Thermal Radiation Heat Transfer*, Taylor & Francis, New York, 5th edition edition, 2011.

[50] E. Magyari and A. Pantokratoras, "Note on the effect of thermal radiation in the linearized Rosseland approximation on the heat transfer characteristics of various boundary layer flows," *International Communications in Heat and Mass Transfer*, vol. 38, no. 5, pp. 554–556, 2011.

[51] C. Fetecau, D. Vieru, C. Fetecau, and S. Akhter, "General solutions for magnetohydrodynamic natural convection flow with radiative heat transfer and slip condition over a moving plat," *Zeitschrift für Naturforschung A*, vol. 68, no. 10-11, pp. 659–667, 2013.

[52] M. Narahari and B. K. Dutta, "Effects of thermal radiation and mass diffusion on free convection flow near a vertical plate with Newtonian heating," *Chemical Engineering Communications*, vol. 199, no. 5, pp. 628–643, 2012.

[53] H. Stehfest, "Algorithm 368: numerical inversion of Laplace transforms [D5]," *Communications of the ACM*, vol. 13, no. 1, pp. 47–49, 1970.

[54] D. Y. Tzou, *Macro to Microscale Heat Transfer: The Behavior*, Tylor and Francis, Washington, 1970.

Hindawi
Advances in Mathematical Physics
Volume 2023, Article ID 1091355, 18 pages
https://doi.org/10.1155/2023/1091355

Research Article

The Modified Exponential Function Method for Beta Time Fractional Biswas-Arshed Equation

Yusuf Pandir,[1] **Tolga Akturk**,[2] **Yusuf Gurefe**,[3] **and Hussain Juya**[3,4]

[1]*Department of Mathematics, Faculty of Science and Arts, Yozgat Bozok University, Yozgat, Turkey*
[2]*Department of Mathematics and Science Education, Faculty of Education, Ordu University, Ordu, Turkey*
[3]*Department of Mathematics, Faculty of Science, Mersin University, Mersin, Turkey*
[4]*Faculty of Information Technology and Communication, Department of Science, Kabul University, Kabul, Afghanistan*

Correspondence should be addressed to Yusuf Gurefe; yusufgurefe@mersin.edu.tr and Hussain Juya; hjuya2021@gmail.com

Received 9 November 2022; Revised 16 December 2022; Accepted 5 April 2023; Published 27 April 2023

Academic Editor: Muhammad Nadeem

In this study, the exact solutions of the Biswas-Arshed equation with the beta time derivative, which has an important role and physically means that it represents the pulse propagation in an optical fiber, nuclear, and particle physics, are obtained using the modified exponential function method. Exact solutions consisting of hyperbolic, trigonometric, rational trigonometric, and rational function solutions demonstrate the competence and relevance of the proposed method. In addition, the physical properties of the obtained exact solutions are shown by making graphical representations according to different parameter values. It is seen that the method used is an effective technique, since these solution functions obtained with all these cases have periodic function properties.

1. Introduction

Differential equations with fractional derivatives have been used very popularly in many fields of science recently, just like integer order derivative equations. It is used effectively in many branches of science such as health, biology, engineering, and stochastic models. Because such equations contain terms that represent many of the behaviors studied in these cases, each equation is defined as a mathematical model. To obtain the solutions of these mathematical models, there are various methods in the literature such as the improved Bernoulli subequation method [1], the trial equation method [2], the extended trial equation method [3], the G'/G method [4, 5], the extended tanh method [6], the Kudryashov method [7, 8], the generalized Kudryashov method [9], the new function method [10], the first integral method [11, 12], the differential transform method [13], the variational iteration method [14], the exp-function method [15, 16], the Adomian decomposition method [17], some numerical methods [18–22], the Chebyshev collocation method [23], the integral transform operator [24], the Chebyshev-Tau method [25], the Taylor expansion method [26], the modified exponential function method [27, 28], and the new type F-expansion method [29].

In this study, the modified exponential function method was applied to obtain the exact solutions of the Biswas-Arshed equation with the beta time derivative.

The outline of this study can be expressed as follows: In the 2nd chapter, some information about the definitions and properties of the Atangana's beta derivative is given. In the third chapter, the modified exponential function method is introduced in detail with its features. In the fourth chapter, the analysis of the nonlinear fractional mathematical model with Atangana's derivative is given. In the last section, there is a conclusion that includes all the outputs presented in this article.

2. The Properties and Definition of Beta Derivative

Definition 1. Khalil et al. added a new fractional derivative term to the fractional derivative topic and brought it to the

literature [30]. Let us analyzed the conformable derivative function $g : [0,\infty)$ of the α order from type $t > 0, \alpha \in (0, 1)$ as follows:

$$ {}_0D_t^{\alpha}\{g(t)\} = \lim_{\varepsilon \longrightarrow 0} \frac{g\left(t + \varepsilon t^{1-\alpha}\right) - g(t)}{\varepsilon}. \tag{1} $$

When g is α-differentiable in the interval of $(0, a), a > 0$ and $\lim_{\varepsilon \longrightarrow 0^+} g^{(\alpha)}(t)$ consists, then it can be defined as $g^{(\alpha)}(0) = \lim_{\varepsilon \longrightarrow 0^+} g^{(\alpha)}(t)$.

Definition 2. The beta derivative term is described by Atangana et al. as follows [31]:

$$ {}_0^A D_t^{\alpha}\{g(t)\} = \lim_{\varepsilon \longrightarrow 0} \frac{g\left(t + \varepsilon(t + (1/(\Gamma(\alpha))))^{1-\alpha}\right) - g(t)}{\varepsilon}. \tag{2} $$

The mathematical model used in the study that consists of the Atangana's fractional derivative is preferred because it provides some features of the basic derivative rules. According to all these cases, the various properties of the conformable derivative are as follows:

(i) Let $h \neq 0$ and g be functions that are differentiable with respect to beta in the range $\beta \in (0, 1]$. Accordingly, the equation that can satisfy all the real numbers q and r is as follows:

$$ {}_0^A D_x^{\alpha}\{q\, g(x) + r\, h(x)\} = q {}_0^A D_x^{\alpha}\{\, g(x)\} + r {}_0^A D_x^{\alpha}\{\, h(x)\}. \tag{3} $$

(ii) p is defined as any constant that satisfies the following equation:

$$ {}_0^A D_x^{\alpha}\{p\} = 0, \tag{4} $$

$$ {}_0^A D_x^{\alpha}\{g(x)h(x)\} = h(x) {}_0^A D_x^{\alpha}\{\, g(x)\} + g(x) {}_0^A D_x^{\alpha}\{\, h(x)\}, \tag{5} $$

$$ {}_0^A D_x^{\alpha}\left\{\frac{g(x)}{h(x)}\right\} = \frac{h(x) {}_0^A D_x^{\alpha}\{\, g(x)\} - g(x) {}_0^A D_x^{\alpha}\{\, h(x)\}}{h^2(x)}. \tag{6} $$

If $\lambda = (x + (1/(\Gamma(\alpha))))^{\alpha-1}\nu$ is written instead of λ in Equation (2) and $\nu \longrightarrow 0$, when $\lambda \longrightarrow 0$, is taken as follows

$$ {}_0^A D_x^{\alpha}\{g(x)\} = \left(x + \frac{1}{\Gamma(\alpha)}\right)^{1-\alpha} \frac{dg(x)}{dx}, \tag{7} $$

with

$$ \eta = \frac{\delta}{\alpha}\left(x + \frac{1}{\Gamma(\alpha)}\right)^{\alpha}, \tag{8} $$

where δ is the constant, and therefore, the following equation is written:

$$ {}_0^A D_x^{\alpha}\{g(\eta)\} = \delta \frac{dg(\eta)}{d\eta}. \tag{9} $$

3. Properties of the Modified Exponential Function Method

In this section, the modified exponential function method, which is an efficient method used to obtain the wave solutions of the nonlinear mathematical model defined by Atangana derivatives, will be explained in detail.

The general form of the nonlinear fractional partial differential equation containing the solution function u with two variables and its beta derivatives is as follows:

$$ P\left(u, |u|^2, {}_0^A D_t^{\beta} u, u_x, u_{xx}, u_{xx}, \cdots\right) = 0, \tag{10} $$

where x and t represent space and time to which the function u given in the general form is dependent.

Let us take the traveling wave transform generated according to the independent variables in the general form of the nonlinear partial differential as follows:

$$ u(x, t) = u(\eta), \eta = \left(x - \frac{\gamma}{\alpha}\left(t + \frac{1}{\Gamma(\beta)}\right)^{\beta}\right), \tag{11} $$

where γ is any constant. When the derivative terms in Equation (10) are written instead of those obtained from the wave transformation (11), the general form of the following nonlinear ordinary differential equation is found:

$$ N\left(u, u^2, u^3, u', u'', \cdots\right) = 0. \tag{12} $$

The solution function of the nonlinear fractional differential equation considered in this study is as follows:

$$ u(\eta) = \frac{\sum_{i=0}^{q} A_i \left[e^{-\vartheta(\eta)}\right]^i}{\sum_{j=0}^{r} B_j \left[e^{-\vartheta(\eta)}\right]^j} = \frac{A_0 + A_1 e^{-\vartheta} + \cdots + A_q e^{-q\vartheta}}{B_0 + B_1 e^{-\vartheta} + \cdots + B_r e^{-r\vartheta}}, \tag{13} $$

where $A_i, B_j, (0 \leq i \leq q, 0 \leq j \leq r)$ are constants and $\vartheta = \vartheta(\eta)$. The terms of derivative in Equation (12) are obtained from Equation (13). However, in this process, while the derivatives of the function u with respect to η are taken, the function ϑ and its derivative with respect to η are required. For this case, the following equation is used as

$$ \vartheta'(\eta) = e^{-\vartheta(\eta)} + \mu\, e^{\vartheta(\eta)} + \lambda. \tag{14} $$

If Equation (14) is arranged, the following equation is obtained:

$$ \frac{e^{\vartheta(\eta)}}{\mu\, e^{2\vartheta(\eta)} + \lambda e^{\vartheta(\eta)} + 1} d\vartheta = d\eta. \tag{15} $$

While integrating Equation (15) according to the functions

η and ϑ, the following family cases are obtained according to the states of the coefficients in the same equation [27, 28]:

Family 1. If $\mu \neq 0$ and $\lambda^2 - 4\mu > 0$,

$$\vartheta(\eta) = \ln\left(-\frac{\lambda}{2\mu} - \frac{\sqrt{\lambda^2 - 4\mu}}{2\mu}\tanh\left(\frac{\sqrt{\lambda^2 - 4\mu}}{2}(\eta + E)\right)\right). \tag{16}$$

Family 2. If $\mu \neq 0$ and $\lambda^2 - 4\mu < 0$,

$$\vartheta(\eta) = \ln\left(-\frac{\lambda}{2\mu} + \frac{\sqrt{-\lambda^2 + 4\mu}}{2\mu}\tan\left(\frac{\sqrt{-\lambda^2 + 4\mu}}{2}(\eta + E)\right)\right). \tag{17}$$

Family 3. If $\mu = 0$, $\lambda \neq 0$, and $\lambda^2 - 4\mu > 0$,

$$\vartheta(\eta) = -\ln\left(\frac{\lambda}{e^{\lambda(\eta+E)} - 1}\right). \tag{18}$$

Family 4. If $\mu \neq 0$, $\lambda \neq 0$, and $\lambda^2 - 4\mu = 0$,

$$\vartheta(\eta) = \ln\left(-\frac{2\lambda(\eta + E) + 4}{\lambda^2(\eta + E)}\right). \tag{19}$$

Family 5. If $\mu = 0$, $\lambda = 0$, and $\lambda^2 - 4\mu = 0$,

$$\vartheta(\eta) = \ln(\eta + E), \tag{20}$$

where E, λ, μ are coefficients.

After determining the function ϑ in Equation (13) according to the conditions stated above, another step that needs to be done is to determine the upper bounds in Equation (13). For this, the balance procedure must be used. In other words, there is a relationship between q and r, which is analyzed as the upper boundary, with the balancing of the highest order derivative term in the nonlinear ordinary differential equation and the highest order nonlinear term. Then, appropriate values are determined to provide this correlation. In this way, the boundaries of Equation (13) are stated. Then, the terms of derivative required in Equation (12) are obtained from Equation (13) and written in their place. The system of algebraic equations consisting of the coefficients of the function ϑ in this equation is obtained. The coefficients in the form of $A_0, A_1, A_2, \cdots, A_q$ and $B_0, B_1, B_2, \cdots, B_r$ are found together with the solution of this system of equations. Then, the obtained coefficients are written in Equation (13). The functions ϑ determined according to the family conditions are also put in their place. It is checked that these functions, which are obtained together with the necessary mathematical operations, provide the nonlinear mathematical model with beta derivatives. Finally, the graphs simulating the physical behavior of wave solutions satisfying the equation are obtained according to the appropriate parameters.

4. Analysis of the Nonlinear Mathematical Model with the Beta Time Derivative

In this section, the traveling wave solutions satisfying the Biswas-Arshed equation with the beta time derivative will be analyzed by using the modified exponential function method. The Biswas-Arshed equation physically means that it represents the pulse propagation in an optical fiber. The Biswas-Arshed equation with the beta time derivative is as follows [32, 33]:

$$\begin{aligned} i{}_0^A D_t^\beta\{u\} + a_1 u_{xx} + a_{20}{}^A D_t^\beta\{u_x\} + i\left(b_1 u_{xxx} + b_{20}{}^A D_t^\beta\{u_{xx}\}\right) \\ - i\left(\sigma\left(|u|^2 u\right)_x + \tau\, u\left(|u|^2\right)_x + \zeta|u|^2 u_x\right) = 0, \end{aligned} \tag{21}$$

where $a_1, a_2, b_1, b_2, \sigma, \tau$, and ζ are arbitrary constants. Here, the functions u_{xx}, u_{xxx}, ${}_0^A D_t^\beta\{u_x\}$, and ${}_0^A D_t^\beta\{u_{xx}\}$ are, respectively, given as the group velocity, the third order, spatiotemporal dispersions, and spatiotemporal third-order dispersions whereas $u = u(x, t)$ is defined as a complex-valued function. Also, $\left(|u|^2 u\right)_x$ is the self-steepening term and $\left(|u|^2\right)_x$ and $|u|^2 u_x$ are the terms of nonlinear dispersions. To solve the nonlinear fractional differential equation, firstly using the wave transform given below, this equation is reduced to a system of nonlinear ordinary differential equations. For this, let us consider the traveling wave transform in the form

$$\begin{aligned} u(x, t) &= \phi(\eta) e^{i\varphi(x,t)}, \\ \eta &= x - \frac{\rho}{\beta}\left(t + \frac{1}{\Gamma(\beta)}\right)^\beta, \\ \varphi(x, t) &= -\kappa x + \frac{\omega}{\beta}\left(t + \frac{1}{\Gamma(\beta)}\right)^\beta + \wp, \end{aligned} \tag{22}$$

where ρ, κ, ω, and $\wp$ are constants. When the terms containing derivatives required in Equation (21) are obtained from the wave transform (22) and written in their place, we get the following system of nonlinear ordinary differential equations:

$$\begin{aligned} &(2\kappa\rho b_2 - 3\kappa b_1 + \omega b_2 + \rho a_2 - a_1)\phi'' + \left(\kappa^3 b_1 - \kappa^2 \omega b_2 + \kappa^2 a_1 - \kappa\omega a_2 + \omega\right)\phi \\ &\quad + (\kappa\sigma + \kappa\zeta)\phi^3 = 0, \end{aligned} \tag{23a}$$

$$\begin{aligned} &(\rho b_2 - b_1)\phi''' + \left(-\kappa^2\rho b_2 + 3\kappa^2 b_1 - 2\kappa\omega b_2 - \kappa\rho a_2 + 2\kappa a_1 - \omega a_2 + \rho\right)\phi' \\ &\quad + (3\sigma + 2\tau + \zeta)\phi^2\phi' = 0. \end{aligned} \tag{23b}$$

By equating the coefficients of Equation (23b) to zero, the following results are obtained:

$$\rho = \frac{b_1}{b_2},$$
$$\sigma = -\frac{2}{3}\tau - \frac{1}{3}\zeta, \tag{24}$$
$$w = \frac{2\kappa^2 b_1 b_2 + 2\kappa a_1 b_2 - \kappa a_2 b_1 + b_1}{b_2(2\kappa b_2 + a_2)}.$$

A nonlinear ordinary differential equation is obtained by substituting the values in Equation (24) into Equation (23a) as follows:

$$\left(-\kappa b_1 + \frac{2\kappa^2 b_1 b_2 + 2\kappa a_1 b_2 - \kappa a_2 b_1 + b_1}{2\kappa b_2 + a_2} + \frac{b_1 a_2}{b_2} - a_1\right)\phi'' + \left(\kappa^3 b_1 - \frac{\left(\kappa^2 b_2 - \kappa a_2 + 1\right)\left(2\kappa^2 b_1 b_2 + 2\kappa a_1 b_2 - \kappa a_2 b_1 + b_1\right)}{b_2(2\kappa b_2 + a_2)} + \kappa^2 a_1\right)\phi + \left(\frac{2\kappa}{3}(\zeta - \tau)\right)\phi^3 = 0. \tag{25}$$

When the balance procedure is applied to Equation (25), the following balance relation is obtained between the term ϕ'' with the highest order derivative and the term ϕ^3 with the highest order nonlinear term:

$$3n - 3m = n - m + 2 \Rightarrow n = m + 1. \tag{26}$$

For $m = 1$, we obtain $n = 2$. In this case, it is assumed that the solution function determined according to Equation (13) is as follows:

$$\phi(\eta) = \frac{\psi}{\varpi} = \frac{A_0 + A_1 e^{-\vartheta} + A_2 e^{-2\vartheta}}{B_0 + B_1 e^{-\vartheta}}. \tag{27}$$

The derivative terms required for Equation (25) are obtained from Equation (27) as follows:

$$u'(\eta) = \frac{\psi'\varpi - \psi\varpi'}{\varpi^2}, \tag{28}$$

$$u''(\eta) = \frac{\left(\left(\psi''\varpi^3 + \psi'\varpi'\varpi^2 - \left(\psi'\varpi'\varpi^2 + \psi\varpi''\varpi^2\right)\right) - 2\varpi\varpi'\left(\psi'\varpi - \psi\varpi'\right)\right)}{\varpi^4}. \tag{29}$$

The system of algebraic equations, observed by substituting the terms obtained in Equations ((27)–(29)) into Equation (25), is solved by using the Mathematica program, and thus, the following coefficients are obtained by this way. In addition, two different cases of solutions such as Case 1 and Case 2, where each case consists of five different solution families, are given below. Now, let us consider these solution cases.

Case 1.

$$A_0 = -\lambda B_0\sqrt{\frac{3b_1}{2\kappa b_2(\zeta - \tau)\left(-4\kappa + \left(2\kappa^2 - \lambda^2 + 4\mu\right)a_2\right)}},$$
$$A_1 = -(2B_0 + \lambda B_1)\sqrt{\frac{3b_1}{2\kappa b_2(\zeta - \tau)\left(-4\kappa + \left(2\kappa^2 - \lambda^2 + 4\mu\right)a_2\right)}},$$
$$A_2 = -B_1\sqrt{\frac{6b_1}{\kappa b_2(\zeta - \tau)\left(-4\kappa + \left(2\kappa^2 - \lambda^2 + 4\mu\right)a_2\right)}},$$
$$a_1 = \frac{b_1\left(2 - 4\kappa a_2 + \left(a_2^2 + b_2\right)\left(2\kappa^2 - \lambda^2 + 4\mu\right)\right)}{b_2\left(-4\kappa + \left(2\kappa^2 - \lambda^2 + 4\mu\right)a_2\right)}. \tag{30}$$

When the coefficients obtained above are, respectively, substituted in Equations (27) and (22), the following wave solutions are found according to the family states.

Family 1. When $\mu \neq 0$ and $\lambda^2 - 4\mu > 0$,

$$u_{1,1}(x,t) = \Theta_1\left(-\lambda + \frac{4\mu}{\lambda + \sqrt{\lambda^2 - 4\mu}\tanh\left[\left(\sqrt{\lambda^2 - 4\mu}/2\right)\left(x - (b_1/\beta b_2)(t + (1/(\Gamma(\beta))))^{\beta} + E\right)\right]}\right) \times e^{i\left(-\kappa x + \left(\left(2\kappa^2 b_1 b_2 + 2\kappa a_1 b_2 - \kappa a_2 b_1 + b_1\right)/(\beta b_2(2\kappa b_2 + a_2))\right)(t + (1/(\Gamma(\beta))))^{\beta} + \varphi\right)}, \tag{31}$$

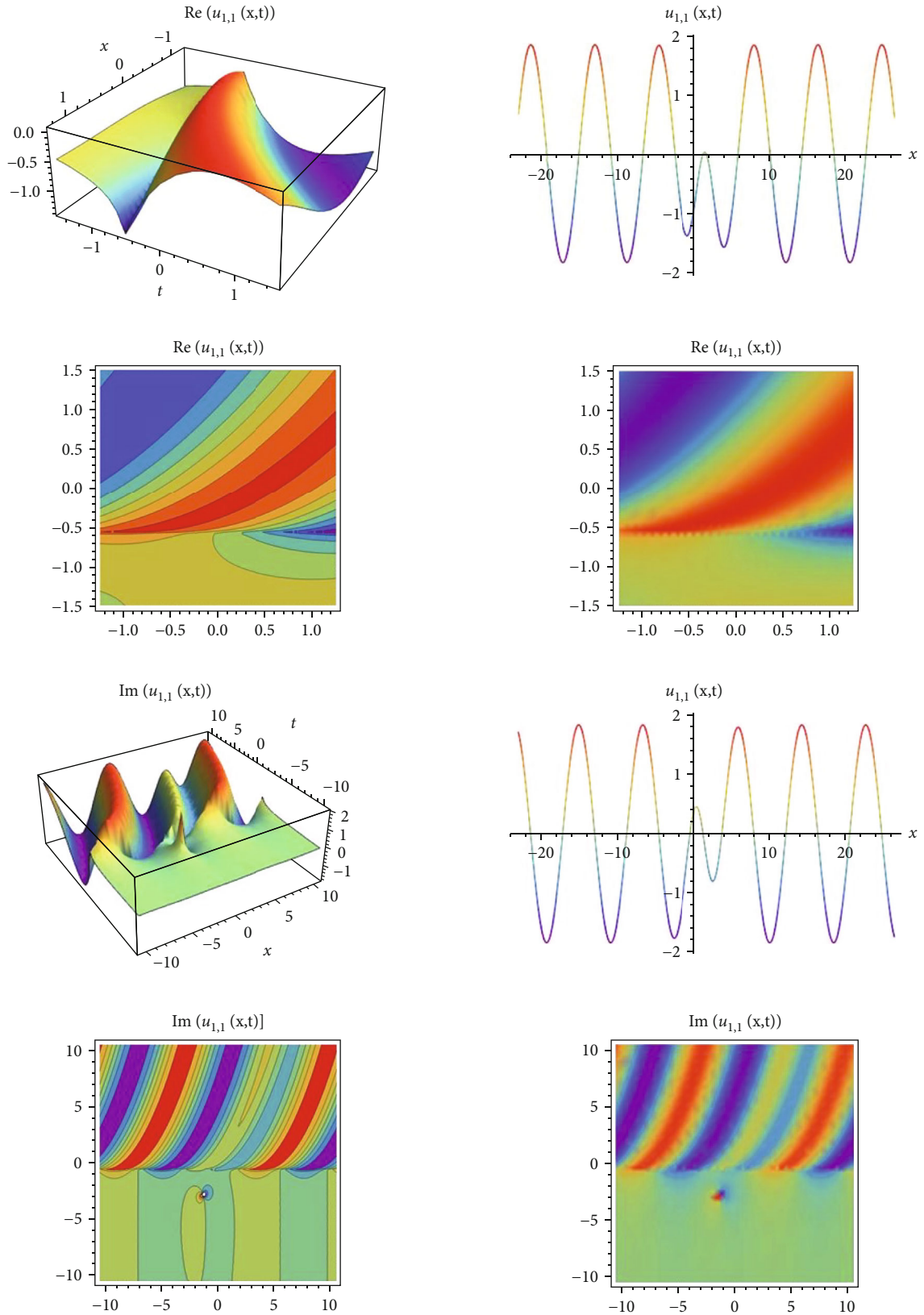

Figure 1: The graphs simulating the behavior of the model (31) for the values of $\delta = 0.96$, $\lambda = 3$, $b_1 = 2.5$, $B_0 = 0.2$, $\kappa = 0.75$, $\zeta = 0.21$, $\tau = 0.45$, $\mu = 2$, $a_2 = 3.6$, $b_2 = 2.4$, $B_1 = 0.85$, $E = 0.65$, $\beta = 0.5$, $A_0 = -1.10702$, $A_1 = -5.44284$, $A_2 = -3.13655$, $a_1 = 2.81046$, $\omega = 0.730188$, $\rho = 1.04167$, and $t = 1$.

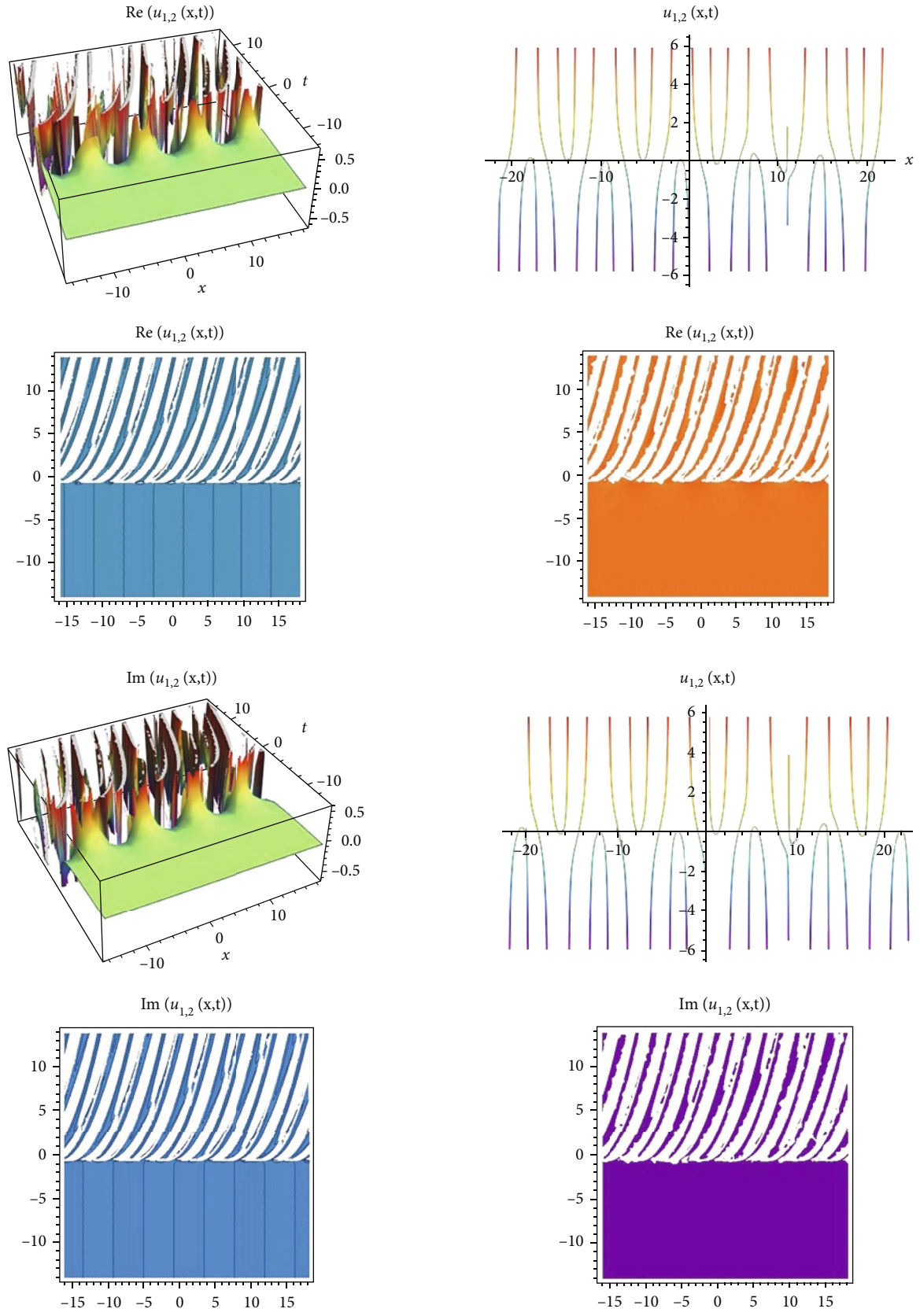

FIGURE 2: The graphs simulating the behavior of the model (32) for the values of $\delta = 0.96$, $\lambda = 2$, $b_1 = 2.5$, $B_0 = 0.2$, $\kappa = 0.75$, $\zeta = 0.45$, $\tau = 0.21$, $\mu = 3$, $a_2 = 3.6$, $b_2 = 2.4$, $B_1 = 0.85$, $E = 0.65$, $\beta = 0.5$, $A_0 = -0.215706$, $A_1 = -1.13245$, $A_2 = -0.916749$, $a_1 = 4.58403$, $\omega = 1.09968$, $\rho = 1.04167$, and $t = 1$.

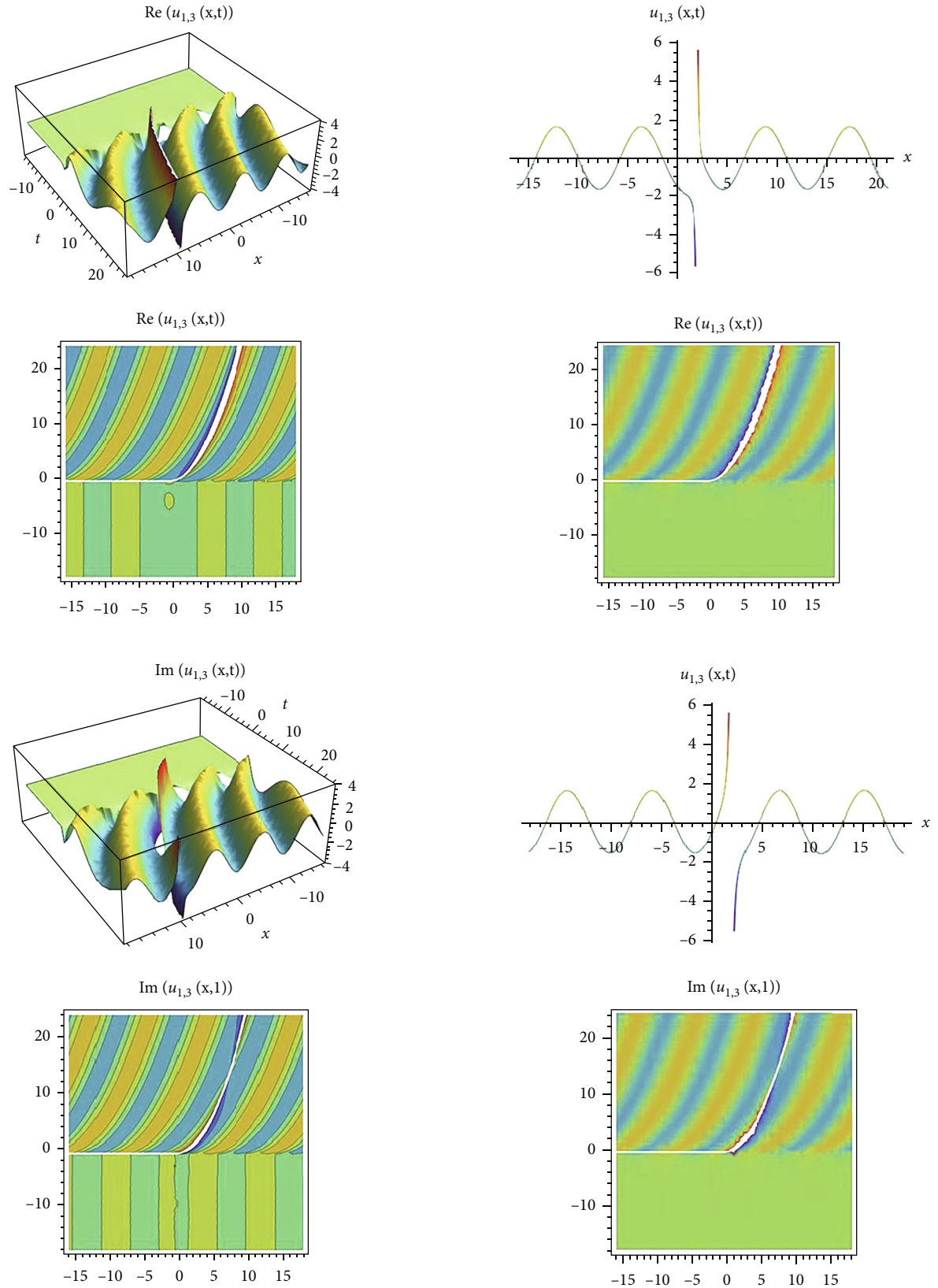

Figure 3: The graphs simulating the behavior of the model (33) for the values of $\delta = 0.96$, $\lambda = 2$, $b_1 = 2.5$, $B_0 = 0.2$, $\kappa = 0.75$, $\zeta = 0.21$, $\tau = 0.45$, $\mu = 0$, $a_2 = 3.6$, $b_2 = 2.4$, $B_1 = 0.85$, $E = 0.65$, $\beta = 0.5$, $A_0 = -0.322547$, $A_1 = -1.69337$, $A_2 = -1.37083$, $a_1 = 4.13233$, $\omega = 1.00558$, $\rho = 1.04167$, and $t = 1$.

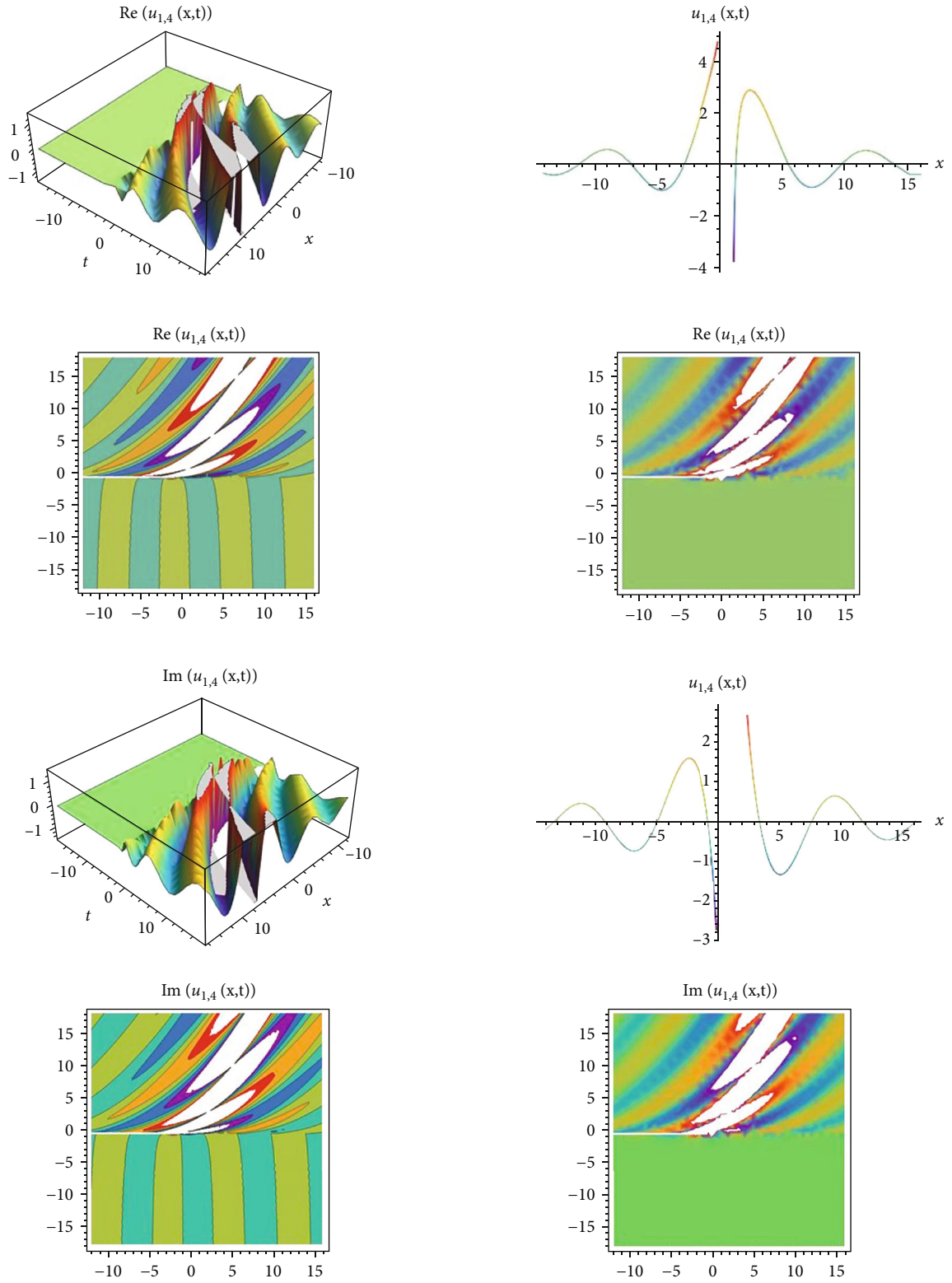

FIGURE 4: The graphs simulating the behavior of the model (34) for the values of $\delta = 0.96$, $\lambda = 2$, $b_1 = 2.5$, $B_0 = 0.2$, $\kappa = 0.75$, $\zeta = 0.45$, $\tau = 0.21$, $\mu = 1$, $a_2 = 3.6$, $b_2 = 2.4$, $B_1 = 0.85$, $E = 0.65$, $\beta = 0.5$, $A_0 = -1.15011$, $A_1 = -6.03807$, $A_2 = -4.88796$, $a_1 = 8.4127$, $\omega = 1.89732$, $\rho = 1.04167$, and $t = 1$.

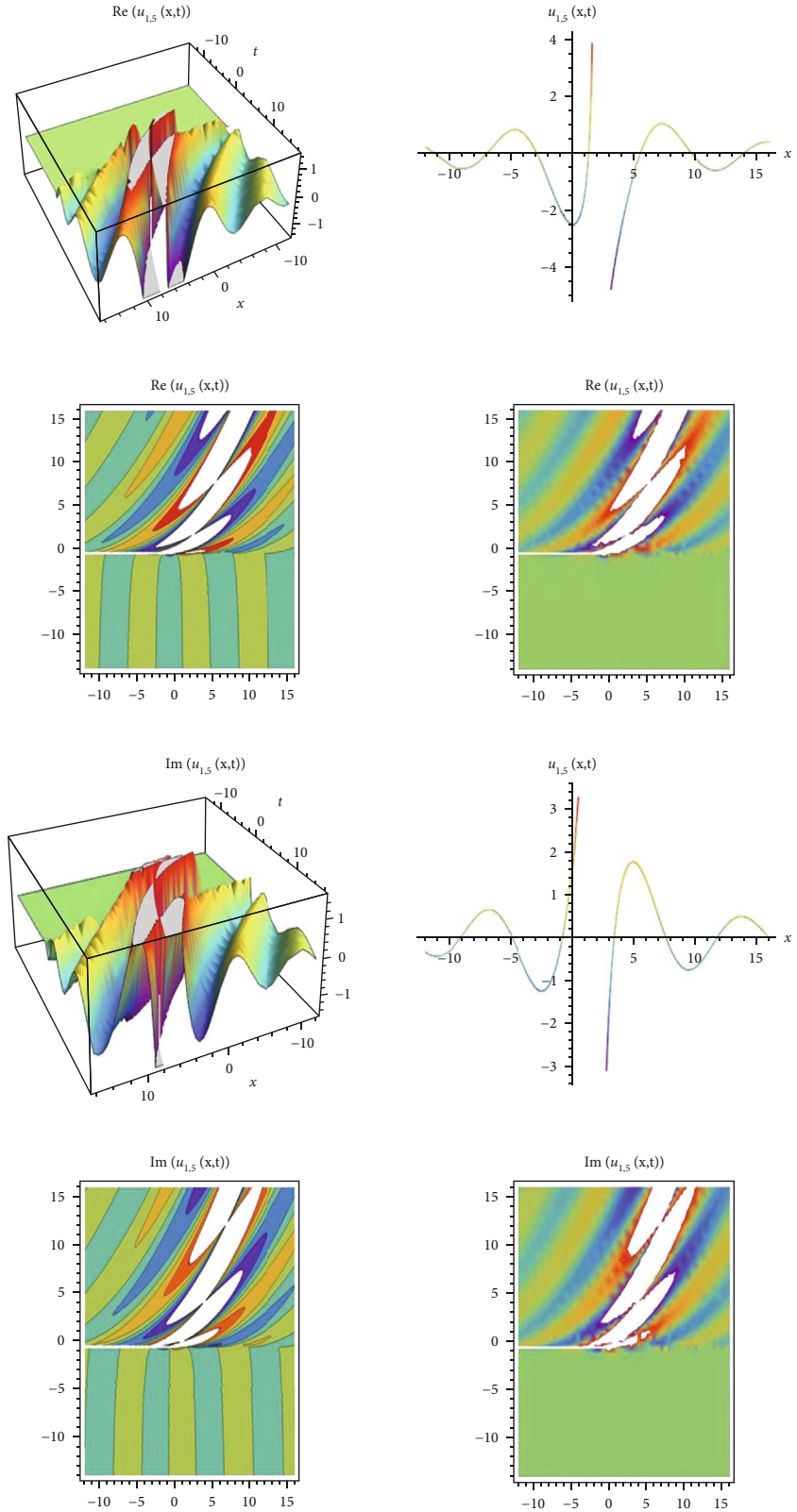

FIGURE 5: The graphs simulating the behavior of the model (35) for the values of $\delta = 0.96$, $\lambda = 0$, $b_1 = 2.5$, $B_0 = 0.2$, $\kappa = 0.75$, $\zeta = 0.45$, $\tau = 0.21$, $\mu = 0$, $a_2 = 3.6$, $b_2 = 2.4$, $B_1 = 0.85$, $E = 0.65$, $\beta = 0.5$, $A_0 = 0$, $A_1 = -1.15011$, $A_2 = -4.88796$, $a_1 = 8.4127$, $\omega = 1.89732$, $\rho = 1.04167$, and $t = 1$.

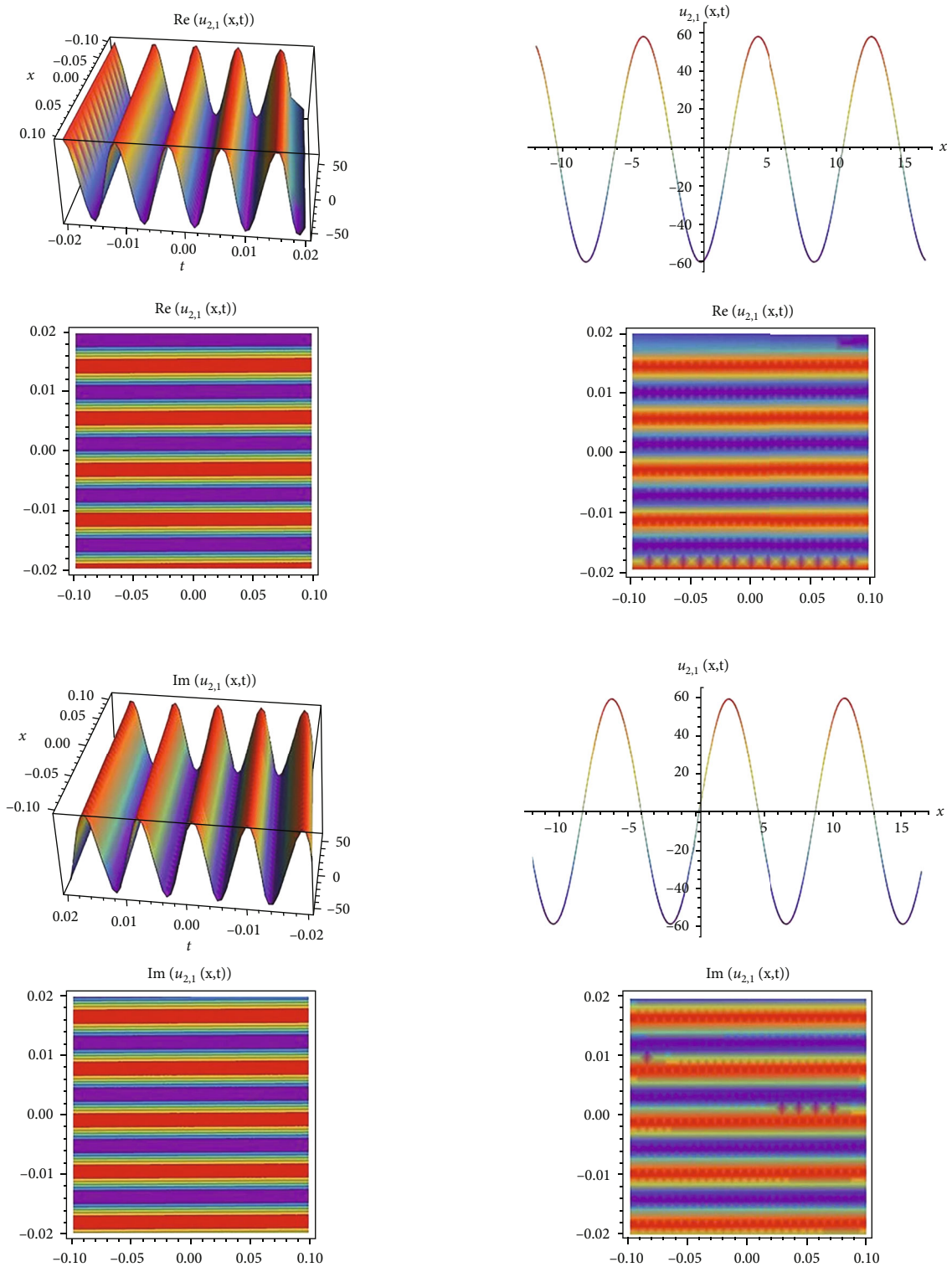

Figure 6: The graphs simulating the behavior of the model (37) for the values of $\delta = 0.96$, $\lambda = 3$, $b_1 = 2.5$, $B_0 = 0.2$, $\kappa = 0.75$, $\zeta = 0.21$, $\tau = 0.45$, $\mu = 2$, $a_2 = 0.6$, $b_2 = 0.4$, $B_1 = 0.85$, $E = 0.65$, $\beta = 0.5$, $A_0 = -11.8153$, $A_1 = -50.215$, $A_2 = 0$, $a_1 = 429.477$, $\omega = 542.055$, $\rho = 6.25$, and $t = 1$.

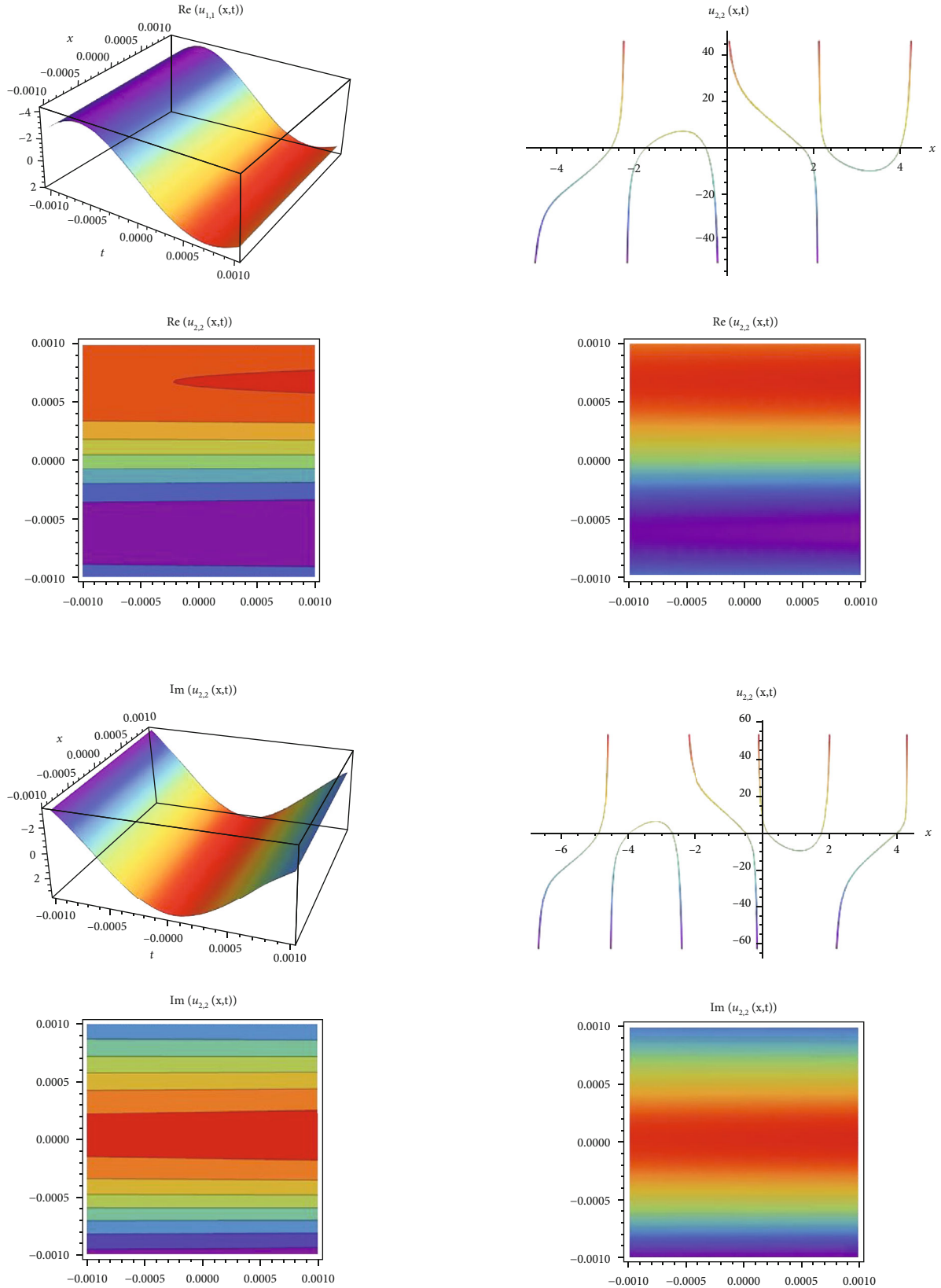

FIGURE 7: The graphs simulating the behavior of the model (38) for the values of $\delta = 0.96$, $\lambda = 2$, $b_1 = 2.5$, $B_0 = 0.2$, $\kappa = 0.75$, $\zeta = 0.21$, $\tau = 0.45$, $\mu = 3$, $a_2 = 0.6$, $b_2 = 0.4$, $B_1 = 0.85$, $E = 0.65$, $\beta = 0.5$, $A_0 = -21.5605$, $A_1 = -91.6323$, $A_2 = 0$, $a_1 = -1442.39$, $\omega = -1797.78$, $\rho = 6.25$, and $t = 1$.

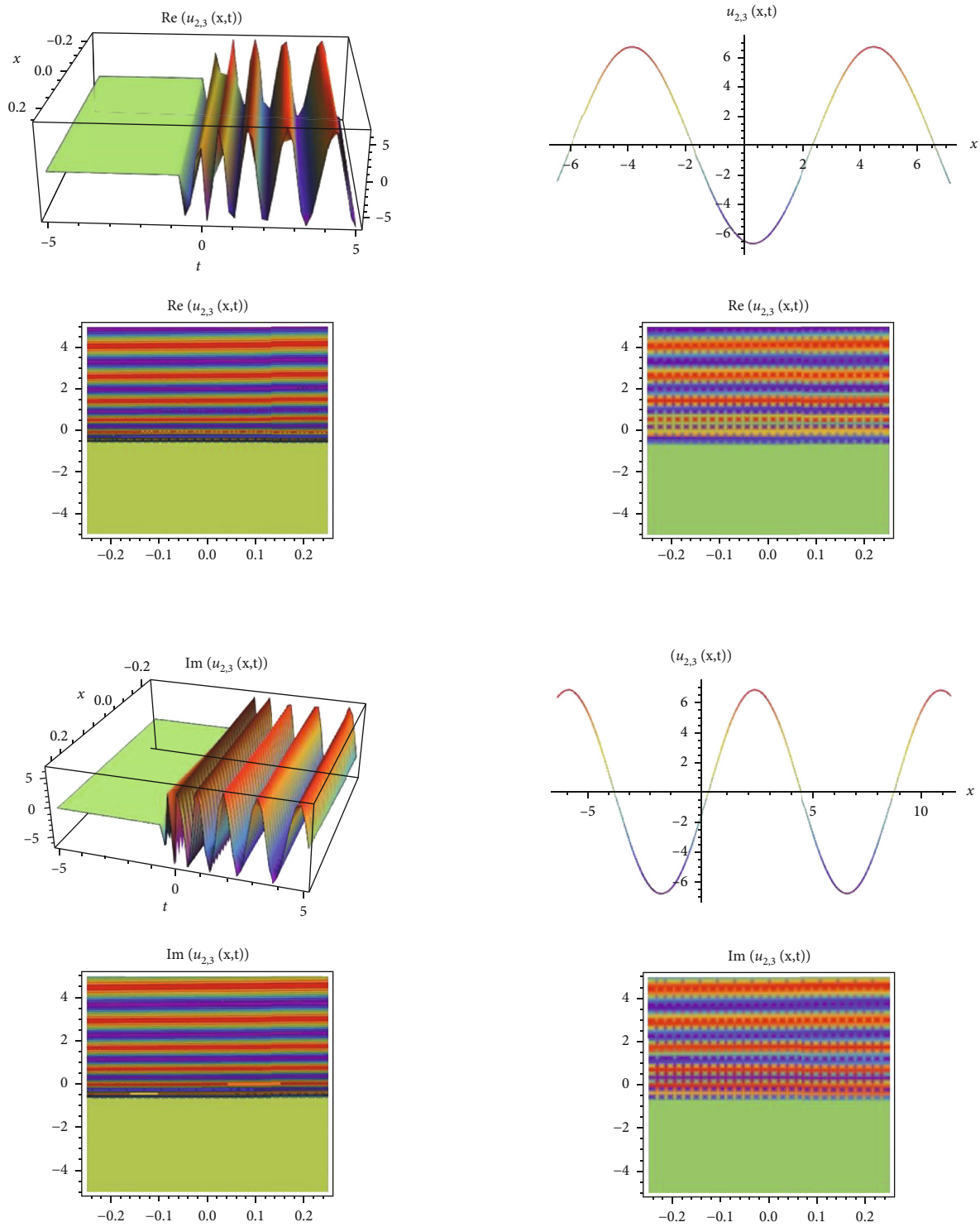

FIGURE 8: The graphs simulating the behavior of the model (39) for the values of $\delta = 0.96$, $\lambda = 2$, $b_1 = 2.5$, $B_0 = 0.2$, $\kappa = 0.75$, $\zeta = 0.21$, $\tau = 0.45$, $\mu = 0$, $a_2 = 0.6$, $b_2 = 0.4$, $B_1 = 0.85$, $E = 0.65$, $\beta = 0.5$, $A_0 = 1.32803$, $A_1 = 5.64414$, $A_2 = 0$, $a_1 = 2.62566$, $\omega = 8.49041$, $\rho = 6.25$, and $t = 1$.

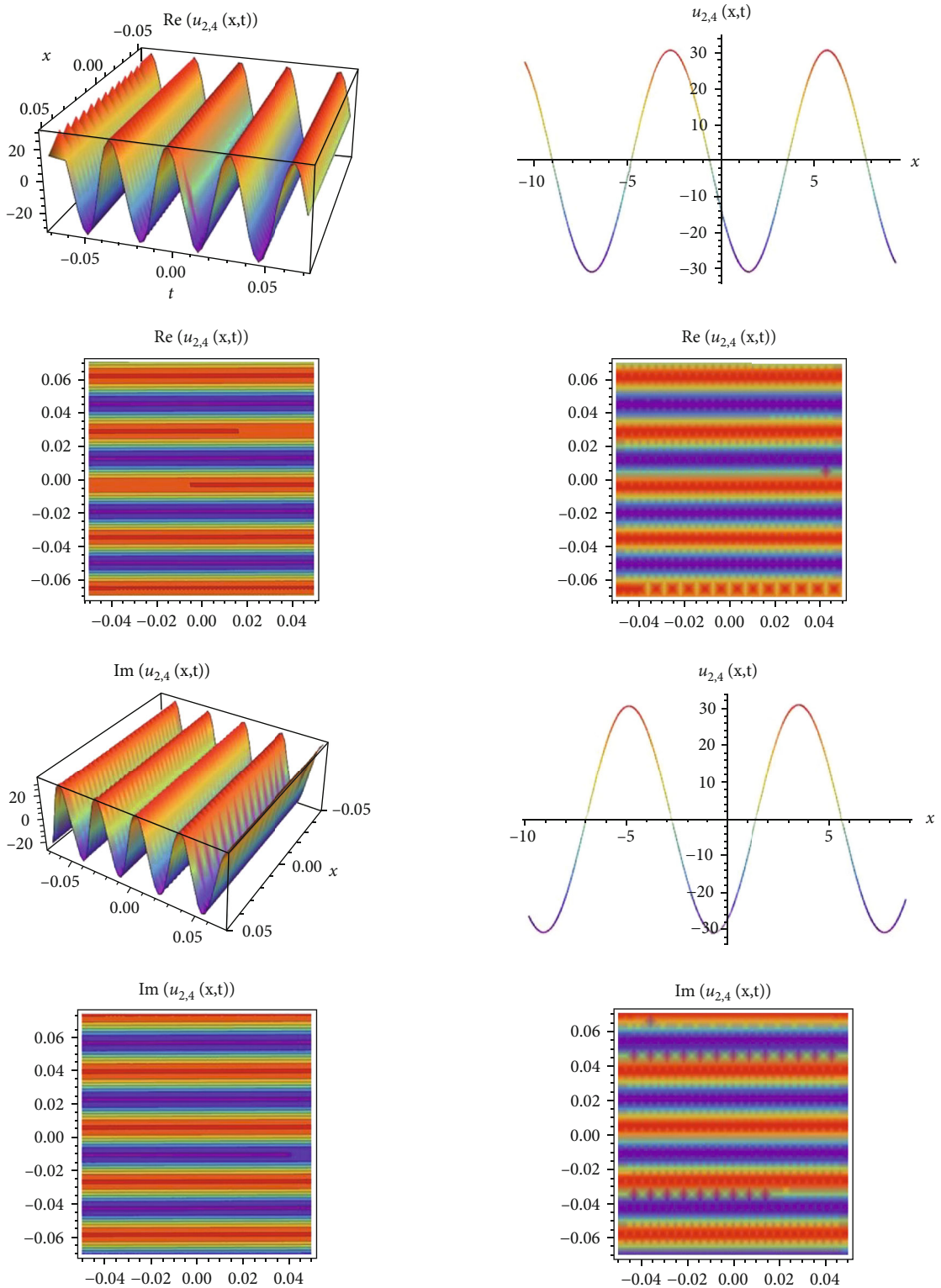

FIGURE 9: The graphs simulating the behavior of the model (40) for the values of $\delta = 0.96$, $\lambda = 2$, $b_1 = 2.5$, $B_0 = 0.2$, $\kappa = 0.75$, $\zeta = 0.21$, $\tau = 0.45$, $\mu = 1$, $a_2 = 0.6$, $b_2 = 0.4$, $B_1 = 0.85$, $E = 0.65$, $\beta = 0.5$, $A_0 = -6.15292$, $A_1 = -26.1499$, $A_2 = 0$, $a_1 = 114.403$, $\omega = 148.212$, $\rho = 6.25$, and $t = 1$.

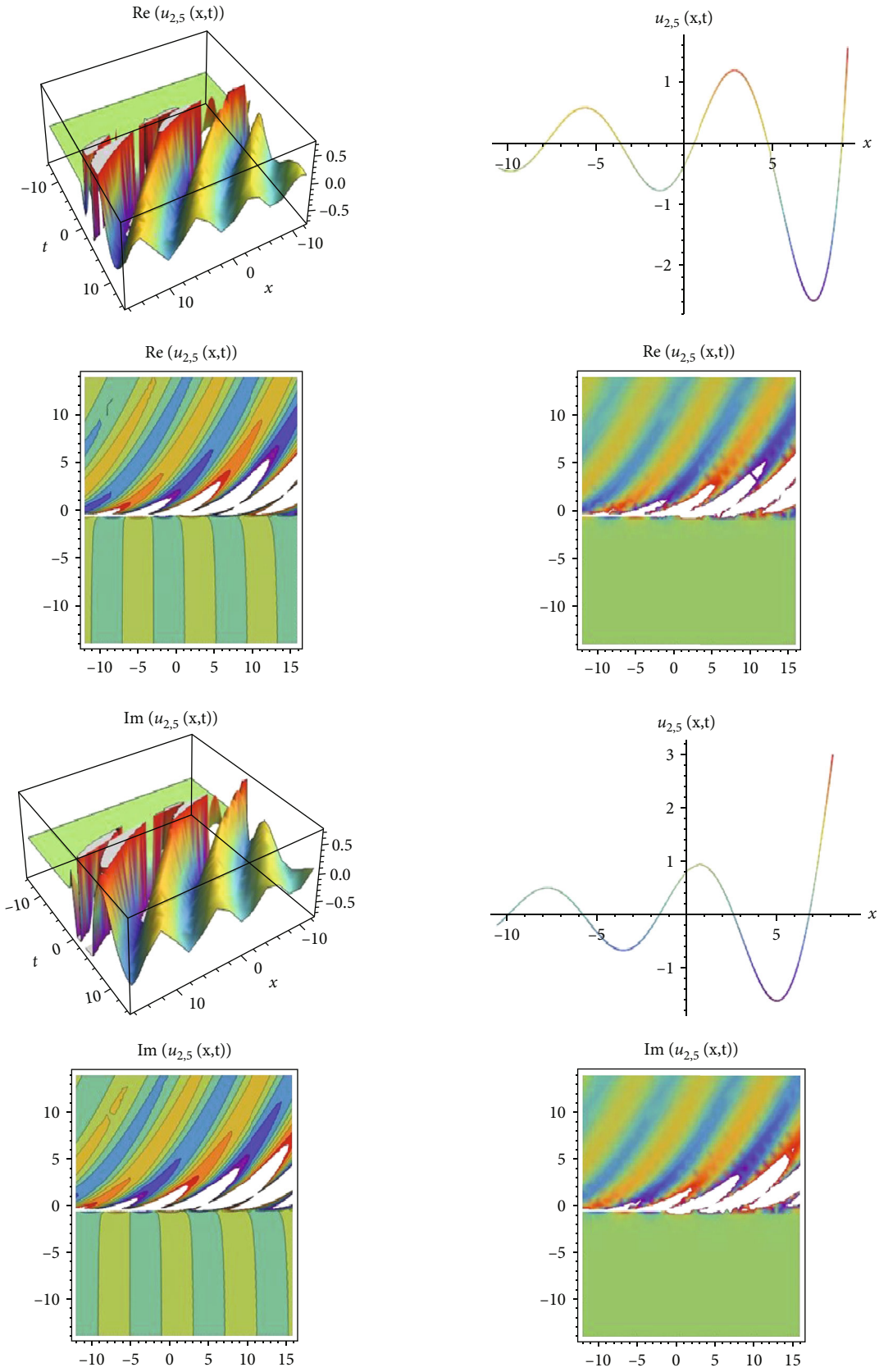

FIGURE 10: The graphs simulating the behavior of the model (41) for the values of $\delta = 0.96$, $\lambda = 2$, $b_1 = 2.5$, $B_0 = 0.2$, $\kappa = 0.75$, $\zeta = 0.21$, $\tau = 0.45$, $\mu = 1$, $a_2 = 0.6$, $b_2 = 0.4$, $B_1 = 0.85$, $E = 0.65$, $\beta = 0.5$, $A_0 = 0$, $A_1 = 1.89321$, $A_2 = 0$, $a_1 = -2.83602$, $\omega = 1.66331$, $\rho = 6.25$, and $t = 1$.

where $\Theta_1 = \sqrt{3b_1/(2b_2\kappa(\zeta-\tau)(-4\kappa+(2\kappa^2-\lambda^2+4\mu)a_2))}$.

Family 2. When $\mu \neq 0$ and $\lambda^2 - 4\mu < 0$,

$$u_{1,2}(x,t) = \Theta_1\left(-\lambda + \frac{4\mu}{\lambda - \sqrt{-\lambda^2+4\mu}\tan\left[\left(\sqrt{-\lambda^2+4\mu}/2\right)\left(x-(b_1/\beta b_2)(t+(1/(\Gamma(\beta))))^{\beta}+E\right)\right]}\right) \cdot \times e^{i\left(-\kappa x+\left(\left(2\kappa^2 b_1 b_2+2\kappa a_1 b_2-\kappa a_2 b_1+b_1\right)/(\beta b_2(2\kappa b_2+a_2))\right)(t+(1/(\Gamma(\beta))))^{\beta}+\wp\right)}, \tag{32}$$

where $\Theta_1 = \sqrt{3b_1/(2b_2\kappa(\zeta-\tau)(-4\kappa+(2\kappa^2-\lambda^2+4\mu)a_2))}$.

Family 3. When $\mu = 0$, $\lambda \neq 0$, and $\lambda^2 - 4\mu > 0$,

$$u_{1,3}(x,t) = \Theta_2 \coth\left[\frac{1}{2}\lambda\left(x-\frac{b_1}{\beta b_2}\left(t+\frac{1}{\Gamma(\beta)}\right)^{\beta}+E\right)\right] e^{i\left(-\kappa x+\left(\left(2\kappa^2 b_1 b_2+2\kappa a_1 b_2-\kappa a_2 b_1+b_1\right)/(\beta b_2(2\kappa b_2+a_2))\right)(t+(1/(\Gamma(\beta))))^{\beta}+\wp\right)}, \tag{33}$$

where $\Theta_2 = \lambda\sqrt{3b_1/(2b_2\kappa(\zeta-\tau)(-4\kappa+(2\kappa^2-\lambda^2)a_2))}$.

Family 4. When $\mu \neq 0$, $\lambda \neq 0$, and $\lambda^2 - 4\mu = 0$,

$$u_{1,4}(x,t) = \frac{\Theta_3 e^{i\left(-\kappa x+\left(\left(2\kappa^2 b_1 b_2+2\kappa a_1 b_2-\kappa a_2 b_1+b_1\right)/(\beta b_2(2\kappa b_2+a_2))\right)(t+(1/((\Gamma(\beta)))))^{\beta}+\wp\right)}}{\left(2+\lambda\left(x-(b_1/\beta b_2)(t+(1/(\Gamma(\beta))))^{\beta}+E\right)\right)}, \tag{34}$$

where $\Theta_3 = \lambda\sqrt{6b_1/(b_2\kappa(\zeta-\tau)(-4\kappa+(2\kappa^2-\lambda^2+4\mu)a_2))}$.

Family 5. When $\mu = 0$, $\lambda = 0$, and $\lambda^2 - 4\mu = 0$,

$$u_{1,5}(x,t) = -\frac{\Theta_4 e^{i\left(-\kappa x+\left(\left(2\kappa^2 b_1 b_2+2\kappa a_1 b_2-\kappa a_2 b_1+b_1\right)/(\beta b_2(2\kappa b_2+a_2))\right)(t+(1/(\Gamma(\beta))))^{\beta}+\wp\right)}}{x-(b_1/\beta b_2)(t+(1/(\Gamma(\beta))))^{\beta}+E}, \tag{35}$$

where $\Theta_4 = \sqrt{3b_1/(b_2\kappa^2(\zeta-\tau)(-2+\kappa a_2))}$.

Case 2.

$$A_0 = \frac{\sqrt{3b_1}(\lambda B_0 - 2\mu B_1)}{\sqrt{2b_2\kappa(\zeta-\tau)\left(-4\kappa+\left(2\kappa^2-\lambda^2+4\mu\right)a_2\right)}},$$

$$A_1 = -\frac{\sqrt{3b_1 b_2}\left(\left(B_0^2-\mu B_1^2\right)+\sqrt{b_1}b_2\left(B_0^2-\lambda B_0 B_1+\mu B_1^2\right)\right)}{\left(2\kappa(\zeta-\tau)\left(-4\kappa+\left(2\kappa^2-\lambda^2+4\mu\right)a_2\right)\right)^{1/2}B_0},$$

$$A_2 = 0,$$

$$a_1 = \frac{2\mu\sqrt{b_1}\sqrt{\kappa(\zeta-\tau)\left(-4\kappa+\left(2\kappa^2-\lambda^2+4\mu\right)a_2\right)b_2}(a_2+2\kappa b_2)\sqrt{\left(\kappa(\zeta-\tau)\left(-4\kappa+\left(2\kappa^2-\lambda^2+4\mu\right)a_2\right)b_2\right)^2 b_1(\lambda B_0-2\mu B_1)^2\left(B_0^2-\lambda B_0 B_1+\mu B_1^2\right)^2+\left(\kappa(\zeta-\tau)\left(-4\kappa+\left(2\kappa^2-\lambda^2+4\mu\right)a_2\right)b_1 b_2\right)(\lambda B_0-2\mu B_1)\left(\begin{array}{c}\left(-4\kappa+a_2\left(2(5\kappa^2+\mu)+\kappa a_2\left(-8\kappa^2+2\lambda^2-8\mu+\kappa\left(2\kappa^2-\lambda^2+4\mu\right)a_2\right)\right)+\right)B_0^2-2\lambda\mu(a_2+2\kappa b_2)B_0 B_1+\\ +\kappa\left(-4\kappa^2+2\lambda^2-4\mu+\kappa\left(2\kappa^2-\lambda^2+4\mu\right)a_2\right)b_2\\ +2\mu^2(a_2+2\kappa b_2)B_1^2\end{array}\right)}{\left(\kappa^2(\zeta-\tau)(-2+\kappa a_2)\left(-4\kappa+\left(2\kappa^2-\lambda^2+4\mu\right)a_2\right)^2 b_2^2 B_0^2(\lambda B_0-2\mu B_1)\right)}. \tag{36}$$

Let us investigate the wave solutions of the following family of solutions according to another set of coefficients obtained by solving the system of algebraic equations.

Family 1. If $\mu \neq 0$ and $\lambda^2 - 4\mu > 0$, then

$$u_{2,1}(x,t) = \frac{\Theta_2\mu(2B_0-\lambda B_1)+\Theta_1(\lambda B_0-2\mu B_1)\left(\lambda+\sqrt{\lambda^2-4\mu}\tanh\left[\left(\sqrt{\lambda^2-4\mu}/2\right)(\eta+E)\right]\right)}{2\mu B_1 - B_0\left(\lambda+\sqrt{\lambda^2-4\mu}\tanh\left[\left(\sqrt{\lambda^2-4\mu}/2\right)(\eta+E)\right]\right)} \times e^{i\left(-\kappa x+\left(\left(2\kappa^2 b_1 b_2+2\kappa a_1 b_2-\kappa a_2 b_1+b_1\right)/(\beta b_2(2\kappa b_2+a_2))\right)(t+(1/(\Gamma(\beta))))^{\beta}+\wp\right)}, \tag{37}$$

where $\eta = x - (b_1/\beta b_2)(t + (1/(\Gamma(\beta))))^{\beta}$, $\Theta_1 = \sqrt{3b_1/(2b_2\kappa(\zeta-\tau)(-4\kappa + (2\kappa^2 - \lambda^2 + 4\mu)a_2))}$, and $\Theta_2 = \sqrt{6b_1/(b_2\kappa(\zeta-\tau)(-4\kappa + (2\kappa^2 - \lambda^2 + 4\mu)a_2))}$.

Family 2. If $\mu \neq 0$ and $\lambda^2 - 4\mu < 0$, then

$$u_{2,2}(x,t) = \frac{\left(\Theta_1 - \Theta_2\mu\left(B_0^2 - \mu B_1^2\right) + \left(B_0^2 - \lambda B_0 B_1 + \mu B_1^2\right)\right)}{B_0(\lambda B_0 - 2\mu B_1)\left(-\lambda + \sqrt{-\lambda^2 + 4\mu}\tan\left[\left(\sqrt{-\lambda^2 + 4\mu}/2\right)\left(x - (b_1/\beta b_2)(t + (1/(\Gamma(\beta))))^{\beta} + E\right)\right]\right)} \times e^{i\left(-\kappa x + \left(\left(2\kappa^2 b_1 b_2 + 2\kappa a_1 b_2 - \kappa a_2 b_1 + b_1\right)/(\beta b_2(2\kappa b_2 + a_2))\right)(t + (1/(\Gamma(\beta))))^{\beta} + \varphi\right)}, \tag{38}$$

where $\Theta_1 = \sqrt{3b_1/(2b_2\kappa(\zeta-\tau)(-4\kappa + (2\kappa^2 - \lambda^2 + 4\mu)a_2))}$ and $\Theta_2 = \sqrt{6b_1/(b_2\kappa(\zeta-\tau)(-4\kappa + (2\kappa^2 - \lambda^2 + 4\mu)a_2))}$.

Family 3. If $\mu = 0$, $\lambda \neq 0$, and $\lambda^2 - 4\mu > 0$, then

$$u_{2,3}(x,t) = \frac{\Theta_1\lambda\left(B_0 - \lambda B_1 + B_0 e^{\lambda\left(x - (b_1/\beta b_2)(t + (1/(\Gamma(\beta))))^{\beta} + E\right)}\right)}{-B_0 + \lambda B_1 + B_0 e^{\lambda\left(x - (b_1/\beta b_2)(t + (1/(\Gamma(\beta))))^{\beta} + E\right)}} e^{i\left(-\kappa x + \left(\left(2\kappa^2 b_1 b_2 + 2\kappa a_1 b_2 - \kappa a_2 b_1 + b_1\right)/(\beta b_2(2\kappa b_2 + a_2))\right)(t + (1/(\Gamma(\beta))))^{\beta} + \varphi\right)}. \tag{39}$$

Family 4. If $\mu \neq 0$, $\lambda \neq 0$, and $\lambda^2 - 4\mu = 0$, then

$$u_{2,4}(x,t) = \Theta_1\left(\begin{array}{c} -\lambda^2\left(B_0^2 - \lambda B_0 + \mu B_1^2\right)\left((E+x)\beta b_2 - b_1\left(t + \dfrac{1}{\Gamma(\beta)}\right)^{\beta}\right) + \\ + \left(\begin{array}{c} i\beta b_2\left(\begin{array}{c} \lambda(4 + (E+x)\lambda)B_0^2 - 4(2 + (E+x)\lambda)\mu B_0 B_1 + \\ +(E+x)\lambda^2\mu B_1^2 \end{array}\right) - \\ -\lambda b_1\left(\lambda B_0^2 - 4\mu B_0 B_1 + \lambda\mu B_1^2\left(t + \dfrac{1}{\Gamma(\beta)}\right)^{\beta}\right) \end{array}\right) \end{array}\right) \times e^{i\left(-\kappa x + \left(\left(2\kappa^2 b_1 b_2 + 2\kappa a_1 b_2 - \kappa a_2 b_1 + b_1\right)/(\beta b_2(2\kappa b_2 + a_2))\right)(t + (1/(\Gamma(\beta))))^{\beta} + \varphi\right)}. \tag{40}$$

Family 5. If $\mu = 0$, $\lambda = 0$, and $\lambda^2 - 4\mu = 0$, then

$$u_{2,5}(x,t) = \frac{\Theta_4 B_0 e^{i\left(-\kappa x + \left(\left(2\kappa^2 b_1 b_2 + 2\kappa a_1 b_2 - \kappa a_2 b_1 + b_1\right)/(\beta b_2(2\kappa b_2 + a_2))\right)(t + (1/(\Gamma(\beta))))^{\beta} + \varphi\right)}}{b_2\left(B_1 + B_0\left(x - (b_1/\beta b_2)(t + (1/(\Gamma(\beta))))^{\beta} + E\right)\right)}, \tag{41}$$

where $a_1 = (b_1((-1 + \kappa a_2)^2 + \kappa^2 b_2))/(\kappa(-2 + \kappa a_2)b_2)$ and $\Theta_4 = \sqrt{3b_1 b_2/(\kappa^2(\zeta-\tau)(-2 + \kappa a_2))}$.

5. Conclusions

In this study, an effective technique, the modified exponential function method for the Biswas-Arshed equation with the beta time derivative, was applied. It can be said that this method is an advantageous technique for obtaining wave solutions of nonlinear partial differential equations. This advantage can be explained as follows. The traveling wave solutions of the mathematical model contain periodic functions. By obtaining these functions, the behavior model obtained in a range can be generalized to an infinite range. In this study, a package program was used for all mathematical operations and graphics that simulate the behavior of the mathematical model and for all the operations related to showing that solution functions provide the mathematical model. Using the method, two case situations consisting of coefficients were analyzed. According to these situations, hyperbolic, trigonometric, and rational solution functions

belonging to the mathematical model were obtained. In addition, in the second case, the solution functions belonging to the mathematical model were obtained in a complex form. For this reason, while determining the graphs simulating the behaviors, they were examined separately as real and imaginary parts in Figures 1–10. When all these results are analyzed, it is concluded that obtaining periodic solution functions is of great importance, because such functions will allow to make comments about a desired range.

Data Availability

No data were used to support this study.

Conflicts of Interest

The authors declare that they have no competing interests.

Authors' Contributions

All authors read and approved the final manuscript.

References

[1] J. Yang, A. Liu, and T. Liu, "Forced oscillation of nonlinear fractional differential equations with damping term," *Advances in Difference Equations*, vol. 2015, no. 1, p. 17, 2015.

[2] C. S. Liu, "A new trial equation method and its applications," *Communications in Theoretical Physics*, vol. 45, no. 3, pp. 395–397, 2006.

[3] Y. Pandir, Y. Gurefe, and E. Misirli, "The extended trial equation method for some time fractional differential equations," *Discrete Dynamics in Nature and Society*, vol. 2013, Article ID 491359, 13 pages, 2013.

[4] M. A. Akbar, N. H. M. Ali, and E. M. E. Zayed, "Abundant exact traveling wave solutions of generalized Bretherton equation via improved (G'/G)-expansion method," *Communications in Theoretical Physics*, vol. 57, no. 2, pp. 173–178, 2012.

[5] A. Akbulut, M. Kaplan, and F. Tascan, "Conservation laws and exact solutions of Phi-four (Phi-4) equation via the (G'/G, 1/G)-expansion method," *Zeitschrift für Naturforschung A*, vol. 71, no. 5, pp. 439–446, 2016.

[6] M. A. Abdou, "The extended tanh method and its applications for solving nonlinear physical models," *Applied Mathematics and Computation*, vol. 190, no. 1, pp. 988–996, 2007.

[7] P. N. Ryabov, D. I. Sinelshchikov, and M. B. Kochanov, "Application of the Kudryashov method for finding exact solutions of the high order nonlinear evolution equations," *Applied Mathematics and Computation*, vol. 218, no. 7, pp. 3965–3972, 2011.

[8] M. Kaplan, A. Bekir, and A. Akbulut, "A generalized Kudryashov method to some nonlinear evolution equations in mathematical physics," *Nonlinear Dynamics*, vol. 85, no. 4, pp. 2843–2850, 2016.

[9] S. T. Demiray, Y. Pandir, and H. Bulut, "Generalized Kudryashov method for time-fractional differential equations," *Abstract and Applied Analysis*, vol. 2014, Article ID 901540, 13 pages, 2014.

[10] T. Akturk, Y. Gurefe, and Y. Pandir, "An application of the new function method to the Zhiber-Shabat equation," *An International Journal of Optimization and Control: Theories & Applications (IJOCTA)*, vol. 7, no. 3, pp. 271–274, 2017.

[11] B. Elma and E. Misirli, "Two reliable techniques for solving conformable space-time fractional PHI-4 model arising in nuclear physics via β-derivative," *Revista Mexicana de Física*, vol. 67, no. 5, article 050707, 2021.

[12] H. Yépez-Martínez, J. F. Gómez-Aguilar, and A. Atangana, "First integral method for non-linear differential equations with conformable derivative," *Mathematical Modelling of Natural Phenomena*, vol. 13, no. 1, p. 22, 2018.

[13] A. Arikoglu and I. Ozkol, "Solution of fractional differential equations by using differential transform method," *Chaos, Solitons & Fractals*, vol. 34, no. 5, pp. 1473–1481, 2007.

[14] B. Batiha, M. S. M. Noorani, and I. Hashim, "Numerical solution of sine-Gordon equation by variational iteration method," *Physics Letters A*, vol. 370, no. 5-6, pp. 437–440, 2007.

[15] A. Bekir, Ö. Güner, and A. C. Cevikel, "Fractional complex transform and exp-function methods for fractional differential equations," *Abstract and Applied Analysis*, vol. 2013, Article ID 426462, 8 pages, 2013.

[16] A. Akbulut, M. Kaplan, and F. Tascan, "The investigation of exact solutions of nonlinear partial differential equations by using exp$(-\Phi(\xi))$ method," *Optik*, vol. 132, pp. 382–387, 2017.

[17] N. T. Shawagfeh, "Analytical approximate solutions for nonlinear fractional differential equations," *Applied Mathematics and Computation*, vol. 131, no. 2-3, pp. 517–529, 2002.

[18] K. Diethelm and N. J. Ford, "Analysis of fractional differential equations," *Journal of Mathematical Analysis and Applications*, vol. 265, no. 2, pp. 229–248, 2002.

[19] P. Kumar and O. P. Agrawal, "An approximate method for numerical solution of fractional differential equations," *Signal Processing*, vol. 86, no. 10, pp. 2602–2610, 2006.

[20] N. J. Ford and A. C. Simpson, "The numerical solution of fractional differential equations: speed versus accuracy," *Numerical Algorithms*, vol. 26, no. 4, pp. 333–346, 2001.

[21] A. Atangana and A. Akgul, "On solutions of fractal fractional differential equations," *Discrete & Continuous Dynamical Systems-S*, vol. 14, no. 10, pp. 3441–3457, 2021.

[22] D. Baleanu, O. G. Mustafa, and R. P. Agarwal, "On the solution set for a class of sequential fractional differential equations," *Journal of Physics A: Mathematical and Theoretical*, vol. 43, no. 38, article 385209, 2010.

[23] M. I. Syam and M. Al-Refai, "Fractional differential equations with Atangana-Baleanu fractional derivative: analysis and applications," *Chaos, Solitons & Fractals*, vol. 2, article 100013, 2019.

[24] A. Atangana and I. Koca, "Chaos in a simple nonlinear system with Atangana-Baleanu derivatives with fractional order," *Chaos, Solitons & Fractals*, vol. 89, pp. 447–454, 2016.

[25] N. Gurefe, E. G. Kocer, and Y. Gurefe, "Chebyshev-tau method for the linear Klein-Gordon equation," *International Journal of Physical Sciences*, vol. 7, no. 43, pp. 5723–5728, 2012.

[26] T. Abdeljawad, "On conformable fractional calculus," *Journal of Computational and Applied Mathematics*, vol. 279, pp. 57–66, 2015.

[27] Y. Pandir, Y. Gurefe, and T. Akturk, "New soliton solutions of the nonlinear Radhakrishnan-Kundu-Lakshmanan equation with the beta-derivative," *Optical and Quantum Electronics*, vol. 54, no. 4, pp. 1–21, 2022.

[28] Y. Gurefe, Y. Pandir, and T. Akturk, "On the nonlinear mathematical model representing the Coriolis effect," *Mathematical*

Problems in Engineering, vol. 2022, Article ID 2504907, 12 pages, 2022.

[29] Y. Pandir and H. H. Duzgun, "New exact solutions of the space-time fractional cubic Schrodinger equation using the new type F-expansion method," *Waves in Random and Complex Media*, vol. 29, no. 3, pp. 425–434, 2019.

[30] R. Khalil, M. Al Horani, A. Yousef, and M. Sababheh, "A new definition of fractional derivative," *Journal of Computational and Applied Mathematics*, vol. 264, pp. 65–70, 2014.

[31] A. Atangana, D. Baleanu, and A. Alsaedi, "New properties of conformable derivative," *Open Mathematics*, vol. 13, no. 1, pp. 889–898, 2015.

[32] K. Hosseini, M. Mirzazadeh, M. Ilie, and J. F. Gómez-Aguilar, "Biswas-Arshed equation with the beta time derivative: optical solitons and other solutions," *Optik-International Journal for Light and Electron Optics*, vol. 217, article 164801, 2020.

[33] T. Han, Z. Li, and J. Yuan, "Optical solitons and single traveling wave solutions of Biswas-Arshed equation in birefringent fibers with the beta-time derivative," *AIMS-Mathematics*, vol. 7, no. 8, pp. 15282–15297, 2022.

Hindawi
Advances in Mathematical Physics
Volume 2022, Article ID 1725110, 10 pages
https://doi.org/10.1155/2022/1725110

Research Article

$\mathscr{ABC}$ Fractional Derivative for Varicella-Zoster Virus Using Two-Scale Fractal Dimension Approach with Vaccination

Jirong Yang,[1] Farkhanda Afzal,[2] and Perpetual Appiah[3]

[1]*Shaanxi University of Chinese Medicine, Xianyang, Shaanxi 712046, China*
[2]*MCS, National University of Sciences and Technology, Islamabad, Pakistan*
[3]*Department of Mathematics, University of Cape Coast, Ghana*

Correspondence should be addressed to Perpetual Appiah; perpetual.appiah@stu.ucc.edu.gh

Received 26 August 2022; Revised 6 September 2022; Accepted 19 September 2022; Published 14 October 2022

Academic Editor: Muhammad Nadeem

Chickenpox or varicella is an infectious disease caused by the varicella-zoster virus ($\mathscr{VZV}$). This virus is the cause of chickenpox (usually a primary infection in the nonimmune host) and herpes zoster. In this paper, a compartmental model for the dynamics of $\mathscr{VZ}$ transmission with the effect of vaccination is solved using the $\mathscr{ABC}$ fractional derivative. The possibility of using the fractal dimension as a biomarker to identify different diseases is being investigated. The problem is investigated in two different levels of research using two scale dimensions. To ascertain the existence and uniqueness of the solution, we qualitatively evaluate the model. We have used the Euler method to compute the numerical solution for the system. At the end, we provide the graphical results showing the effectiveness of two-scale dimension and fractional calculus in the current model.

1. Introduction

Chickenpox, or varicella, is caused by the varicella-zoster virus($\mathscr{VZV}$), a globally distributed herpes virus [1]. Chickenpox occurs in all countries, killing about 7,000 people annually. This is a common illness in children in temperate countries, ten with them. [2, 3]. The itchy blister rash caused by a chickenpox infection appears for 10 to 21 days and usually lasts about 5 to 10 days. Other signs and symptoms that may appear 1-2 days before the rash appears are fever, decreased appetite, headache, and general malaise. Chickenpox spreads from one individual to another by direct contact with the blisters, saliva, or mucus of an infected individual. The virus can also spread in the air by coughing or sneezing. There are different theories about the origin of the name of this disease. After infection, the skin appeared to have been picked out from the chicken. Another reason is that the rash mimics chickpea seeds. The most usual interpretation is that the disease is a type of "chickenpox" because it is not as severe as smallpox. Chickenpox occurs differently depending on the geographical area. Anyhow, the occurrence of chickenpox in these regions increased between adolescents and adults [4], which may in part be due to an increase in global tourism and economic migration. In most tropical areas, situation is changed, with 60 percent of the immunized adult population [5]. Previously, the said virus infects almost the whole population, causing significant morbidity and mortality from both primary varicella zoster and reactivation of herpes zoster. The first approved vaccine for varicella was used in 1995 reducing the severity, morbidity, and mortality rate significantly. In 2006, due to the outbreak of illness caused by a single vaccination schedule, the children were recommended to receive their second dose vaccination series. The innovation of the shingles vaccine has also benefited the elders. For those over 60, the Food and Drug Administration approved the use of a shingles vaccination in 2006 that contained high amounts of the primary varicella vaccine's live attenuated vaccine. Millions of individuals could help prevent the disease caused by the varicella-zoster virus by lowering the prevalence and mortality of shingles and postherpetic neuralgia.

Compared to integer-order calculus, many real-world problems can be better explained when using fractional operators. Fractional calculus is recognized as a promising

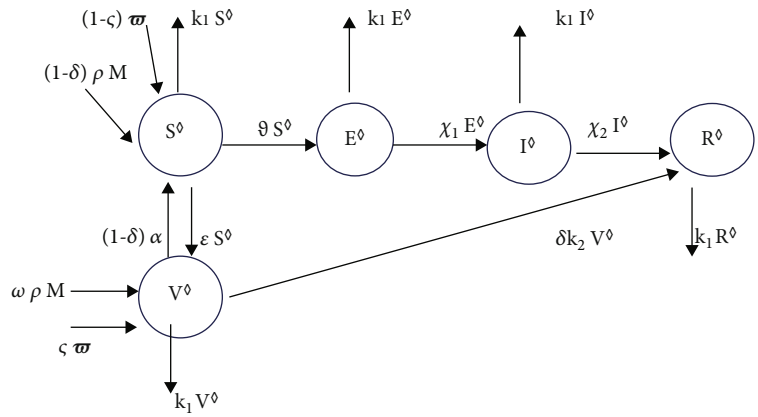

Figure 1: Flow diagram of VZV.

mathematical tool for efficiently characterizing historical memories and global correlations of complex dynamical systems, phenomena, or structures. Fractional-order PDEs dominate the majority of models of physical fluid dynamics events, electricity, ecological structure, quantum physics, and many others. Understanding positive integer order derivatives and integrals are of great importance for the development of modern theoretical and practical problems of science. Properties of integral, differential operators, and mathematical functions are as follows: gamma, beta, and other special functions where the integral takes the form of convolution, and there are singularities are useful.

Development of fractal theory was formulated by Mandelbrot. The second half of the 20th century generally integrated the work of many other early mathematicians and scientists, opening a new perspective on this goal. Since then, several attempts have been made to interpret the relationship between fractional operators and this new geometry. As the dynamic foundations of fractional calculus and fractal dimensions, fractal theory and FDE theory are rapidly gaining popularity as disciplines around the world.

Physical memory and heredity are clearly defined by fractions. Special functions, elliptic integrals, and elliptic functions are used in various physical systems. Their inclusion in solving nonlinear differential equations is well known. You can examine these functions and integrals using the references. Fractional differential operators are becoming robust, and systematic mathematical tools for studying various scientific and biological events nowadays, for example, childhood disease [14, 16], HIV, coronary heart disease [15], hepatitis C [17], Chikungunya virus [18], and Crimean-Congo hemorrhagic fever (CCHF) [19], can be seen in the references. Fractional-order differential equations, in contrast to integer-order differential equations, can show nonlocal interactions with memory cores in time and space [6, 7].

1.1. Motivation. The complexity, validity, implementation, prevention, therapy, and control strategies of mathematical models have been improving. Following the research, the entire population is divided into three categories: susceptible, infectious, and eliminated with lifelong acquired immunity. This approach is known as the SIR model. In real life situations after a time, in the infectious compartment, the individuals, recovered or removed individuals, lose immunity and return to the susceptible compartment. These models are known as SIRS models. Following the same assumptions, the model 2 can be written in the following form [13].

$$\begin{aligned}
\frac{d\mathcal{S}^{\circ}}{dt} &= (1-\omega)\rho M + (1-\varsigma)\varpi + (1-\delta)\alpha\mathcal{V}^{\circ} - (\vartheta + \kappa_1 + \epsilon)\mathcal{S}^{\circ},\\
\frac{d\mathcal{V}^{\circ}}{dt} &= \omega\rho M + \varsigma\varpi + \kappa_1\mathcal{S}^{\circ} - ((1-\delta)\alpha + \delta\kappa_2 + \epsilon))\mathcal{V}^{\circ},\\
\frac{d\mathcal{E}^{\circ}}{dt} &= \vartheta\mathcal{S}^{\circ} - (\chi_1 + \epsilon)\mathcal{E}^{\circ},\\
\frac{dI^{\circ}}{dt} &= \chi_1\mathcal{E}^{\circ} - (\chi_2 + \epsilon)\mathcal{I}^{\circ},\\
\frac{d\mathcal{R}^{\circ}}{dt} &= \chi_2\mathcal{I}^{\circ} + (\delta\kappa_2)\mathcal{V}^{\circ} - \epsilon\mathcal{R}^{\circ}.
\end{aligned} \tag{1}$$

Figure 1 shows the block diagram of the model under consideration. It can be seen that susceptible vaccinated classes have direct relationship. And engineering and science fields like biotechnology, medicine, biological processes, artificial intelligence, and space sciences all make extensive use of mathematical modeling of physical systems. Scientists, engineers, and mathematicians are turning to the broad field of mathematical modeling to solve the numerous issues they face. We take into account the Atangana-Baleanu fractional operator in the sense of Caputo to investigate the fractional dynamics of a model under consideration. The utilization of the Atangana-Baleanu partial derivatives is based on their nonlocal characteristics. This operator is better for capturing complex behaviors. Table 1 gives definitions of variables.

2. Contribution and Novelty

Mathematical methods are based on the application of some basic principles of fractional differentiation and first-order

Table 1: Variables' definitions.

Variables & Parameters	Interpretation
$\mathcal{S}^{\circ}(t)$	Susceptible individuals
$\mathcal{V}^{\circ}(t)$	Vaccinated individuals
$\mathcal{E}^{\circ}(t)$	Exposed individuals
$I^{\circ}(t)$	Infected individuals
$R^{\circ}(t)$	Recovered individuals
ρ	Per capita birth rate
κ_1	Natural mortality rate
$\chi 2$	Rate has permanent immunity after recovery
ϖ	Consistent recruitment rate
ς	Vaccinated recruit
ω	Vaccinated infants
ϑ	Rate of first-dose vaccine received by susceptible individuals

interpolation. An analysis is conducted on the existence and uniqueness of the model. According to the interesting attractors obtained in this study, these new fractal-fractional operators may be able to explain new elements of the behavior of these systems rather than fractional derivatives. Some of these properties go beyond the traditional integer-order operators. It is trendy to examine the real life problems using fractional approaches because the fractional derivative covers a broad spectrum of variables as compared to integer order derivatives. Two-scale dimension is a new approach for dealing with the problems involving more than one scale of observation. This paper combines the benefits of fractional derivative and $_{85}$ efficacy of two-scale dimension to study a wide spread virus model [24].

This study differs from previous studies on schemes due to the involved new formulation of a two-scale fractal fractional derivative. Atangana and his colleagues first published some of these new derivative theories in 2017. They combine the concepts of fractional and fractal derivatives, taking into account nonlocality, memory, and fractal effects. This model takes into account processes such as power law, fading memory, and crossovers. Note that this article uses a significantly different numerical approach and analysis than [13], which describes the integer ordering problem. It has been shown that the two-scale fractal dimension has a significant impact on the dynamics of the system.

$$
\begin{aligned}
&{}_0^{\mathcal{HBC}}\mathcal{D}_t^{\nu}\mathcal{S}^{\circ} = (1-\omega)\rho M + (1-\varsigma)\varpi + (1-\delta)\alpha\mathcal{V}^{\circ} - (\vartheta+\kappa_1+\epsilon)\mathcal{S}^{\circ},\\
&{}_0^{\mathcal{ABC}}\mathcal{D}_t^{\nu}\mathcal{V}^{\circ} = \omega\rho M + \varsigma\varpi + \kappa_1\mathcal{S}^{\circ} - \left((1-\delta)\alpha + \delta\kappa_2 + \kappa_1\right)\Big)\mathcal{V}^{\circ},\\
&{}_0^{\mathcal{ABC}}\mathcal{D}_t^{\nu}\mathcal{E}^{\circ} = \vartheta\mathcal{S}^{\circ} - (\chi_1+\kappa_1)\mathcal{E}^{\circ},\\
&{}_0^{\mathcal{ABC}}\mathcal{D}_t^{\nu}\mathcal{I}^{\circ} = \chi_1\mathcal{E}^{\circ} - (\chi_2+\kappa_1)I^{\circ},\\
&{}_0^{\mathcal{ABC}}\mathcal{D}_t^{\nu}\mathcal{R}^{\circ} = \chi_2 I^{\circ} + (\delta\kappa_2)\mathcal{V}^{\circ} - \kappa_1\mathcal{R}^{\circ}.
\end{aligned}
\tag{2}
$$

Definition 1. Let ς be a function which is continuous in the domain (a, b) with $\nu \in (0, 1]$. The $\mathcal{ABC}$ fractional derivative is defined as [8]

$$
{}_0^{\mathcal{ABC}}\mathcal{D}_t^{\nu}\varsigma(t) = \frac{\mathcal{M}(\nu)}{1-\nu}\frac{d}{dt}\int_0^t \varsigma(\zeta)E_{\nu}\left[\frac{-\nu}{1-\nu}(t-\zeta)^{\nu}\right]d\zeta. \tag{3}
$$

The normalization constant $\mathcal{M}(\nu)$ gives $\mathcal{M}(0) = \mathcal{M}(1) = 1$.

Definition 2. The fractional integral related with the fractional derivative is given as [8, 9]

$$
{}_0^{\mathcal{ABC}}I_t^{\nu}S(t) = \frac{1-\nu}{\mathcal{M}(\nu)}\varsigma(t) + \frac{\nu}{\mathcal{M}(\nu)\Gamma(\nu)}\int_0^t \left[(t-\zeta)^{\nu-1}\right]\varsigma(\zeta)d\zeta. \tag{4}
$$

2.1. $\mathcal{ABC}$ Fractional Order Model for $\mathcal{VEV}$. Over the last few decades, some researchers and scientists have emphasized fractional calculus and have shown that it is a better tool to study natural events by fractional order than the integer order. Fractional calculus supported the popularity and benefits of fractal modeling. This section explains the adoption of the numerical method for Atangana-Baleanu's fractional differential operator [23]. The iterative expression obtains via $\mathcal{ABC}$ fractional model to Eq. (2) as follows:

$$
\begin{aligned}
\mathcal{S}^{\circ}(t) - \mathcal{S}^{\circ}(0) = {}& \frac{1-\nu}{\mathcal{M}(\nu)}\left[(1-\omega)\rho M + (1-\varsigma)\varpi + (1-\delta)\alpha\mathcal{V}^{\circ}\right.\\
&\left. - (\vartheta+\kappa_1+\epsilon)\mathcal{S}^{\circ}\right] + \frac{\nu}{\mathcal{M}(\nu)\Gamma(\nu)}\\
&\cdot\int_0^t \left[(t-\zeta)^{\nu-1}\right]\left[(1-\omega)\rho M + (1-\varsigma)\varpi\right.\\
&\left. + (1-\delta)\alpha\mathcal{V}^{\circ} - (\vartheta+\kappa_1+\epsilon)\mathcal{S}^{\circ}\right]d\zeta.
\end{aligned}
\tag{5}
$$

For simplification, we write

$$
\begin{aligned}
\Theta_1(t, \mathcal{S}^{\circ}) = {}& (1-\omega)\rho M + (1-\varsigma)\varpi + (1-\delta)\alpha\mathcal{V}^{\circ}\\
&- (\vartheta+\kappa_1+\epsilon)\mathcal{S}^{\circ}.
\end{aligned}
\tag{6}
$$

3. Two-Scale Dimension

Mathematics plays a vital role in the science of measurement. Mathematical models are needed to recognize how powerful dimensional systems are structured and to investigate the results they produce. How about measuring a coastline? In this example, the concept of length is not applicable. Land mass features exist on multiple scales, but there is no clear scale of minimum features to consider when measuring. The smooth and idealized length of the metal rod can be precisely measured with the help of measuring instrument to determine whether the length is less than one value and greater than the other. The accuracy of the true value depends on the accuracy of the instrument. However, improving the measuring instrument does not improve the accuracy of coastline surveying. As with metal rods, there

is no way to give a specific value to the length of the coastline.

The coastline problem applies to the idea of a fractal surface in $3D$ space where the area of the surface changes with the measurement scale. Many laws of physics are scale-dependent and give scale-dependent results. In these systems, behavior is "scale dependent" and can be assumed to be accompanied by drastic changes in behavior associated with an exclusive regime. Einstein's theory of relativity made researchers believed that applying the theory of relativity to a similar scale could account for the usage of scale dependence in practical problems, see [10] to study the details of the two-scale transformation.

$$\Delta S = \frac{\Delta t^{\nu}}{\Gamma(1+\nu)}, \tag{7}$$

where ΔS is the smaller scale, Δt is the larger scale, and ν is two-scale dimension. Two scales provide a logical explanation in terms of existing fractal calculus theories. This is a modern concept that emphasizes the importance of scale in the examination of practical problem [20, 21]. In [11, 12], the work presented was the source of our motivation. As an illustration of the concepts presented in the aforementioned articles, we will present our own work.

Theorem 3. *Θ_1 fulfills the Lipschitz condition and contraction if the following inequality holds:*

$$0 \le (\vartheta + \kappa_1 + \epsilon) < 1. \tag{8}$$

Proof. Let $a = (\vartheta + \kappa_1 + \epsilon)$. For $S^{\diamond}$, we have

$$\begin{aligned}\Theta_1(t, S^{\circ}) - \Theta_1(t, S_1^{\circ}) &= -(\vartheta + \kappa_1 + \epsilon)(\mathcal{S}^{\circ} - S_1^{\circ}(t)) \\ &\le (\vartheta + \kappa_1 + \epsilon)(\mathcal{S}^{\circ} - S_1^{\circ}(t)).\end{aligned} \tag{9}$$

□

We get the following result:

$$\Theta_1(t, S^{\circ}) - \Theta_1(t, S_1^{\diamond}) \le a(\mathcal{S}^{\circ}(t) - \mathcal{S}_1^{\diamond}(t)). \tag{10}$$

Consequently, for Θ_1, the Lipschitz condition is achieved. Likewise, the Lipschitz condition for Θ_i for $i = 2, \cdots, 5$ also holds.

With the help of above concept, one can write

$$\begin{aligned}\mathcal{S}^{\circ}(t) = \mathcal{S}^{\circ}(0) &+ \frac{1-\nu}{\mathcal{M}(\nu)}\Theta_1(t, \mathcal{S}^{\circ}) \\ &+ \frac{\nu}{\mathcal{M}(\nu)\Gamma(\nu)}\int_0^t \left[(t-\zeta)^{\nu-1}\right]\Theta_1(t, S^{\circ})d\zeta.\end{aligned} \tag{11}$$

We can write the above formula as

$$\begin{aligned}\mathcal{S}_n^{\circ}(t) = \mathcal{S}^{\circ}(0) &+ \frac{1-\nu}{\mathcal{M}(\nu)}\Theta_1(t, \mathcal{S}_{n-1}^{\circ}) \\ &+ \frac{\nu}{\mathcal{M}(\nu)\Gamma(\nu)}\int_0^t \left[(t-\zeta)^{\nu-1}\right]\Theta_1(t, S_{n-1}^{\circ})d\zeta.\end{aligned} \tag{12}$$

$S(0) = S_0^{\diamond}$ is an initial condition, and the terms following in order of difference are defined as follows:

$$\begin{aligned}\Lambda_n = S_n^{\circ}(t) - S_{n-1}^{\circ}(t) &= \frac{1-\nu}{\mathcal{M}(\nu)}(\Theta_1(t, S_{n-1}^{\circ}) - \Theta_1(t, S_{n-2}^{\diamond})) \\ &+ \frac{\nu}{\mathcal{M}(\nu)\Gamma(\nu)}\int_0^t \left[(t-\zeta)^{\nu-1}\right](\Theta_1(t, S_{n-1}^{\circ}) - \Theta_1(t, \mathcal{S}_{n-2}^{\circ}))d\zeta.\end{aligned} \tag{13}$$

We get

$$\mathcal{S}_n^{\diamond}(t) = \sum_{i=0}^{n} \Lambda_{1i}(t). \tag{14}$$

Also, we define

$$S_{1_{-1}}^{\diamond}(0) = 0. \tag{15}$$

As a result, we get

$$\Lambda_n \le \frac{1-\nu}{\mathcal{M}(\nu)}\beta_1\Lambda_n + \frac{\beta_1\nu}{\mathcal{M}(\nu)\Gamma(\nu)}\int_0^t \Lambda_{1_{n-1}}(\zeta)(t-\zeta)^{\nu-1}d\zeta, \tag{16}$$

where $(\beta_1, \beta_2, \beta_3, \cdots, \beta_5) \in (0, 1)^5$. The existence of the solution is assured by using these results.

Theorem 4. *If there exists τ_0 in the considered model, then its solution exists such that*

$$\frac{1-\nu}{\mathcal{M}(\nu)}\beta_1 + \frac{\tau_0^{\nu}\beta_1}{\mathcal{M}(\nu)\Gamma(\nu)} < 1. \tag{17}$$

Proof. Let us suppose that the bounded functions exist in the considered system; so, one can obtain

$$\Lambda_n \le S^{\circ}(0)\left[\frac{1-\nu}{\mathcal{M}(\nu)}\beta_1 + \frac{\tau_0^{\nu}\beta_1}{\mathcal{M}(\nu)\Gamma(\nu)}\right]^n. \tag{18}$$

To express (13) as a solution of (22), we assume that

$$\mathcal{S}^{\circ}(t) - \mathcal{S}^{\circ}(0) = \mathcal{S}_n^{\circ}(t) - U_{1_n}(0). \tag{19}$$

We conclude

$$U_{1_n} \le \left[\frac{1-\nu}{\mathcal{M}(\nu)} + \frac{\tau^{\nu}}{\mathcal{M}(\nu)\Gamma(\nu)}\right]^{n-1}\beta_1^{n-1}, \tag{20}$$

for $\tau = \tau_0$.

$$U_{1_n} \leq \left[\frac{1-\nu}{\mathscr{M}(\nu)} + \frac{\tau_0^{\nu}}{\mathscr{M}(\nu)\Gamma(\nu)}\right]^{n-1} \beta_1^{n-1}. \tag{21}$$

By applying limit, we have

$$U_{1_n}(t) \longrightarrow \infty. \tag{22}$$

By following the same process, we get

$$U_{i_n}(t) \longrightarrow \infty, \tag{23}$$

for $i = 1, 2, \cdots, 5$. □

Theorem 5. *The considered model has a unique solution if*

$$\left[1 - \frac{1-\nu}{\mathscr{M}(\nu)}\beta_1 + \frac{\tau^{\nu}\beta_1}{\mathscr{M}(\nu)\Gamma(\nu)}\right] > 0. \tag{24}$$

4. Proof

We suppose that the model has another solution, that is, S

$$\begin{aligned}\mathscr{S}^{\circ}(t) - \mathscr{S}_1^{\circ}(t) = {} & \frac{1-\nu}{\mathscr{M}(\nu)}(\Theta_1(t, \mathscr{S}^{\circ} - \Theta_1(t, \mathscr{S}_1^{\circ})) \\ & + \frac{\nu}{\mathscr{M}(\nu)\Gamma(\nu)}\int_0^t \left[(t-\zeta)^{\nu-1}\right](\Theta_1(t, \mathscr{S}^{\circ}) \\ & - \Theta_1(t, \mathscr{S}_1^{\circ}))d\zeta.\end{aligned} \tag{25}$$

By the properties of norm, the following inequality is obtained:

$$\mathscr{S}^{\circ}(t) - \mathscr{S}_1^{\circ}(t)\left[1 - \frac{1-\nu}{\mathscr{M}(\nu)}\beta_1 + \frac{\tau^{\nu}\beta_1}{\mathscr{M}(\nu)\Gamma(\nu)}\right] \leq 0. \tag{26}$$

If condition of (19) is satisfied, then

$$\mathscr{S}^{\circ}(t) - \mathscr{S}_1^{\circ}(t) = 0. \tag{27}$$

Clearly, one can see that

$$\mathscr{S}^{\circ}(t) - \mathscr{S}_1^{\circ}(t). \tag{28}$$

For the other components of the model, one can follow the same pattern.

5. Problem Formulation

With the $\mathscr{ABC}$ fractional derivative, we assume the initial-value problem

$${}_0^{\mathscr{ABC}}D_{\tau}^{\nu}g(\tau) = f(\tau, g(\tau)). \tag{29}$$

$\mathscr{ABC}$-PIR ($\mathscr{BC}$ fractional product integral rule) is given in [24]:

$$g_j = g_0 + \frac{\nu h^{\nu}}{\mathscr{M}(\nu)}\left(\nu_j f(\tau_0, g_0) + \sum_{i=1}^{n} \xi_{j-i} f(\tau_i, g_i)\right), \tag{30}$$

where

$$\nu_j = \frac{(j-1)^{\nu+1} - j^{\nu}(j-\nu-1)}{\Gamma(\nu+2)}, \tag{31}$$

and ξ_k:

$$\begin{aligned}\xi_k &= \frac{1}{\Gamma(\nu+2)} + \frac{1-\nu}{\nu h h^{\nu}}, \text{for } k = 0, \\ \xi_k &= \frac{(k-1)^{\nu+1} - 2k^{\nu+1} + (k+1)^{\nu+1}}{\Gamma(\nu+2)}. \text{for } k = 1, 2, ,\cdots, j\text{-}1.\end{aligned} \tag{32}$$

By using Eq. (21), we get

$$\begin{aligned}\mathscr{S}_n^{\circ} = \mathscr{S}_0^{\circ} + {} & \frac{\nu h^{\nu}}{\mathscr{M}(\nu)}\left[a_j z_1(t_0, \mathscr{S}_0^{\circ}, \mathscr{V}_0^{\circ}, \mathscr{E}_0^{\circ}, \mathscr{I}_0^{\circ}, \mathscr{R}_0^{\circ},\right. \\ & \left. + \sum_{i=1}^{j} \xi_{j-i} z_1(t_i, \mathscr{S}_i^{\circ}, \mathscr{V}_i^{\circ}, \mathscr{E}_i^{\circ}, \mathscr{I}_i^{\circ}, \mathscr{R}_i^{\circ}\right].\end{aligned} \tag{33}$$

For the remaining equations, we adopt the same pattern as we did above, and we get

$$\begin{aligned}\mathscr{V}_n^{\circ} = {} & \mathscr{V}_0^{\circ} + \frac{\nu h^{\nu}}{\mathscr{M}(\nu)}\left[a_j z_2(t_0, \mathscr{S}_0^{\circ}, \mathscr{V}_0^{\circ}, \mathscr{E}_0^{\circ}, \mathscr{I}_0^{\circ}, \mathscr{R}_0^{\circ},\right. \\ & \left. + \sum_{i=1}^{j} \xi_{j-i} z_2(t_i, S_i^{\circ}, \mathscr{V}_i^{\circ}, \mathscr{E}_i^{\circ}, \mathscr{I}_i^{\circ}, \mathscr{R}_i^{\circ}\right], \\ \mathscr{E}_n^{\circ} = {} & \mathscr{E}_0^{\circ} + \frac{\nu h^{\nu}}{\mathscr{M}(\nu)}\left[a_j z_3(t_0, \mathscr{S}_0^{\circ}, \mathscr{V}_0^{\circ}, \mathscr{E}_0^{\circ}, \mathscr{I}_0^{\circ}, \mathscr{R}_0^{\circ},\right. \\ & \left. + \sum_{i=1}^{j} \xi_{j-i} z_3(t_i, \mathscr{S}_i^{\circ}, \mathscr{V}_i^{\circ}, \mathscr{E}_i^{\circ}, I_i^{\circ}, \mathscr{R}_i^{\circ}\right], \\ \mathscr{I}_n^{\circ} = {} & \mathscr{I}_0^{\circ} + \frac{\nu h^{\nu}}{\mathscr{M}(\nu)}\left[a_j z_4(t_0, \mathscr{S}_0^{\circ}, \mathscr{V}_0^{\circ}, \mathscr{E}_0^{\circ}, \mathscr{I}_0^{\circ}, \mathscr{R}_0^{\circ},\right. \\ & \left. + \sum_{i=1}^{j} \xi_{j-i} z_4(t_i, S_i^{\circ}, \mathscr{V}_i^{\circ}, \mathscr{E}_i^{\circ}, \mathscr{I}_i^{\circ}, \mathscr{R}_i^{\circ}\right], \\ \mathscr{R}_n^{\circ} = {} & \mathscr{R}_0^{\circ} + \frac{\nu h^{\nu}}{\mathscr{M}(\nu)}\left[a_j z_5(t_0, S_0^{\circ}, \mathscr{V}_0^{\circ}, \mathscr{E}_0^{\circ}, \mathscr{I}_0^{\circ}, \mathscr{R}_0^{\circ},\right. \\ & \left. + \sum_{i=1}^{j} \xi_{j-i} z_5(t_i, \mathscr{S}_i^{\circ}, \mathscr{V}_i^{\circ}, \mathscr{E}_i^{\circ}, \mathscr{I}_i^{\circ}, \mathscr{R}_i^{\circ}\right].\end{aligned} \tag{34}$$

6. Numerical Simulation

This study's primary goal was to evaluate how vaccination strategies affected the dynamics of disease transmission. Graphs are depicting the parametric variation with regard to various variables that are offered here to support the analytical conclusions. Since the majority of the parameters are not immediately available, it is deemed appropriate to estimate solely for the purpose of illustrative purposes to show how the model would react in various real-world scenarios as given in Table 2. The Euler method has been used for numerical simulation of the problem [22].

Figure 2 depicts simulations with various vaccination rates for neonates. As the outbreak develops later, the vaccination drive begins to have an impact, reducing the 160 overall population of individuals who are susceptible; this reduction in susceptible people will naturally result in a reduction in the number of sick people, controlling the disease outbreak.

Figure 3 depicts simulations with various vaccination rates for neonates. As the outbreak spreads later, the vaccination drive begins to have an impact, reducing the overall number of infected people; this reduction in sick people will automatically result in the elimination of VZV from the neighborhood. Although a newborn-focused vaccination effort is ideal for a nation's future, it does not immediately result in the illness being eradicated. Random mass vaccination must be used to have immediate results, which necessitates immunizing a sizeable portion of the population.

Figure 4 shows that when vaccination rates for susceptible adults rise, the fraction of susceptible people tends to decline. As a result, there are fewer people who become ill, which lowers the incidence of chickenpox.

Figure 5 shows that there is a small decline in the compartment of susceptible people when the double dose population increases. This is because susceptible people are not necessarily those who receive the second dose; instead, they only receive second dose two when they are already vaccinated. This circumstance is what caused the slight decrease in the susceptible population. In order to reduce the disease, this method generally has a minor yet considerable effect.

Figure 6 shows that there are more recovered people as newborn vaccination rates rise. Conversely, when newborns are not vaccinated, there are more recovered people. This may be because the sick people have natural immunity, and a corresponding decline may be caused by immunity loss that actually wane with time. It can be seen in Figure 6 that there is a noticeable rise in the number of recovered people when almost a half of neonates receive vaccinations. However, with the passage of time, one can observe a fall in the compartment of recovered persons. The results are consistent with our hypothesis that the effectiveness of the first dosage of vaccine waned over the period of time, necessitating the need for the second vaccine to enhance vaccination rates. When vaccination covers the population 100 percent, the slope of the graph increases, and then nearly remains constant after reaching the maximum point, indicating that the 190 infection can be completely eradicated from the community.

Table 2: Parameters' values.

Parameters	Value
κ_1	0.7
κ_2	0.8
ς	0.5
ρ	0.45
α	0.36
$\delta 2$	0.7
χ_2	0.6
χ_1	0.3
ϵ	0.2

From Figure 1, it is evident that suspected population increases with decrease in the fractional order and two-scale dimension. And it is the lowest when the problem reaches the order 1. The case is opposite for vaccinated population and exposed population, that is, compartments V and E reach its maximum value for the lowest two-scale dimension and fractional order as shown in Figures 2 and 3. Recovered population increases exponentially for the lowest value of fractal dimension.

7. Results and Discussion

In this work, a noninteger order model of SIVER models with two viruses is formulated through ABC operator. The existence theory is provided with the help of fixed-point theorem. We used an iterative strategy to find a unique solution to the hypothesized fractional SIRS model with two viruses. Numerical findings are produced for various values of the fractional parameters. As a result, the government must take steps to educate people in rural regions, provide vaccinations, and provide proper treatment in hospitals and other health care facilities. Because we applied the concept of two-scale with Atangana-Baleanu fractional derivatives, the current study will be more useful than prior studies. Our findings predicted that the outcomes of fractional derivative are more precious than the ordinary system.

7.1. Effect of κ_1. When the entire adult population received the first dosage of the vaccine, the number of susceptible and infectious people quickly decreased (in the case of $\kappa_1 = 1$). This indicates that the first dose of vaccination had a major impact. Figure 4 demonstrates that as the proportion of adults who are susceptible to the disease is increased by vaccination, the proportion of susceptible adults tends to decrease. As a result, there are fewer sick people and, consequently, fewer cases of chicken pox. As the effects of the initial dose started to wear off, this reduction in the proportion of susceptible and infectious shifted. The entire population contracted the disease, which caused it to reappear. If this tendency is not reversed soon, it could cause future outbreaks of the illness, which could eventually become endemic. This calls for the second dosage of the vaccine to be administered.

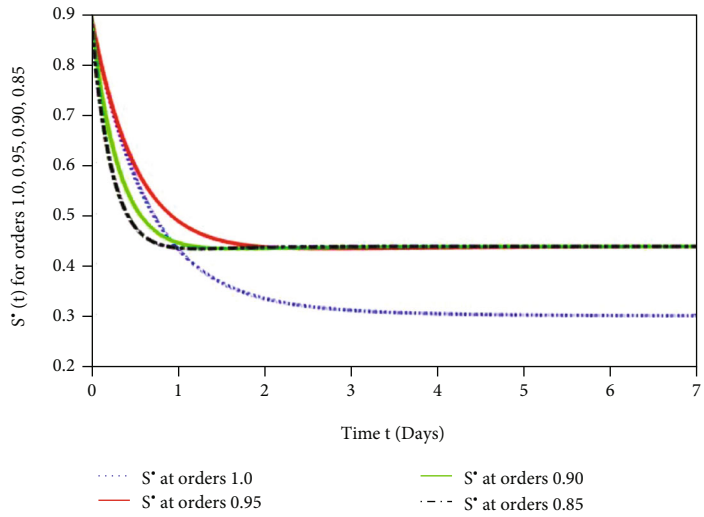

Figure 2: Susceptible population.

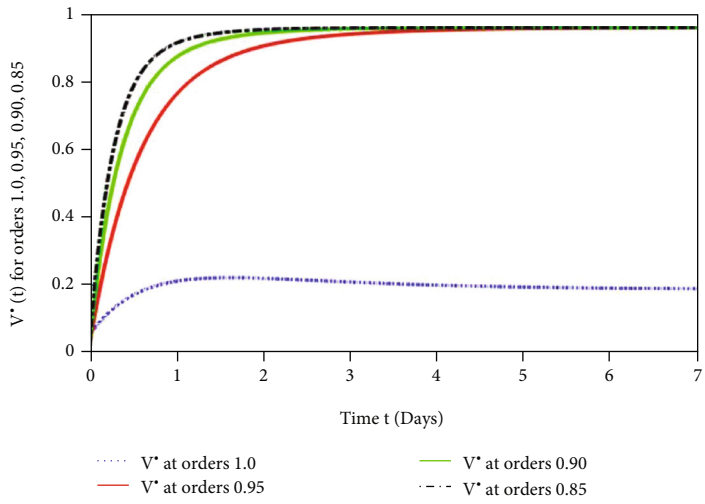

Figure 3: Vaccinated population.

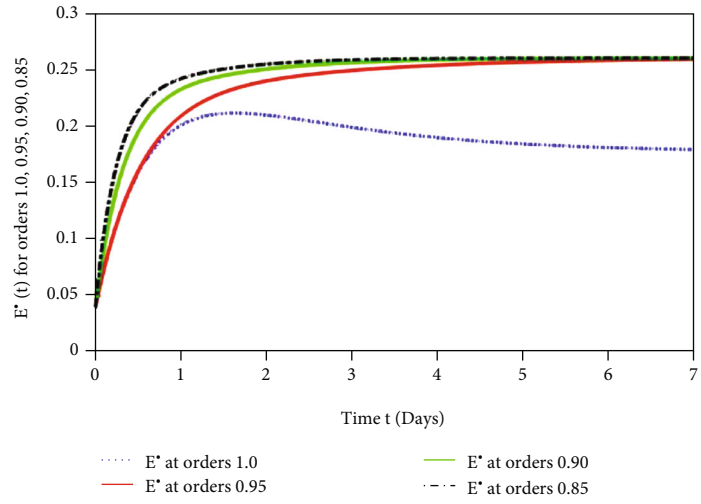

Figure 4: Exposed population.

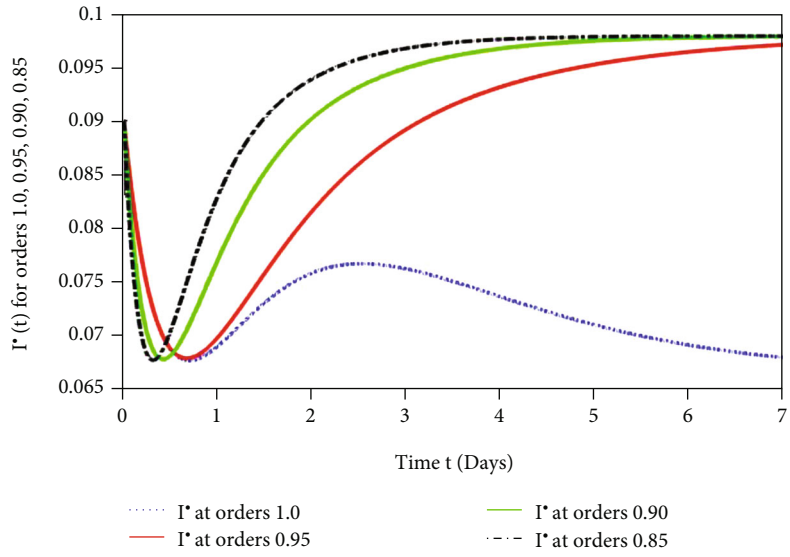

Figure 5: Infected population.

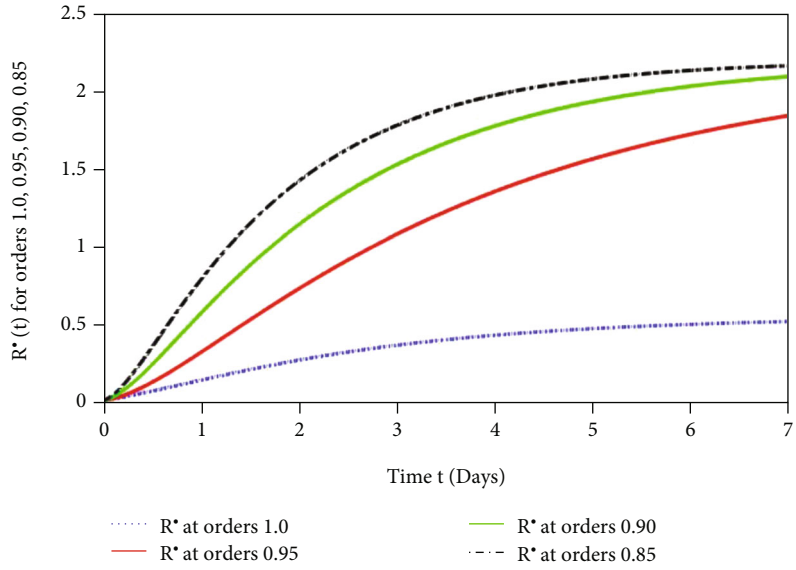

Figure 6: Recovered population.

7.2. Effect of κ_2. Figure 3 shows that there is a slight but significant decrease in the fraction of sensitive individuals as dosage two coverage among humans increases. This is because the individuals that received the second dose are not directly connected to susceptible persons. Humans who are susceptible will only take dosage two if they have already gotten dose one; otherwise, they will not. Due to the possibility that these individuals may be newborns or recruits, who would not or would have a minimal impact on the population of susceptible, this circumstance led to a minor fall in the insusceptible population even though more people received dosage two of the vaccination. Therefore, this practice generally has a minor but considerable effect in lowering the sickness.

7.3. Recovery Rate. Figure 6 demonstrates how the quantity of recovered people rises as infant immunization coverage does. Additionally, it may be observed that when neonates are not immunized, the proportion of the population that recovers gradually decreases, possibly as a result of the sick people's innate immunity. Immunity loss, which worsens over time, may be the cause of this decline in the recovery percentage. The grey line in Figure 6's graph shows that when 50 percent of newborns receive immunizations, there is a discernible increase in the number of recovered humans.

Numerous studies have used the ABC fractional operator to depict different sickness models, and the results support the validity of the concept. We investigated $\mathscr{VIV}$ using the same methodology in order to come up with a

workable solution. The graphical findings were obtained using MATLAB 2020. We draw the conclusion from these graphical results that one can achieve more accurate results and gain a better understanding of both an enzyme reaction equation system and real-world problems in science and engineering by using this new notion of the two-sale and ABC fractional operator.

8. Concluding Remarks

We used a new fractional ABC derivative in arithmetic to solve the problemunder consideration. To incorporate the scale effect in the model under consideration, the concept of two-scale fractal dimension has been taken into consideration. The results of fractional order are demonstrated by numerical simulation. The outcomes demonstrate the effectiveness of the fractional derivative operator, integral operators, and two-scale transform in ABC approach. So, we can conclude that the strategy under consideration is effective. The nature of a large class of nonlinear fractional-order mathematical models in engineering and research can be studied using this method.

9. Future Recommendation

In the current research era, fractal theory and fractional calculus have become particularly popular topics. A new step forward in understanding natural fractals and hierarchical structures is the two-scale fractal theory. The idea that all physical laws are scale-dependent and that each law is only true on the specified scale above which there are stochastic features is projected by the two-scale dimension. To address a specific issue, two observational scales can be chosen. Three scales may be proposed in the future for computations that are more accurate.

To solve the mathematical model of varicella-zoster virus, two-scale dimension has been used. In future, fractal derivative, distance, velocity, and two-scale transform can be applied. To strengthen the mathematical underpinnings of two-scale fractal theory, additional mathematical definitions may be added in the future.

Data Availability

All the data are available within the article.

Conflicts of Interest

The authors declare that they have no competing of interest.

References

[1] M. Almuneef, Z. A. Memish, H. H. Balkhy, B. Alotaibi, and M. Helmy, "Chickenpox complications in Saudi Arabia: is it time for routine varicella vaccination," *275 International journal of infectious diseases*, vol. 10, no. 2, pp. 156–161, 2006.

[2] A. A. Gershon, "Varicella-zoster virus infections," *Pediatrics in Review*, vol. 29, no. 1, 2008.

[3] L. Gregorakos, P. Myrianthefs, N. Markou, D. Chroni, and E. Sakagianni, "Severity of illness and outcome in adult patients with primary varicella pneumonia," *Respiration*, vol. 69, no. 4, pp. 330–334, 2002.

[4] C. K. Fairley and E. Miller, "Varicella-zoster virus epidemiology-a changing scene," *Journal of infectious diseases.*, vol. 174, Supplement 3, pp. S314–S319, 1996.

[5] B. W. Lee, "Review of varicella zoster seroepidemiology in India and South-East Asia," *Tropical medicine & international health: TM & IH.*, vol. 3, no. 11, pp. 886–890, 1998.

[6] C. Cattani, H. M. Srivastava, and X. J. Yang, *Fractional dynamics*, Walter de Gruyter Gmb H & Co KG, 2015.

[7] K. M. Kolwankar and A. D. Gangal, *Local fractional calculus: a calculus for fractal space-time*, InFractals, Springer, London, 1999.

[8] A. Atangana, "Fractal-fractional differentiation and integration: connecting fractal calculus and fractional calculus to predict complex system," *Chaos, solitons & fractals*, vol. 102, pp. 396–406, 2017.

[9] A. Atangana and S. Qureshi, "Modeling attractors of chaotic dynamical systems with fractal-fractional operators," *Chaos, solitons & fractals*, vol. 123, pp. 320–337, 2019.

[10] Q. T. Ain and J.-H. He, "On two-scale dimension and its applications," *Thermal Science*, vol. 23, no. 3 Part B, pp. 1707–1712, 2019.

[11] J.-H. He and Q.-T. Ain, "New promises and future challenges of fractal calculus: from two-scale thermodynamics to fractal variational principle," *Thermal Science*, vol. 24, no. 2 Part A, pp. 659–681, 2020.

[12] J.-H. He, G. M. Moatimid, and M. H. Zekry, *Forced Nonlinear Oscillator in a Fractal Space, Facta Universitatis*, Series: Mechanical Engineering, 2022.

[13] A. Elisha, T. Aboiyar, and A. R. Kimbir, "Mathematical analysis of varicella zoster virus model," *Applied and Computational Mathematics*, vol. 6, no. 2, 2021.

[14] F. Haq, M. Shahzad, S. Muhammad, H. A. Wahab, and G. ur Rahman, "Numerical analysis of fractional order epidemic model of childhood diseases," *Discrete Dynamics in Nature and Society.*, vol. 2017, Article ID 4057089, 7 pages, 2017.

[15] I. Ameen, M. Hidan, Z. Mostefaoui, and H. M. Ali, "Fractional optimal control with fish consumption to prevent the risk of coronary heart disease," *Complexity*, vol. 2020, Article ID 9823753, 13 pages, 2020.

[16] A. Ullah, T. Abdeljawad, S. Ahmad, and K. Shah, "Study of a fractional-order epidemic model of childhood diseases," *Journal of Function Spaces.*, vol. 2020, Article ID 5895310, 8 pages, 2020.

[17] H. M. Alshehri and A. Khan, "A fractional order hepatitis C mathematical model with Mittag-Leffler kernel," *Journal of Function Spaces.*, vol. 2021, Article ID 2524027, 10 pages, 2021.

[18] M. Helikumi, G. Eustace, and S. Mushayabasa, "Dynamics of a fractional-order chikungunya model with asymptomatic infectious class," *Computational and Mathematical Methods in Medicine.*, vol. 2022, Article ID 5118382, 19 pages, 2022.

[19] H. Mohammadi, M. K. Kaabar, J. Alzabut, A. Selvam, and S. Rezapour, "A complete model of Crimean-Congo hemorrhagic fever (CCHF) transmission cycle with nonlocal fractional derivative," *Journal of Function Spaces*, vol. 2021, Article ID 1273405, 12 pages, 2021.

[20] A. Harir, S. Melliani, H. El Harfi, and L. S. Chadli, "Variational iteration method and differential transformation method for solving the SEIR epidemic model," *International Journal of*

Differential Equations., vol. 2020, Article ID 3521936, 7 pages, 2020.

[21] A. Elias-Zuniga, "On two-scale dimension and its application for deriving a new analytical solution for the fractal DUFFINGS equation," *Fractals*, vol. 30, no. 3, 2022.

[22] H. Yuan, "Some properties of numerical solutions for semilinear stochastic delay differential equations driven by G-Brownian motion," *Mathematical Problems in Engineering*., vol. 2021, Article ID 1835490, 26 pages, 2021.

[23] A. Din, Y. Li, F. M. Khan, Z. U. Khan, and P. Liu, "On analysis of fractional order mathematical model of hepatitis B using Atangana Baleanu Caputo (ABC) derivative," *Fractals*, vol. 30, no. 1, 2022.

[24] A. Din, "The stochastic bifurcation analysis and stochastic delayed optimal control for epidemic model with general incidence function," *Journal of Nonlinear Science*., vol. 31, no. 12, article 123101, 2021.

Hindawi
Advances in Mathematical Physics
Volume 2022, Article ID 2847993, 10 pages
https://doi.org/10.1155/2022/2847993

Research Article

Analysis of Fractional Thin Film Flow of Third Grade Fluid in Lifting and Drainage via Homotopy Perturbation Procedure

Mubashir Qayyum,[1] **Farnaz Ismail**,[2] **Syed Inayat Ali Shah**,[2] **Muhammad Sohail**,[3] **Kanayo Kenneth Asogwa**,[4] **and Fatema Tuz Zohra**[5]

[1]*Department of Sciences and Humanities, National University of Computer & Emerging Sciences FAST Lahore, Pakistan*
[2]*Department of Mathematics, Islamia College University Peshawar, Pakistan*
[3]*Department of Mathematics, Khawaja Fareed University of Engineering & Information Technology, Rahim Yar Khan, Pakistan*
[4]*Department of Mathematics, Nigeria Maritime University, Okerenkoko, Delta State, Nigeria*
[5]*Department of Mathematics, Faculty of Science and Technology, American International University Bangladesh, Dhaka 1229, Bangladesh*

Correspondence should be addressed to Fatema Tuz Zohra; fatema.tz28@gmail.com

Received 17 July 2022; Revised 23 August 2022; Accepted 10 September 2022; Published 23 September 2022

Academic Editor: Qura Tul Ain

Analysis of thin film flows is an important topic in fluid dynamics due to the large number of industrial applications such as food processing, chip manufacturing, irrigation, oil refining process, painting finishing, etc. Analysis involves studying the effects of various parameters in absolute conditions. These parameters may be film thickness, volumetric flux, liquid velocity profile, viscosity, shear stress, gravity, density, and different boundary formations. We have expanded the formulations of non-Newtonian third grade fluid for lifting and draining in fractional space. Fractional calculus along with Homotopy Perturbation Method is used for the solution and analysis purposes. The suitability and consistency of the solutions is determined by detecting residuals in each case. Velocity profile, average velocity, and volume flow for lifting and drainage cases are calculated. To the best of authors knowledge, thin film flow of fractional third grade fluid is not attempted before in lifting and drainage. Investigation shows increase in value of fractional parameter that decreases the velocity profile in lifting while increases the velocity in drainage scenario. Also, the frictional parameter and the gravitational parameter have opposite, while material constant has direct relationship with the velocity profile in lifting case. All the parameters showed inverse effect on the velocity in drainage case.

1. Introduction

Thin film flows can be seen in many natural situations such as raindrops on the window, water-filled eyes, and lava. Free drainage refers to a phenomenon in which a fluid flows along a vertical object in such a way that adheres to the form of objects and viscous forces [1]. Paint finishing, oil refining processes, chip production, construction and public works, and laser cutting are industrial applications of these flows [2–4]. The first work on thin films was performed based on Newtonian fluids in [3]. Although this procedure works for a long time, it was not sufficient for the nonlinear analysis of non-Newton liquid such as melted plastics gels, lubricants containing polymeric additives, blood, and foods such as ketchup and honey [5, 6]. Siddiqui et al. address the drainage problems in relation with Phan-Thein-Tanner (PTT) and third grade fluids which flows along an inclined plane in [7, 8]. Siddiqui et al. also analyzed thin film scenario using fourth-grade fluids on vertical cylinders in [9]. Alam et al. [10] investigated thin film of pseudoplastic fluid. Deiber and Cruz analyzed non-Newtonian fluid flow through a circular tube [11]. In terms of flow types, Yih [12] performed the first studies regarding laminar flows in free surface. Landau [13] and Stuart [14] have extended the analysis to the turbulent flows. Nakaya [15] and Lin [16] performed stability analysis taking into account surface

tension. Zangooee et al. [17] performed hydrothermal analysis of hybrid nanofluid on a vertical plate with slip effects. Gulzar et al. analyzed magneto-hyperbolic-tangent liquid for different features in [18]. Fallah et al. analyzed nanofluid in a vertical channel taking polynomial boundary [19]. Nayak et al. [20] numerical examine the mixed convection nanofluid over an isothermal thin needle metallic nanomaterial. Ebrahem et al. investigated the significance of Lorentz forces on radiative nanofluid under multiple constraints [21]. Zaher et al. solved boundary layer flow of a non-Newtonian fluid with planktonic microorganism in [22]. Sara et al. analyzed thin blood stream through electroosmotic forces in hybrid nanofluid [23].

In the past few decades, various numerical and homotopy-based techniques have been proposed by many researchers for BVPs [16, 24, 25]. In 1992, Liao proposed homotopy analysis method for BVPs [26, 27]. After that, professor He proposed a combination of homotopy with perturbation for solution of BVPs in [28–30] and has been used successfully to solve many linear and nonlinear [31–33]. Yıldırım [34], Golbabai et al. [35], and Ghasemi et al. [36] solved integro-differential and integral equations through HPM. FDEs have been modelled and studied in signal processing, physics, and biology due to their ability to capture more complex nonlinear phenomena [37–39]. Spasic and Lazarevic discussed the electro viscoelasticity of fractional-order model in [40]. In this continuation, in current paper, we extend the study of thin film flow of fractional third grade fluid in lifting and drainage cases. We formulate the phenomena in the form of fractional differential equations and compute series solutions using homotopy perturbation method (HPM). In the rest of the manuscript, Section 2 is presenting governing equations. Formulation and solution in lifting case are given in Sections 3 and 4. Sections 5 and 6 contain formulation and solution related to drainage case. Results and discussion is in Section 7, while conclusion is given in Section 8.

2. Governing Equations

The fundamental equations are as follows [7, 8]:

$$\operatorname{div} \mathbf{V} = 0, \tag{1}$$

$$\rho\left[\frac{\partial \mathbf{V}}{\partial t} + (\mathbf{V}.\nabla)\mathbf{V}\right] = \nabla.\mathbf{T} + \rho\mathbf{b}, \tag{2}$$

where $\mathbf{T}$, $\mathbf{V}$ and ρ are Cauchy stress tensor, velocity and density, respectively. Where

$$\mathbf{T} = -p\mathbf{I} + \mathbf{S}, \tag{3}$$

where $\mathbf{I}$ is the unit tensor, p is the pressure, and $\mathbf{S}$ the extra stress tensor.

$$\mathbf{S} = \left[a + b\left|\sqrt{\frac{1}{2}\operatorname{tr}(\mathbf{A_1})^2}\right|^{n-1}\right]\mathbf{A_1}, \tag{4}$$

where a, b, and n are constants.

$$\begin{aligned}\mathbf{S} + \lambda_1\frac{\mathrm{D}\mathbf{S}}{\mathrm{D}t} + \frac{\lambda_3}{2}(\mathbf{S}\mathbf{A_1} + \mathbf{A_1}\mathbf{S}) + \frac{\lambda_5}{2}(\operatorname{tr}\mathbf{S})\mathbf{A_1} \\ = \mu\left(\mathbf{A_1} + \lambda_2\frac{\mathrm{D}\mathbf{A_1}}{\mathrm{D}t} + \lambda_4\mathbf{A_1}^2\right), \mathbf{A_1} = \mathbf{L} + \mathbf{L}^{\mathrm{T}},\end{aligned}$$

$$\mathbf{L} = \operatorname{grad}\ \mathbf{V}, \tag{5}$$

where $\mu, \lambda_1, \lambda_2, \lambda_3, \lambda_4$ and λ_5 are material constant, and $\mathbf{A_1}$ is the Rivlin-Ericksen tensor.

3. Formulation of the Problem in Lifting Case [7, 8]

Substituting Equations (3) and (4) in Equation (2), we get

$$\begin{aligned}-\frac{dp_1}{dx} &= 0, \\ -\frac{dp_1}{dy} + \rho g + a\frac{d^2v}{dx^2} + b\frac{d}{dx}\left(\frac{dv}{dx}\right)^{\mathrm{n}} &= 0.\end{aligned} \tag{6}$$

From above we deduce that $p_1 = p_1(y)$,

$$a\frac{d^2v}{dx^2} + nb\left(\frac{dv}{dx}\right)^{\mathrm{n}-1}\frac{d^2v}{dx^2} + \rho g = \frac{dp_1}{dx}. \tag{7}$$

Equation (9) becomes

$$a\frac{d^2v}{dx^2} + nb\left(\frac{dv}{dx}\right)^{\mathrm{n}-1}\frac{d^2v}{dx^2} - \rho\mathrm{g} = 0, \tag{8}$$

$$\text{with } v = U_0 \text{at } x = 0 \text{ and } S_{xy} = 0 \text{ at } x = \delta, \tag{9}$$

where

$$S_{xy} = a\frac{dv}{dx} + b\left[\frac{dv}{dx}\right]^{\mathrm{n}}. \tag{10}$$

Using Equation (10) in Equation (9), we get

$$\frac{dv}{dx} = 0 \text{ at } x = \delta, \tag{11}$$

$$\frac{d^2v}{dx^2} + \frac{nb}{a}\left(\frac{dv}{dx}\right)^{\mathrm{n}-1}\frac{d^2v}{dx^2} - \frac{\rho g}{a} = 0. \tag{12}$$

Substituting $n = 3, b = 2(\beta_2 + \beta_3)$ and $a = \mu$ in Equation (12), we have

$$\frac{d^2v}{dx^2} + \frac{6(\beta_2 + \beta_3)}{\mu}\left(\frac{dv}{dx}\right)^2\frac{d^2v}{dx^2} - \frac{\rho g}{\mu} = 0, \tag{13}$$

$$\left.\begin{aligned} v &= U_0 \text{at } x = 0, \\ \frac{dv}{dx} &= 0 \text{ at } x = \delta. \end{aligned}\right\} \tag{14}$$

$v^* = v/U_0, x^* = x/\delta, \beta^* = 6(\beta_2 + \beta_3){U_0}^2/\mu, {g_p}^* = \rho g/\mu U_0$ are dimensionless parameters.

The dimensionless form without '*' of Equation (13) subject to Equation (14) is

$$\frac{d^2v}{dx^2} + \beta\left(\frac{dv}{dx}\right)^2 \frac{d^2v}{dx^2} - g_p = 0, \tag{15}$$

$$\text{with } \frac{dv}{dx} = 0 \text{ at } x = 1 \text{ and } v = 1 \text{ at } x = 0, \tag{16}$$

Using definitions of fractional calculus, Equation (16) can be written as fractionally

$$\frac{d^2v(x)}{dx^2} + \beta(D^\alpha v(x))^2 \frac{d^2v(x)}{dx^2} - g_p = 0, \tag{17}$$

$$\text{with } v'(1) = 0, v(0) = 1, 0 < \alpha < 1. \tag{18}$$

4. Homotopy Solution of Third Grade Fluid in Lifting Case

For Equation (17), the homotopy $\Omega \times [0, 1] \longrightarrow R$ is defined as follows [24]:

$$(1-p)\frac{d^2v(x)}{dx^2} + p\left[\frac{d^2v(x)}{dx^2} + \beta(D^\alpha v(x))^2 \frac{d^2v(x)}{dx^2} - g_p\right] = 0. \tag{19}$$

Using Equations (18) and (19) different order problems are given as follows:

0^{th} order

$${v_0}''(\mathrm{x}) = 1, v_0'(1) = 0, v_0(0) = 1. \tag{20}$$

1^{st} order

$$-g_p + \beta(D^\alpha v_0(\mathrm{x}))^2 {v_0}''(\mathrm{x}) + {v_1}''(\mathrm{x}) = 0, {v_1}'(1) = 0, v_1(0) = 0 \tag{21}$$

2^{nd} order

$$\begin{aligned} 2\beta(D^\alpha v_0(\mathrm{x}))(D^\alpha v_1(\mathrm{x})){v_0}''(\mathrm{x}) + \beta(D^\alpha v_0(\mathrm{x}))^2 {v_1}''(\mathrm{x}) \\ + {v_2}''(\mathrm{x}) = 0, {v_2}'(1) = 0, v_2(0) = 0 \end{aligned} \tag{22}$$

3^{rd} order

$$\begin{aligned} \beta(D^\alpha v_1(\mathrm{x}))^2 {v_0}''(\mathrm{x}) + 2\beta(D^\alpha v_0(\mathrm{x}))(D^\alpha v_2(\mathrm{x})){v_0}''(\mathrm{x}) \\ + 2\beta(D^\alpha v_0(\mathrm{x}))(D^\alpha v_1(\mathrm{x})){v_1}''(\mathrm{x}) \\ + \beta(D^\alpha v_0(\mathrm{x}))^2 {v_2}''(\mathrm{x}) + {v_3}''(\mathrm{x}) \\ = 0, v_3(0) = 0, {v_3}'(1) = 0 \end{aligned} \tag{23}$$

4^{th} order

$$\begin{aligned} 2\beta(D^\alpha v_1(\mathrm{x}))(D^\alpha v_2(\mathrm{x})){v_0}''(\mathrm{x}) + 2\beta(D^\alpha v_0(\mathrm{x}))(D^\alpha v_3(\mathrm{x})){v_0}''(\mathrm{x}) \\ + \beta(D^\alpha v_1(\mathrm{x}))^2 {v_1}''(\mathrm{x}) \\ + 2\beta(D^\alpha v_0(\mathrm{x}))(D^\alpha v_2(\mathrm{x})){v_1}''(\mathrm{x}) \\ + 2\beta(D^\alpha v_0(\mathrm{x}))(D^\alpha v_1(\mathrm{x})){v_2}''(\mathrm{x}) \\ + \beta(D^\alpha v_0(\mathrm{x}))^2 {v_3}''(\mathrm{x}) \\ + {v_4}''(\mathrm{x}) = 0, v(0) = 0, {v_4}'(1) = 0 \end{aligned} \tag{24}$$

Using Caputo definition while $\alpha = 0.8$, $\beta = 1$ and $g_p = 0.8$ fixed, the approximate solution is

$$\begin{aligned} V(x) = 1 &+ \frac{1}{2}\left(-1.6x + 0.8x^2\right) \\ &+ \frac{1}{x^{1.6}} 0.01787764010524059\left(7.612661760000037x^{2.6}\right. \\ &- 10.110566399999996x^4 + 6.938624000000001x^5 \\ &\left. - 1.5769600000000001x^6\right. \end{aligned}$$

$$\text{The residual is } R = \frac{d^2V(x)}{dx^2} + \beta(D^\alpha V(x))^2 \frac{d^2V(x)}{dx^2} - g_p \tag{25}$$

4.1. Flow Rate and Average Velocity in Lifting Case [7]. The average velocity is

$$Q = \int_0^1 V(x)dx,$$

$$Q = \frac{(-3+2\alpha)\left(-3{g_p}^3(-3+\alpha)^2(-16+\alpha(25+\alpha(-13+2\alpha)))\beta/-7+2\alpha-2\left(-3+g_p\right)(-5+2\alpha)\Gamma[4-\alpha]^2\right)}{6(15-16\alpha+4\alpha^2)\Gamma[4-\alpha]^2}. \tag{26}$$

$$\bar{V} = Q.$$

Table 1: Results for α in lifting case where $\beta = 0.5$ and $g_p = 0.001$ are fixed.

x	$\alpha = 0.2$		$\alpha = 0.6$		$\alpha = 0.99$	
	$V(x)$	Error	$V(x)$	Error	$V(x)$	Error
0.1	9.9998e−1	-4.54216e−18	9.9991e−1	-1.54976e−17	9.9981e−1	-2.1073e−16
0.2	9.9981e−1	-1.23994e−17	9.9984e−1	-3.1282e−17	9.9985e−1	-1.53593e−16
0.3	9.9974e−1	-2.16777e−17	9.9982e−1	-4.36903e−17	9.9973e−1	-1.01302e−16
0.4	9.9962e−1	-3.07258e−17	9.9972e−1	-5.10537e−17	9.9965e−1	-6.13372e−17
0.5	9.9963e−1	-3.81183e−17	9.9975e−1	-5.31326e−17	9.9959e−1	-3.37629e−17
0.6	9.9958e−1	-4.2865e−17	9.9968e−1	-5.06284e−17	9.9956e−1	-1.65235e−17
0.7	9.9954e−1	-4.45033e−17	9.9964e−1	-4.47699e−17	9.9955e−1	-6.95404e−18
0.8	9.9952e−1	-4.30865e−17	9.9952e−1	-3.69744e−17	9.9954e−1	-2.42827e−18
0.9	9.9998e−1	-4.54216e−18	9.9991e−1	-1.54976e−17	9.9981e−1	-2.1073e−16
1.	9.9981e−1	-1.23994e−17	9.9984e−1	-3.1282e−17	9.9985e−1	-1.53593e−16

Table 2: Results for g_p in lifting case where $\alpha = 0.95$ and $\beta = 0.1$ are fixed.

x	$g_p = 0.001$		$g_p = 0.01$		$g_p = 0.1$	
	$V(x)$	Error	$V(x)$	Error	$V(x)$	Error
0.1	9.9988e−1	-8.42917e−18	9.9985e−1	-8.42917e−13	9.9989e−1	-8.42614e−8
0.2	9.9985e−1	-6.14371e−18	9.9982e−1	-6.14371e−13	9.9986e−1	-6.14184e−8
0.3	9.9982e−1	-4.05208e−18	9.9978e−1	-4.05208e−13	9.9984e−1	-4.05108e−8
0.4	9.9972e−1	-2.45348e−18	9.9975e−1	-2.45348e−13	9.9975e−1	-2.453e−8
0.5	9.9971e−1	-1.35051e−18	9.9973e−1	-1.35051e−13	9.9972e−1	-1.35031e−8
0.6	9.9968e−1	-6.60931e−19	9.9969e−1	-6.60941e−14	9.9968e−1	-6.60868e−9
0.7	9.9964e−1	-2.78159e−19	9.9965e−1	-2.78161e−14	9.9964e−1	-2.78139e−9
0.8	9.9962e−1	-9.71282e−20	9.9964e−1	-9.7131e−15	9.9952e−1	-9.71257e−10
0.9	9.9952e−1	-2.8262e−20	9.9955e−1	-2.82618e−15	9.9951e−1	-2.82607e−10
1.	9.9951e−1	-6.02955e−20	9.992e−1	-6.03165e−16	9.995e−1	-6.03129e−11

Table 3: Results for β in lifting case where $\alpha = 0.99$ and $g_p = 0.001$ are fixed.

x	$\beta = 0.1$		$\beta = 0.5$		$\beta = 0.9$	
	$V(x)$	Error	$V(x)$	Error	$V(x)$	Error
0.1	9.9998e−1	-1.03899e−17	9.9984e−1	-2.59749e−16	9.9979e−1	-8.41587e−16
0.2	9.9991e−1	-6.69572e−18	9.9981e−1	-1.67394e−16	9.9975e−1	-5.42356e−16
0.3	9.9984e−1	-4.02215e−18	9.9974e−1	-1.00554e−16	9.9974e−1	-3.25794e−16
0.4	9.9978e−1	-2.22459e−18	9.9972e−1	-5.56148e−17	9.9962e−1	-1.80192e−16
0.5	9.9973e−1	-1.10445e−18	9.9963e−1	-2.76114e−17	9.9963e−1	-8.9461e−17
0.6	9.9968e−1	-4.71565e−19	9.9961e−1	-1.17891e−17	9.9956e−1	-3.81967e−17
0.7	9.9964e−1	-1.60686e−19	9.9954e−1	-4.01724e−18	9.9954e−1	-1.30159e−17
0.8	9.9962e−1	-3.81773e−20	9.9952e−1	-9.54481e−19	9.9952e−1	-3.09255e−18
0.9	9.9951e−1	-5.30469e−21	9.9951e−1	-1.326e−19	9.995e−1	-4.29646e−19
1.	9.994e−1	-2.27581e−22	9.995e−1	-5.66682e−21	9.994e−1	-1.83058e−20

5. Mathematical Formulation in Drainage Case [7, 8]

Considering the fluid falling on the stationary infinite stationary belt, the flow is in the downward direction due to gravity, so Equation (15) becomes

$$\frac{d^2v}{dx^2} + \beta\left(\frac{dv}{dx}\right)^2 \frac{d^2v}{dx^2} + g_p = 0, \tag{27}$$

Table 4: Results for α in drainage case keeping $\beta = 0.1$ and $g_p = 0.001$ are fixed.

x	$\alpha = 0.2$		$\alpha = 0.6$		$\alpha = 0.99$	
	$V(x)$	Error	$V(x)$	Error	$V(x)$	Error
0.1	9.41e−5	1.81686e−19	9.52e−5	2.04663e−18	9.62e−5	1.03899e−17
0.2	1.71e−4	4.95977e−19	1.73e−4	2.82993e−18	1.81e−4	6.69572e−18
0.3	2.62e−4	8.67109e−19	2.65e−4	2.98548e−18	2.64e−4	4.02215e−18
0.4	3.42e−4	1.22903e−18	3.43e−4	2.74607e−18	3.53e−4	2.22459e−18
0.5	3.65e−4	1.52473e−18	3.62e−4	2.29456e−18	3.65e−4	1.10445e−18
0.6	4.12e−4	1.7146e−18	4.11e−4	1.76941e−18	4.52e−4	4.71565e−19
0.7	4.52e−4	1.78013e−18	4.54e−4	1.26636e−18	4.61e−4	1.60686e−19
0.8	4.91e−4	1.72346e−18	4.93e−4	8.42172e−19	4.89e−4	3.81773e−20
0.9	4.95e−4	1.56378e−18	4.91e−4	5.20346e−19	$4.95e{-4}^4$	5.30469e−21
1.	5.11e−4	1.33187e−18	5.21e−4	2.98346e−19	5.01e−4	2.27581e−22

Table 5: Results for g_p in drainage case where $\alpha = 0.99$ and $\beta = 0.1$ are fixed.

x	$g_p = 0.1$		$g_p = 0.01$		$g_p = 0.001$	
	$V(x)$	Error	$V(x)$	Error	$V(x)$	Error
0.1	9.41e−5	1.81686e−19	9.52e−5	2.04663e−18	9.62e−5	1.03899e−17
0.2	1.71e−4	4.95977e−19	1.73e−4	2.82993e−18	1.81e−4	6.69572e−18
0.3	2.62e−4	8.67109e−19	2.65e−4	2.98548e−18	2.64e−4	4.02215e−18
0.4	3.42e−4	1.22903e−18	3.43e−4	2.74607e−18	3.53e−4	2.22459e−18
0.5	3.65e−4	1.52473e−18	3.62e−4	2.29456e−18	3.65e−4	1.10445e−18
0.6	4.12e−4	1.7146e−18	4.11e−4	1.76941e−18	4.52e−4	4.71565e−19
0.7	4.52e−4	1.78013e−18	4.54e−4	1.26636e−18	4.61e−4	1.60686e−19
0.8	4.91e−4	1.72346e−18	4.93e−4	8.42172e−19	4.89e−4	3.81773e−20
0.9	4.95e−4	1.56378e−18	4.91e−4	5.20346e−19	$4.95e{-4}^4$	5.30469e−21
1.	5.11e−4	1.33187e−18	5.21e−4	2.98346e−19	5.01e−4	2.27581e−22

Table 6: Results for β in drainage case where $\alpha = 0.95$ and $g_p = 0.001$ are fixed.

x	$\beta = 0.1$		$\beta = 0.3$		$\beta = 0.7$	
	$V(x)$	Error	$V(x)$	Error	$V(x)$	Error
0.1	9.41e−5	1.81686e−19	9.52e−5	2.04663e−18	9.62e−5	1.03899e−17
0.2	1.71e−4	4.95977e−19	1.73e−4	2.82993e−18	1.81e−4	6.69572e−18
0.3	2.62e−4	8.67109e−19	2.65e−4	2.98548e−18	2.64e−4	4.02215e−18
0.4	3.42e−4	1.22903e−18	3.43e−4	2.74607e−18	3.53e−4	2.22459e−18
0.5	3.65e−4	1.52473e−18	3.62e−4	2.29456e−18	3.65e−4	1.10445e−18
0.6	4.12e−4	1.7146e−18	4.11e−4	1.76941e−18	4.52e−4	4.71565e−19
0.7	4.52e−4	1.78013e−18	4.54e−4	1.26636e−18	4.61e−4	1.60686e−19
0.8	4.91e−4	1.72346e−18	4.93e−4	8.42172e−19	4.89e−4	3.81773e−20
0.9	4.95e−4	1.56378e−18	4.91e−4	5.20346e−19	4.95e−4	5.30469e−21
1.	5.11e−4	1.33187e−18	5.21e−4	2.98346e−19	5.01e−4	2.27581e−22

$$\left.\begin{array}{l} v = 0 \text{ at } x = 0, \\ \text{with } \dfrac{dv}{dx} = 0 \text{ at } x = 1. \end{array}\right\} \tag{28}$$

Using definitions of fractional calculus, Equation (27) can be written fractionally as follows:

$$\frac{d^2v(x)}{dx^2} + \beta\left(D^{\alpha}v(x)\right)^2\frac{d^2v(x)}{dx^2} + g_p = 0, \tag{29}$$

$$\text{with } v(0) = 0, v'(1) = 0, 0 < \alpha < 1. \tag{30}$$

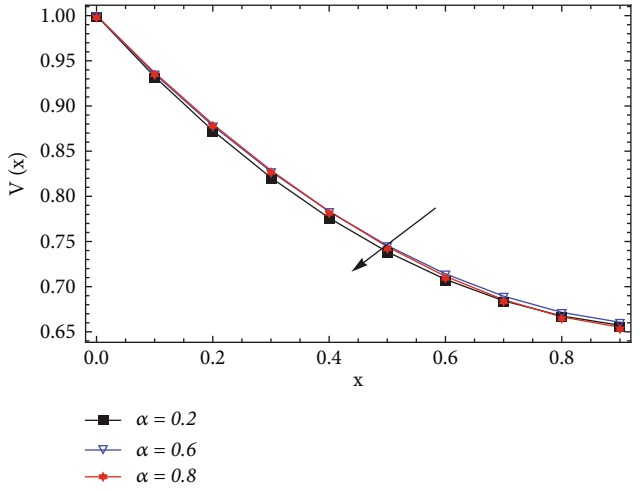

Figure 1: In lifting case effect of α on $V(x)$ where $g_p = 0.8$ and $\beta = 1$ are fixed.

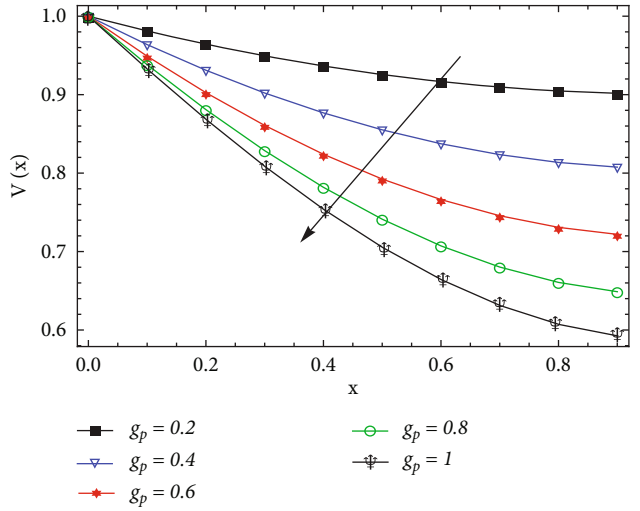

Figure 2: In lifting case effect of g_p on $V(x)$ where $\alpha = 0.95$ and $\beta = 1$ are fixed.

6. Homotopy Solution of Third Grade Fluid in Drainage Case

For Equation (29), the homotopy $\Omega \times [0, 1] \longrightarrow R$ is defined as follows [24]:

$$(1-p)\frac{d^2v(x)}{dx^2} + p\left[\frac{d^2v(x)}{dx^2} + \beta(D^{\alpha}v(x))^2\frac{d^2v(x)}{dx^2} + g_p\right] = 0. \tag{31}$$

Using Equations (30) and (31) different order problems are given as follows:

0^{th} order

$$v_0''(\mathrm{x}) = 0, v_0'(1) = 0, v_0(0) = 0. \tag{32}$$

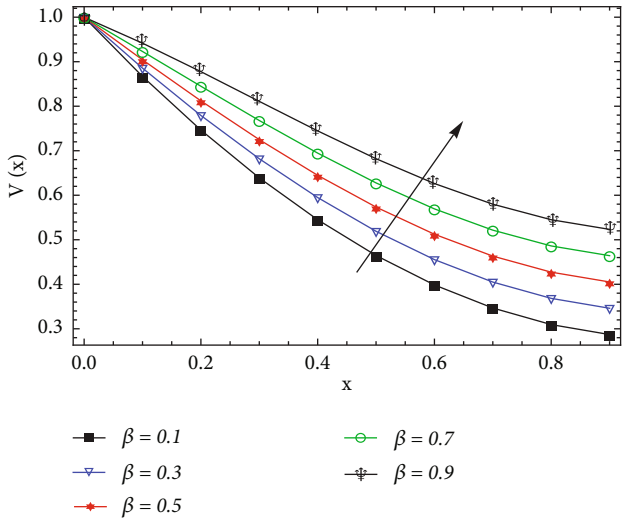

Figure 3: In lifting case effect of β on $V(x)$ where $\alpha = 0.95$ and $g_p = 1.5$ are fixed.

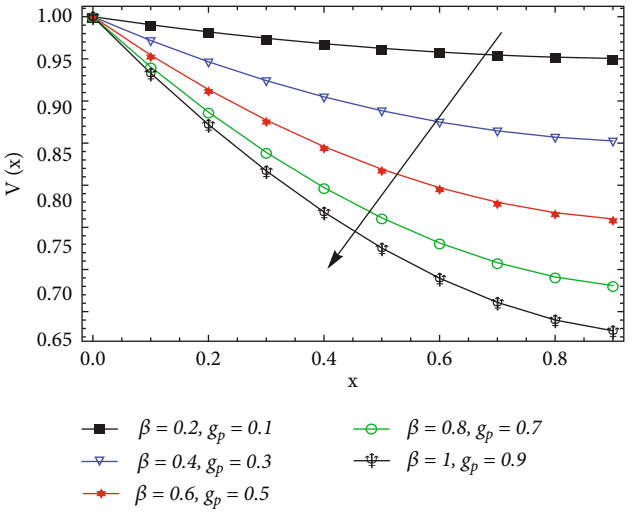

Figure 4: In lifting case effect of increasing β and g_p on $V(x)$ where $\alpha = 0.8$ is fixed.

1^{st} order

$$g_p + \beta(D^{\alpha}v_0(\mathrm{x}))^2 v_0''(\mathrm{x}) + v_1''(\mathrm{x}) = 0, v_1'(1) = 0, v_1(0) = 0. \tag{33}$$

2^{nd} order

$$2\beta(D^{\alpha}v_0(\mathrm{x}))(D^{\alpha}v_1(\mathrm{x}))v_0''(\mathrm{x}) + \beta(D^{\alpha}v_0(\mathrm{x}))^2 v_1''(\mathrm{x}) + v_2''(\mathrm{x}) = 0, v_2(0) = 0, v_2'(1) = 0. \tag{34}$$

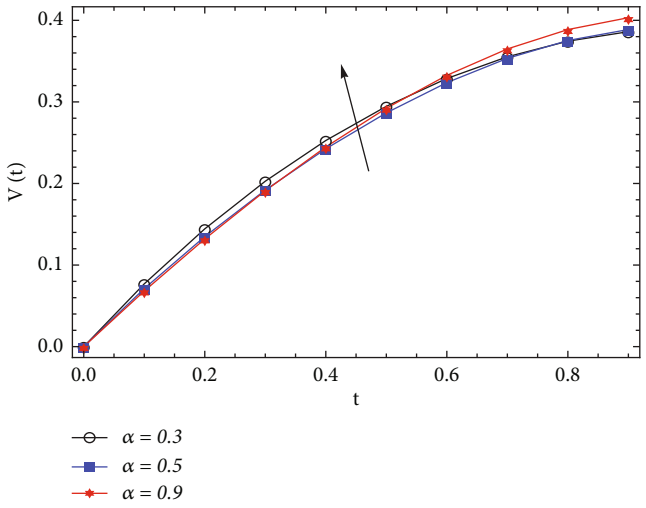

Figure 5: In drainage case effect of α on $V(x)$ where $g_p = 1$ and $\beta = 1$ are fixed.

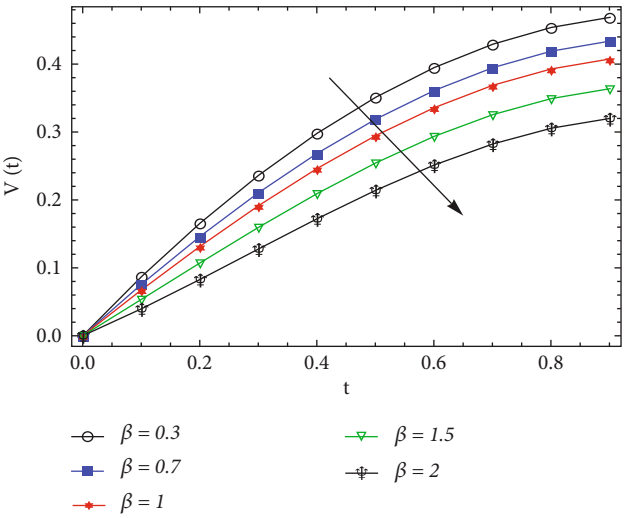

Figure 7: In drainage case effect of β on $V(x)$ where $g_p = 1$ and $\alpha = 0.95$ are fixed.

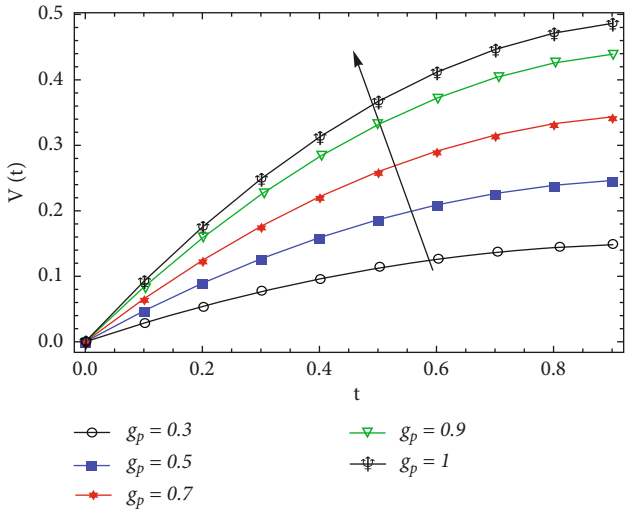

Figure 6: In drainage case effect of g_p on $V(x)$ keeping $\alpha = 0.95$ and $\beta = 1$ are fixed.

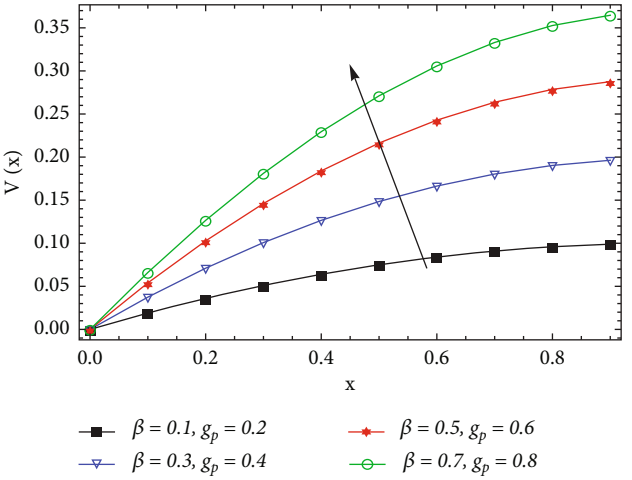

Figure 8: In drainage case effect of increasing β and g_p on $V(x)$ where $\alpha = 0.95$ is fixed.

3^{rd} order

$$\begin{aligned}\beta(D^{\alpha}v_1(x))^2 {v_0}''(x) + 2\beta(D^{\alpha}v_0(x))(D^{\alpha}v_2(x)){v_0}''(x)\\ + 2\beta(D^{\alpha}v_0(x))(D^{\alpha}v_1(x)){v_1}''(x)\\ + \beta(D^{\alpha}v_0(x))^2 {v_2}''(x) + {v_3}''(x)\\ = 0, v_3(0) = 0, {v_3}'(1) = 0.\end{aligned} \tag{35}$$

4^{th} order

$$\begin{aligned}2\beta(D^{\alpha}v_1(x))(D^{\alpha}v_2(x)){v_0}''(x) + 2\beta(D^{\alpha}v_0(x))(D^{\alpha}v_3(x)){v_0}''(x)\\ + \beta(D^{\alpha}v_1(x))^2 {v_1}''(x)\\ + 2\beta(D^{\alpha}v_0(x))(D^{\alpha}v_2(x)){v_1}''(x)\\ + 2\beta(D^{\alpha}v_0(x))(D^{\alpha}v_1(x)){v_2}''(x)\\ + \beta(D^{\alpha}v_0(x))^2 {v_3}''(x)\\ + {v_4}''(x) = 0, v(0) = 0, {v_4}'(1) = 0.\end{aligned} \tag{36}$$

By using definition where $\alpha = 0.8$, $\beta = 1$ and $g_p = 0.8$ are fixed, we get the following approximate solution:

$$V(x) = 1/2\left(0.002\,x - 0.001\,x^2\right) + \frac{\left(0.0269608\left(-1.08662\times10^{-9}\,x^{2.8} + 1.55232\times10^{-9}\,x^4 - 1.0584\times10^{-9}x^5 + 2.52\times10^{-10}x^6\right)\right)}{x^{1.8}}.$$

$$\text{The residual is } R = \frac{d^2V(x)}{dx^2} + \beta\left(D^\alpha V(x)\right)^2\frac{d^2V(x)}{dx^2} + g_p. \tag{37}$$

6.1. Average Velocity and Flow Rate in Drainage Case. The average velocity is

$$Q = \int_0^1 V(x)dx,$$
$$Q = \frac{g_p(-3+2\alpha)\left(3{g_p}^2(-3+\alpha)^2(-16+\alpha(25+\alpha(-13+2\alpha)))\beta + (70+8(-6+\alpha)\alpha)\Gamma[4-\alpha]^2\right)}{2(-21+6\alpha)(15-16\alpha+4\alpha^2)\Gamma[4-\alpha]^2}.\bar{V} = Q. \tag{38}$$

7. Result and Discussion

In this article, series solution of fractional thin film of third grade fluid is obtained in case of lifting and drainage. For the validity check, modelled problems are solved for different values of involved parameters, and the results are presented in Tables 1–6. Tables 1 and 4 are showing solutions and residual errors for different values of fractional parameter α. Tables 2 and 5 present solution and errors against different numerical values of gravitational parameter g_p. Similarly, Tables 3 and 6 show the solutions along with errors for different values of non-Newtonian parameter β. Analysis of these tables clearly indicates that obtained solutions are valid and consistent. Graphical analysis of the involved parameters is provided in Figures 1–8. Figures 1–4 capture the effect of involved parameter on the velocity in lifting case. Figures 1, 2, and 3 show the effects of fractional, gravitational, and material parameter on the velocity profile. It is observed that α and g_p have inverse, while β has direct relationship with the fluid velocity in lifting case. The effect of simultaneous increase in β and g_p on the velocity is shown in Figure 4. It has been observed that g_p effect is more dominant as compared to β in case of lifting. Effects of above mentioned parameters in drainage case are shown in Figures 5–8. Figures 5, 6, and 7 fractional, gravitational, and material parameter on the velocity profile. It is observed that α and g_p have direct while β has inverse relationship with the fluid velocity in drainage case. The effect of simultaneous increase in β and g_p on the velocity is shown in Figure 8. It has been observed that the effect of g_p is more dominant as compared to β in drainage as well.

8. Conclusions

In this article, homotopy based solutions of fractional thin film of third grade fluid are obtained. The validity and convergence of the obtained solutions are confirmed by finding residual errors in each case. The effects of different parameters (fluid and fractional) are also explored on the fluid velocity in fractional environment. Analysis reveals that fractional parameter showed inverse behavior on the fluid velocity in lifting and drainage cases. Moreover, gravitational parameter is prevailing parameter as compared to other fluid parameters in this study.

Nomenclature

T: Cauchy stress tensor
V: Velocity vector
ρ: Density
S: Extra stress tensor
$\mathbf{A_1}$: Rivlin-Ericksen tensor
β: Non-Newtonian Parameter
g: Gravitational force
μ: Material constant
λ_i: Material constants
g_p: gravitational parameter
β_i: Material constants
α: Fractional parameter.

Data Availability

All the data is available with in the manuscript.

Conflicts of Interest

Authors have no conflict of interest on the publication of this article.

References

[1] B. R. Munson and D. F. Young, *Fundamentals of Fluid Mechanics*, John Wiley and Sons, New York, second edition, 1994.

[2] C. Denson, "The drainage of Newtonian liquids entrained on a vertical surface," *Industrial and Engineering Chemistry Fundamentals*, vol. 9, no. 3, pp. 443–448, 1970.

[3] S. B. G. O. Brien and L. W. Schwartz, "Theory and modeling of thin film flows," *Encyclopedia of Surface and Colloid Science*, vol. 1, pp. 5283–5297, 2002.

[4] H. Jeffreys, *The draining of a vertical plate*, St Johns College, 1930.

[5] J. J. V. Rossum, "Viscous lifting and drainage of liquid," *Applied Scientific Research*, vol. 7, pp. 141–145, 1958.

[6] G. Astarita and G. Marrucci, *Principle of Non-Newtonian Fluid Mechanics*, McGraw-Hill, London, 1974.

[7] A. M. Siddiqui, R. Mahmood, and Q. K. Ghori, "Homotopy perturbation method for thin film flow of a third grade fluid down an inclined plane," *Chaos, Solitons & Fractals*, vol. 35, no. 1, pp. 140–147, 2008.

[8] A. M. Siddiqui, R. Mahmood, and Q. K. Ghori, "Some exact solutions for the thin film flow of a PTT fluid," *Physics Letters A*, vol. 356, no. 4-5, pp. 353–356, 2006.

[9] A. M. Siddiqui, R. Mahmood, and Q. K. Ghori, "Homotopy perturbation method for thin film flow of a fourth grade fluid down a vertical cylinder," *Physics Letters A*, vol. 352, no. 4-5, pp. 404–410, 2006.

[10] M. K. Alam, A. M. Siddiqui, M. T. Rahim, S. Islam, E. J. Avital, and J. J. R. Williams, "Thin film flow of magnetohydrodynamic (MHD) pseudo-plastic fluid on vertical wall," *Applied Mathematics and Computation*, vol. 245, pp. 544–556, 2014.

[11] J. A. Deiber and A. S. M. Santa Cruz, "On non-Newtonian fluid flow through a tube of circular cross section," *Latin American journal of chemical engineering and applied chemistry*, vol. 14, pp. 19–38, 1984.

[12] C. S. Yih, "Stability of parallel laminar flow with a free surface," in *Proceedings of the Second U.S. National Congress of Applied Mechanics, ASME*, pp. 623–628, New York, 1955.

[13] L. D. Landau, "On the problem of turbulence," *Comptes Rendus de L'Academie des Sciences de L'URSS*, vol. 44, pp. 311–314, 1944.

[14] J. T. Stuart, "On the role of Reynolds stresses in stability theory," *Journal of Aerospace Sciences*, vol. 23, pp. 86–88, 1956.

[15] C. Nakaya, "Equilibrium states of periodic waves on the fluid film down a vertical wall," *Journal of the Physical Society of Japan*, vol. 36, no. 3, pp. 921–926, 1974.

[16] S. P. Lin, "Finite amplitude side-band stability of a viscous film," *Journal of Fluid Mechanics*, vol. 63, no. 3, pp. 417–429, 1974.

[17] M. R. Zangooee, K. Hosseinzadeh, and D. D. Ganj, "Hydrothermal analysis of hybrid nanofluid flow on a vertical plate by considering slip condition," *Theoretical and Applied Mechanics Letters*, vol. 100357, 2022.

[18] M. M. Gulzar, A. Aslam, M. Waqas, M. A. Javed, and K. Hosseinzadeh, "A nonlinear mathematical analysis for magneto-hyperbolic-tangent liquid featuring simultaneous aspects of magnetic field, heat source and thermal stratification," *Applied Nanoscience*, vol. 10, no. 12, pp. 4513–4518, 2020.

[19] M. Fallah Najafabadi, H. TalebiRostami, K. Hosseinzadeh, and D. D. Ganji, "Investigation of nanofluid flow in a vertical channel considering polynomial boundary conditions by Akbari-Ganji's method," *Theoretical and Applied Mechanics Letters*, vol. 100356, 2022.

[20] M. K. Nayak, A. Wakif, I. L. Animasaun, and M. S. H. Alaoui, "Numerical differential quadrature examination of steady mixed convection nanofluid flows over an isothermal thin needle conveying metallic and metallic oxide nanomaterials: a comparative investigation," *Arabian Journal for Science and Engineering*, vol. 45, no. 7, pp. 5331–5346, 2020.

[21] E. A. Algehyne, A. Wakif, G. Rasool, A. Saeed, and Z. Ghouli, "Significance of Darcy-Forchheimer and Lorentz forces on radiative alumina-water nanofluid flows over a slippery curved geometry under multiple convective constraints: a renovated Buongiorno's model with validated thermophysical correlations," *Waves in Random and Complex Media*, pp. 1–30, 2022.

[22] A. Z. Zaher, K. K. Ali, and K. S. Mekheimer, "Electroosmosis forces EOF driven boundary layer flow for a non-Newtonian fluid with planktonic microorganism: Darcy Forchheimer model," *International Journal of Numerical Methods for Heat & Fluid Flow*, vol. 31, no. 8, pp. 2534–2559, 2021.

[23] S. I. Abdelsalam, K. S. Mekheimer, and A. Z. Zaher, "Alterations in blood stream by electroosmotic forces of hybrid nanofluid through diseased artery: aneurysmal/stenosed segment," *Chinese Journal of Physics*, vol. 67, pp. 314–329, 2020.

[24] J. H. He, "Homotopy perturbation technique," *Computer Methods in Applied Mechanics and Engineering*, vol. 178, no. 3-4, pp. 257–262, 1999.

[25] N. H. Hamad, A. Wakif, and A. Alshehri, "Towards the dynamics of a radiative-reactive magnetized viscoelastic nanofluid involving gyrotactic microorganisms and flowing over a vertical stretching sheet under multiple convective and stratification constraints," *Waves in Random and Complex Media*, pp. 1–31, 2022.

[26] M. T. Inayat Ullah, H. K. Rahim, and M. Qayyum, "Homotopy analysis solution for magnetohydrodynamic squeezing flow in porous medium," *Adv. Math. Phys.*, vol. 2016, article 3541512, 9 pages, 2016.

[27] K. H. Hosseinzadeh, M. R. Mardani, S. Salehi, M. Paikar, and D. D. Ganji, "Investigation of micropolar hybrid nanofluid (iron oxide–molybdenum disulfide) flow across a sinusoidal cylinder in presence of magnetic field," *International Journal of Applied and Computational Mathematics*, vol. 7, no. 5, 2021.

[28] J. H. He, "A coupling method of a homotopy technique and a perturbation technique for non-linear problems," *International Journal of Non-Linear Mechanics*, vol. 35, no. 1, pp. 37–43, 2000.

[29] J. H. He, "Homotopy perturbation method: a new nonlinear analytical technique," *Applied Mathematics and Computation*, vol. 135, no. 1, pp. 73–79, 2003.

[30] J. H. He, "A simple perturbation approach to Blasius equation," *Applied Mathematics and Computation*, vol. 140, no. 2-3, pp. 217–222, 2003.

[31] J. H. He, "Application of homotopy perturbation method to nonlinear wave equations," *Chaos, Solitons and Fractals*, vol. 26, no. 3, pp. 695–700, 2005.

[32] S. Abbasbandy, "Homotopy perturbation method for quadratic Riccati differential equation and comparison with Adomian's decomposition method," *Applied Mathematics and Computation*, vol. 172, no. 1, pp. 485–490, 2006.

[33] J. H. He, "Homotopy perturbation method for solving boundary value problems," *Physics Letters A*, vol. 350, no. 1-2, pp. 87-88, 2006.

[34] A. Yıldırım, "Solution of BVPs for fourth-order integro-differential equations by using homotopy perturbation method," *Computers & Mathematcs with Applications*, vol. 56, no. 12, pp. 3175–3180, 2008.

[35] A. Golbabai and B. Keramati, "Modified homotopy perturbation method for solving Fredholm integral equations," *Chaos, Solitons and Fractals*, vol. 37, no. 5, pp. 1528–1537, 2008.

[36] M. Ghasemi, M. Tavassoli Kajani, and E. Babolian, "Numerical solutions of non linear Volterra Fredholm integral equations by using homotopy perturbation method," *Applied Mathematics and Computation*, vol. 188, pp. 446–449, 2007.

[37] R. Hilfer, Ed., *Applications of Fractional Calculus in Physics*, Academic Press, Orlando, 1999.

[38] I. Podlubny, *Fractional Differential Equations*, Academic Press, NewYork, 1999.

[39] R. Gorenflo and F. Mainardi, *Fractional Calculus: Integral and Differential Equations of Fractional Order*, Springer, Wien and NewYork, 1997.

[40] A. M. Spasic and M. P. Lazarevic, "Electroviscoelasticity of liquid/liquid interfaces: fractional-order model," *Journal of Colloid and Interface Science*, vol. 282, no. 1, pp. 223–230, 2005.

Hindawi
Advances in Mathematical Physics
Volume 2022, Article ID 2706122, 10 pages
https://doi.org/10.1155/2022/2706122

Research Article

Recent Developments and the Causes of Globalization for the Chinese Yuan Based on Statistical Analysis

Tao Ma[1] **and Dali Wang**[2]

[1]*School of Mathematics and Statistics, Qujing Normal University, 655011 Qujing, China*
[2]*School of Physical Education, Yunnan Normal University, 650500 Kunming, China*

Correspondence should be addressed to Dali Wang; king2012310@163.com

Received 9 August 2022; Revised 2 September 2022; Accepted 10 September 2022; Published 21 September 2022

Academic Editor: Qura Tul Ain

We analyze the spatial evolutionary path and spatial evolutionary features of Renminbi (RMB) internationalization from three aspects: transaction intermediary, invoicing unit, and value storage. The main results show that: Firstly, the internationalization of RMB exhibits a certain path expansion pattern, such as initially expands to East Asian countries and regions, then gradually moves to Southeast Asia, Europe, South America, and Australia, and participating countries in the Belt and Road initiative. Secondly, the RMB settlement of cross-border trade presents the "coast-border-inland" spatial characteristics. Thirdly, bilateral currency swap shows "rapid growth" and "unbalanced growth." Finally, the spatial structure of RMB internationalization has the significant features such as "from points to the area and from lines to the area."

1. Introduction

The process of a currency growing from national to international is a process that continuously expands its currency functions performed in the international context. An international currency can simultaneously play the role of transaction intermediary, invoicing unit, and value storage [1]. The internationalization processes of the world's major international currencies (sterling, dollar, euro, etc.) all display geospatial evolutionary features (Lin Lefen, Wang Shaonan, [2]). Because of the influences of economics, politics, and other factors under different historical backgrounds, the world's major international currencies appear different spatial evolutionary structural characteristics.

From the spatial evolutionary characteristics and determinants of Sterling, Dollars, and Euro, currency internationalization is inseparable from a strong economic and political foundation. However, the internationalization path of each currency is different under a specific historical background. Therefore, they provide different insights and experiences for advancing the process of RMB internationalization.

After 44 years of deepening market-oriented reforms, China's economy has grown rapidly and has made remarkable achievements in terms of economic volume and trade volume. China is starting to play a significant role on the international historical stage both in economics and politics. Correspondingly, the RMB is also gradually advancing the internationalization process through cross-border trade settlement, the establishment of bilateral domestic currency trade agreements, and the layout of offshore RMB financial centers. By 2018, cross-border RMB receipt and payment business have been launched in 242 countries and regions, bilateral local currency swap agreements have been signed in 39 countries and regions, and RMB settlement arrangements have been established in 24 countries and regions. In 2021, the aggregate amount of China's cross-border RMB receipt and payment has reached RMB36,600 billion. This paper focuses on the spatial expansion paths and structural characteristics of RMB in the internationalization process, which would be different from the world's major international currencies discussed above. The analysis is demonstrated from the three major functions of a currency: transaction intermediary, invoicing unit, and value storage.

The rest of the paper is organized as follows. The second section is the main body of this paper. We analyze the spatial evolutionary path of RMB internationalization. The process of RMB internationalization is studied with the following five aspects; settlement in cross-border trades, bilateral currency swap agreements, as an international reserve currency, offshore financial centers, and Belt and Road iniative (Wu Shuyu, Li Daokui, [3]). Section 3 analyzes the structural characteristics of the spatial evolution of RMB internationalization and the main factors to determine the evolutionary pattern. The fourth section concludes there were 40 countries and regions in which the central banks or monetary authorities have signed bilateral currency swap agreements with the People's Bank of China by the end of June 2022, and 25 countries and regions have established RMB clearing mechanisms with China by the end of 2020 [4](source: http://www.pbc.gov.cn).

The internationalization of the RMB is a process in which the spatial scope of the monetary function continues to expand. It is essentially a spatiotemporal phenomenon; that is, based on the comprehensive strength of the country, and driven by national policies, the spatial scope of RMB performing its international monetary function is expanding with the migration of time.

The Chinese Yuan is the only currency of a developing country that entered into the Special Drawing Rights (SDR) basket of the International Monetary Fund (IMF). The process of RMB internationalization has been deeply developed in various forms such as cross-border business, currency swaps, and offshore business since RMB is official to be used in cross-border trade settlement in July 2009. Some breakthroughs have been achieved in major areas such as that the ranking of RMB used as international payments has continuously increased, RMB has joined the special drawing rights (SDR) in 2016, and different spatial divisions have been formed. The process of RMB internationalization has formed its spatial structure and spatial characteristics. To our knowledge, there is not much research on the geospatial evolutionary path and evolutionary characteristics of currency internationalization in the literature. The main current situation of RMB internationalization is as follows [5].

In the aspect of international payments, according to SWIFT data, the RMB is the fifth largest global payment currency in the world, accounting for 2.20% of all global currency payments in July 2022 (source: http://www.swift.com).

In the aspect of cross-border trade RMB settlement and cross-border RMB receipts and payments, it has officially promoted the internationalization of the RMB in China through cross-border trade using RMB settlement since 2009. The cross-border trade RMB settlement amount was only 3.580 billion Yuan in 2009. China's cross-border trade RMB settlement amount reached 7.94 trillion Yuan in 2021, which is about 2218 times compared that of 2009. The RMB has been China's second largest international payment currency for eight consecutive years, and the cross-border RMB payment in 2020 reached 45.27 trillion Yuan by CIPS (Cross-border Interbank Payment System). There were 75.07% of the RMB offshore market receipts and payments occurred in Hong Kong in June 2020 (source: http://www.pbc.gov.cn).

In the aspect of reserve currency, the RMB entered the currency basket of the International Monetary Fund as a separate currency and became one of the world's eight official foreign exchange reserve currencies in the fourth quarter of 2016 with a share of 10.92%. The absolute value of the RMB as a foreign exchange reserve currency was US$90.288 billion, accounting for 1.07% of the world's eight major currencies, ranking seventh among the world's eight major foreign exchange reserves, only higher than the Swiss franc in the fourth quarter of 2016. There were at least 70 central banks or monetary authorities around the world which take RMB as their foreign exchange reserves, making the RMB the fifth largest reserve currency in the world by the end of the fourth quarter of 2019. The RMB continues to maintain its international status as the world's fifth largest reserve currency in the first quarter of 2022. The absolute value of the RMB as foreign exchange reserves in quarter 1 of 2022 was 336.39 billion US dollars, accounting for 2.88%, surpassing Canadian dollars, Australian dollars, and Swiss francs. The share of RMB in the IMF currency basket increased to 12.28% in May 2022 (Source: http://www.imf.org).

In addition, the RMB has become the world's third largest trade financing currency, accounting for 3.07% in July 2022. It is the fifth largest spot foreign exchange currency (source: http://www.swift.com).

There are tons of research works and literature on RMB internationalization. Cheung et al. (2019) studied the spatial pattern of the geographical distribution and diffusion of RMB; however, they focused on offshore transactions. Based on the meaning of international currency which is a natural extension process from the national scope to the international scope (Li 2013), we comprehensively examine the spatial structure characteristics formed by RMB's currency functions exceeding its original using areas. Li (2009) interprets currency internationalization as a dynamic process that some or all functions of a currency expand from its original using area to neighboring countries or regions and finally evolve into a global universal currency. From circulation means, payment, invoicing and value storage, and the four major functions of currency, we examine the spatial pattern formed by the gradual expansion of using RMB in the world. Thereby, we try to refine the rules and insights in the process of RMB internationalization [6–8].

The rest of the article is as follows: Part 2 mainly analyzes the performance of RMB's international currency functions, including circulation, payment and settlement, and value storage. Part 3 mainly analyzes the reasons for RMB's spatial evolution and its spatial characteristics. Part 4 is the conclusion and outlook.

2. RMB Performs International Currency Functions

We discuss the space expansion paths of the RMB in the past ten years from the perspective of RMB fulfilling different functions such as the means of circulation, means of payment, and value storage.

2.1. RMB Performs International Circulation Currency. The RMB has gradually become a currency in circulation in some regions outside China, mainly in parts of the three Southeast Asian countries, including Myanmar, Vietnam, and Laos, which border China's Yunnan Province. Due to China's political stability, sustained and stable economic growth, and stable currency value of RMB, the RMB has gradually been trusted and accepted by people in these border areas. In some areas, the RMB has even replaced the local currency, becoming the local hard currency and circulated and used locally. For example, in the second special zone of Shan State in Myanmar (Myanmar Wa State), the RMB has become the local currency instead of the Myanmar kyat and the US dollar. In the three northern provinces of Phongsali, Nanta, and Urumsai in Laos, the usage of RMB in cash is greater than that of Laos Kip. Vietnamese residents on the Sino-Vietnamese border also generally hold RMB in cash as the main currency in circulation [7–10].

2.2. RMB Performs Payment and Settlement Functions

2.2.1. The Ranking and Proportion of RMB as an International Payment Currency. When China officially promoted the internationalization of the RMB, the ranking of the RMB among international payment currencies was relatively low. In the second year of China officially promoting its internationalization, the RMB as an international payment currency ranked only 35th in October 2010 [11]. In recent years, the RMB's ranking among international payment currencies has greatly improved, and is roughly stable between the 5th and 7th international payment currencies, as shown in Table 1.

Table 1: RMB as an international payment currency.

Time	Ranking of RMB as an international payment currency	Proportion (%)
Oct. 2010	35	
Oct. 2011	17	0.29
Oct. 2012	16	0.42
Oct. 2013	12	0.84
Oct. 2014	7	1.59
Oct. 2015	5	1.92
Oct. 2016	6	1.67
Oct. 2017	7	1.46
Oct. 2018	6	1.7
Oct. 2019	6	1.65
Oct. 2020	6	1.66
Oct. 2021	5	1.85
July. 2022	5	2.20

Source: http://www.swift.com.

2.2.2. Cross-Border Trade RMB Settlement and Its Geospatial Evolution Characteristics. The geospatial evolution of RMB settlement in cross-border trade has gone through the following three stages.

In July 2009, China officially launched the RMB settlement in cross-border trade. There were only Shanghai and 4 cities in Guangdong Province (Guangzhou, Shenzhen, Zhuhai, and Dongwan) within the inland territory of the settlement pilot, and only Hong Kong, Macao, and ASEAN countries within the overseas territory [12, 13].

In June 2010, the People's Bank of China and other 5 ministries and commissions jointly issued the "Notice on Relevant Issues Concerning the Work of Expanding the Pilots for RMB Settlement in Cross-border Trade." The inland pilots have been expanded to 20 provinces (autonomous regions and municipalities)[①] Specifically, these regions include Shanghai, Guangdong, Beijing, Tianjin, Neimenggu, Liaoning, Jilin, Heilongjiang, Jiangsu, Zhejiang, Fujian, Shandong, Hubei, Guangxi, Hunan, Chongqing, Sichuan, Yunnan, Xizang, and Xinjiang., and the overseas pilots have covered all countries and regions [14].

In July 2011, the People's Bank of China and other 5 ministries and commissions again jointly issued the "Notice on expanding the RMB settlement areas in cross-border trade." RMB settlement in cross-border trade within an inland territory has expanded to the whole country [15].

Figure 1 exhibits the spatial evolutionary process of the cross-border RMB settlement pilot areas from July 2009 to July 2011. China started to introduce RMB internationalization in 2009, which is why we took the data from 2009 to 2011 for this study. We cannot choose the data from 2000 to 2011 as the RMB internationalization pilot was not launched in these years. One can see that it is a quick process that the cross-border RMB settlement areas increased from 5 cities to the whole world. The spatial evolutionary structure shows a "coast—border—inland" characteristic.

The spatial expansion process of the RMB settlement pilots for cross-border trade in the domestic territory presents the spatial structure characteristic of "coastal—border—inland." There are three main reasons for this kind of characteristic:

Firstly, the degree of openness and the level of international trade in coastal cities is relatively high in China. According to the data from the National Bureau of Statistics, in the first year of the pilot RMB settlement in cross-border trade (2009), the total import and export volume was 220.7535 billion US dollars in the whole country. As the first group of domestic pilot regions, Shanghai, Guangzhou, and Shenzhen contributed 28.3% of the total import and export trade volume, which was as high as 624.622 billion US dollars. The relatively high degree of openness and the high level of international trade is the main reason why these coastal cities were selected as the first batch of pilots (source: http://www.pbc.gov.cn).

Secondly, the provinces along the border have relatively geographical advantages. As shown in Figure 1, the second batch of pilots not only included coastal provinces but also expanded to all provinces along China's borders. These provinces have geographical advantages over different countries in Asia. One of the important reasons to identify this pilot is to expand the cross-border use of RMB in international trade through geographical advantages.

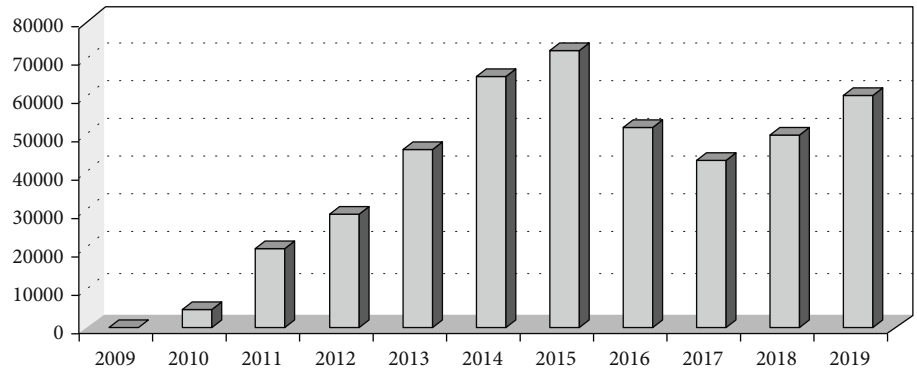

Figure 1: The cross-border RMB Settlement from 2009 to 2019. Source: http://www.pbc.gov.cn.

Thirdly, RMB internationalization is the strategic requirement for a complete national plan. After two pilot schemes, to accelerate the pace of RMB internationalization, it is necessary to concentrate the resources of all provinces across the country to further expand the cross-border use of RMB worldwide. In terms of the degree of openness, international trade, and geographical advantages, inland provinces and regions are less than coastal cities. However, the national development strategy of RMB internationalization determines that the cross-border RMB settlement business inevitably spreads to the whole country.

Unlike the gradual expansion in space of the domestic cross-border RMB settlement pilot areas, the overseas RMB cross-border settlement pilot expanded directly from the "Hong Kong, Macao, and ASEAN" regions to the whole world without any other transition. As the two special administrative regions under the condition of "one country, two systems" in China, Hong Kong and Macau were selected to be the first pilot areas, which is reasonable because of their historical and geological advantages.

As a whole, ASEAN plays an increasingly important role in the regional economy, and it is also the most important cooperation area among Chinese trade partners except the USA. Moreover, there does not exist a strong international currency in ASEAN countries and regions. There also exist certain geographical advantages between ASEAN and China. Therefore, there are special geographical factors and economic reasons that Hong Kong, Macao, and ASEAN were selected in the first group [16].

There are potential possibilities for all countries and regions that have international trade with China to use RMB for cross-border trade settlement. Therefore, to promote RMB internationalization through cross-border trade settlement, it is necessary to practice RMB settlement in cross-border trade around the whole world and explore the possibility that RMB performs international currency functions in a wider space.

It can be seen clearly from Figure 1 that the volume of cross-border RMB settlement was increasing rapidly over the above-mentioned three stages. The accumulated volume of cross-border RMB settlements handled by commercial banks has increased from 3.58 billion Yuan in 2009 to 6.04 trillion Yuan in 2019, an increase of about 1,687 times. The RMB settlement business of cross-border trade showed an upward trend in volatility from 2009 to 2019.

Table 2: Cross-border RMB settlement or receipt and payment from 2015 to 2021.

Year	Amount	One hundred million Yuan Remarks
2014	6550,000.00	Cross-border RMB settlement
2015	12,100,000.00	Cross-border RMB receipt and payment
2016	9,850,000.00	Cross-border RMB receipt and payment
2017	9,190,000.00	Cross-border RMB receipt and payment
2018	15,850,000.00	Cross-border RMB receipt and payment
2019	19,700,000.00	Cross-border RMB receipt and payment
2020	28,400,000.00	Cross-border RMB receipt and payment
2021	36,600,000.00	Cross-border RMB receipt and payment

Source: http://www.pbc.gov.cn, *China Monetary Policy Implementation Report from 2014 to 2021.*

2.2.3. The Situation of Cross-Border RMB Receipts and Payments. Since 2015, the "Monetary Policy Implementation Report" issued by the People's Bank of China has transformed the RMB from the original concept of simple cross-border trade RMB settlement to a broader concept of cross-border RMB receipts and payments, covering both the current account and capital account, as shown in Table 2.

2.3. RMB Performs Value Storage Function: The Spatial Evolutionary Characteristics of RMB as an International Reserve Currency. More than 70 central banks or monetary authorities around the world have included RMB in foreign exchange reserves, and RMB was the world's fifth largest reserve currency in the 1st quarter of 2022 [17] (source: http://www.imf.org).

In addition, the number of countries holding RMB as official foreign currency assets has increased so has in amount. According to a survey of 130 member countries conducted by the IMF in 2015, there were 27 countries holding RMB as official foreign currency assets in the world in 2013, and the number has been up to 38 by 2014 [18] (source: http://www.imf.org).

The number of RMB assets held worldwide was equivalent to 29 billion special drawing rights (SDR) in 2013, which is about 0.7% of total official foreign currency assets. This number reached 51 billion SDR by 2014, which is equivalent to 1.1% of total official foreign currency assets [19]. By the end of June 2021, overseas entities holding RMB financial assets reach RMB10.26 trillion (source: http://www.imf.org).

3. The Motivation Mechanism and Spatial Evolutionary Features of RMB Internationalization

The reasons why the internationalization of the RMB presents such spatial evolutionary features can be summarized in two main aspects: the basic momentum driven by market demand and proactively promoted by national strategies and policies.

3.1. Analysis of the Basic Momentum Driven by Market Demand. In terms of market demand, because of the foundations of China, such as China's total economic volume, international trade level, international investment, and the relative stability of the RMB currency, the demand for RMB for international usage has been increasing in the international markets. The specific manifestations are as follows.

3.1.1. China's Economy. In terms of economic strength, China has achieved world-renowned achievements in economic development since its reform and opening up in 1978. China's GDP was already comparable with Japan and ranked second in the world by 2008. China's total GDP reached $5,122 billion, following the USA ($14,418.73 billion) ranked second in the world, and surpassing Japan ($5,035.140 billion) for the first time in 2009. China officially started a pilot program of RMB settlement for cross-border trade to promote the internationalization of the RMB in July 2009. From the perspective of time, it should not be just a coincidence, but a strategy taken proactively when the country's economic strength reached a certain stage. Since 2009, China's GDP has remained second in the world, and the total amount has further increased. China became the second country in the world to reach 10 trillion US dollars after the USA when China's GDP reached $10,557.64 billion in 2014. While further narrowing the gap with the USA, the gap in GDP between China and Japan was getting wider. China's GDP was $13,118.69 billion, a year-on-year increase of 6.1% in 2019. In 2021, China's GDP was USD17,458.04 billion, and it continued to maintain its status as the world's second largest economic capacity (source: http://www.imf.org).

3.1.2. China's International Trade. Merchandise import and export trade is China's main body of international trade. From the perspective of total merchandise import and export trade, China's merchandise import and export trade volume broke through the 4 trillion US dollar for the first time in 2013, reaching $41,589.99 billion. For the first time, China's trade volume surpassed the USA which was $39,086.53 billion. China became the largest country in terms of trade volume in commodity imports and export in the world. China's total merchandise import and export trade continued to rank first in the world in 2014 and 2015. China's total merchandise import and export trade continued to maintain a high level, ranking second in the world in 2016. China's total import and export volume was $4.11 trillion with a year-on-year increase of 11.4% in 2017, $4.62 trillion with an increase of 12.6% in 2018, $4.57 trillion in 2019, and USD6.05 trillion in 2021. In general, China's total international trade scale is already the second largest in the world. The huge scale of international trade objectively requires the RMB to become the invoicing and settlement currency in international trade, which helps to avoid foreign exchange rate fluctuations causing exchange losses to the majority of importers and exporters. International trade is becoming one of the main economic factors driving the internationalization of the RMB (source: http://www.wto.org).

3.1.3. China's International Investment. Global foreign direct investment outflows declined for the third consecutive year until 2018. According to the statistics of the World Investment Report 2019 of the United Nations Conference on Trade and Development, the global foreign direct investment (FDI) flow was $1,014.17 billion in 2018, a decrease of 28.9% from the previous year's $1,425.44 billion. Facing the complex international investment environment, China thoroughly implements new development proposals, fulfilled high-quality development requirements, and increased the effort of policy guidance and public services. China's foreign investment made steady progress in 2021 with an aggregate amount of USD145.19 billion. The global share of FDI stock further increased, and the influence of global FDI has further expanded (source: http://www.mofcom.gov.cn/).

China's FDI flow was $153.71 billion in 2021, taking 1st place in the world. From third place in the world in 2017, it returned to first place which reached the highest value in history (source: http://www.mofcom.gov.cn/).

3.2. Actively Propelling through National Strategies and Policies

3.2.1. National Strategies. "Peace, development, cooperation, and win-win" is China's development strategy for a big and powerful country which was proposed in the report of the 18th National Congress of the Communist Party of China. This strategy is an important and scientific ideology for China to actively face the challenges of economic globalization. The most important part of economic globalization is the globalization of finance. In particular, the global financial crisis has obvious international shocks, which indicates that the current international monetary system is overreliance on the US dollar, and the US dollar standard system faces many problems and contradictions. Therefore, the internationalization of the RMB is the key and core to propelling the evolution of the international currency system and constructing a diversified international reserve currency system. It is the joint choice by the international markets and China's development strategy. China's strategy of "peace, development, cooperation, and win-win" is completely different from the

historical rise of colonialism and imperialism relying on aggression and plunder. Instead, it achieves a mutually beneficial and win-win situation between the international society and other countries and regions through the reform of its economic system and economic cooperation.

The internationalization of the RMB has *de facto* become one of the national strategies related to national economic and social development when it was officially written into China's "13th Five-Year Plan." It is an important part and manifestation of the financial development strategy. The process of RMB internationalization should be based on the transformation of China's economy and finance. The internationalization of the RMB will be naturally realized driven by both markets and national strategy when the economic and financial transformation is succeeded, and China becomes a country not only with GDP in scale but also with powerful GDP and strengthened finance. Therefore, as one of the national strategies, the process of internationalization of the RMB is propelled by the government and the market. On the one hand, it is a natural result when the development of China's economy and international trade reaches a certain level. On the other hand, it is undoubtedly the right choice for the current government.

Before the official internationalization of the RMB, the reliance of the RMB on the international monetary system (IMS) exhibits a dependence on the US dollar due to the strong position of the US dollar in the IMS. The RMB has changed into a reformer in the IMS from a follower since the official implementation of the RMB internationalization strategy. This strategic change has already achieved some results; for instance, the RMB has joined the IMF's SDRs currency basket and has begun to appear in the world's official foreign exchange reserves as an independent currency.

In summary, the RMB internationalization strategy is an important part of China's development strategies for a big country and a powerful country. It emphasizes "peace, development, cooperation, and win-win" with other countries and regions, which fulfills both China's national interests and the interests of other countries in the world.

3.2.2. The Belt and Road Initiative and RMB Internationalization. In 2013, Chinese President Xi Jinping successively proposed the cooperation initiatives of the "New Silk Road Economic Belt" and the "21st Century Maritime Silk Road." Using the historical symbols of the ancient Silk Road, this initiative aims to expand the current cooperation in various fields and at various levels, such as political mutual trust, economic trade, and culturally inclusive. This cooperation is referred to as the Belt and Road initiative (Benjamin J Cohen, [6]; Zhang F, Yu M, Yu J, et al. [19]).

The Belt and Road has an obvious linear characteristic in geographical space. Since the initiative is proposed, high-level visits between countries along the route have become more frequent, economic and trade exchanges have been closer, and financial cooperation has been further strengthened (Eichengreen B, [8]). In this process, the usage scope of RMB has expanded in these countries along the route. Various measures have been made, such as projects investment in the "Silk Road Fund", and the establishment of branches of Chinese banks such that the China union pay cards and ATMs covered more than 50 countries along the route.

SWIFT evaluates the situation of UMB usage in countries along the Belt and Road using the RMB payment amount issued by China from January 2014 to June 2017. Based on these data, it is pointed out that RMB usage in the Belt and Road regions has four characteristics.

First, the amount of RMB usage in commercial payments in the four countries, Kazakhstan, Kyrgyzstan, Tajikistan, and Turkmenistan, shows favorable signs of growth. The absolute amount of paying in RMB is still relatively low compared to countries such as France or Germany; however, China's RMB payments to these countries display a growth rate of higher than 100%.

Second, the RMB business growth prospects in Southeast Asian countries of the "Maritime Silk Road" are favorable. China's RMB commercial payments to Indonesia, Malaysia, Thailand, and Vietnam have increased significantly.

Third, the adoption rate of RMB in other markets of the "Maritime Silk Road" is low. The countries along the "Maritime Silk Road" such as Egypt, Kenya, Greece, and India RMB payments received were lower.

Fourth, the RMB payment situation was more diversified in the Western European markets. China's RMB payments to Germany, Poland, and the Czech Republic have grown strongly, while China's payments to the Netherlands, France, and Italy have fallen sharply.

In general, the usage of RMB in the regions of Belt and Road was concentrated in the main offshore RMB centers by June 2017.

The increase in the layout of offshore RMB centers implies that the internationalization of the RMB presents a "multi-point" spatial distribution status in geographic space, while the Belt and Road has obvious a feature of lines. No matter which features appears, points, or lines, it will eventually provide a possibility of spatial expansion of the RMB internationalization to more areas from points or lines.

3.2.3. Bilateral Local Currency Swap Agreement. From October 2008 to the end of 2009, there were only 6 countries and regions (South Korea, Hong Kong, Malaysia, Indonesia, Belarus, and Argentina) signed bilateral local currency swap agreements with the People's Bank of China, with a total amount of 650 billion Yuan.

The People's Bank of China has signed bilateral local currency swap agreements with central banks or monetary authorities of 39 countries and regions by the end of 2019. It covers most developed and emerging economies around the world, as well as major offshore RMB markets, with a total amount exceeding 3.7 Trillion Yuan.

As the most important portal city to connect mainland of China and the outside world, Hong Kong is the core city of RMB internationalization and the most important RMB offshore market. The currency swaps in Hong Kong increased from 200 billion Yuan in 2009 to 400 billion Yuan/470 billion HKD in 2017.

As one can be seen from Table 3, by the end of July 2017, more than 50 countries and regions have signed bilateral

Table 3: Countries and regions which have signed bilateral currency swap agreements with the Central Bank of China from 2008 to 2019.

Year	Countries or regions
2008	Republic of Korea, Hong Kong, China, Malaysia, Indonesia, Belarus, Argentina
2010	Singapore, Iceland
2011	Thailand, New Zealand, People's Republic of Mongolia, Pakistan, Uzbekistan
2012	Australia, the United Arab Emirates, Turkey, Ukraine
2013	Brasil, UK, Hungary, Albania, Central Bank of Europe
2014	Russia, Canada, Argentina, Swiss, Kazakhstan, Sri Lanka, Qatar
2015	South Africa, Surinam, Armenia, Chile, Tajikistan
2016	Morocco, Egypt
2018	Japan
2019	Macao China
2020	Laos

currency swap agreements with China. From the geographic point of view, the number of bilateral currency swap agreements exhibits a trend of further expansion.

Since 2009, the countries and regions that have signed bilateral currency swap agreements with China have not only increased rapidly in number, from 6 in 2009 to 52 in early 2020, but also covered Europe, Asia, Africa, South America, Oceania, and North America. The geographic spatial distribution of countries and regions that have signed agreements with China shows an uneven feature of growth. This uneven feature is demonstrated most significantly when we compare North America, Oceania, and Africa.

3.2.4. RMB Offshore Financial Center. China has established 26 RMB clearing banks in 24 countries and regions outside of China by June 2020, covering Asia, America, Europe, Oceania, and Africa, for the foreign entities' convenience holding and using RMB. Except for JPMorgan Chase Bank in the USA and Mitsubishi UFJ Bank in Japan, these RMB clearing banks are all held by major Chinese banks (see Table 4 for details).

These RMB clearing banks facilitate offshore RMB transactions and cross-border RMB payments.

At present, the most important five *points* are Hong Kong, China, the UK, Russian Federation, Singapore, and the USA. The offshore RMB market share of the 5 offshore centers accounts for about 87.93 percent of the global offshore RMB market share. China has designated 24 offshore RMB financial centers scattered around the world by 2021, and it will be possible to spread the international usage of RMB to the "areas" involved in these "points." The Belt and Road initiative has continuously strengthened the use of RMB in financial investment and financial services in countries along the route, which plays a role in the expansion of RMB internationalization from "points" to "areas" (source: http://www.swift.com).

As the world's largest and most efficient offshore RMB center, Hong Kong has always played an important role in the process of RMB internationalization since its offshore RMB business started in 2004. The RMB business maintains rapid growth or above a high level in Hong Kong. It plays an important role in various fields such as RMB deposits, RMB settlement in cross-border trade, RMB direct investment, RMB investment in financial markets, and RMB international bond issuance. In July 2022, Hong Kong still takes the 1st place of offshore RMB businesses with a share of 70.93% (source: http://www.swift.com).

London is the first offshore RMB center outside Asia that can carry out RMB clearing business. It is the second largest RMB offshore clearing center. Its market share of offshore RMB business accounts for 6.35% of the global share in July 2022. It plays an important role in expanding the usage of RMB overseas and accelerating the process of RMB internationalization (source: http://www.swift.com).

The offshore financial center in Russian Federation allows its qualified institutional investors to enter China's security markets and make RMB offshore investments. It also allows qualified institutional investors from Mainland China to invest in Russian capital markets using RMB. The usage scope of RMB has been further expanded through the Russian offshore financial center. The share of offshore RMB business accounts for 3.90% of the global share in July 2022 which takes the 3rd place in all the offshore RMB centers (source: http://www.swift.com).

3.3. Adjustment of International Political and Economic Relations and Opportunities for Reform of the International Monetary System. The world economy has shown a development trend from "one super" to "one super, multiple powers" since World War II. Regional economic integration and global economic integration have been further strengthened.

From the period after World War II to the early 1970s, the USA occupied a dominant position in the world economy, with strong industrial strength and abundant gold reserves. It controlled the international financial market and world markets of commodity and trade services by establishing and controlling the Bretton Woods system and the General Agreement on Tariffs and Trade.

The USA also implemented the "Marshall Plan" during this period to help Western European countries revive from the damages of war. From the 1970s to the late 1980s, the unbalanced economic development of capitalist countries still existed. The European Community and Japan made great progress in many economic fields, and then, the capitalist world presented a three-polar situation of the USA, the European Community, and Japan.

Since the 1990s, the degree of the economic interdependence of countries has further deepened, and the trend of world economic regional clustering and global economic integration has continued to strengthen, with a further strengthening of production and division of labor and the huge impact of the new technological revolution. At this stage, the process of European economic integration has accelerated; ASEAN regional cooperation has been further

Table 4: Offshore RMB clearing center and clearing banks.

Item	Cities	Clearing bank	Start time	Belongs to
1	Hong Kong China	Bank of China	Dec. 2003	Asia
2	Macao, China	Bank of China	Sep. 2004	Asia
3	Vientiane, Laos	Industrial and Commercial Bank of China	Jun. 2012	Asia
4	Taiwan, China	Bank of China	Dec. 2012	Asia
5	Singapore	Industrial and Commercial Bank of China	Feb. 2013	Asia
6	Phnom Penh, Cambodia	Industrial and Commercial Bank of China	Mar. 2014	Asia
7	London, UK	China Construction Bank	Jun. 2014	Europe
8	Frankfurt, Germany	Bank of China	Jun. 2014	Europe
9	Seoul, Korea	Bank of Communications	Jul. 2014	Asia
10	Paris, France	Bank of China	Sep. 2014	Europe
11	Luxembourg	Industrial and Commercial Bank of China	Sep. 2014	Europe
12	Doha, Qatar	Industrial and Commercial Bank of China	Nov. 2014	Asia
13	Toronto, Canada	Industrial and Commercial Bank of China	Nov. 2014	North America
14	Kuala Lumpur, Malaysia	Bank of China	Jan. 2015	Asia
15	Bangkok, Thailand	Industrial and Commercial Bank of China	Jan. 2015	Asia
16	Sydney, Australia	Bank of China	Feb. 2015	Oceania
17	Santiago, Chile	China Construction Bank	May. 2015	South America
18	Budapest, Hungary	Bank of China	Jun. 2015	Europe
19	Johannesburg, South Africa	Bank of China	Jul. 2015	Africa
20	Argentina	Industrial and Commercial Bank of China	Sep. 2015	South America
21	Lusaka, Zambia	Bank of China	Sep. 2015	Africa
22	Zurich, Switzerland	China Construction Bank	Nov. 2015	Europe
23	New York, USA	Bank of China	Sep. 2016	North America
24	New York, USA	JP Morgan Chase Bank	Feb. 2018	North America
25	Tokyo, Japan	Bank of China	Oct. 2018	Asia
26	Tokyo, Japan	Mitsubishi UFJ Bank	Jun. 2019	Asia

Source: according to public information.

strengthened; China's economy has risen and become an important role in the world economy; and Japan remains the third largest economy in the world.

Neoliberalism quickly became popular and gradually formed an international financial system with the collapse of the Bretton Woods system in 1973. The Washington Consensus was formed in 1990. Global economic integration and economic financialization were rapidly developed, and financial centers rapidly evolved and formed networks (CFCI, 2019).

The adjustment and evolution of international political and economic relations inevitably brought about the adjustment of the international multipolar political and economic structure. The currency is a manifestation of the political and economic strength of a country or region. Therefore, the opportunity for diversified adjustment of the international politics and economy provided an opportunity for China to adjust its international position and the internationalization of the RMB.

The subprime mortgage crisis originated in the USA and brought financial turmoil that hit the world in 2008. This financial crisis further highlighted the shortcomings of the US dollar standard in the international monetary system.

The European Union and Russia also advocate reforms to the international monetary system, although they have different concerns. This requirement proposed by major economic entities and regions in the world has caused the reform of the international monetary system to develop from theoretical discussions to practical policies.

The Chinese Ministry of Finance issued 3 billion offshore RMB bonds in London in May 2016, which accelerated the internationalization of the RMB. The overseas investment by Chinese companies has greatly increased since China joined the WTO. China's industry-wide FDI reached US$117.12 billion in 2019. By the end of 2021, the number of investors outside China who hold RMB bonds reached 4 trillion. China participates in the global economy and promotes the internationalization of the RMB (Source: https://www.bbtnews.com.cn/).

The RMB officially joined the SDR (Special Drawing Rights) currency basket on October 1, 2016, with a share of 10.92%. After continuous efforts, which created a new situation in the international monetary system, that is, as the currency of a developing country, the RMB joined the international monetary system first, which provides new possibilities for countries to choose more diversified reserve currencies, trade settlement currencies, and payment

currencies in the international monetary system. On August 1, 2022, RMB's share in the SDR currency basket rises to 12.28% (source: http://www.imf.org).

3.4. The Rational Choice of the Geographic Status Quos of Asian Currencies. Currently, there are huge differences in various political situations such as social systems, political systems, and state formation among Asian countries. It does not meet Mundell's criteria of "the optimum currency area" which is only suitable for areas that are continuously integrated with politics. In other words, the term "Asian Dollar" proposed in academics does not work in terms of political integration. At present, the vast majority of Asian countries are still issuing and circulating their currencies in their respective territories. However, due to historical, political, economic, and other reasons, some Asian countries and regions have shown other different characteristics in currency geography, which are prominently shown in the following three aspects:

First, multiple currencies are issued and circulated within the territory of a country. For instance, there exist four currencies in China issued in Mainland, Hong Kong, Macao, and Taiwan.

Second, a currency with a higher degree of internationalization is adopted as the local currency. For example, Cyprus has joined the Eurozone and fully adopts the Euro as its domestic currency; East Timor adopts the US dollar as its domestic currency; and the country only issues coins as fractional currency, which is equivalent to the US dollar in value.

Third, there are no currencies issued but two currencies circulating in the country at the same time. For instance, Palestine does not yet have its currency, and both Israeli currency (shekel) and Jordanian currency (dinar) are circulated in the country.

The concept of the "Asian Dollar" can only stay at the stage of conception. McKinnon (2004) has been aware of this issue. He said, "At present, the political will for full-scale economic and monetary integration with neighboring countries simply does not exist elsewhere. However, a less politically demanding common monetary standard based on a key currency might achieve much – although certainly not all – of the benefits of a common currency." This argument still applies to the current situation in Asia. In other words, the "Asian Dollar" does not apply to Asia at the moment. Regarding the RMB as a key currency, firmly propelling the internationalization of the RMB is another way to realize the internationalization of the RMB. It also meets the McKinnon criteria of "a less politically demanding common monetary standard based on a key currency."

McKinnon further pointed out that a successful common monetary standard requires two key interrelated conditions:

(1) A credible anchoring mechanism so that countries that attach themselves to the standard succeed in stabilizing the purchasing powers of their national monies

(2) Close trading partners who attach themselves convincingly to the same standard

With the continuous strengthening of China's economy, the RMB has joined the IMF's currency basket and has continued to rise in the rankings of international payment currencies. The status of the RMB in the international currency system is continuously improving. The credit anchoring mechanism with RMB as the key currency might be mature. It is more realistic and feasible to steadily promote the internationalization of the RMB than the assumptions of the "Asian Dollar" or "China Dollar."

4. Conclusions and Outlook

We analyzed the spatial evolutionary characteristics of RMB internationalization and further explained the mechanism of the spatial evolutionary structure of RMB internationalization from the perspective of domestic and foreign motivations.

The main findings are as follows:

Firstly, the RMB has evolved from the pure simple RMB settlement in cross-border trade to a broader concept of cross-border RMB payment since the official launch of RMB internationalization in 2009, which covered both the current account and capital account.

Secondly, the spatial evolutionary path of RMB internationalization presents a certain spatiotemporal pattern. It initially expanded to East Asian countries and regions, gradually expanded to developing countries in Southeast Asia, and then advanced to developed countries in Europe, South America, and Australia and participating countries along the Belt and Road.

Thirdly, the RMB settlement of cross-border trade presents the "coast-border-inland" spatial characteristics.

Fourthly, bilateral currency swaps show "rapid growth" and "unbalanced growth."

Fifthly, the spatial structure of RMB internationalization has obvious characteristics of "from points to areas, and from lines to areas" because of the impetus from the RMB offshore financial centers, RMB clearing banks, and the Belt and Road initiative. The "points" mainly refer to the spatial characteristics of RMB offshore financial centers, and the "lines" mainly refer to the linear characteristics of the Belt and Road.

Sixthly, China's economic strength is still the decisive factor in the internationalization of the RMB, and import and export trade volume and foreign investment are important driving forces.

Looking into the future, the role of the RMB as an international payment currency, foreign exchange reserve currency, and trade settlement currency will be further strengthened. The RMB will inevitably perform various functions of an international currency in a broader geographic space in the future. However, the strong position of the US dollar and the Euro in the existing international monetary system remains, and the historical advantages of the British pound and the Japanese yen still exist. The currency competition faced by the internationalization of the RMB is mainly the above four international currencies. However, from the absolute amount and proportion perspective, the difference between the RMB, as a foreign exchange reserve currency, and international payment currency, the British pound, and the Japanese yen is not too

big. As China's economic strength, international trade, and foreign investment are continuously enhanced, it is hopefully expected that the RMB will surpass the British pound and the Japanese yen in a near future. The position of the RMB in the international monetary system will be further enhanced, too.

Data Availability

The data on the Renminbi ranking and proportion are obtained from the official website of SWIFT. Other data regarding RMB cross-border receipt and payment are obtained from the official website of the People's Bank of China. All the data are available from the corresponding author upon request.

Conflicts of Interest

The authors declare that there are no conflicts of interest regarding the publication of this paper.

Acknowledgments

This research is supported by the Key National Natural Science Foundation of China, "Research on the Heterogeneous Constraints of Financial Cooperation Between Yunnan and Surrounding Countries and the Realization Mechanism and Path of RMB Regionalization" (No. U2002201).

References

[1] P. B. Kenen, "The international position of the dollar in a changing world," *International Organization, Cambridge University Press*, vol. 23, no. 3, pp. 705–718, 1969.

[2] L. Lefen and W. Shaonan, "An empirical analysis of the influencing factors of RMB internationalization in the process of "the Belt and Road" [J]," *Studies of International Finance*, vol. 2, pp. 75–83, 2016.

[3] W. Shuyu and L. Daokui, "A new measure of currency internationalization—an analysis based on the perspective of international financial investment[J]," *Economic Perspectives*, vol. 2, pp. 146–158, 2018.

[4] People's Bank of China, *Renminbi Internationalization Report[R]*, People's Bank of China, 2017, 2021.

[5] P. Bottelier and U. Dadush, "The future of the Renminbi as an international currency[N]," *International Economic Bulletin*, vol. 2, 2011.

[6] B. J. Cohen, "The yuan tomorrow? Evaluating China's currency internationalisation strategy," *New Political Economy*, vol. 17, no. 3, pp. 361–371, 2012.

[7] C. Yuanzheng, *The Strategy of RMB Internationalization[M]*, Hainan Press, Haikou, 2013.

[8] B. Eichengreen, "Adb distinguished lecture renminbi internationalization: tempest in a teapot?," *Asian Development Review*, vol. 30, no. 1, pp. 148–164, 2013.

[9] H. Weidong, *The Study of RMB-ZONE[M]*, People Press, Beijing, 2015.

[10] S. Hall, "Rethinking international financial centres through the politics of territory: renminbi internationalisation in London's financial district," *Transactions of the Institute of British Geographers*, vol. 42, no. 4, pp. 489–502, 2017.

[11] P. B. Kenen, *The Role of Dollar as an International Currency*, Occasional Paper 13, Group of Thirty, New York, 1983.

[12] L. Jing, *The Impacts of the Renminbi Regionalization on the Chinese Economy and Countermeasures[M]*, China Financial Publishing House, Beijing, 2009.

[13] L. Daokui, *Research on RMB Internationalization [M]*, Science press, Beijing, 2013.

[14] L. Xuemei, *Research on the RMB Internationalization and Regionalization[M]*, Economic Science Press, Beijing, 2013.

[15] L. Lefen and W. Shaonan, "An empirical analysis on the factors of the RMB's internationalization in the process of the Belt and Road initiative of China [J]," *Studies of International Finance*, vol. 2, pp. 75–83, 2016.

[16] C. A. McNally and J. Gruin, "A novel pathway to power? Contestation and adaptation in China's internationalization of the RMB," *Review of International Political Economy*, vol. 24, no. 4, pp. 599–628, 2017.

[17] The People's Bank of China, *The People's Bank Issued RMB Settlement Pilot Management Rules on Cross-Border Trade[EB/OL]*, 2009, [2015-06-04].

[18] L. M. Töpfer and S. Hall, "London's rise as an offshore RMB financial centre: state–finance relations and selective institutional adaptation," *Regional Studies*, vol. 52, no. 8, pp. 1053–1064, 2018.

[19] F. Zhang, M. Yu, J. Yu, and Y. Jin, "The effect of RMB internationalization on belt and road initiative: evidence from bilateral swap agreements," *Emerging Markets Finance and Trade*, vol. 53, no. 12, pp. 2845–2857, 2017.

Hindawi
Advances in Mathematical Physics
Volume 2022, Article ID 2881207, 9 pages
https://doi.org/10.1155/2022/2881207

Research Article

A Fractional-Order Discrete Lorenz Map

Yanyun Xie

School of General Education, Chongqing Water Resources and Electric Engineering College, Chongqing 40216, China

Correspondence should be addressed to Yanyun Xie; xieyanyun2022@126.com

Received 1 July 2022; Revised 25 August 2022; Accepted 6 September 2022; Published 20 September 2022

Academic Editor: Qura tul Ain

In this paper, a discrete Lorenz map with the fractional difference is analyzed. Bifurcations of the map in commensurate-order and incommensurate-order cases are studied when an order and a parameter are varied. Hopf bifurcation and periodic-doubling cascade are found by the numerical simulations. The parameter values of Hopf bifurcation points are determined when the order is taken as a different value. It can be concluded that the parameter decreases as the order increases. Chaos control and synchronization for the fractional-order discrete Lorenz map are studied through designing the suitable controllers. The effectiveness of the controllers is illustrated by numerical simulations.

1. Introduction

Fractional calculus has been studied for a fairly long time in the field of pure mathematics [1]. At the primary stage, its development is slow because of the absence of geometrical interpretation and applications. Until the last few decades, researchers gradually noticed that fractional calculus has superior characteristics over the classical calculus. Nowadays, fractional calculus has been analyzed deeply in theoretical research and practical applications.

It is well known that discrete fractional calculus was put forward by Diaz and Olser [2]. Within the past decade, people are more and more interested in discrete fractional calculus. In [3–7], definitions and stability for discrete fractional calculus are introduced and investigated. Based on these, many fractional-order maps are proposed and studied in detail, such as fractional sine map, standard map, Hénon map, and Ikeda map [8–14]. For the long-term memory characteristic of the operator, this kind of maps is a better fit for application in secure communications and encryption [15–17]. The main reasons are that fractional-order discrete maps are not only sensitive to the small disturbance of parameters and initial conditions but also to the variation of fractional orders, which are the unique advantages of fractional-order systems. On the other hand, fractional-order discrete maps have simple forms and rich dynamics, which are good for model analysis and numerical computation. Therefore, investigation of a fractional-order discrete map including dynamics, stabilization, and synchronization is necessary and important for the development of fractional calculus.

In this paper, we will investigate a fractional-order discrete Lorenz map. Bifurcations of the map in commensurate-order and incommensurate-order cases are analyzed. Hopf bifurcation and periodic-doubling cascade are found by the numerical simulations. The parameter values of Hopf bifurcation points are determined when the order is varied. The fractional-order discrete Lorenz map has several advantages such as unpredictability, diffusion properties, sensitivity to initial conditions, orders, and parameters. It is very suitable for application in secure communication and encryption. Therefore, chaos control and synchronization for the fractional-order Lorenz map are studied through designing the suitable controllers based on the adaptive method. The advantages of the method are follows: the principle of the adaptive method is simple based on the stability theory of fractional difference maps; the designing controllers for control and synchronization are easy to realize in simulations. It should be noted that the research of fractional-order maps is at an early stage. Many control and synchronization methods and strategies need to be studied further.

The paper is organized into seven sections. Section 2 gives the related theories of discrete fractional calculus. A

fractional-order discrete Lorenz map is described in Section 3. Bifurcations in two cases are studied in Section 4. Control and synchronization for map are investigated, respectively, in Sections 5 and 6. The summarization of the paper is given in Section 7.

2. Discrete Fractional Calculus

In this section, some theories related to discrete fractional calculus will be listed. The symbol ${}^{C}\Delta_b^q Y(t)$ represents the Caputo type fractional difference of a function $Y(\mathrm{t})$: $\mathrm{N}_b \longrightarrow \mathbb{R}$ with $\mathrm{N}_b = \{b, b+1, b+2, \cdots\}$ [18], which is marked as

$$ {}^{C}\Delta_b^q Y(t) = \Delta_b^{-(n-q)} \Delta_b^n Y(t) = \frac{1}{\Gamma(n-q)} \sum_{s=b}^{t-(n-q)} (t-s-1)^{(n-q-1)} \Delta_s^n Y(s). \tag{1} $$

Here, $q \notin N$ is the fractional order, and $n = \lceil q \rceil + 1$.The fractional sum in (1) can be expressed as [19, 20]

$$ \Delta_b^{-q} Y(t) = \frac{1}{\Gamma(q)} \sum_{s=b}^{t-q} (t-s-1)^{(q-1)} Y(s). \tag{2} $$

Here, $t \in N_{b+q}$, $q > 0$, and the falling function $t^{(q)}$ is written as follows:

$$ t^{(q)} = \frac{\Gamma(t+1)}{\Gamma(t+1-q)}, \tag{3} $$

where $\Gamma(\cdot)$ denotes the gamma function, which is defined as $\Gamma(t) = \int_0^{+\infty} x^{t-1} e^{-x} dx$ for $t > 0$.

We can determine the numerical solutions of a fractional difference equation via the method below. A fractional difference equation with initial conditions is

$$ \begin{cases} {}^{C}\Delta_b^q u(t) = f(t+q-1, u(t+q-1)), \\ \Delta^k u(b) = u_k . n = \lceil q \rceil + 1, k = 0, 1, 2, \cdots, n-1. \end{cases} \tag{4} $$

The corresponding discrete integral equation is

$$ u(t) = u_0(t) + \frac{1}{\Gamma(q)} \sum_{s=b+n-q}^{t-q} (t-s-1)^{(q-1)} f(s+q-1, u(s+q-1)), t \in \mathrm{N}_{b+n}. \tag{5} $$

Here, $u_0(t) = \sum_{k=0}^{n-1} ((t-b)^{(k)} / \Gamma(k+1)) \Delta^k u(b)$.

The below theorem can be used to determine the stability of the equilibrium point for a fractional-order difference system. You can refer to the literature [21] for the detail of the proof.

Theorem 1. *For a linear fractional-order difference discrete system,*

$$ {}^{C}\Delta_b^q X(t) = \mathbf{A} Y(t+q-1). \tag{6} $$

Here, $Y(t) = (y_1(t), y_2(t), \cdots, y_n(t))^T$, $0 < q < 1$, $\mathbf{A} \in R^{n \times n}$ *and* $\forall t \in N_{b+1-q}$, *and the zero equilibrium is asymptotically stable if all the eigenvalues of matrix* $\mathbf{A}$ *satisfy*

$$ |\lambda_i| < \left(2 \cos \frac{|\arg \lambda_i| - \pi}{2 - q} \right)^q \text{ and } |\arg \lambda_i| > \frac{q\pi}{2}, i = 1, 2, \cdots, n. \tag{7} $$

Definition 2. For a fractional-order system, which can be described by ${}^{C}\Delta_a^q = f(\mathbf{x}(\mathrm{t}))$, where $\mathbf{x} = (x_1, x_2, \cdots, x_n)^{\mathrm{T}}$ is the state vector, $\mathbf{q} = (q_1, q_2, \cdots, q_n)^{\mathrm{T}}$ is the fractional derivative orders vector, and $q_i > 0$. The fractional-order system is in commensurate order when all the derivative orders satisfy $q_1 = q_2 = \cdots = q_n$; otherwise, it is an incommensurate-order system [22].

3. A Discrete Lorenz Map with Fractional Difference Operator

Recently, a Lorenz map was studied deeply and successfully applied in encryption [23–25]. A Lorenz chaotic map was presented which is given as follows:

$$ \begin{cases} x(n+1) = (1 + \gamma\delta) x(n) - \delta y(n) x(n), \\ y(n+1) = (1 - \delta) y(n) + \delta x^2(n). \end{cases} \tag{8} $$

Here, $x(n)$ and $y(n)$ denote state variables, and γ and δ represent system parameters. The corresponding first-order difference for (8) is expressed as

$$ \begin{cases} \Delta x(n) = x(n+1) - x(n) = (1 + \gamma\delta) x(n) - \delta y(n) x(n) - x(n), \\ \Delta y(n) = y(n+1) - y(n) = (1 - \delta) y(n) + \delta x^2(n) - y(n). \end{cases} \tag{9} $$

By using the Caputo-like delta difference operator to replace the first order difference in (9) with a starting point b, the fractional-order Lorenz map can be obtained, which is the following form [26]:

$$ \begin{cases} {}^{C}\Delta_b^q x(t) = (1 + \gamma\delta) x(t-1+q) - \delta y(t-1+q) x(t-1+q) - x(t-1+q), \\ {}^{C}\Delta_b^q y(t) = (1 - \delta) y(t-1+q) + \delta x^2(t-1+q) - y(t-1+q). \end{cases} \tag{10} $$

Here, $0 < q < 1$ denotes the derivative order. If all the orders in (10) are identical, then the map is a commensurate-order one. Otherwise, it is an incommensurate-order one which is expressed by the following difference equations:

$$ \begin{cases} {}^{C}\Delta_b^{q_1} x(t) = (1 + \gamma\delta) x(t-1+q_1) - \delta y(t-1+q_1) x(t-1+q_1) - x(t-1+q_1), \\ {}^{C}\Delta_b^{q_2} y(t) = (1 - \delta) y(t-1+q_2) + \delta x^2(t-1+q_2) - y(t-1+q_2). \end{cases} \tag{11} $$

The derivative orders satisfy $0 < q_1, q_2 < 1$.

The numerical formulas of commensurate-order map (10) are

$$\begin{cases} x(n) = x(b) + \dfrac{1}{\Gamma(q)} \displaystyle\sum_{j=1}^{n} \dfrac{\Gamma(n-j+q)}{\Gamma(n-j+1)} (\gamma\delta x(j-1) - \delta y(j-1)x(j-1)), \\ y(n) = y(b) + \dfrac{1}{\Gamma(q)} \displaystyle\sum_{j=1}^{n} \dfrac{\Gamma(n-j+q)}{\Gamma(n-j+1)} \left(\delta\left(-y(j-1) + x^2(j-1)\right)\right), \end{cases} \tag{12}$$

and the numerical recipes of (11) are as follows:

$$\begin{cases} x(n) = x(b) + \dfrac{1}{\Gamma(q_1)} \displaystyle\sum_{j=1}^{n} \dfrac{\Gamma(n-j+q_1)}{\Gamma(n-j+1)} (\gamma\delta x(j-1) - \delta y(j-1)x(j-1)), \\ y(n) = y(b) + \dfrac{1}{\Gamma(q_2)} \displaystyle\sum_{j=1}^{n} \dfrac{\Gamma(n-j+q_2)}{\Gamma(n-j+1)} \left(\delta\left(-y(j-1) + x^2(j-1)\right)\right). \end{cases} \tag{13}$$

In here, we fix the low limit b as 0. When the parameters are taken as $\gamma = 1.25, \delta = 0.75$, and the order q is 0.99, the commensurate-order map (10) has a chaotic attractor, see Figure 1.

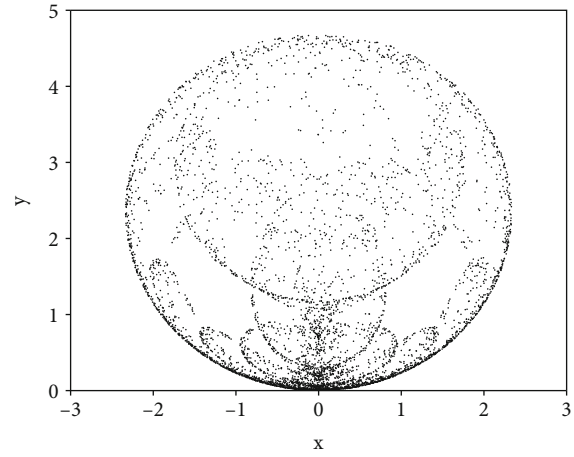

Figure 1: The chaotic attractor of map (10).

4. Bifurcations of Fractional-Order Discrete Lorenz Map

We will study the bifurcations of the fractional-order discrete Lorenz map in commensurate-order and incommensurate-order cases in this section.

4.1. Bifurcations of Map (10). Firstly, parameter γ is fixed as 1.25, and the intervals of δ and the order q are taken as $[0.2, 1]$ and $[0.6, 0.99]$, respectively. The bifurcation of the commensurate-order discrete Lorenz map, which is corresponding to the difference equations (10), is studied when δ and q are varied, see Figure 2(a), from which it is clear that that map (10) has very abundant dynamics. Period-doubling cascades and Hopf bifurcations can be observed. The chaos region becomes large as the order increases from 0.65 to 0.99. In order to obtain the order of chaos appears firstly in the map (10), a bifurcation diagram with the variation of the order in the interval $[0.6, 0.65]$ and parameter δ is plotted in Figure 2(b). It is clear that the map (10) is periodic when $q < 0.62$ and is chaotic when $q \geq 0.62$. Based on this, we can get the total order for the map (10) to remain chaos that is 1.24. The phase diagrams of map (10) with initial conditions $(x_0, y_0) = (0.1, 0)$ and $(x_0, y_0) = (-0.1, 0)$ belonging to different basins of attraction are plotted in Figure 3, in which the parameter δ increases from 0.30 to 0.60, and the order is taken as 0.95. Typical Hopf bifurcation can be observed from Figures 3(a) and 3(b). The two limit cycles become large as δ increases (Figure 3(c)). When $\delta = 0.60$, the two attractors merge into a chaotic one, see Figure 3(d).

Secondly, the parameter δ is chosen as 0.75, and the intervals of γ and the order are $[0.2, 1.3]$ and $[0.7, 0.99]$, respectively. Bifurcation of the map (10) when the parameter γ and the order q are varied is displayed in Figure 4(a). The region of chaos becomes large as the order increases from 0.65 to 0.99. A bifurcation diagram with the variation of the order in the interval $[0.70, 0.75]$ and parameter γ is plotted in Figure 4(b) to show the appearance of chaos in the map at the first time. It is clear that the map (10) is periodic when $q < 0.74$ and is chaotic when $q \geq 0.74$. Therefore, the total order of the map (10) to remain chaos is 1.48 in this case.

From Figures 2 and 4, we can see clearly that the route leading to chaos for map (10) is Hopf bifurcation. The Hopf bifurcation points (HPFs for short) for different values of the order q are listed in Table 1. It is clear that HPFs decrease as the order increases. An example is taken to show the Hopf bifurcation when the order $q = 0.95$. Map (10) converges to a fixed point for $\delta = 0.46$ (Figure 5(a)) and to a limit cycle for $\delta = 0.47$ (Figure 5(b)).

4.2. Bifurcations of Map (11). In this subsection, bifurcations of the incommensurate-order discrete Lorenz map which is corresponding to the difference equations (11) will be studied. Parameter γ is fixed as 1.25 and order $q_2 = 1$, and the interval of δ is $[0.2, 1]$. Figure 6(a) is the bifurcations of map (11) when δ and q_1 are varied. We can see that period-doubling and Hopf bifurcations occur when the parameter and the order are varied. The chaos region becomes large as the order increases from 0.4 to 0.99. From Figure 6(b), we can see that map (11) is periodic for $q_1 < 0.45$ and chaotic for $q_1 \geq 0.45$. Then, the total order for map (11) to remain chaos is 1.45 in this case.

Secondly, the order q_1 is fixed as 1, and the interval of q_2 is taken as $[0.35, 0.99]$. The bifurcations with the variation of the parameter δ and the order q_2 are shown in Figure 7. It can be seen that that the region of chaos becomes large as the order increases from 0.35 to 0.99. We can determine that the total order for map (11) to remain chaos is 1.4 based on Figure 7(b).

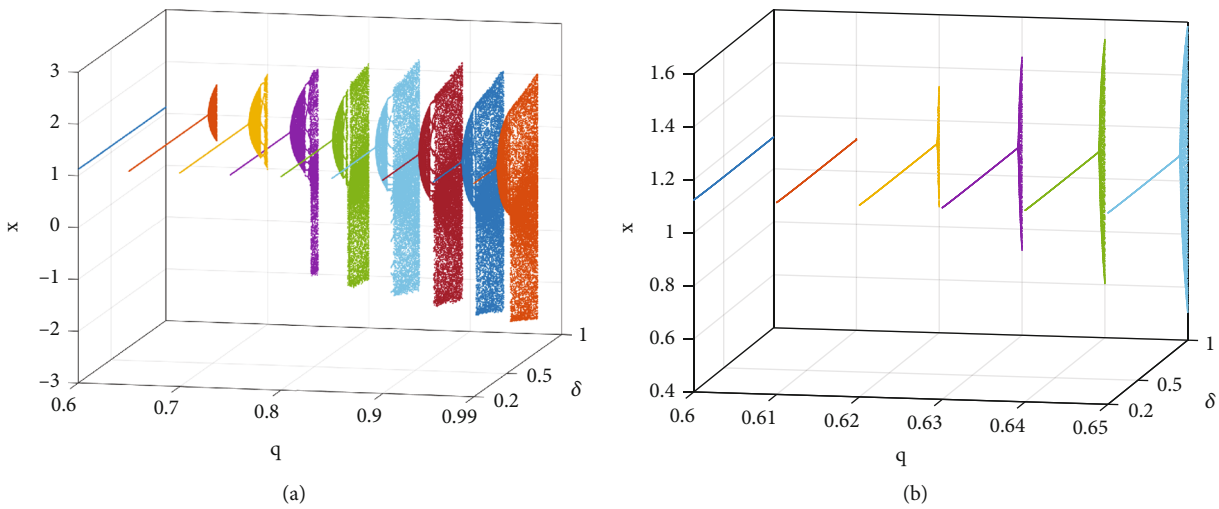

Figure 2: The bifurcation diagrams of map (10) when δ and q are varied. (a) $q \in [0.6, 0.99]$. (b) $q \in [0.6, 0.65]$.

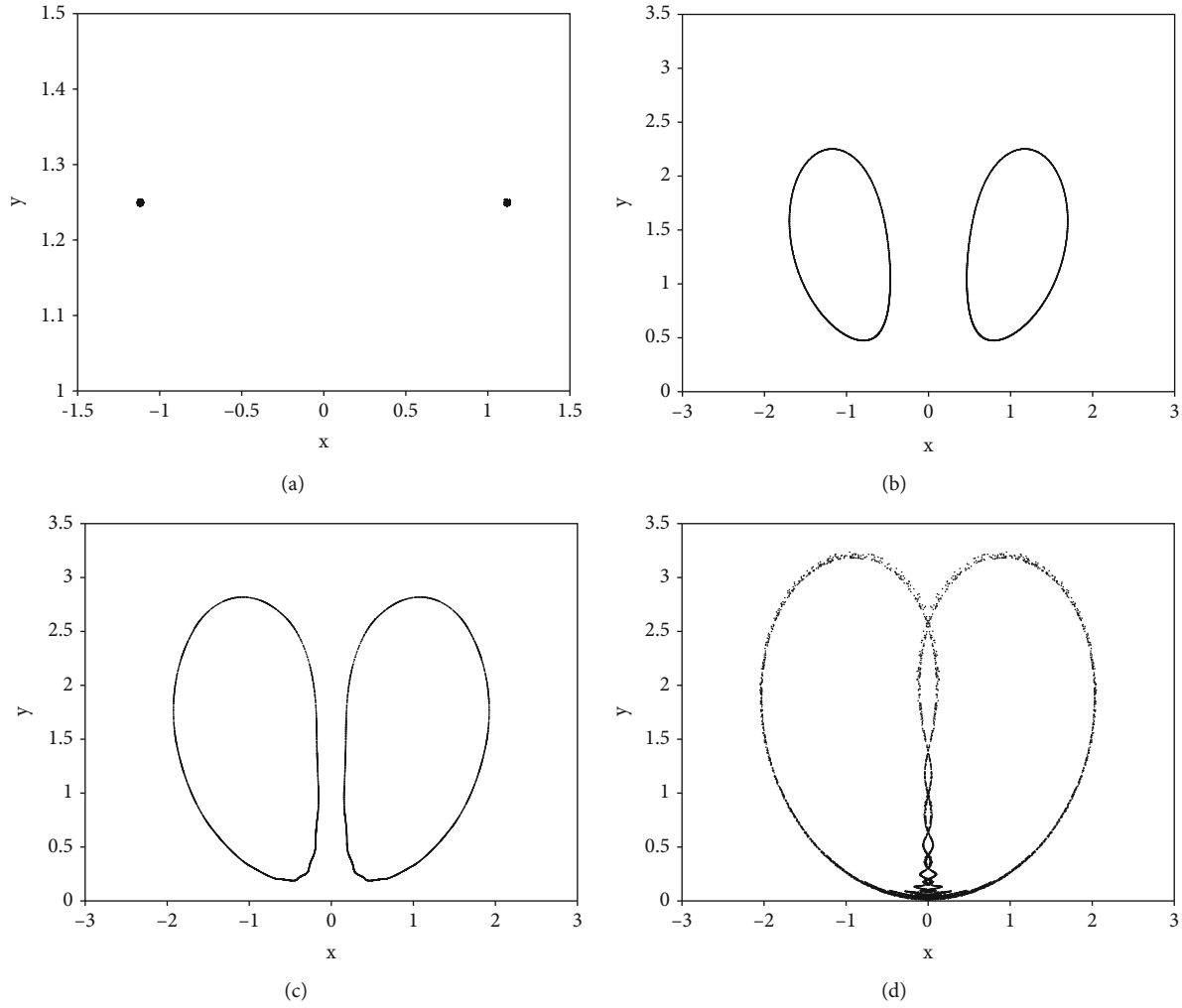

Figure 3: Phase diagrams of map (10) with different initial conditions $(x_0, y_0) = (0.1, 0)$ and $(x_0, y_0) = (-0.1, 0)$. (a) $\delta = 0.30$. (b) $\delta = 0.50$. (c) $\delta = 0.55$. (d) $\delta = 0.60$.

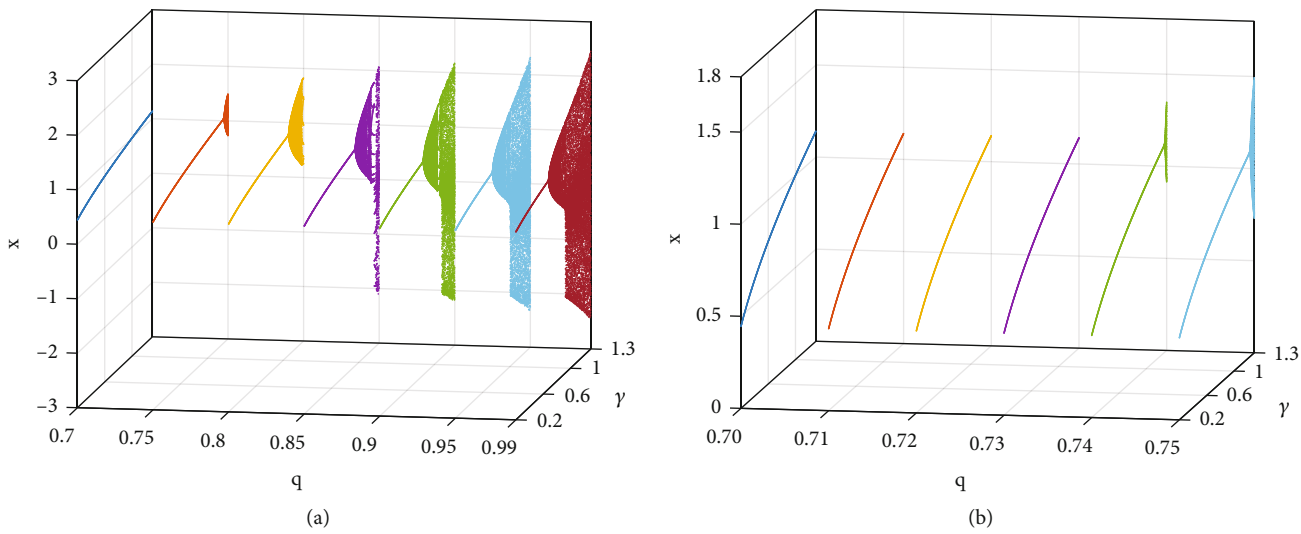

Figure 4: Bifurcation diagrams of map (10) when γ and q are varied. (a) $q \in [0.7, 0.99]$. (b) $q \in [0.7, 0.75]$.

Table 1: Hopf bifurcation points of map (10) for different values of q.

q	δ	q	δ
0.60	—	0.75	0.75
0.61	—	0.80	0.68
0.62	0.98	0.85	0.60
0.63	0.97	0.90	0.54
0.64	0.95	0.95	0.47
0.65	0.93	0.99	0.42
0.70	0.84		

5. Chaos Control

In this section, chaos control for map (10) will be analyzed. Firstly, map (10) with controllers is the follows:

$$\begin{cases} {}^{C}\Delta_b^q x(t) = (1+\gamma\delta)x(t-1+q) - \delta y(t-1+q)x(t-1+q) - x(t-1+q) + u_1(t-1+q), \\ {}^{C}\Delta_b^q y(t) = (1-\delta)y(t-1+q) + \delta x^2(t-1+q) - y(t-1+q) + u_2(t-1+q), \end{cases} \tag{14}$$

where u_1 and u_2 denote the chaos controllers.

Theorem 3. *If the controllers are taken as the following form,*

$$\begin{cases} u_1(t-1+q) = -(1+\gamma\delta)x(t-1+q) + \delta y(t-1+q)x(t-1+q)), \\ u_2(t-1+q) = -(1-\delta)y(t-1+q) - \delta x^2(t-1+q), \end{cases} \tag{15}$$

then the chaotic behavior of map (10) can be controlled.

Proof. By substituting (15) into (14), then map (14) can be rewritten as

$$\begin{cases} {}^{C}\Delta_b^q x(t) = -x(t-1+q), \\ {}^{C}\Delta_b^q y(t) = -y(t-1+q). \end{cases} \tag{16}$$

The compact form of map (16) is

$${}^{C}\Delta_b^q (x(t), y(t))^{\mathrm{T}} = \mathbf{B} \times (x(t-1+q), y(t-1+q))^{\mathrm{T}}, \tag{17}$$

where $\mathbf{B} = \begin{pmatrix} -1 & 0 \\ 0 & -1 \end{pmatrix}$. The eigenvalues of $\mathbf{B}$ satisfy $|\arg \lambda_i| = \pi$ and $|\lambda_i| = 2^q$, for $i = 1, 2$. It means that the chaotic behavior of map (10) can be controlled to the zero equilibrium based on Theorem 1.

The system parameters are fixed as $\gamma = 1.25$, $\delta = 0.75$ and order $q = 0.99$. Map (10) is stabilized by using the controllers when the iteration $n = 1000$, see Figure 8. We can see clear that $x(n), y(n)$ converge to zero as time n toward to 2000. □

6. Adaptive Synchronization

In here, adaptive synchronization for the Lorenz map in fractional form will be studied. Firstly, map (10) is chosen as the drive system and is rewritten as follows

$$\begin{cases} {}^{C}\Delta_b^q x_1(t) = \gamma\delta x_1(t-1+q) - \delta y_1(t-1+q)x_1(t-1+q), \\ {}^{C}\Delta_b^q y_1(t) = \delta\left(-y_1(t-1+q) + {x_1}^2(t-1+q)\right). \end{cases} \tag{18}$$

The response system with synchronization controllers $u_x(t-1+q)$ and $u_y(t-1+q)$ is designed as the following

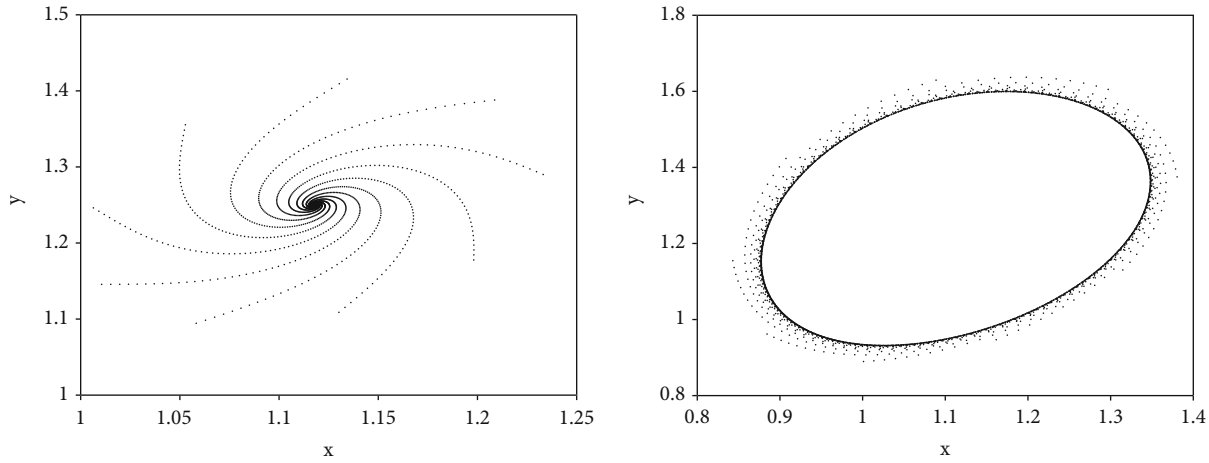

Figure 5: Phase diagrams of map (10) for $q = 0.95$. (a) $\delta = 0.46$. (b) $\delta = 0.47$.

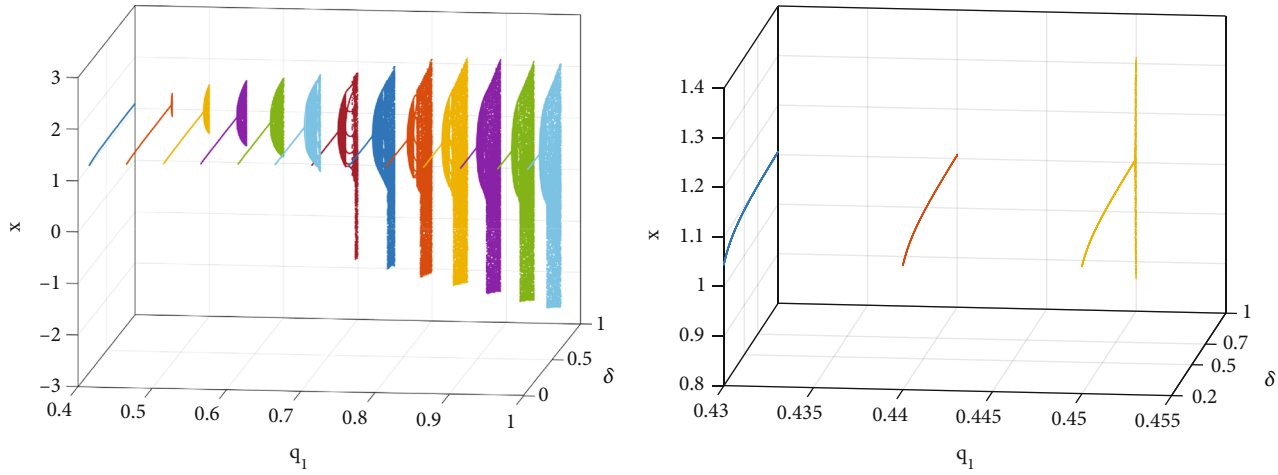

Figure 6: The bifurcation diagrams of map (11) when δ and q_1 are varied. (a) $q_1 \in [0.4, 0.99]$. (b) $q_1 \in [0.43, 0.45]$.

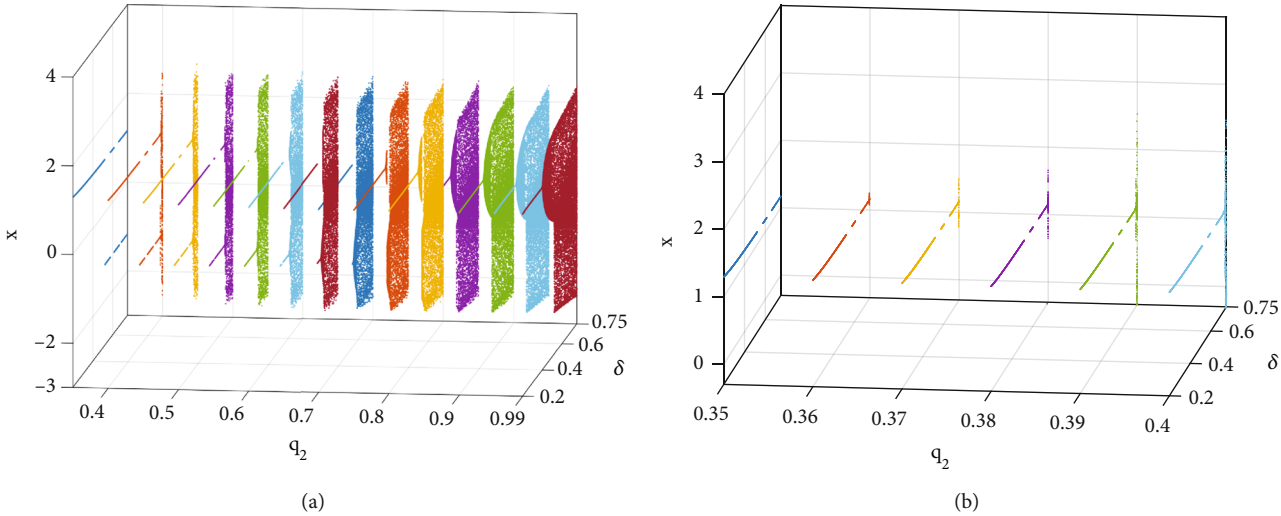

Figure 7: The bifurcation diagrams of map (11) when δ and q_2 are varied. (a) $q_2 \in [0.35, 0.99]$. (b) $q_2 \in [0.35, 0.4]$.

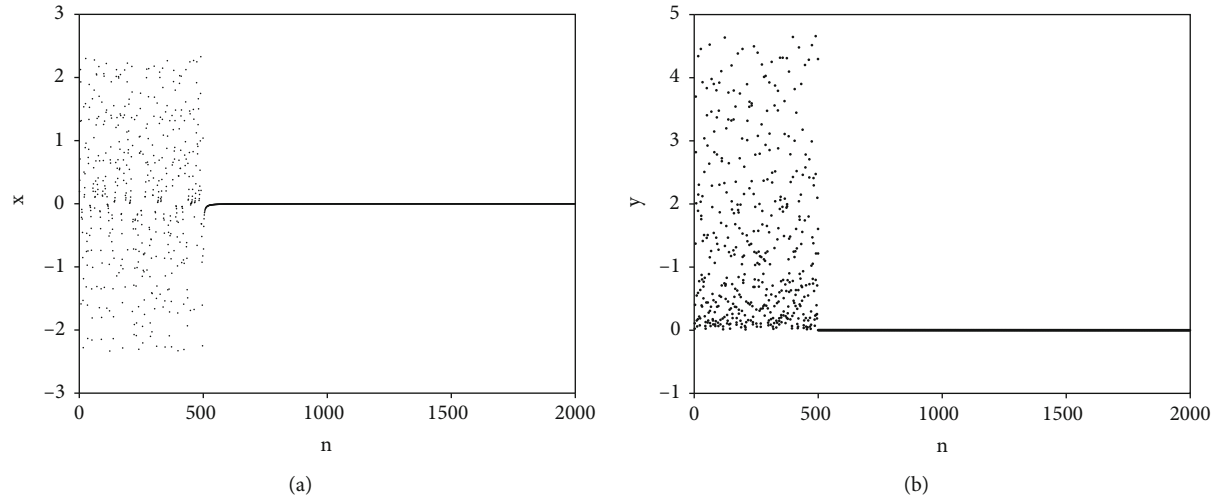

Figure 8: The controlled results for map (10). (a) The state variable x with n (b) the state variable y with n.

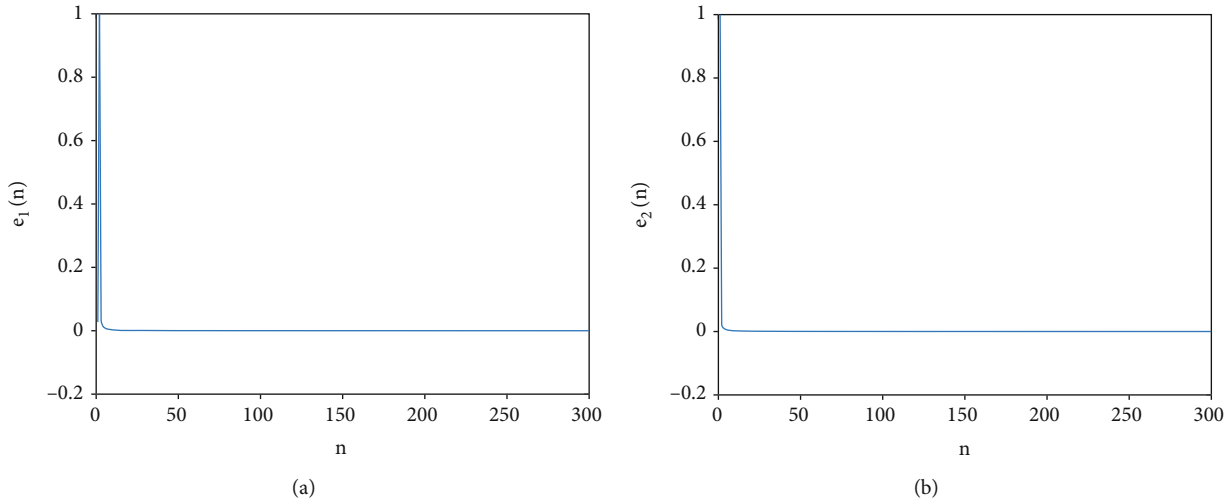

Figure 9: The synchronization results. (a) $e_1(n)$ with n. (b) $e_2(n)$ with n.

form:

$$\begin{cases} {}^{C}\Delta_b^{v} x_2(t) = \gamma\delta x_2(t-1+q) - \delta y_2(t-1+q)x_2(t-1+q) + u_x(t-1+q), \\ {}^{C}\Delta_b^{v} y_2(t) = \delta\left(-y_2(t-1+q) + {x_2}^2(t-1+q)\right) + u_y(t-1+q). \end{cases} \tag{19}$$

The error state variables of the synchronization are defined as

$$\begin{cases} e_1(t-1+q) = x_2(t-1+q) - x_1(t-1+q), \\ e_2(t-1+q) = y_2(t-1+q) - y_1(t-1+q). \end{cases} \tag{20}$$

It is well known that if the two error states variables converge to 0 as the time t tends to infinity, then maps (18) and (19) is synchronized under the controllers.

Theorem 4. *The synchronization between two maps (18) and (19) is realized if the controllers are designed as follows:*

$$\begin{cases} u_x(t-1+q) = (\delta y_2(t-1+q) - \gamma\delta - 1)e_1(t-1+q) + \delta x_1(t-1+q)e_2(t-1+q), \\ u_y(t-1+q) = (\delta - 1)e_2(t-1+q) - \delta(x_2(t-1+q) + x_1(t-1+q))e_1(t-1+q). \end{cases} \tag{21}$$

Proof. We can obtain the error system via simple computation

$$\begin{cases} {}^{C}\Delta_b^q e_1(t) = \gamma\delta x_2(t-1+q) - \delta y_2(t-1+q)x_2(t-1+q) - \gamma\delta x_1(t-1+q) + \delta y_1(t-1+q)x_1(t-1+q) + u_x(t-1+q), \\ {}^{C}\Delta_b^q e_2(t) = \delta\left(-y_2(t-1+q) + {x_2}^2(t-1+q)\right) - \delta\left(-y_1(t-1+q) + {x_1}^2(t-1+q)\right) + u_y(t-1+q). \end{cases} \tag{22}$$

By substituting the controllers (21) into (22), error dynamical system can be determined as the following:

$$\begin{cases} {}^{C}\Delta_a^q e_1(t) = -e_1(t-1+q), \\ {}^{C}\Delta_a^q e_2(t) = -e_2(t-1+q). \end{cases} \tag{23}$$

For the convenience of analysis, we give the compact form of system (23)

$${}^{C}\Delta_a^q(e_1(t), e_2(t)) = \mathbf{C} \times (e_1(t-1+q), e_2(t-1+q))^{\mathrm{T}}, \tag{24}$$

where $\mathbf{C} = \begin{bmatrix} -1 & 0 \\ 0 & -1 \end{bmatrix}$. Matrix $\mathbf{C}$ satisfies the stability condition

$$|\lambda_i| < \left(2\cos\frac{|\arg\lambda_i| - \pi}{2-q}\right)^q \text{ and } |\arg\lambda_i| > \frac{q\pi}{2}, i = 1, 2. \tag{25}$$

Therefore, synchronization between maps (18) and (19) is realized based on Theorem 1. In other words, the equilibrium point of (23) is asymptotically stable. □

In here, parameters are fixed as $\gamma = 1.25, \delta = 0.75$ and order $q = 0.99$. The initial conditions of maps (18) and (19) are chosen as $(0.2, 0.1), (0.7, 0.3)$. The synchronization results are plotted in Figure 9, from which we can see that e_1 and e_2 converge to zero rapidly as n towards to 300.

7. Conclusions

A fractional-order discrete Lorenz map is analyzed in this paper. Bifurcations of the map in commensurate-order and incommensurate-order cases are studied. The bifurcation diagrams in a three-dimension space are shown when a derivative order and a parameter are varied. Hopf and periodic-doubling bifurcations can be observed. Based on the analysis, parameter values of Hopf bifurcation points are determined with different orders. We can conclude that the critical values of the parameter decreases as the order increases. It is very important for us to observe the dynamical evolution of the map with the variation of an order and a system parameter. It is worth mentioning that it is the first time to show the dynamics of the fractional-order Lorenz map in a three-dimension space, from which we can see that the order is a very important parameter which affects the dynamics of a fractional-order map. Therefore, the map with an order has more extensively parametric space and abundant dynamics. Meanwhile, it is very important for the application of the map in secure communications and encryption. Chaos control and synchronization for the fractional-order discrete Lorenz map are studied through designing the suitable controllers. The effectiveness of the controllers is illustrated by numerical simulations. From the results, we can also see that a high speed of stabilization and synchronization is obtained.

Data Availability

The data for the bifurcation diagrams used to support the findings of this study are included within the supplementary information file(s) (available here).

Conflicts of Interest

The author declares no conflicts of interest regarding this article.

Authors' Contributions

The author has accepted responsibility for the entire content of this submitted manuscript and approved submission.

References

[1] C. Goodrich and A. C. Peterson, *Discrete fractional calculus*, Springer, Berlin, 2015.

[2] J. B. Diaz and T. J. Olser, "Differences of fractional order," *Mathematics of Computation*, vol. 28, no. 125, pp. 185–202, 1974.

[3] H. G. Sun, Y. Zhang, D. Baleanu, W. Chen, and Y. Q. Chen, "A new collection of real world applications of fractional calculus in science and engineering," *Communications in Nonlinear Science and Numerical Simulation*, vol. 64, pp. 213–231, 2018.

[4] M. Buslowicz and A. Ruszewski, "Necessary and sufficient conditions for stability of fractional discrete-time linear state-space systems," *Bulletin of the Polish Academy of Sciences. Technical Sciences*, vol. 61, no. 4, pp. 779–786, 2013.

[5] F. M. Atici and P. W. Eloe, "Discrete fractional calculus with the Nabla operator," *Electronic Journal of Qualitative Theory of Differential Equations*, vol. 3, no. 3, pp. 1–12, 2009.

[6] C. Goodrich, "Some new existence results for fractional difference equations," *International Journal of Dynamical Systems and Differential equations*, vol. 3, no. 1-2, pp. 145–162, 2011.

[7] D. Baleanu, G. Wu, Y. Bai, and F. Chen, "Stability analysis of Caputo-like discrete fractional systems," *Communications in Nonlinear Science and Numerical Simulation*, vol. 48, pp. 520–530, 2017.

[8] J. Mumkhamar, "Chaos in a fractional order logistic map," *Fractional Calculus and Applied Analysis*, vol. 16, no. 3, pp. 511–519, 2013.

[9] G. C. Wu, D. Baleanu, and S. D. Zeng, "Discrete chaos in fractional sine and standard maps," *Physics Letters A*, vol. 378, no. 5-6, pp. 484–487, 2014.

[10] C. Ma, J. Mou, P. Li, and T. Liu, "Dynamic analysis of a new two-dimensional map in three forms: integer-order, fractional-order and improper fractional-order," *The European Physical Journal Special Topics*, vol. 230, no. 7-8, pp. 1945–1957, 2021.

[11] T. Hu, "Discrete chaos in fractional Hénon map," *Applications of Mathematics*, vol. 5, no. 15, pp. 2243–2248, 2014.

[12] Y. Liu, "Chaotic synchronization between linearly coupled discrete fractional Hénon maps," *Indian Journal of Physics*, vol. 90, no. 3, pp. 313–317, 2016.

[13] O. Megherbi, H. Hamiche, S. Djennoune, and M. Bettayeb, "A new contribution for the impulsive synchronization of fractional-order discrete–time chaotic systems," *Nonlinear Dynamics*, vol. 90, no. 3, pp. 1519–1533, 2017.

[14] A. Ouannas, A. A. Khennaoul, Z. Odibat, and V. T. Pham, "On the dynamics, control and synchronization of fractional-order Ikeda map," *Chaos Solitions Fractals*, vol. 123, pp. 108–115, 2019.

[15] Z. Y. Liu, T. C. Xia, and Y. P. Wang, "Image encryption technology based on fractional two-dimensional discrete chaotic map accompanied with menezes-vanstone elliptic curve cryptosystem," *Fractals*, vol. 29, no. 3, p. 2150064, 2021.

[16] G. C. Wu, D. Baleanu, and Z. X. Lin, "Image encryption technique based on fractional chaotic time series," *Journal of Vibration and Control*, vol. 22, no. 8, pp. 2092–2099, 2016.

[17] J. X. Liu, Z. X. Wang, M. L. Shu, F. F. Zhang, S. Leng, and X. H. Sun, "Secure communication of fractional complex chaotic systems based on fractional difference function synchronization," *Complexity*, vol. 2019, Article ID 7242791, 10 pages, 2019.

[18] T. Abdeljawad, "On Riemann and Caputo fractional differences," *Computers & Mathematcs with Applications*, vol. 62, no. 3, pp. 1602–1611, 2011.

[19] H. I. Gray and N. F. Zhang, "On a new definition of the fractional difference," *Mathematics of Computation*, vol. 50, no. 182, pp. 513–529, 1988.

[20] K. S. Miller and B. Ross, *Univalent Functions, Fractional Calculus, and their Applications*, Eills Howard, Chichester, 1989.

[21] J. Čermák, I. Györi, and L. Něchvátal, "On explicit stability conditions for a linear fractional difference system," *Fractional Calculus and Applied Analysis*, vol. 18, no. 3, pp. 651–672, 2015.

[22] M. T. Shatnawi, N. Djenina, A. Ouannas, I. M. Batiha, and G. Grassi, "Novel convenient conditions for the stability of nonlinear incommensurate fractional-order difference systems," *Alexandria Engineering Journal*, vol. 61, no. 2, pp. 1655–1663, 2022.

[23] O. M. Al-Hazaimeh, M. F. Al-Jamal, N. Alhindawi, and A. Omari, "Image encryption algorithm based on Lorenz chaotic map with dynamic secret keys," *Neural Computing and Applications*, vol. 31, no. 7, pp. 2395–2405, 2019.

[24] O. M. Al-Hazaimeh, "A new dynamic speech encryption algorithm based on Lorenz chaotic map over internet protocol," *International Journal of Electrical and Computer Engineering*, vol. 10, no. 5, pp. 4824–8708, 2020.

[25] M. Itoh, T. Yang, and L. O. Chua, "Conditions for impulsive synchronization of chaotic and hyperchaotic SYSTEMS," *International Journal of Bifurcation and Chaos*, vol. 11, no. 2, pp. 551–560, 2001.

[26] A. A. Khennaoui, A. Ouannas, S. Bendoukha, G. Grassi, R. P. Lozi, and V. T. Pham, "On fractional-order discrete-time systems: Chaos, stabilization and synchronization," *Chaos Solitions Fractals*, vol. 119, pp. 150–162, 2019.

Hindawi
Advances in Mathematical Physics
Volume 2022, Article ID 3073782, 9 pages
https://doi.org/10.1155/2022/3073782

Research Article

The Study of Cross-Border Trade with Third-Party Payment Institutions in China

Yina Zhu

School of Finance, Anhui University of Finance & Economics, Bengbu 233030, China

Correspondence should be addressed to Yina Zhu; 20201840@aufe.edu.cn

Received 30 July 2022; Accepted 30 August 2022; Published 19 September 2022

Academic Editor: Muhammad Nadeem

The cross-border Renminbi (RMB) business volume of third-party payment institutions makes up a small share of China's total cross-border business, but there is still an absolute amount of trade that cannot be disregarded. The third-party payment institutions are subject to policy restrictions in the process of seeking development and business promotion and hope to obtain policy support in the business, transaction amount limit, identification, and other aspects. Recently, China has made a strict policy for third-party payment institutions and warned against issuing any new licenses concerning payment. On the other hand, 39 payment institutions' licenses have been canceled for various reasons. Under the premise that strict supervision becomes normal, all payment institutions should be more cautious to develop businesses legally.

1. Introduction

In the past few decades, the internationalization of RMB has made some achievements, but the bottleneck has emerged, and the current international political and economic environment has been very different from that in 2009 [1]. Under the background of the current world political and economic environment, how to further promote the internationalization of RMB is a common concern of Chinese officials and academia.

With the rapid development of cross-border e-commerce, third-party payment may be a breakthrough for the internationalization of RMB. With the continuous maturity of Internet technology and advanced transportation and communication means, the world is more closely connected. At present, China's total economy, total import and export trade volume, the flow of foreign students, the number of inbound and outbound tourists, and other indicators are at the forefront of the world. Trade development and personnel flow provide the basis for cross-border payment and give birth to the vigorous development of cross-border payment business. China's payment licenses have been issued since 2011. Since then, the number of third-party payment institutions has experienced the reality of a gradual decline to rapid growth [2]. To serve the internationalization of RMB, national financial stability, third-party payment industry, and corresponding enterprises and individuals, this paper carries out corresponding research.

Firstly, the ultimate purpose of the cross-border RMB business of third-party payment institutions is to serve the national strategy of RMB internationalization [3].

Secondly, policy suggestions for financial stability are provided. With the rapid development of financial technology and the change and innovation of international trade mode in recent years, the degree of innovation and facilitation of payment mode has been continuously improved. The third-party payment provides payment convenience for economic development; meanwhile, the risk problem cannot be ignored. The risk problems in the third-party payment will bring some adverse aspects to China's financial stability. Objectively, we need to encourage development to adapt to appropriate supervision and serve the overall situation of national economic construction [4, 5].

Thirdly, a reference for industries and enterprises is provided. On how to promote the healthy development of third-party payment institutions on a benign track and standardize the behavior of third-party payment institutions, it is not enough to rely on the self-discipline of enterprises

and industries, and regulatory intervention is needed. Why regulation? What are the main regulatory aspects? Through the research of this paper, we hope to provide some useful references for the third-party payment industry and enterprises and hope that the industry and enterprises can consciously integrate into the cause of national financial development and make different contributions in their respective fields.

Theoretically, at present, there are many research articles both home and abroad on third-party payment institutions. However, with the vigorous development and prominent innovation of third-party payment, from the existing literature that can be retrieved, the research results of direct research on the cross-border RMB support policy and supervision of third-party payment institutions are relatively rare [6]. Therefore, this study has specific significance from the theoretical and academic levels.

Practically, the latest first-hand information can be obtained through the distribution, recovery, and sorting of the questionnaire. Through the analysis and judgment of the first-hand information, it can provide policy support for the national financial management institutions and provide some reference for the legal and compliant business of the industrial sector.

2. Overview of Cross-Border RMB Business of Third-Party Payment Institutions in China

At present, banking financial institutions have absolute advantages in the processing scale of payment business. They are the main force in China's payment industry. The influence of nonbanking payment institutions in China's retail payment market is prominent.

2.1. Issuance of Payment Business License. A payment business license is also known as a payment license. According to regulatory regulations, nonbanking financial institutions need a license first to carry out cross-border payment business. These licenses include the business license of cross-border payment, which is specifically divided into cross-border foreign exchange payment business license and cross-border RMB payment business license. Liu et al. [7] claimed that 56 institutions carried out cross-border payment businesses by the end of 2019. According to the newest data from the Payment & Clearing Association of China, in 2021, 43 payment institutions launched cross-border businesses with an aggregate amount of RMB972.36 billion.

2.2. Business Model of Cross-Border Payment of Third-Party Payment Institutions. There is no precedent for domestic payment institutions to participate in the payment and clearing system of other countries (regions). There are three modes of cross-border payment business of payment institutions: the first, cooperation with overseas payment institutions; the second, direct cooperation with overseas e-commerce platforms; and the third, cooperation with domestic banks.

2.2.1. Cooperation with Overseas Payment Institutions. Payment institutions can cooperate with overseas and local payment institutions that have obtained financial supervision licenses, including overseas subsidiaries with relevant business qualifications established by domestic payment companies and overseas and local payment institutions. If an overseas cooperative institution establishes an overseas bank account, its funds may be paid through the overseas bank account. By 2020, Alipay connects with more than 80 million companies and 2000 financial institutions. its Chinese users have exceeded 1 billion, and its users outside China have exceeded 0.3 billion, thus greatly improving the ease of cross-border settlement. Alipay's technical strategy is *BASIC*, that is, Blockchain, AI, Security, the Internet of Things, and Cloud Computing, in which, the blockchain cross-border payment is derivative. Xiuting [8] used the technical ability to support Alipay for the successful payment in industrial fields.

2.2.2. Cooperation with Overseas e-Commerce Platforms. Payment institutions can directly provide services for overseas e-commerce platforms. In terms of cross-border RMB payment, in the import business, the domestic e-commerce platform will pay the payment to the reserve account of the payment institution, then transfer it to the cross-border RMB reserve account, and complete the cross-border payment by sending the customer's cross-border payment instruction to the cooperative bank. In the export business, the cross-border collection cooperative institution paid the payment to the cross-border RMB reserve account of the payment institution. Junwen et al. [9] studied that the cooperative bank can automatically transfer it to the reserve account of the payment institution after completing the cross-border income declaration, and the payment institution can complete the merchant capital settlement.

2.2.3. Cooperation with Domestic Banks. Payment institutions provide payment services for both parties of cross-border transactions, and domestic cooperative banks provide payment institutions with cross-border RMB collection and payment, cross-border foreign currency collection and payment, foreign exchange settlement and sales, the balance of payments declaration, and other services. When cooperating with domestic banks, payment institutions are faced with the problems of channel rate and deposit of reserves. However, since the provision was implemented in 2019 that deposit reserves should be 100%, it has been a great blow to the payment institutions. The profit space of the third-party payment institutions that could obtain the interest difference under the provision has disappeared. However, some studies believe that interest rate spread is not the key, and the bargaining power of channel fees is the key [10, 11].

2.3. Overview of Cross-Border RMB Collection and Payment Business of Third-Party Payment Institutions. In 2019, China's cross-border RMB receipts and payments amounted to RMB19.7 trillion. In the same year, the cross-border RMB collection and payment amount of third-party payment institutions reached RMB500.424 billion, accounting for

about 2.5% of the total people's collection and payment amount in that year. In terms of data comparison, the proportion of third-party payment institutions in China's cross-border RMB collection and payment is small, which can only add to the overall situation of RMB internationalization.

3. Cross-Border RMB Support Policies of the Third-Party Payment Institutions: Analysis Based on Questionnaire

On May 20, 2021, a total of 56 questionnaires were distributed to third-party payment institutions with cross-border RMB qualifications. On June 9, 2021, the first batch of questionnaires was returned, and a total of 47 questionnaires were recovered, including 42 valid questionnaires and 5 invalid questionnaires.

3.1. Overview of Cross-Border RMB Business of Third-Party Payment Institutions in 2020. Among the 42 valid questionnaires, the third-party payment institution with the largest cross-border RMB business scale in 2020 had a cross-border RMB business scale of about RMB189.2 billion, accounting for about 40% of the total business scale of the 42 questionnaires, which was prominent. In addition to the payment institution, there are nine third-party payment institutions with a cross-border people's business scale of more than 10 billion. The total scale of the top 10 cross-border RMB businesses accounts for about 94% of the total scale of cross-border RMB business of all surveyed third-party payment institutions, and the scale of the last 32 accounts for only 6% of the total scale (refer to Figure 1 for details).

3.2. Policy Basis for the Development of Third-Party Payment Institutions. According to the feedback of the questionnaire, the main policy basis of China's third-party payment institutions in the process of exhibition involves 9 aspects: laws, regulations, measures, interim measures, and detailed rules, notices, opinions, announcements, and guidelines, both local and repealed. In particular, the abolition category is due to the rapid development and change of business; some policies can no longer adapt to the current business development, and some original policies have been abolished.

3.3. Difficulties and Pain Points of Third-Party Payment Institutions under the Existing Policy Framework. Concerning the main problems encountered by third-party payment institutions in the process of business development, among the feedback questionnaires, 7 payment institutions made it clear that there is no problem at present.

Other third-party payment institutions with cross-border RMB payment business have more or less fed back the main problems or difficulties in the process of exhibition. Generally speaking, it involves seven aspects. Firstly, I think the business process is cumbersome. Secondly, they believe that the policies related to cross-border RMB payment are not clear and unified. They hope that the policies will be unified and that there will be standardized business guidance.

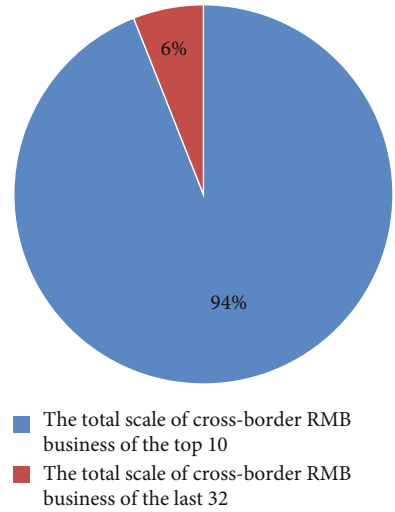

Figure 1: The total scale of cross-border RMB business.

Thirdly, they believe that there are practical obstacles in overseas business, including authenticity verification, the limited scope of a license, etc. Fourthly, we believe that we should deepen cooperation with domestic and foreign banks and further expand business areas. Because banks have strong customer relationships, they can provide high-quality customer protection to third-party payment institutions, which are supported by advanced digital technology, good computer analysis, and processing ability; the two complement each other. Fifthly, it is believed that there are other factors affecting business development, such as COVID-19 and identity. Sixthly, with the increasing use of third-party payment, the third-party payment platform user fund precipitation problem is serious and easily causes huge financial risks. As the use of third-party payments gradually increased, the number of funds invested significantly increased, and third-party payment institutions will be charged a large amount of interest, due to implicit improper handling of financial risks. Seventhly, in the industry of oligopoly competition, Alipay, Tenpay, and Yiqianbao occupy more than 90% of the third-party payment market share; most of the resources are monopolized by the oligopoly (refer to Figure 2 for details).

3.4. Cross-Border RMB Support Policies That Third-Party Payment Institutions Want to Obtain

3.4.1. They Hope to Promulgate Specific Measures for the Management of the Exhibition Industry, Allowing the Business Scope of the Exhibition Industry to Be Broader and Clearer. Because WTO divides trade mode into merchandise trade and commercial service trade, this article divides the trade mode into goods trade and nongoods trade based on WTO standards.

In terms of goods trade, only cross-border e-commerce B2C business is supported at present, but there are more legal and compliant businesses in the current market. For third-party payment institutions, such businesses have more market space, such as B2B and other industries. Therefore, it

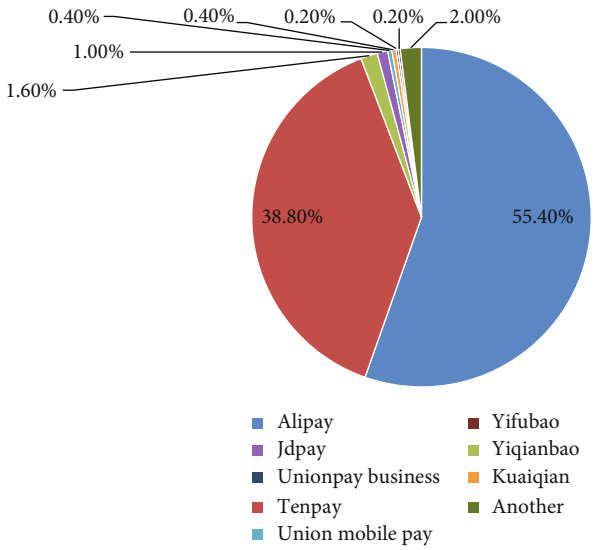

Figure 2: Third-party payment institution's market share. Data resource: https://www.sohu.com/a/317379295_120057347.

is hoped that relevant departments can give third-party payment institutions a wider scope of business development, to facilitate their further expansion of cross-border RMB business.

In terms of nongoods trade, due to different business types, the relevant requirements of the government for information collection may affect the compliance of certain businesses. For example, in the digital industry, the whole payment and transaction are completed on the Internet, and there is no logistics delivery link because it is impossible to collect logistics information, resulting in the inability of third-party payment institutions to cooperate with similar industries. Similar problems are also reflected in online car rental, house rental, various member services, games, and other industries.

For many cross-border e-commerce providers, while recovering the sales revenue of overseas e-commerce platforms to China, there is also a demand for funds to continue to be used for normal operating expenses such as overseas warehouse, procurement, tax payment, and commercial insurance expenses. Based on this demand and the product basis of cross-border e-commerce collection, some third-party payment institutions are also constantly exploring their business or extending the service scope from the collection of existing cross-border e-commerce platforms. After receiving the sales revenue of e-commerce platforms, they continue to provide one-stop payment services and pay the received funds directly to their domestic goods suppliers or service providers, It is expected to provide good payment services for more domestic enterprises or individuals engaged in cross-border trade.

3.4.2. It Is Hoped That the Single Transaction Limit of Service Trade Can Be Classified. In principle, it is not allowed to exceed RMB300,000 for current trade and other service items. Some third-party payment institutions encounter the problem of a single transaction limit in the actual cross-border RMB business exhibition. For example, in the payment scenario of studying abroad, college tuition fees are generally paid according to different school disciplines and years, which is generally more than RMB300,000. However, since split payment is not allowed, the third-party payment institutions are very limited in carrying out such business. In addition, for example, in other service trade scenarios under the current account, such as exhibition and conference services, there will also be more than RMB300,000 business scenarios, which will bring difficulties to the exhibition industry of third-party payment institutions according to the current regulations. It is hoped that the regulatory authorities can conduct research and analysis on such service trade based on the real transaction background and finally realize the classification limit [12–14].

3.4.3. It Is Hoped That Relevant Departments Can Promulgate Cross-Border RMB Management Measures or Operation Guidelines as Soon as Possible. At present, the standards for cross-border RMB business are not unified, and the regulatory provisions are diverse, resulting in no unified standard for third-party payment institutions to refer to when engaging in cross-border RMB business. If relevant departments can issue specific management measures or operation guidelines on cross-border RMB business and guide all third-party payment institutions to adopt unified cross-border RMB business standards, there will be a better and unified policy basis for the development of cross-border RMB business of third-party payment institutions, which is conducive to the further expansion of business of third-party payment institutions.

3.5. They Hope to Improve the Relevant Policies of Export Tax Rebate. There is a demand for an export tax rebate for cross-border e-commerce, but the RMB transaction flow distributed by domestic payment companies across the border cannot be used as the basis for the export collection of this e-commerce because the currency is RMB and the payment source is the provision of payment institutions, so the tax rebate cannot be handled. It is suggested to improve the export tax rebate policy to facilitate the export tax rebate of cross-border export e-commerce.

3.6. They Hope to Further Improve the Facilitation of Cross-Border Trade Settlement. In the current goods trade collection business, some third-party payment institutions will collect and review the customer's transaction information one by one in advance to meet the requirements of trade authenticity verification, resulting in increased system docking costs for customers, and some concerns about the impact of commercial privacy disclosure and transaction timelines. Therefore, some third-party payment institutions suggest further improving the facilitation of cross-border goods trade settlement based on risk and taking more convenient monitoring measures for the relevant businesses of high-quality platforms instead of the way of preaudit one by one, such as post transaction spot check. In addition, the development of trade under cross-border RMB services mainly depends on the risk control of various banks. It is

hoped that policy development will be given based on risk control. For example, each customer can encourage relevant businesses to leave the country and drive the growth of cross-border RMB business through facilitation measures such as annual restrictions on the amount of foreign exchange purchased and paid by cross-border people.

3.7. It Is Hoped That the Explanation and Implementation of Policies by Relevant Departments Are Unified. For cross-border RMB-related policies, in practice, both e-commerce enterprises and payment institutions are faced with the problem that many departments involved in cross-border policies fail to reach an agreement on policies. After the introduction of relevant policies, different institutions may have different understanding and interpretations of the policies, which brings confusion to the payment institutions engaged in cross-border RMB business. Therefore, the payment institutions hope that the relevant government departments can be more detailed and unified in the interpretation of the policies, to facilitate the smooth development of relevant businesses. At the same time, in terms of cooperation with banks, third-party payment institutions also hope that the cross-border audit standards and cross-border material requirements of banks can be unified, the operation process can be standardized, and the audit time can be shortened, to make cross-border transactions more smooth and fast.

4. Supervision of Cross-Border RMB-Related Businesses of Third-Party Payment Institutions

The core of financial supervision is the supervision of financial risks (Huang Da, 2003). The core of the supervision of cross-border RMB business for third-party payment institutions is still the supervision of financial risks. To prevent such financial risks, the supervision of cross-border RMB-related businesses of third-party payment institutions mainly includes the following three aspects.

4.1. Legal and Administrative Supervision: Mainly Payment Licenses from Scratch, from Loose to Tight. When the payment business license was first issued, it was issued quickly. However, from the issuance of payment licenses during the period from May 2011 to March 2015, it is obviously in a high open low trend (refer to Figure 3 for details).

In terms of the total amount, from May 2011 to December 2015, the total number of payment licenses issued in China reached 271.

Since December 2015, among the licenses issued, some licenses have been revoked due to violations, and some institutions have been merged for other reasons. Due to the rapid issuance of licenses in previous years, the whole payment industry ushered in a period of rapid development, but then, there began to be problems in provisions, clearing and settlement, second clearing, code set, false preauthorization (this event is the fuse for punishing third-party payment), machine cutting, cash out, and direct channel. The state began to rectify the whole payment industry. From 2015 to

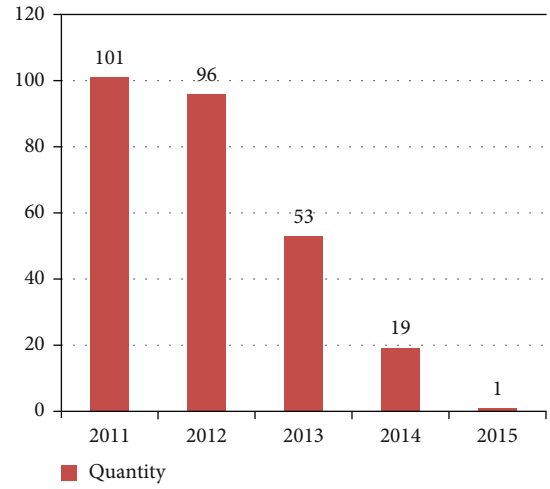

Figure 3: The license quantity authorized from May 2011 to December 2015. Data resource: https://www.sohu.com/a/317379295_120057347.

February 2021, 39 payment licenses have been canceled for various reasons, including voluntary applications for cancellation, merger cancellation, and more because of noncompliance or illegality of business, and no new institutions have been approved by the People's Bank of China ever since 2015 [15].

The number of payment institutions in China from 2015 to February 2021 is shown in Figure 4.

According to the above and Figure 4, the number of third-party payment institutions with payment licenses in China has dropped from a historical high of 271 to only 232 (by the end of September 2021). Judging from the number of licensed institutions since the end of 2015, there will be no significant change in the tightening trend of national licenses.

At the same time, the state will continue to maintain a high pressure on the unlicensed operation and payment business and coordinate the implementation of special inspection and "double random inspection." For regions and overseas merchants with a high risk of gambling and black ash industry, organize special inspection and patrol, establish an account blacklist system, and effectively control the fund settlement activities of suspected online gambling and black ash industry. Based on the reform of individual account classification, we will consolidate the risk prevention responsibilities of class II and III accounts, improve the risk monitoring mechanism, and strengthen the risk warning [16]. In short, the state's supervision situation is tightened for both unlicensed operations and payment institutions that operate with certificates but violate laws and regulations [17].

4.2. Technical Supervision, That Is, "Cut Off the Direct Connection." Under the current supervision system of third-party payment institutions in China, Huoqi (2020) pointed out that "cut off the direct connection" and full deposit of reserves are the two core policies [18].

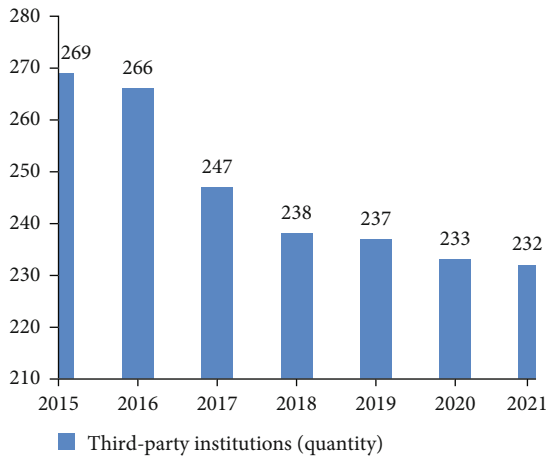

Figure 4: The quantity of China's third-party payment institution from 2015 to September 2021.

"Cut off the direct connection" refers to cutting off the direct data connection between the third-party payment institution and the bank.

In the "direct connection" mode, the third-party payment institution directly connects with the bank and sends the user's down payment request directly to the bank in the form of instructions to request payment. The customer's instructions are in the charge of the third-party payment institution, and the bank can only transfer funds according to the instructions of the third-party payment institution. Under the direct connection business mode, it is difficult for the regulator to grasp the capital flow of the third-party payment institution's transactions in time, so it is difficult to control the risk.

The establishment of the Internet connection platform can effectively solve this problem. It provides a connection between payment institutions and banks. By November 2018, the business migration of "disconnection and direct connection" will be completed. All network transactions involving bank cards in the business of third-party payment institutions need to be carried out through the Internet connection platform. Through the Internet connection platform, we can clearly grasp the flow of transactions and effectively improve the supervision efficiency of third-party payment institutions, It also improves the transparency of clearing between payment institutions and banks and plays an important role in preventing financial risks.

4.3. Economic Supervision

4.3.1. Deposit of Reserves. China's first third-party payment institution was founded in 1998, but till January 14, 2019, 100% of the reserves are required to be deposited. In the 20 years or so from the establishment of the third-party payment institution to the full deposit of the reserves, the payment institution has accumulated a large number of precipitated funds in its hands by taking advantage of its industry convenience. Meiling (2019) thought this part of funds once brought huge benefits to the payment institution by collecting interest. It is not too much to call it "lying and winning" [19]. In the era when the provisions were not required to be deposited, there was industry chaos in which third-party payment institutions misappropriated the provisions of customers, with large financial risk exposure. After January 14, 2019, the people's Bank of China successfully implemented the full deposit of reserves, firmly grasped the initiative of risk management, and made government supervision more confident.

4.3.2. Transaction Authenticity. Controlling the authenticity of transactions helps to prevent cross-border money laundering, cross-border gambling, cross-border online fraud, cross-border bribery capital outflow, and other cross-border illegal transactions. These funds may have a huge amount and bring huge risks to the whole financial system.

From the perspective of third-party payment institutions, the gradually tightened regulatory policies contradict the increasing requirements of customers for business facilitation. In the current market, customers will choose the most convenient payment institution to carry out business according to the principle of lower compliance and risk control requirements such as data and order information. At this time, institutions with high compliance and risk control requirements very easily lose customers, resulting in the phenomenon of "bad money expels good money." Nevertheless, the regulatory policy will only impose stricter requirements on the authenticity of transactions. In the long run, strict regulation will bring benefits to the future living space for good third-party institutions.

Liping and Pinxian [20] thought transaction authenticity includes the authenticity of the transaction subject and the authenticity of the transaction background or transaction content.

As for the authenticity of the transaction subject, cross-border e-commerce and third-party payment institutions should conduct due diligence and identify the identity of the transaction subject, mainly involving natural person transaction subjects and institutional transaction subjects [21–23].

(1) Natural Person Transaction Subject. For the identification of domestic natural persons, you may apply to join the "citizen network identification system" and "identity online verification system" developed and launched by the Ministry of Public Security to verify the identity information of customers and effectively reduce risks. However, at present, third-party payment institutions have not used such a system, resulting in the difficulty of identity verification. Various authors [24, 25] showed that the identification of overseas natural persons is more difficult because the other party is not willing to provide relevant identity information.

(2) Institutional Transaction Subject. At present, when examining the qualification of domestic online enterprises, third-party payment institutions cannot directly query the list of key supervision of RMB settlement enterprises and the list and enterprise level (A/B/C) classification of ASONE (digital foreign exchange management platform of the State Administration of Foreign Exchange), which must rely on

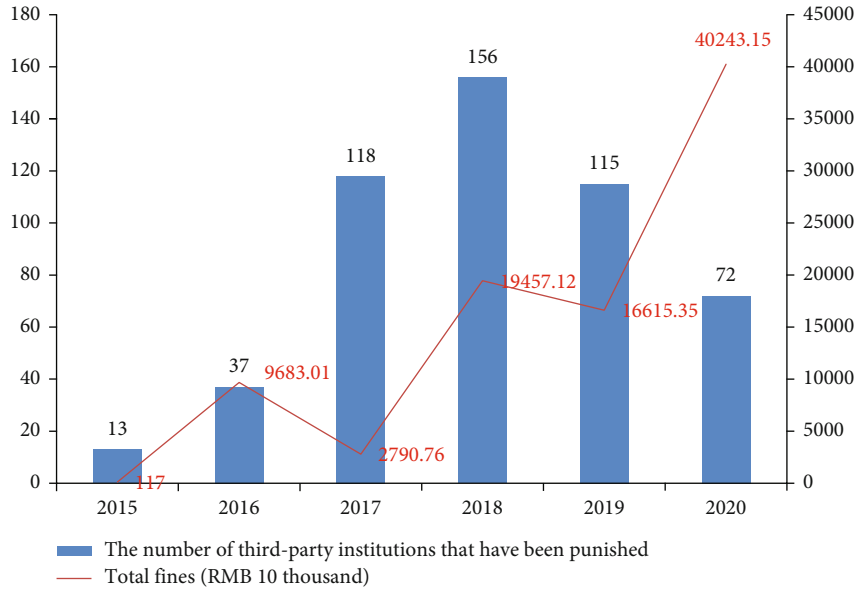

Figure 5: The economic punishment from 2015 to 2020 to the third-party institutions.

cooperative banks, resulting in audit delay. For the transaction subject of overseas legal person institutions, there are some difficulties in KYC (know your customer) work when the third-party payment institutions access overseas merchants [26, 27].

4.3.3. Economic Punishment for Violation of Laws and Regulations. Since 2015, China has gradually increased the intensity of economic punishment for the illegal acts of third-party payment institutions, confiscated the illegal income, and imposed a fine at the same time. Overall, from 2015 to 2020, the number of punished third-party payment institutions reached 156 in 2018, the highest in history (see Figure 5 for details).

In terms of amount, the amount of fines and confiscations for third-party payment institutions in 2020 has exceeded RMB400 million. Compared with the fine of RMB1.17 million in 2015, by 2020, the amount of fines and confiscations has become the main means of economic supervision, and the cost of violations is too high, which is enough for more third-party payment institutions to reflect on whether their business is standardized. It can be predicted that the means of economic punishment has become one of the main means to supervise third-party payment institutions and relevant senior executives [28–30].

5. Conclusions

5.1. There Are Good Basic Conditions for the Development of Third-Party Payment Institutions in China. The new forms of international trade have developed rapidly, such as the rapid development of cross-border e-commerce. In 2020, the import and export volume of cross-border e-commerce in China reached 1.69 trillion yuan, an increase of 31.1%. The total volume of the market procurement trade also exceeded 100 billion US dollars. Taking advantage of these basic conditions, some payment institutions have made their contributions to the overall strategy of RMB internationalization while achieving the development of cross-border RMB business. Generally speaking, the foundation is good, which provides conditions for the rapid, healthy, and standardized development of China's third-party payment institutions.

5.2. The Cross-Border RMB Business of Third-Party Payment Institutions Plays a Supporting Role in the Overall Situation of RMB Internationalization. From the past data analysis, commercial banks are still the absolute main body of China's current cross-border RMB business. Indeed, the share of third-party payment institutions in China's overall cross-border RMB business is small (2.5% in 2019), but in absolute terms, it has exceeded 500 billion yuan in 2019, which cannot be ignored. The standardized development of the cross-border RMB business of third-party payment institutions is a useful supplement to China's cross-border RMB business and will help the overall situation of China's RMB internationalization.

5.3. Third-Party Payment Institutions Hope to Get Policy Support in Cross-Border RMB Business. According to the questionnaire and relevant references, third-party payment institutions have made some achievements in carrying out cross-border RMB business, but at the same time, they also feel that some policy restrictions have bound their hands. Generally speaking, third-party payment institutions hope to obtain policy support from relevant national departments in terms of cross-border RMB business, such as exhibition guidance, license scope, transaction limit, export tax rebate, and consistency of policy implementation and understanding. It is hoped that relevant departments will earnestly consider the reasonable demands of third-party payment institutions and give more business autonomy and convenience to third-party payment institutions within the scope permitted by laws and policies, to promote their better and

faster development. Because of the above investigation and analysis, the following suggestions are put forward.

First: it is suggested that the regulators should give policy support to third-party payment institutions in respect of routine business, unconventional business, and innovative business. Of course, these support policies should be based on the principles of real transaction background and controllable risk, and the support policies should be flexible and in line with market development, with support and inclusiveness as the starting point, to better understand and support the new things encountered by third-party payment institutions in the forefront of cross-border RMB payment.

Second: it is suggested to realize the classified limit instead of treating all similar cross-border RMB businesses with a unified limit standard. At present, the single transaction of service trade and other current accounts shall not exceed 300,000 yuan in principle, which restricts the normal development of third-party payment institutions and is not conducive to their development.

Third: it is suggested to provide more convenient policy support for third-party payment institutions that conduct business legally and in compliance, specifically to include export tax rebate, identity recognition, unified methods, consistent policy implementation standards, etc., to solve the embarrassing situation faced by third-party payment institutions in the process of business development.

5.4. Third-Party Payment Institutions Engaged in Cross-Border RMB Business Should Develop in a Standardized Manner under Strict Supervision. The state's supervision of third-party payment institutions is becoming more and more strict. Third-party payment institutions engaged in cross-border RMB business face a more complex business environment due to their cross-border business, so they should be more cautious in terms of business legitimacy and compliance. Thus, the situation of "bad money expelling good money" may occur in the past with the continuous development and progress of the state in legal, administrative, technical, economic, and other regulations. The third-party payment institutions engaged in business in violation of laws and all other guidelines will face a heavy blow from the regulators. Strict supervision is a long-term trend of supervision in the financial field. Any third-party payment institution should standardize its development and win the future for itself.

Data Availability

The data in the paper are obtained from an open website. All the data are available from the corresponding author upon request.

Conflicts of Interest

The author declares that there are no conflicts of interest regarding the publication of this paper.

References

[1] C. Weidong and Z. Xueqing, "Research on the development path of RMB internationalization," *International Economic Review*, vol. 148, no. 4, pp. 28–37, 2020.

[2] X. Qing, W. Yufei, X. Qianyu, Z. Weiwei, and Y. Zhihui, "Research on anti money laundering supervision of third-party payment from the perspective of game theory," *Journal of Harbin University*, vol. 40, no. 5, pp. 32–36, 2019.

[3] C. Chunzhu and L. Zhaolin, "Third party payment money laundering: characteristics, risks, punishment difficulties and countermeasures," *Chongqing Social Sciences*, vol. 311, no. 10, pp. 66–78, 2020.

[4] L. Gang, "Realistic thinking on the development of third-party payment and industry supervision in China," *Exploration of Financial Theory*, vol. 192, no. 4, pp. 62–70, 2020.

[5] Y. Song and Z. Bo, "Research on the regulatory policy of third-party payment based on text analysis," *Rule of Law and Society*, vol. 1051, no. 3, pp. 99–102, 2021.

[6] F. Sixian and B. Lihong, "International comparison and enlightenment of third-party payment supervision mechanism," *Shanghai Economic Research*, vol. 317, no. 11, pp. 47–54, 2015.

[7] L. Che, P. Xin, P. Hongwei, and F. Li, "International experience comparison of third-party payment supervision," *Southwest Finance*, vol. 231, pp. 42–47, 2018.

[8] Y. Xiuting, "Third party payment internet market development and regulation," *People's Tribune*, vol. 698, no. 7, pp. 82–85, 2021.

[9] Z. Junwen et al., "Objectives and institutional arrangements of third-party payment supervision," *Research on Financial Regulation*, vol. 87, no. 3, pp. 79–97, 2019.

[10] G. Binbin, *Empirical Study on Consumer Personal Information Protection in Third-Party Payment*, vol. 35, Zhengzhou University, 2020.

[11] W. Lizi, *Research on Legal Issues of Third-Party Payment and Consumer Protection*, vol. 44, Hebei University, 2020.

[12] Q. Jianbo, X. Lili, and Z. Xinjian, "Research on third party payment risk and countermeasures," *Jilin Financial Research*, vol. 80, no. 4, pp. 68–71, 2021.

[13] L. Lianke and C. Bo, "China Payment and Clearing Association China Payment Industry Annual Report 2020," vol. 3, China Finance Press, 2020.

[14] G. Shuqing, "To solve the new challenges facing by financial technology development," *Financial View*, vol. 301, no. 1, p. 38, 2021.

[15] C. Ting, "Research on the impact of third-party payment business on commercial banking business in China," *Enterprise Technology and Development*, vol. 435, no. 3, pp. 146–148, 2021.

[16] Y. Lihua, "Competitive impact assessment of business concentration in third-party payment industry," *Gansu Social Sciences*, vol. 238, no. 6, pp. 182–188, 2019.

[17] P. Jiadong and C. Haodong, "Has the Internet third-party payment platform formed a monopoly – a study based on the measurement of market power," *Journal of Guangdong University of Finance and economics*, vol. 36, no. 4, pp. 29–37, 2021.

[18] H. Qi, "Supervision logic and system innovation of third party payment under the background of "cutting off direct

connection"," *Shanghai Jiao Tong University*, vol. 467, no. 5, pp. 1–39, 2020.

[19] M. Ling, "The era of third-party payment lying win is over," *China Quality Wanli travel*, vol. 302, no. 2, pp. 94-95, 2019.

[20] Z. Liping and Y. Pinxian, "Cross border e-commerce payment status, risks and regulatory countermeasures," *Shanghai Finance*, vol. 430, no. 5, pp. 73–78, 2016.

[21] G. Lei, "Legal risks prevention and control measures facing by China's third-party cross-border payment institutions," *Practice in Foreign Economic Relations and Trade*, vol. 448, no. 4, pp. 73–76, 2020.

[22] L. Jingjing and D. Peng, "Research on the risk and governance of illegal application of aggregate payment," *Journal of People's Public Security University of China (Social Sciences Edition)*, vol. 37, no. 6, pp. 79–86, 2021.

[23] C. Wencui, "Research on evolutionary game between commercial banks and third-party payment institutions in China," *Journal of Nanjing University of Technology (Social Sciences Edition)*, vol. 16, no. 6, pp. 115–121, 2017.

[24] D. Liuqing, *Comparative Study on the Supervision of Precipitated Funds of Third-Party Payment Platforms between China and Germany*, vol. 24, Nanjing University, 2020.

[25] Y. Ting, "The post era of "Disconnection and direct connection": research on the sustainable development of network connected platform," *Journal of Hubei University of Economics (Humanities and Social Sciences)*, vol. 16, no. 4, pp. 79–82, 2019.

[26] Q. Chen and L. Kaishen, "A preliminary study on the cross-border development of third-party payment enterprises——taking Alipay as an example," *SEZ Economy*, vol. 296, no. 9, pp. 208–210, 2013.

[27] W. Jin and W. Yongqi, "Research on the legal supervision of the third-party payment platform of Internet in our country," *Business Economy*, vol. 553, no. 9, pp. 147–149, 2022.

[28] Z. Yuxin, G. Rui, W. Huiyu, and T. Xiaofeng, "The development course and trend analysis of the third party payment in our country," *Modern Business*, vol. 588, no. 12, pp. 3–5, 2022.

[29] Y. Luo, L. Cunjin, and L. Bin, "Study on the competitive evolution mechanism of third-party payment institution and commercial bank based on double-layer network," *Chinese Management Science*, vol. 229, pp. 1–14.

[30] L. Nan, "Discussion on the impact of third-party payment on financial accounting of public hospitals and standardized management," *Assets and Finance of administrative Undertakings*, vol. 327, no. 6, pp. 94-95, 2021.

Hindawi
Advances in Mathematical Physics
Volume 2022, Article ID 6815685, 10 pages
https://doi.org/10.1155/2022/6815685

Research Article

The K Extended Laguerre Polynomials Involving ${}_rF_r, r > 2$

Adnan Khan,[1] **M. Haris Mateen**,[2] **Ali Akgül**,[3] **and Md. Shajib Ali**[4]

[1]*Department of Mathematics, National College of Business Administration & Economics, Lahore, Pakistan*
[2]*Department of Management Science, National University of Modern Languages, Lahore, Pakistan*
[3]*Department of Mathematics, Art and Science Faculty, Siirt University, Siirt 56100, Turkey*
[4]*Department of Mathematics, Islamic University, Kushtia 7003, Bangladesh*

Correspondence should be addressed to Md. Shajib Ali; shajib_301@yahoo.co.in

Received 9 June 2022; Revised 4 August 2022; Accepted 17 August 2022; Published 5 September 2022

Academic Editor: Qura Tul Ain

In this manuscript, we present the generalized hypergeometric function of the type ${}_rF_r, r > 2$ and extension of the K Laguerre polynomial for the K extended Laguerre polynomials $\{A_{r,n,k}^{(\alpha)}(x)\}$. Additionally, we describe the K generating function, K recurrence relations, and KS Rodrigues formula.

1. Introduction

Laguerre polynomials are utilized to investigate non-central Chi-square distribution. Many works are existed in the literature with implementation to classical orthogonal polynomials. There many extensions of Laguerre polynomials.

A large number of properties of Laguerre polynomials have been described in classical works, e.g., Erdélyi et al. [1] and Bell [2]; also we can refer to Wang and Guo [3] and Mathai [4].

Chak [5] has given a representation for the Laguerre polynomials. Carlitz [6] proved the recurrence relations involving Laguerre polynomials. Al-Salam [7] proved several results involving Laguerre polynomials. Prabhakar [8] introduced that generating functions, integrals, and recurrence relations are obtained for the polynomials $Z_n^{\alpha}(x;k)$ in x^k..

Andrews et al. [9], Chen and Srivastava [10], Trickovic and Stankovic [11], Radulescu [12], and Doha et al. [13] have done a lot of work for properties of Laguerre polynomials. Akbary et al. [14] can be referred for other application of Laguerre polynomials. Li [15], Aksoy et al. [16], Wang [17], and Krasikov and Zarkh [18] studied problems of permutation of polynomials; bijection that can induce polynomials with integer coefficients is modulo m.

In this manuscript, we present the properties of the extending Laguerre polynomial including ${}_rF_r, r > 2$; we consider

$$L_n^{(\alpha)}(x) = \frac{(1+\alpha)_n}{n!}\,{}_1F_1(-n;1+\alpha;x). \tag{1}$$

Shively [19] extended the Laguerre polynomials as

$$R_n(a,x) = \frac{(a)_{2n}}{n!(a)_n}\,{}_1F_1(-n;a+n;x). \tag{2}$$

Habibullah [20] demonstrated the Rodrigues formula as

$$\begin{aligned} R_n(a+1,x) &= \frac{e^x x^{-\alpha-n}}{n!} D^n\left(x^{\alpha+2n}e^{-x}\right), \\ L_n^{(\alpha)}(x) &= \frac{e^x x^{-\alpha}}{n!} D^n\left(x^{\alpha+n}e^{-x}\right). \end{aligned} \tag{3}$$

Erdélyi et al. [1] introduced

$$D^m\left[x^{\alpha+m}L_n^{(\alpha+m)}(x)\right] = \frac{\Gamma(\alpha+m+n+1)}{\Gamma(\alpha+n+1)} x^{\alpha}L_n^{(\alpha)}(x), D = \frac{d}{dx}. \tag{4}$$

Khan and Habibullah [21] introduced $A_{2,n}(x) = {}_2F_2(-n/2, (-n+1/2); 1/2, 1; x^2)$.

Khan and Kalim [22] introduced

$$A_{3,m}^{(\alpha)}(y) = \frac{(1+\alpha)_m}{m!}\,{}_3F_3\left(\frac{-m}{3}, \frac{-m+1}{3}, \frac{-m+2}{3}; \frac{1+\alpha}{3}, \frac{2+\alpha}{3}, \frac{3+\alpha}{3}; y^3\right). \tag{5}$$

Khan et al. [23] proposed extended Laguerre polynomials $\left\{ A_{q,n}^{(\alpha)}(x) \right\}$.

Parashar [24] presented a new set of Laguerre polynomials $L_n^{(\alpha,h)}(x)$ related to the Laguerre polynomials $L_n^{(\alpha)}(x)$. Sharma and Chongdar [25] proved an extension of bilateral generating functions of the modified Laguerre polynomials.

Researchers [26–28] found additional properties of k gamma and k beta functions. Then, Mubeen and Habibullah [29] introduced k fractional integrals and discussed its application. Mubeen and Habibullah [30] introduced an integral representation of some k hypergeometric functions. Krasniqi [31] derived some properties of the k gamma and k beta function. Mubeen [32] proved the properties of confluent k integrals by using k fractional integrals. There is a tremendous scope to study k polynomials using k gamma, k beta, and k hypergeometric functions. Kokologiannaki and Krasniqi [33] introduced k analogue of the Riemann Zeta function and also proved some inequities relating to Riemann Zeta function and k gamma functions.

Din et al. [34] understand the dynamical behavior such diseases; they fitted a susceptible-infectious quarantined model for human cases with constant proportions. Din et al. [35] investigated a newly constructed system of equation for hepatitis B disease in sense of Atanganaa–Baleanu Caputo (ABC) fractional order derivative. Din et al. [36] developed the analysis of a non-integer-order model for hepatitis B (HBV) under singular type Caputo fractional order derivative. They investigated proposed system for an approximate or semi-analytical solution using Laplace transform along with decomposition techniques by Adomian polynomial of nonlinear terms and some perturbation techniques of homotopy (HPM). Din [37] investigated the spread of such contagion by using a delayed stochastic epidemic model with general incidence rate, time-delay transmission, and the concept of cross immunity.

Ain et al. [38] impression of activated charcoal is shaped by the fractional dynamics of the problem, which leads to speedy and low-cost first aid. Ain et al. [39] presented an impulsive differential equation system, which is useful in examining the effectiveness of activated charcoal in detoxifying the body with methanol poisoning. Din and Ain [40] developed a model based on a stochastic process that could be utilized to portray the effect of arbitrary-order derivatives. A nonlinear perturbation is used to study the proposed stochastic model with the help of white noises.

Rehman et al.'s [41] unsaturated porous media were analyzed by solving Burger's equation using the variational iterative modeling and homotopy perturbation method. Wang and Wang [42] described two different types of plasma models with variable coefficients by using the fractal derivative. Wang [43] investigated the fractal nonlinear dispersive Boussineq-like equation by variational perspective for the first time. The fractal variational principle of the fractal Boussineq-like equation was established via fractal semi-inverse method (FSM).

2. Extended Polynomials

Lemma 1.

If $k, j \in \mathbb{Z}^+$ and n is any non-negative integer. Then, we will get

$$\left(\frac{-n}{r}\right)_{kj}\left(\frac{-n+1}{r}\right)_{kj}\cdots\left(\frac{-n+r-1}{r}\right)_{kj} = (-1)^{rkj}\frac{n!}{r^{rkj}(n-rkj)!}. \tag{6}$$

Proof.

$$\begin{aligned}
&\left(\frac{-n}{r}\right)_{kj}\left(\frac{-n+1}{r}\right)_{kj}\cdots\left(\frac{-n+r-1}{r}\right)_{kj}\\
&= \left(\frac{-n}{r}\right)\left(\frac{-n}{r}+1\right)\left(\frac{-n}{r}+2\right)\cdots\\
&\left(\frac{-n}{r}+kj-1\right)\left(\frac{-n+1}{r}\right)\left(\frac{-n+1}{r}+1\right)\left(\frac{-n+1}{r}+2\right)\cdots\\
&\left(\frac{-n+1}{r}+kj-1\right)\left(\frac{-n+r-1}{r}\right)\left(\frac{-n+r-1}{r}+1\right)\\
&\left(\frac{-n+r-1}{r}+2\right)\cdots\left(\frac{-n+r-1}{r}+kj-1\right)\\
&= \left(\frac{-n}{r}\right)\left(\frac{-n+r}{r}\right)\left(\frac{-n+2r}{r}\right)\cdots\left(\frac{-n+rkj-r}{r}\right)\left(\frac{-n+1}{r}\right)\\
&\left(\frac{-n+r+1}{r}\right)\left(\frac{-n+2r+1}{r}\right)\cdots\left(\frac{-n+rkj-r+1}{r}\right)\\
&\left(\frac{-n+r-1}{r}\right)\left(\frac{-n+2r-1}{r}\right)\left(\frac{-n+3r-1}{r}\right)\cdots\left(\frac{-n+rkj-1}{r}\right).
\end{aligned} \tag{7}$$

By simplification we get our desired result. □

Lemma 2.

If $k \in \mathbb{Z}^+$ and n is any non-negative integer, thus

$$(\alpha)_{kn} = k^{kn}\left(\frac{\alpha}{k}\right)_n\left(\frac{\alpha+1}{k}\right)_n\cdots\left(\frac{\alpha+k-1}{k}\right)_n. \tag{8}$$

Rainville [44] (p 22)).

Lemma 3.

Assume that $k \in \mathbb{Z}^+$ and n is any non-negative integer. Then, we reach

$$\sum_{n=0}^{\infty}\sum_{k=0}^{n}B(k,n) = \sum_{n=0}^{\infty}\sum_{k=0}^{\infty}B(k,n+k). \tag{9}$$

Rainville [44] (p 57)).

Table 1: .

The extended Laguerre polynomials $A_{q,n}^{(\alpha)}(x)$ Khan et al. [23]
The K extended Laguerre polynomials $A_{r,n,k}^{(\alpha)}(x)$
$A_{q,n}^{(\alpha)}(x) = \frac{e^x(q+\alpha)_n}{n!}\,{}_qF_q\left(\begin{matrix}\frac{-n}{q}, \frac{-n+1}{q}, \cdots, \frac{-n+q-1}{q}\\ \frac{q+\alpha}{q}, \frac{q+1+\alpha}{q}, \cdots, \frac{2q+\alpha-1}{q}\end{matrix}; x^q\right)$
$A_{r,n,k}^{(\alpha)}(x) = \frac{e^x(rk+\alpha)_{n,k}}{(n;k)!}\,{}_rF_{r,k}\left(\begin{matrix}\left(\frac{-n}{r},k\right), \left(\frac{-n+k}{r},k\right), \cdots, \left(\frac{-n+rk-1}{r},k\right);\\ \left(\frac{\alpha+kr}{r},k\right), \left(\frac{\alpha+rk+1}{r},k\right), \cdots, \left(\frac{\alpha+2rk-1}{r},k\right)\end{matrix}; x^r\right).$
If we put $k=1$ in our paper, then we get the result of Khan et al. [23].

Lemma 4.

Assume that $k \in \mathbb{Z}^+$ and n is any non-negative integer. Thus, we have

$$\sum_{n=0}^{\infty}\sum_{k=0}^{\infty} B(k,n) = \sum_{n=0}^{\infty}\sum_{k=0}^{n} B(k,n-k). \tag{10}$$

Rainville [44] (p 56)).

3. The K Extended Laguerre Polynomials $A_{r,n,k}^{(\alpha)}(x)$

We describe the K extended Laguerre polynomial set $\{A_{r,n,k}^{(\alpha)}(x)\}$ as

$$A_{r,n,k}^{(\alpha)}(x) = \frac{e^x(rk+\alpha)_{n,k}}{(n;k)!}\,{}_rF_{r,k}\left(\begin{matrix}\left(\frac{-n}{r},k\right), \left(\frac{-n+k}{r},k\right), \cdots, \left(\frac{-n+rk+1}{r},k\right);\\ \left(\frac{\alpha+kr}{r},k\right), \left(\frac{\alpha+rk+1}{r},k\right), \cdots, \left(\frac{\alpha+2rk-1}{r},k\right)\end{matrix}; x^r\right), \tag{11}$$

where $\alpha \in \mathbb{R}, n, r, k \in \mathbb{Z}^+$.

Theorem 5.

If $\{A_{r,n,k}^{(\alpha)}(x)\}$, are the K extended Laguerre polynomials. Then

$$A_{r,n,k}^{(\alpha)}(x) = e^x(rk+\alpha)_{n,k}\sum_{j=0}^{[n/rk]}\frac{(-1)^{rkj}}{(n-rkj;k)!(rk+\alpha)_{rkj}}\frac{(x)^{rkj}}{(rkj;k)!}, \tag{12}$$

$$\alpha \in \mathbb{R}, n, r, k \in \mathbb{Z}^+. \tag{13}$$

Proof.

Consider

$$A_{r,n,k}^{(\alpha)}(x) = \frac{e^x(rk+\alpha)_{n,k}}{(n;k)!}\,{}_qF_{q,k}\left(\begin{matrix}\left(\frac{-n}{r},k\right), \left(\frac{-n+k}{r},k\right), \cdots, \left(\frac{-n+rk+1}{r},k\right);\\ ;x^r\\ \left(\frac{\alpha+rk}{r},k\right), \left(\frac{\alpha+rk+1}{r},k\right), \cdots, \left(\frac{\alpha+2rk-1}{r},k\right)\end{matrix}\right).$$
$$= \frac{e^x(rk+\alpha)_{n,k}}{(n;k)!} \times \sum_{j=0}^{[n/rk]}\left\{\frac{((-n/r),k)_j((-n+k/r),k)_j \cdots ((-n+rk+1/r),k)_j}{((\alpha+kq/r),k)_j((\alpha+qk+1/r),k)_j \cdots ((\alpha+2rk-1/r),k)_j}\right\}\frac{(x)^{rkj}}{(rkj;k)!}. \tag{14}$$

By using Lemma (1)

$$A_{r,n,k}^{(\alpha)}(x) = \frac{e^x(rk+\alpha)_{n,k}}{(n;k)!} \times \sum_{j=0}^{[n/rk]}\left[\frac{(-1)^{rkj}(n;k)!}{r^{rj}(n-rkj;k)!((\alpha+rk/r),k)_j((\alpha+rk+1/r),k)_j \cdots ((\alpha+2rk-1/r),k)_j}\right]\frac{(x)^{rkj}}{(rkj;k)!}. \tag{15}$$

Now, by applying Lemma (2), we get our desired result. □

4. K Generating Functions

Theorem 6.
Suppose that $n, j, k \in \mathbb{Z}^+$. Thus, we reach

$$\sum_{n=0}^{\infty}\sum_{j=0}^{[n/rk]}\frac{(-1)^{rkj}e^x t^n}{(n-rkj\,;k)!(rk+\alpha)_{rkj}}\frac{(x)^{rkj}}{(rkj\,;k)!} = e^x M_k(t)\,{}_0F_{r,k}\left(--;\left(\frac{rk+\alpha}{r}\,;k\right),\left(\frac{rk+1+\alpha}{r}\,;k\right),\cdots,\left(\frac{2rk+\alpha-1}{r}\,;k\right);\left(\frac{-xt}{r}\right)^r\right). \tag{16}$$

Proof.
We have

$$\begin{aligned}&\sum_{n=0}^{\infty}\sum_{j=0}^{[n/rk]}\frac{(-1)^{rkj}e^x t^n}{(n-rkj\,;k)!(rk+\alpha)_{rkj}}\frac{(x)^{rkj}}{(rkj\,;k)!}\\ &=\sum_{n=0}^{\infty}\sum_{j=0}^{\infty}\frac{(-1)^{rkj}e^x t^{n+rkj}}{(n\,;k)!(rk+\alpha)_{rkj}}\frac{(x)^{rkj}}{(rkj\,;k)!}\\ &=e^x\left[\sum_{n=0}^{\infty}\frac{t^n}{(n\,;k)!}\right]\left[\sum_{j=0}^{\infty}\frac{(-1)^{rkj}t^{rkj}}{(rk+\alpha)_{rkj}}\frac{(x)^{rkj}}{(rkj\,;k)!}\right]\\ &=e^x M_k(t)\sum_{j=0}^{\infty}\frac{(-xt)^{rkj}}{(rk+\alpha)_{rkj}(rkj\,;k)!}\end{aligned} \tag{17}$$

By applying Lemma (2), we get

$$\begin{aligned}&\sum_{n=0}^{\infty}\sum_{j=0}^{[n/rk]}\frac{(-1)^{rkj}e^x t^n}{(n-rkj\,;k)!(rk+\alpha)_{rkj}}\frac{(x)^{rkj}}{(rkj\,;k)!}\\ &=e^x M_k(t)\\ &\times\sum_{j=0}^{\infty}\frac{(-xt)^{rkj}}{r^{rkj}((rk+\alpha/r)\,;k)_j((rk+1+\alpha/r)\,;k)_j\cdots((2rk+\alpha-1/r)\,;k)_j(rkj\,;k)!}.\end{aligned} \tag{18}$$

After simplification, we get our result. □

Corollary 7.
Suppose that $\alpha \in \mathbb{R}$and $n, r, j, k \in \mathbb{Z}^+$. Thus, we reach

$$\sum_{n=0}^{\infty}\frac{A\begin{matrix}(\alpha)\\ r,n,k\end{matrix}(x)t^n}{(rk+\alpha)_{n,k}} = e^x M_k(t)\,{}_0F_{r,k}\left(\begin{matrix}--;\\ \left(\frac{-xt}{r}\right)^r\\ \left(\frac{rk+\alpha}{r}\,;k\right),\left(\frac{rk+1+\alpha}{r}\,;k\right),\cdots,\left(\frac{2rk+\alpha-1}{r}\,;k\right);\end{matrix}\right). \tag{19}$$

Proof.
From Equation (12), we acquire

$$\sum_{n=0}^{\infty}\left[\frac{A\begin{matrix}(\alpha)\\ r,n,k\end{matrix}(x)}{(rk+\alpha)_{n,k}}\right]t^n = \sum_{n=0}^{\infty}\left[\sum_{j=0}^{[n/rk]}\left[\frac{(-1)^{rkj}}{(n-rkj\,;k)!(rk+\alpha)_{rkj}}\right]\frac{(x)^{rkj}}{(rkj\,;k)!}\right]t^n. \tag{20}$$

Then, we have our result. □

Theorem 8.
If $c \in \mathbb{Z}^+$, then

$$\sum_{n=0}^{\infty}\frac{(c)_{n,k}A\begin{matrix}(\alpha)\\ r,n,k\end{matrix}(x)t^n}{(\alpha+rk)_{n,k}} = \frac{e^x}{(1-kt)_k^{c/k}}\times{}_rF_{r,k}\left(\begin{matrix}\left(\frac{c}{r},k\right),\left(\frac{c+k}{r},k\right),\cdots,\left(\frac{c+rk+1}{r},k\right);\left(\frac{-xt}{(1-kt)_k^{1/k}}\right)^r\\ \left(\frac{\alpha+rk}{r},k\right),\left(\frac{\alpha+rk+1}{r},k\right),\cdots,\left(\frac{\alpha+2rk-1}{r},k\right);\end{matrix}\right). \tag{21}$$

Proof.
From Equation (20), we note that

$$\sum_{n=0}^{\infty}(c)_n\left[\frac{A\begin{matrix}(\alpha)\\ r,n,k\end{matrix}(x)}{(rk+\alpha)_{n,k}}\right]t^n = \sum_{n=0}^{\infty}(c)_n e^x\left[\sum_{j=0}^{[n/rk]}\left[\frac{(-1)^{rkj}}{(n-rkj\,;k)!(rk+\alpha)_{rkj}}\right]\frac{(x)^{rkj}}{(rkj\,;k)!}\right]t^n. \tag{22}$$

We get

$$\begin{aligned}\sum_{n=0}^{\infty}\frac{(c)_{n,k}A\begin{matrix}(\alpha)\\ r,n,k\end{matrix}(x)t^n}{(rk+\alpha)_{n,k}} &= \sum_{n=0}^{\infty}\sum_{j=0}^{\infty}\frac{(c)_{n+rkj,k}e^x t^{n+rkj}}{(n\,;k)!}\frac{(-1)^{rj}(x)^{rkj}}{(rk+\alpha)_{rkj,k}(rkj)!}\\ &=\sum_{j=0}^{\infty}\left[\sum_{n=0}^{\infty}\frac{(c+rkj)_{n,k}t^n}{(n\,;k)!}\right]\left[\frac{(c)_{rj,k}}{(\alpha+rk)_{rj,k}}\right]\frac{e^x(-xt)^{rkj}}{(rkj\,;k)!},\end{aligned} \tag{23}$$

Since $(c)_{n+rkj,k} = (c+rkj)_{n,k}(c)_{rj,k}$, and $(1-kt)_k^{-(m/k)} = \sum_{n=0}^{\infty}(m)_{n,k}t^n/(n\,;k)!$ it thus implies that

$$\begin{aligned}\sum_{n=0}^{\infty}\frac{(c)_{n,k}A\begin{matrix}(\alpha)\\ r,n,k\end{matrix}(x)t^n}{(\alpha+rk)_{n,k}} &= \sum_{j=0}^{\infty}\left[\frac{(c)_{rkj,k}}{\left[(1-t)^{c+rkj}\right](\alpha+rk)_{rj,k}}\right]\frac{e^x(-xt)^{rkj}}{(rkj\,;k)!}\\ &=\frac{e^x}{(1-kt)_k^{c/k}}\sum_{j=0}^{\infty}\left[\frac{(c)_{rkj,k}}{(rk+\alpha)_{rj,k}}\right]\frac{\left(-xt/(1-kt)_k^{1/k}\right)^{rjk}}{(rjk\,;k)!}\end{aligned} \tag{24}$$

□

Corollary 9.

Assume that $\alpha \in \mathbb{R}$ and $n, r, j, k \in \mathbb{Z}^+$. Thus, we reach

$$\sum_{n=0}^{\infty} A_{r,n,k}^{(\alpha)}(x)t^n = \frac{1}{(1-kt)_k^{(\alpha+qk)/k}} exp\left(\frac{x-2xt}{1-t}\right). \tag{25}$$

Proof.

We choose $c = r + \alpha$ in Equation (21). We can reach the desired results. □

5. K Recurrence Relations

Theorem 10.

Assume that $\alpha \in \mathbb{R}$ and $n, j, k \in \mathbb{Z}^+$. Thus, we reach

$$xDA_{r,n,k}^{(\alpha)}(x) = (n+x)A_{r,n,k}^{(\alpha)}(x) - (rk+\alpha+n-1)A_{r,n-1,k}^{(\alpha)}(x), D = \frac{d}{dx}. \tag{26}$$

Proof.

From Equation (16)

$$\sum_{n=0}^{\infty} \frac{A_{r,n,k}^{(\alpha)}(x)t^n}{(rk+\alpha)_{n,k}} = e^x M_k(t) {}_0F_{r,k}\left(\begin{matrix} --; \left(\frac{-xt}{r}\right)^r \\ \left(\frac{rk+\alpha}{r}; k\right), \left(\frac{rk+1+\alpha}{r}; k\right), \cdots, \left(\frac{2rk+\alpha-1}{r}; k\right); \end{matrix}\right). \tag{27}$$

Let

$$\sigma_{r,n,k}(x) = \frac{A_{r,n,k}^{(\alpha)}(x)}{(\alpha+rk)_{n,k}}. \tag{28}$$

Suppose that

$${}_0F_{r,k}\left(\begin{matrix} --; \left(\frac{-xt}{r}\right)^r \\ \left(\frac{rk+\alpha}{r}; k\right), \left(\frac{rk+1+\alpha}{r}; k\right), \cdots, \left(\frac{2rk+\alpha-1}{r}; k\right); \end{matrix}\right) = \psi\left(\frac{x^r t^r}{r}\right). \tag{29}$$

Then

$$F = e^x M_k(t)\psi\left(\frac{x^r t^r}{r}\right) = \sum_{n=0}^{\infty} \sigma_{r,n,k}(x)t^n. \tag{30}$$

By taking partial derivatives,

$$\frac{\partial F}{\partial x} = e^x M_k(t)\psi + x^{r-1}t^r e^x M_k(t)\psi', \tag{31}$$

$$\frac{\partial F}{\partial t} = e^x M_k(t)\psi + x^r t^{r-1} e^x M_k(t)\psi', \tag{32}$$

$$x\frac{\partial F}{\partial x} - t\frac{\partial F}{\partial t} = xF - tF. \tag{33}$$

Since

$$F = \sum_{n=0}^{\infty} \sigma_{r,n,k}(x)t^n, \tag{34}$$

therefore $\partial F/\partial x = \sum_{n=0}^{\infty} \sigma'_{r,n,k}(x)t^n$, and $t(\partial F/\partial t) = \sum_{n=0}^{\infty} n\sigma_{r,n,k}(x)t^n$.

Equation (33), then yields

$$\begin{aligned} x\sum_{n=0}^{\infty} \sigma'_{r,n,k}(x)t^n - \sum_{n=0}^{\infty} n\sigma_{r,n,k}(x)t^n \\ = x\sum_{n=0}^{\infty} \sigma_{r,n,k}(x)t^n - \sum_{n=0}^{\infty} \sigma_{r,n,k}(x)t^{n+1} = x\sum_{n=0}^{\infty} \sigma_{r,n,k}(x)t^n \\ - \sum_{n=1}^{\infty} \sigma_{r,n-1,k}(x)t^n. \end{aligned} \tag{35}$$

We get $\sigma'_{r,0}(x) = 0$, and for $n > 1$, we get our result. □

Theorem 11.

If $\alpha \in \mathbb{R}$ and $n \geq 2$, then

$$DA_{r,n,k}^{(\alpha)}(x) = DA_{r,n-1,k}^{(\alpha)}(x) + A_{r,n,k}^{(\alpha)}(x) - 2A_{r,n-1,k}^{(\alpha)}(x). \tag{36}$$

Proof.

By (25), we reach

$$(1-t)^{-rk-\alpha} \exp\left[x\left(\frac{1-2t}{1-t}\right)\right] = \sum_{n=0}^{\infty} A_{r,n,k}^{(\alpha)}(x)t^n. \tag{37}$$

Let

$$F = A(t)\exp\left[x\left(\frac{1-2t}{1-t}\right)\right] = \sum_{n=0}^{\infty} y_{r,n,k}(x)t^n, \tag{38}$$

$$\frac{\partial F}{\partial x} = \left(\frac{1-2t}{1-t}\right)A(t)\exp\left[x\left(\frac{1-2t}{1-t}\right)\right], \tag{39}$$

$$(1-t)\frac{\partial F}{\partial x} = (1-2t)A(t)\exp\left[x\left(\frac{1-2t}{1-t}\right)\right]. \tag{40}$$

By using Equation (38), we obtain

$$(1-t)\frac{\partial F}{\partial x} = (1-2t)F. \tag{41}$$

$$\text{Since } F = \sum_{n=0}^{\infty} y_{r,n,k}(x)t^n, \text{ we reach } \frac{\partial F}{\partial x} = \sum_{n=0}^{\infty} y'_{r,n,k}(x)t^n. \tag{42}$$

Equation (41) can be expressed as

$$\sum_{n=0}^{\infty} y'_{r,n,k}(x)t^n - \sum_{n=0}^{\infty} y'_{r,n,k}(x)t^{n+1} = \sum_{n=0}^{\infty} y_{r,n,k}(x)t^n - 2\sum_{n=0}^{\infty} y_{r,n,k}(x)t^{n+1}. \tag{43}$$

We get $y'_{r,0,k}(x) = 0$, $y'_{r,1,k}(x) = 0$, and for $n > 2$, we get our result. □

Theorem 12.
If $\alpha \in \mathbb{R}$ and $n \geq r$, then

$$DA\,{}^{(\alpha)}_{r,n,k}(x) = A\,{}^{(\alpha)}_{r,n,k}(x) - \sum_{j=0}^{n-1} A\,{}^{(\alpha)}_{r,j,k}(x). \tag{44}$$

Proof.
We have

$$\frac{\partial F}{\partial x} = \left[1 - \frac{t}{1-t}\right]F. \tag{45}$$

Applying Equation (38) yields

$$\frac{\partial F}{\partial x} = \left[1 - \frac{t}{1-t}\right]\sum_{n=0}^{\infty} y_{r,n,k}(x)t^n. \tag{46}$$

By using Equation (42), we obtain

$$\begin{aligned}\sum_{n=0}^{\infty} y'_{r,n,k}(x)t^n &= \sum_{n=0}^{\infty} y_{r,n,k}(x)t^n - \left[\sum_{n=0}^{\infty} t^{n+1}\right]\left[\sum_{n=0}^{\infty} y_{r,n,k}(x)t^n\right] \\ &= \sum_{n=0}^{\infty} y_{r,n,k}(x)t^n - \sum_{n=0}^{\infty}\sum_{j=0}^{\infty} y_{r,j,k}(x)t^j t^{n+1}\end{aligned} \tag{47}$$

By using Lemma (4), we get

$$\begin{aligned}\sum_{n=0}^{\infty} y'_{r,n,k}(x)t^n &= \sum_{n=0}^{\infty} y_{r,n,k}(x)t^n - \sum_{n=0}^{\infty}\sum_{j=0}^{n} y_{r,j,k}(x)t^{n+1} \\ &= \sum_{n=0}^{\infty} y_{r,n,k}(x)t^n - \sum_{n=1}^{\infty}\sum_{j=0}^{n-1} y_{r,j,k}(x)t^n\end{aligned} \tag{48}$$

□

Then, we have $y'_{r,0,k}(x) = 0$, $y'_{r,1,k}(x) = 0$, and for $n > r$,

$$y'_{r,n,k}(x) = y_{r,n,k}(x) - \sum_{j=0}^{n-1} y_{r,j,k}(x). \tag{49}$$

We get our desired result.

Theorem 13.
Suppose that $\alpha \in \mathbb{R}$ and $n \geq r+1$. Thus, we get

$$nA\,{}^{(\alpha)}_{r,n,k}(x) = (3x - rk - \alpha)A\,{}^{(\alpha)}_{r,n-1,k}(x) - (rk + \alpha + n - 2)A\,{}^{(\alpha)}_{r,n-2,k}(x). \tag{50}$$

Proof.
We have

$$\begin{aligned}0 = nA\,{}^{(\alpha)}_{r,n,k}(x) - xDA\,{}^{(\alpha)}_{r,n-1,k}(x) + (2x - rk - \alpha - n + 1)A\,{}^{(\alpha)}_{r,n-1,k}(x), \\ nA\,{}^{(\alpha)}_{r,n,k}(x) = xDA\,{}^{(\alpha)}_{r,n-1,k}(x) - (2x - rk - \alpha - n + 1)A\,{}^{(\alpha)}_{r,n-1,k}(x).\end{aligned} \tag{51}$$

Then, after simplification, we get our result. □

Theorem 14.
Assume that $\alpha \in \mathbb{R}$ and $n, r, j, k \in \mathbb{Z}^+$. Thus, we obtain

$$A\,{}^{(1+\alpha)}_{r,n-1,k}(x) + A\,{}^{(\alpha)}_{r,n,k}(x) = A\,{}^{(1+\alpha)}_{r,n,k}(x). \tag{52}$$

Proof.
From Equation (12), we obtain

$$A\,{}^{(1+\alpha)}_{r,n-1,k}(x) = e^x(rk+1+\alpha)_{n-1,k} \sum_{j=0}^{[(n-1)/rk]} \frac{(-1)^{rkj}}{(n-1-rkj;k)!(r+1+\alpha)_{rkj}}\frac{x^{rkj}}{(rkj;k)!}, \tag{53}$$

so

that-

$$A_{r,n,k}^{(\alpha)}(x) = e^x(rk+\alpha)_{n,k}\sum_{j=0}^{[n/rk]}((-1)^{rkj}/(n-rkj;k)!(rk+\alpha)_{rkj})((x)^{rkj}/(rkj;k)!).$$

$$\begin{aligned}
&A_{r,n-1,k}^{(1+\alpha)}(x) + A_{r,n,k}^{(\alpha)}(x) = e^x(rk+1+\alpha)_{n-1,k}\sum_{j=0}^{\left[\frac{n-1}{rk}\right]}\frac{(-1)^{rkj}}{(n-1-rkj;k)!(r+1+\alpha)_{rkj}}\frac{x^{rkj}}{(rkj;k)!}e^x(rk+\alpha)_{n,k}\sum_{j=0}^{\left[\frac{n}{rk}\right]}\frac{(-1)^{rkj}}{(n-rkj;k)!(rk+\alpha)_{rkj}}\frac{(x)^{rkj}}{(rkj;k)!}\\
&= e^x\left[\sum_{j=0}^{\left[\frac{n-1}{rk}\right]}\frac{(rk+\alpha+n-1)!(-1)^{rkj}}{(n-1-rkj;k)!(r+\alpha+rkj)!}\frac{x^{rkj}}{(rkj;k)!} + \sum_{k=0}^{\left[\frac{n}{rk}\right]}\frac{(rk+\alpha+n-1)!(-1)^{rkj}}{(n-rkj;k)!(r+\alpha+rkj-1)!}\frac{x^{rkj}}{(rkj;k)!}\right]\\
&= e^x\left[\sum_{j=0}^{\left[\frac{n-1}{rk}\right]}\frac{(rk+\alpha+n-1)!(-1)^{rkj}}{(n-1-rkj;k)!(r+\alpha+rkj)!}\frac{x^{rkj}}{(rkj;k)!} + \sum_{k=0}^{\left[\frac{n-1}{rk}\right]}\frac{(rk+\alpha+n-1)!(-1)^{rkj}}{(n-rkj;k)!(r+\alpha+rkj-1)!}\frac{x^{rkj}}{(rkj;k)!} + \frac{x^{rkn}}{(rkn;k)!}\right]\\
&= e^x\left[\begin{array}{c}\displaystyle\sum_{j=0}^{\left[\frac{n-1}{rk}\right]}\frac{(r+\alpha+n-1)!x^{rkj}(-1)^{rkj}}{(rkj;k)!}\\ \displaystyle\left\{\frac{1}{(n-1-rkj;k)!(r+\alpha+rkj)!}+\frac{1}{(n-rkj;k)!(r+\alpha+rkj-1)!}\right\}+\frac{x^{rkn}}{(rkn;k)!}\end{array}\right]\\
&= e^x\left[\sum_{j=0}^{\left[\frac{n-1}{rk}\right]}\frac{(r+\alpha+n-1)!(-1)^{rkj}}{(n-rkj;k)!(r+\alpha+rkj)!}\{r+\alpha+n\}\frac{x^{rkj}}{(rkj;k)!}+\frac{x^{rkn}}{(rkn;k)!}\right] = e^x\left[\sum_{j=0}^{\left[\frac{n-1}{rk}\right]}\frac{(r+\alpha+n)!(-1)^{rkj}}{(n-rkj;k)!(r+\alpha+rkj)!}\frac{x^{rkj}}{(rkj;k)!}+\frac{x^{rkn}}{(rkn;k)!}\right]\\
&= e^x\left[(r+1+\alpha)_{n,k}\sum_{j=0}^{\left[\frac{n-1}{rk}\right]}\frac{(-1)^{rkj}}{(n-rkj;k)!(r+1+\alpha)_{rj,k}}\frac{x^{rkj}}{(rkj;k)!}+\frac{x^{rkn}}{(rkn;k)!}\right] = e^x(r+1+\alpha)_{n,k}\sum_{j=0}^{\left[\frac{n}{rk}\right]}\frac{(-1)^{rkj}}{(n-rkj;k)!(r+1+\alpha)_{rj,k}}\frac{x^{rkj}}{(rkj;k)!} = A_{r,n,k}^{(1+\alpha)}(x).
\end{aligned} \tag{54}$$

6. K Differential Equation

Theorem 15.
Assume that $\alpha \in \mathbb{R}$ and $n \geq q$. Thus, we reach

$$xD^2A_{r,n,k}^{(\alpha)}(x) + (rk+\alpha-3x)DA_{r,n,k}^{(\alpha)}(x) + (2x+n-rk-\alpha)A_{r,n,k}^{(\alpha)}(x) = 0. \tag{55}$$

Proof.
We have

$$xD^2A_{r,n,k}^{(\alpha)}(x) + DA_{r,n,k}^{(\alpha)}(x) = (n+x)DA_{r,n,k}^{(\alpha)}(x) + A_{r,n,k}^{(\alpha)}(x) - (rk+\alpha+n-1)DA_{r,n-1,k}^{(\alpha)}(x). \tag{56}$$

By using Equation (36), we get

$$\begin{aligned}
&xD^2A_{r,n,k}^{(\alpha)}(x) + DA_{r,n,k}^{(\alpha)}(x) = (n+x)DA_{r,n,k}^{(\alpha)}(x) + A_{r,n,k}^{(\alpha)}(x)\\
&-(rk+\alpha+n-1)\left[DA_{r,n,k}^{(\alpha)}(x) - A_{r,n,k}^{(\alpha)}(x) + 2A_{r,n-1,k}^{(\alpha)}(x)\right],
\end{aligned} \tag{57}$$

or

$$xD^2A_{r,n,k}^{(\alpha)}(x) + (rk+\alpha-x)DA_{r,n,k}^{(\alpha)}(x) = (rk+\alpha+n)A_{r,n,k}^{(\alpha)}(x) - 2(rk+\alpha+n-1)A_{r,n-1,k}^{(\alpha)}(x). \tag{58}$$

Then, we acquire

By using Equation (26), we have

$$\begin{aligned}
&xD^2A_{r,n,k}^{(\alpha)}(x) + (rk+\alpha-x)DA_{r,n,k}^{(\alpha)}(x)\\
&= (rk+\alpha+n)A_{r,n,k}^{(\alpha)}(x) + 2xDA_{r,n,k}^{(\alpha)}(x)\\
&\times\ -2(n+x)DA_{r,n,k}^{(\alpha)}(x),
\end{aligned} \tag{59}$$

or

$$xD^2A_{r,n,k}^{(\alpha)}(x) + (rk+\alpha-3x)DA_{r,n,k}^{(\alpha)}(x) + (2x+n-rk-\alpha)A_{r,n,k}^{(\alpha)}(x) = 0. \tag{60}$$

□

7. K Rodrigues Formula

Theorem 16.
Assume that $\alpha \in \mathbb{R}$ and $n, j, k \in \mathbb{Z}^+$. Thus, we reach

$$A_{r,n,k}^{(\alpha)}(x) = \frac{x^{-(rk-1)-\alpha}e^{2x}}{(n;k)!}D_k^n\left(x^{(rk-1)+\alpha+nk}e^{-x}\right). \tag{61}$$

Proof.
We take into consideration the K extended Laguerre polynomials involving

$r > 2_2F_2, r > 2,$

$$A_{r,n,k}^{(\alpha)}(x) = \frac{e^x(rk+\alpha)_{n,k}}{(n;k)!}\,{}_rF_{r,k}\left(\begin{matrix}\left(\frac{-n}{r},k\right),\left(\frac{-n+k}{r},k\right),\cdots,\left(\frac{-n+rk+1}{r},k\right);\\ \left(\frac{\alpha+rk}{r},k\right),\left(\frac{\alpha+rk+1}{r},k\right),\cdots,\left(\frac{\alpha+2rk-1}{r},k\right)\end{matrix};x^r\right). \tag{62}$$

By Theorem (12), we have

$$\begin{aligned}A_{r,n,k}^{(\alpha)}(x) &= \frac{e^x}{(n;k)!}\sum_{j=0}^{[n/rk]}\left[\frac{(n;k)!}{(n-rkj;k)!(rkj;k)!}\right]\frac{(rk+\alpha)_{n,k}x^{rkj}}{(rk+\alpha)_{rj,k}}\\ &= \frac{e^x x^{-(rk-1)-\alpha}}{(n;k)!}\sum_{j=0}^{[n/r]}\left[\frac{(-1)^{rkj}(n;k)!}{(n-rkj)!(rkj;k)!}\right]\frac{(\alpha+rk)_{n,k}x^{rkj+\alpha+(rk-1)}}{(\alpha+rk)_{rj,k}}.\end{aligned} \tag{63}$$

Since $D^{nk-rjk}\left(x^{n+\alpha+(r-1)}\right) = (\alpha+rk)_{n,k}x^{rj+\alpha+(r-1)}/(\alpha+rk)_{rj,k}$, we get

$$\begin{aligned}A_{r,n,k}^{(\alpha)}(x) &= \frac{x^{-(r-1)-\alpha}e^{2x}}{(n;k)!}\sum_{j=0}^{[n/rk]}\left[\frac{(n;k)!}{(n-rjk;k)!(rj)!}\right]\left[(-1)^{rkj}e^{-x}\right]\left[D^{nk-rkj}\left(x^{n+\alpha+(rk-1)}\right)\right]\\ &= \frac{x^{-(r-1)-\alpha}e^{2x}}{(n;k)!}\sum_{j=0}^{[n/rk]^n}C_{rjk;k}D^{nk-rkj}\left(x^{n+\alpha+(rk-1)}\right)D^{rkj}\left(e^{-x}\right)\end{aligned} \tag{64}$$

Then, we get our desired result. □

8. Special Properties

Theorem 17.
Suppose that $\alpha, \beta \in \mathbb{R}$ and $n, j, r, k \in \mathbb{Z}^+$. Thus, we acquire

$$A_{r,n,k}^{(\alpha)}(x) = \sum_{j=0}^{[n/rk]}\frac{(\alpha-\beta)_{rkj}A_{r,n-rkj}^{(\beta)}(x)}{(rkj;k)!}. \tag{65}$$

Proof.
From Equation (25),

$$\sum_{n=0}^{\infty}A_{r,n,k}^{(\alpha)}(x)t^n = \frac{1}{(1-t)^{rk+\alpha}}\exp\left(\frac{x-2xt}{1-t}\right). \tag{66}$$

Also, consider

$$\begin{aligned}&\frac{1}{(1-t)^{rk+\alpha}}\exp\left(x\left(\frac{1-2t}{1-t}\right)\right) = (1-t)^{-(\alpha-\beta)}(1-t)^{-rk-\beta}\exp\left(x\left(\frac{1-2t}{1-t}\right)\right),\\ &\sum_{n=0}^{\infty}A_{r,n,k}^{(\alpha)}(x)t^n = (1-t)^{-(\alpha-\beta)}\sum_{n=0}^{\infty}A_{r,n,k}^{(\beta)}(x)t^n = \sum_{n=0}^{\infty}\frac{(\alpha-\beta)_{rn}t^{rn}}{(rn;k)!}\sum_{n=0}^{\infty}A_{r,n,k}^{(\beta)}(x)t^n = \sum_{n=0}^{\infty}\sum_{j=0}^{\infty}\frac{(\alpha-\beta)_{rkj}t^{rkj}A_{r,n,k}^{(\beta)}(x)t^n}{(rkj;k)!}.\end{aligned} \tag{67}$$

By using Lemma (4) yields

$$\sum_{n=0}^{\infty}A_{r,n,k}^{(\alpha)}(x)t^n = \sum_{n=0}^{\infty}\sum_{j=0}^{[n/rk]}\frac{(\alpha-\beta)_{rkj}t^{rkj}A_{r,n-rkj,k}^{(\beta)}(x)t^{n-rkj}}{(rkj;k)!} = \sum_{n=0}^{\infty}\sum_{j=0}^{[n/rk]}\frac{(\alpha-\beta)_{rkj}A_{r,n-rkj,k}^{(\beta)}(x)t^n}{(rkj;k)!}. \tag{68}$$

Then, we get our result. □

Theorem 18.
If $\alpha \in \mathbb{R}$ and $n, j, k \in \mathbb{Z}^+$, then

$$A_{r,n,k}^{(\alpha+\beta+qk)}(x+y) = \sum_{j=0}^{[n/rk]}A_{r,n-rkj,k}^{(\beta)}(y)A_{r,rkj,k}^{(\alpha)}(x). \tag{69}$$

Proof.

Consider

$$\begin{aligned}&(1-t)^{-rk-\alpha}\exp\left(x\left(\frac{1-2t}{1-t}\right)\right)(1-t)^{-rk-\beta}\exp\left(y\left(\frac{1-2t}{1-t}\right)\right)\\ &= (1-t)^{-rk-(\alpha+\beta+rk)}\exp\left\{(x+y)\left(\frac{1-2t}{1-t}\right)\right\}.\end{aligned} \tag{70}$$

Then, we get

$$\sum_{n=0}^{\infty}A\begin{matrix}(\alpha)\\ r,n,k\end{matrix}(x)t^n\sum_{n=0}^{\infty}A\begin{matrix}(\beta)\\ r,n,k\end{matrix}(y)t^n = \sum_{n=0}^{\infty}A\begin{matrix}(\alpha+\beta+q)\\ r,n,k\end{matrix}(x+y)t^n. \tag{71}$$

By using Lemma (4), we acquire

$$\sum_{n=0}^{\infty} A_{r,n,k}^{(\alpha+\beta+qk)}(x+y)t^n = \sum_{n=0}^{\infty}\sum_{j=0}^{[n/rk]} A_{r,n-rkj,k}^{(\beta)}(y) A_{r,rkj,k}^{(\alpha)}(x)t^n. \tag{72}$$

On comparing the coefficients of t^n, we acquire our result. □

9. Conclusion

We constructed the K extended Laguerre polynomials $\{A_{r,n,k}^{(\alpha)}(x)\}$ relied on the ${}_rF_r$, $r > 2$. We acquired K generating functions, K recurrence relations and K Rodrigues formula for these K extended Laguerre polynomials. We will use the integral transformations on the results of K extended Laguerre polynomials in our future works (Table 1). We can also apply Laplace transformation on our results.

Data Availability

No data were used to support this work.

Conflicts of Interest

The authors declare that they have no conflicts of interest.

Authors' Contributions

The authors declare that the study was realized in collaboration with equal responsibility. All authors read and approved the final manuscript.

References

[1] A. Erdélyi, W. Magnus, F. Oberhettinger, and F. G. Tricomi, *Higher Transcendental Functions*, I. I. Vol and M. Graw, Eds., Hill Book Co, New York, 1953.

[2] W. W. Bell, *Special Functions for Scientists and Engineers*, D. Van Nostrand Co, London, 1968.

[3] Z. X. Wang and D. R. Guo, *Special functions*, World Scientific Publishing Co. Pvt. Ltd, 1989.

[4] A. M. Mathai, *A Hand Book of Generalized Special Functions for Statistical and Physical Sciences*, University Press Inc., New York, 1993.

[5] A. M. Chak, "A class of polynomials and a generalization of Stirling numbers," *Duke Mathematical Journal*, vol. 23, no. 1, pp. 45–56, 1956.

[6] L. Carlitz, "A note on certain biorthogonal polynomials," *Pacific Journal of Mathematics*, vol. 24, no. 3, pp. 425–430, 1968.

[7] W. A. Al-Salam, "Operational representations for the Laguerre and other polynomials," *Duke Mathematical Journal*, vol. 31, no. 1, pp. 127–142, 1964.

[8] T. R. Prabhakar, "On a set of polynomials suggested by Laguerre polynomials," *Pacific Journal of Mathematics*, vol. 35, no. 1, pp. 213–219, 1970.

[9] G. Andrews, R. Askey, and R. Roy, *Special Functions*, Cambridge University Press, 2004.

[10] K. Y. Chen and H. M. Srivastava, "A limit relationship between Laguerre and Hermite polynomials," *Integral Transforms and Special Functions*, vol. 16, no. 1, pp. 75–80, 2005.

[11] S. B. Trickovic and M. S. Stankovic, "A new approach to the orthogonality of the Laguerre and Hermite polynomials," *Integral Transforms and Special Functions*, vol. 17, no. 9, pp. 661–672, 2006.

[12] V. Radulescu, "Rodrigues-type for Hermite and Laguerre polynomials," *Analele stiintifice ale Universitatii Ovidius Constanta*, vol. 2, pp. 109–116, 2008.

[13] E. H. Doha, H. M. Ahmed, and S. I. El-Soubhy, "Explicit formulae for the coefficients of integrated expansions of Laguerre and Hermite polynomials and their integrals," *Integral Transforms and Special Functions*, vol. 20, no. 7, pp. 491–503, 2009.

[14] A. Akbary, D. Ghioca, and Q. Wang, "On permutation polynomials of prescribed shape," *Finite Fields and Their Applications*, vol. 15, no. 2, pp. 195–206, 2009.

[15] S. Li, "Permutation polynomials modulo m," *Finite Fields and Their Applications*, vol. 11, pp. 321–325, 2005.

[16] E. Aksoy, A. Cesmelioglu, W. Meidl, and A. Topuzoglu, "On the Carlitz rank of permutation polynomials," *Finite Fields and Their Applications*, vol. 15, no. 4, pp. 428–440, 2009.

[17] Q. Wang, "On inverse permutation polynomials," *Finite Fields and Their Applications*, vol. 15, no. 2, pp. 207–213, 2009.

[18] I. Krasikov and A. Zarkh, "Equioscillatory property of the Laguerre polynomials," *Journal of Approximation Theory*, vol. 162, no. 11, pp. 2021–2047, 2010.

[19] R. L. Shively, *On pseudo-Laguerre polynomials, Michigan thesis*, 1953.

[20] G. M. Habibullah, "An integral equation involving Shively's polynomials," *The Journal of Natural Sciences and Mathematics*, vol. 10, pp. 209–214, 1970.

[21] A. Khan and G. M. Habibullah, "Extended Laguerre polynomials," *International Journal of Contemporary Mathematical Sciences*, vol. 7, no. 22, pp. 1089–1094, 2012.

[22] A. Khan and M. Kalim, "The extended Laguerre polynomials $A_{3,m}^{(a)}(x)$ involving ${}_3F_3$," *Pakistan Journal of Statistics*, vol. 38, no. 1, pp. 89–98, 2022.

[23] A. Khan, M. Kalim, A. Akgul, and F. Jarad, "The extended Laguerre polynomials $\{A_{q,n}^{(a)}(x)\}$ involving ${}_qF_q$, $q > 2$," *Journal of Function Spaces*, vol. 2022, Article ID 7326760, 14 pages, 2022.

[24] B. P. Parashar, "The difference operators and extended Laguerre polynomials," *Bulletin of the Australian Mathematical Society*, vol. 28, no. 1, pp. 111–119, 1983.

[25] R. Sharma and A. K. Chongdar, "An extension of bilateral generating functions of modified Laguerre polynomials," *Proceedings of the Indian Academy of Sciences - Mathematical Sciences*, vol. 101, no. 1, pp. 43–47, 1991.

[26] C. G. Kokologiannaki, "Properties and inequalities of generalized k - gamma, beta and zeta functions," *International Journal of Contemporary Mathematical Sciences*, vol. 5, pp. 653–660, 2010.

[27] M. Mansour, "Determining the k - generalized gamma function $\Gamma_k(x)$ by functional equations," *International Journal of Contemporary Mathematical Sciences*, vol. 4, pp. 1037–1042, 2009.

[28] F. Merovci, "Power product inequalities for the Γ_k function. International journal mathematical," *Analysis*, vol. 4, pp. 1007–1012, 2010.

[29] S. Mubeen and G. M. Habibullah, "K–fractional integrals and application," *International Journal of Contemporary Mathematical Sciences*, vol. 7, no. 2, pp. 89–94, 2012.

[30] S. Mubeen and G. M. Habibullah, "An integral representation of some k–hypergeometric functions," *International Mathematics Forum*, vol. 7, no. 4, pp. 203–207, 2012.

[31] V. Krasniqi, "A limit for the k-gamma and k-beta function," *International Mathematical Forum*, vol. 5, pp. 1613–1617, 2010.

[32] S. Mubeen, "Solution of some integral equations involving confluent k-hypergeometric functions," *Applied Mathematics*, vol. 4, no. 7, pp. 9–11, 2013.

[33] C. G. Kokologiannaki and V. Krasniqi, "Some properties of the k - gamma function," *Le Matematiche*, vol. 1, pp. 13–22, 2013.

[34] A. Din, Y. Li, T. Khan, and G. Zaman, "Mathematical analysis of spread and control of the novel corona virus (COVID-19) in China," *Chaos, Solitons and Fractals*, vol. 141, article 110286, 2020.

[35] A. Din, Y. Li, F. M. Khan, Z. U. Khan, and P. Liu, "On analysis of fractional order mathematical model of hepatitis B using Atangana–Baleanu Caputo (ABC) derivative," *Fractals*, vol. 30, no. 1, article 2240017, 2022.

[36] A. Din, Y. Li, A. Yusuf, and A. Ali, "Caputo type fractional operator applied to Hepatitis B system," *Fractals*, vol. 30, no. 1, 2022.

[37] A. Din, "The stochastic bifurcation analysis and stochastic delayed optimal control for epidemic model with general incidence function," *Chaos*, vol. 31, no. 12, article 123101, 2021.

[38] Q. T. Ain, T. Sathiyaraj, S. Karim, M. Nadeem, and P. K. Mwanakatwe, "ABC fractional derivative for the alcohol drinking model using two-scale fractal dimension," *Complexity*, vol. 2022, Article ID 8531858, 11 pages, 2022.

[39] Q. T. Ain, A. Khan, M. I. Ullah, M. A. Alqudah, and T. Abdeljawad, "On fractional impulsive system for methanol detoxification in human body," *Chaos, Solitons & Fractals*, vol. 160, article 112235, 2022.

[40] A. Din and Q. T. Ain, "Stochastic optimal control analysis of a mathematical model: theory and application to non-singular kernels," *Fractal and Fractional*, vol. 6, no. 5, p. 279, 2022.

[41] G. Rehman, S. Qin, Q. T. Ain et al., "A study of moisture content in unsaturated porous medium by using homotopy perturbation method (HPM) and variational iteration method (VIM)," *International Journal on Geo Mathematics*, vol. 13, no. 3, 2022.

[42] K. Wang and H. Wang, "Fractal variational principles for two different types of fractal plasma models with variable coefficients," *Fractals*, vol. 30, no. 3, article 2250043, 2022.

[43] K. Wang, "Fractal solitary wave solutions for fractal nonlinear dispersive Boussinesq-like models," *Fractals*, vol. 30, no. 4, article 2250083, 2022.

[44] E. D. Rainville, *Special Functions*, The Macmillan Company, New York, 1965.

Hindawi
Advances in Mathematical Physics
Volume 2022, Article ID 7087481, 8 pages
https://doi.org/10.1155/2022/7087481

Research Article

Modified Homotopy Perturbation Method and Approximate Solutions to a Class of Local Fractional Integrodifferential Equations

Bo Xu[1,2,3] **and Sheng Zhang**[2]

[1]*School of Mathematics, China University of Mining and Technology, Xuzhou 221116, China*
[2]*School of Mathematical Sciences, Bohai University, Jinzhou 121013, China*
[3]*School of Educational Sciences, Bohai University, Jinzhou 121013, China*

Correspondence should be addressed to Sheng Zhang; szhangchina@126.com

Received 10 July 2022; Revised 14 August 2022; Accepted 17 August 2022; Published 27 August 2022

Academic Editor: Muhammad Nadeem

In this paper, the local fractional version of homotopy perturbation method (HPM) is established for a new class of local fractional integral-differential equation (IDE). With the embedded homotopy parameter monotonously changing from 0 to 1, the special easy-to-solve fractional problem continuously deforms to the class of local fractional IDE. As a concrete example, an explicit and exact Mittag–Leffler function solution of one special case of the local fractional IDE is obtained. In the process of solving, two initial solutions are selected for the iterative operation of local fractional HPM. One of the initial solutions has a critical condition of convergence and divergence related to the fractional order, and the other converges directly to the real solution. This paper reveals that whether the sequence of approximate solutions generated by the iteration of local fractional HPM can approach the real solution depends on the selection of the initial approximate solutions and sometimes also depends on the fractional order of the selected initial approximate solutions or the considered equations.

1. Introduction

Fractals, solitons, and chaos together constitute three important branches of nonlinear sciences. In fractal space, there exist some magical functions which are continuous everywhere but nondifferentiable everywhere. The local fractional calculus [1] developed in recent years provides a powerful mathematical tool to handling with such type of nondifferentiable functions. Fractional calculus, which is widely believed to have originated more than 300 years ago, has attracted much attention [2–17]. It is of theoretical and practical value to solve fractional differential equations (DEs) directly connecting with fractional dynamical processes in a great many fields. For this reason, people often construct exact solutions of fractional DEs to obtain useful clues in these fractional dynamical processes for specific applications.

With the development of fractional calculus, many numerical and analytical methods for fractional DEs have been developed, such as integral transform method [1], series expansion method [3], Adomian decomposition method [4], Fan subequation method [5], variational iteration method (VIM) [6], variable separation method [7], finite difference method [8], homotopy perturbation method (HPM) [9], combined the HPM with Laplace transform [10], exp-function method [11], and Hirota bilinear method [12]. The HPM proposed by He [18] couples the homotopy method and the perturbation technique, which needs no the small parameters embedded in differential equations. More importantly, it is indicated in [19] that the HPM can truly eliminate the limitations existing in traditional perturbation methods.

One of the advantages of local fractional derivative is that it has been successfully used to describe some nondifferential problems appearing in science and engineering [1]. The concept of local fractional derivative, which is based on Riemann-Liouville fractional derivative, can be retrospected

to Kolwankar and Gangal's pioneering work [13]. More specifically, if the following limit exists and is finite for a given continuous function $u(x)$: $[0, 1] \longrightarrow R$,

$$D^{\alpha}u(x_0) = \lim_{x \longrightarrow x_0} \frac{d^q(u(x) - u(x_0))}{d(x - x_0)^q}, (0 < q < 1), \quad (1)$$

then $D^{\alpha}u(x_0)$ is called q-order fractional derivative of $u(x)$ at the point $x = x_0$. Later, inspired by the relation $d^{\alpha}u(x) = \Gamma(1 + \alpha)du(x)$ of Jumarie [20], the local fractional derivative of a local fractional continuous but nondifferentiable function $u(x)$ is defined as another form ([4], see Definition 1). Recently, the theory of local fractional calculus has been significantly developed. Yang and his collaborators [1, 3, 17] have made a series of achievements in the development of local fractional calculus. Benefiting from the graceful properties of local fractional calculus, some existing methods like those [5, 11, 12], originally proposed for DEs with integer orders, have successfully been extended to fractional DEs and many methods are meeting more and more challenges for solving fractional DEs.

The paper is aimed at establishing the local fractional HPM for a new class of local fractional IDEs:

$$\frac{d^{\alpha}u(x)}{dx^{\alpha}} - f(x) - \frac{1}{\Gamma(1 + \alpha)} \int_0^1 g(x, t)u(t)(dt)^{\alpha} = 0, \quad (2)$$

where $0 < \alpha \leq 1$, $u(x)$, $f(x)$, and $g(x, t)$ are the local fractional continuous but nondifferentiable functions, $d^{\alpha}u(x)/dx^{\alpha}$ and $(1/\Gamma(1 + \alpha))\int_0^1 g(x, t)u(t)(dt)^{\alpha}$ represent the local fractional derivative and integral [1], respectively, and $\Gamma(1 + \alpha)$ is the well-known Euler's Gamma function:

$$\Gamma(1 + \alpha) = \int_0^{\infty} t^{\alpha}e^{-t}dt. \quad (3)$$

Considering a concrete application of the established local fractional HPM, we would like to solve a special case of Equation (2):

$$\frac{d^{\alpha}u(x)}{dx^{\alpha}} - 3E_{\alpha}(3x^{\alpha}) + \left(\frac{E_{\alpha}(3)}{\Gamma(1 + \alpha)} - \frac{E_{\alpha}(3) - 1}{3}\right)x^{\alpha} - \frac{1}{\Gamma(1 + \alpha)} \int_0^1 \frac{3x^{\alpha}t^{\alpha}}{\Gamma(1 + \alpha)} u(t)(dt)^{\alpha} = 0, \quad (4)$$

where the Mittag–Leffler function

$$E_{\alpha}(x^{\alpha}) = \sum_{k=0}^{\infty} \frac{x^{k\alpha}}{\Gamma(1 + k\alpha)}, \quad (5)$$

which is defined on a fractal set [1].

The organization of the rest of this paper is as follows. Section 2 recalls the local fractional derivative and integral and some basic properties. Section 3 establishes the local fractional HPM for the class of local fractional IDEs (2). Section 4 takes the local fractional IDE (4), a special case of Equation (2), to test the established local fractional HPM and discuss the influence of not only the initial approximate solutions but also the fractional order on whether the sequence of approximate solutions can approach the real solution. Section 5 employs He-Laplace method coupling the HPM with Laplace transform to solve the local fractional IDE (4) and compares the obtained results. Section 6 summarizes the whole paper.

2. Local Fractional Derivative and Integral and Some Basic Properties

In this section, we recall the local fractional derivative and integral and some basic properties.

Definition 1 (see [1]). Let $u(x)$ be a local fractional continuous but nondifferentiable function; then, α-order local fractional derivative of $u(x)$ at the point $x = x_0$ reads

$$D_x^{\alpha}u(x_0) = \left.\frac{d^{\alpha}u(x)}{dx^{\alpha}}\right|_{x=x_0} = \lim_{x \longrightarrow x_0} \frac{\Delta^{\alpha}(u(x) - u(x_0))}{(x - x_0)^{\alpha}}, (0 < \alpha \leq 1), \quad (6)$$

where $\Delta^{\alpha}(u(x) - u(x_0)) \cong \Gamma(1 + \alpha)(u(x) - u(x_0))$.

The local fractional derivative has some basic properties [1]:

$$\begin{aligned} D_x^{\alpha}(\lambda u(x) + \mu v(x)) &= \lambda D_x^{\alpha}u(x) + \mu D_x^{\alpha}v(x), \\ D_x^{\alpha}(u(x)v(x)) &= (D_x^{\alpha}u(x))v(x) + u(x)(D_x^{\alpha}v(x)), \\ D_x^{\alpha}\frac{u(x)}{v(x)} &= \frac{D_x^{\alpha}u(x)}{v(x)} - \frac{u(x)(D_x^{\alpha}v(x))}{v^2(x)}, \\ D_x^{\alpha}(C) &= 0, \\ D_x^{\alpha}\frac{x^{k\alpha}}{\Gamma(1 + k\alpha)} &= \frac{x^{(k-1)\alpha}}{\Gamma(1 + (k - 1)\alpha)}, \\ D_x^{\alpha}E_{\alpha}(qx^{\alpha}) &= qE_{\alpha}(qx^{\alpha}), \\ D_x^{\alpha}\sin_{\alpha}(x^{\alpha}) &= \cos_{\alpha}(x^{\alpha}), D_x^{\alpha}\cos_{\alpha}(x^{\alpha}) = -\sin_{\alpha}(x^{\alpha}), \end{aligned} \quad (7)$$

where λ, μ, C, and q are constants and k is an integer, while $\sin_{\alpha}(x^{\alpha}) = \sum_{k=0}^{\infty}(-1)^k x^{(2k+1)\alpha}/\Gamma(1 + (2k + 1)\alpha)$ and $\cos_{\alpha}(x^{\alpha}) = \sum_{k=0}^{\infty}(-1)^k x^{2k\alpha}/\Gamma(1 + 2k\alpha)$.

Definition 2 (see [1]). Let function $u(x) \in C_{\alpha}[a, b]$; then, the definition of α-order local fractional integral of $u(x)$ in the integral $[a, b]$ is as follows:

$$\begin{aligned} {}_aI_b^{\alpha}u(x) &= \frac{1}{\Gamma(1 + \alpha)} \int_a^b u(t)(dt)^{\alpha} \\ &= \frac{1}{\Gamma(1 + \alpha)} \lim_{\Delta x_k \longrightarrow 0} \sum_{k=0}^{N-1} u(x_k)(\Delta x_k)^{\alpha}, (0 < \alpha \leq 1), \end{aligned} \quad (8)$$

where $\Delta x_k = x_{k+1} - x_k$ with $x_0 = a < x_1 < \cdots < x_{N-1} < x_N = b$.

The local fractional integral has some basic properties [1]:

$$
\begin{aligned}
&{}_aI_b^\alpha(\lambda f(x)+\mu g(x)) = \lambda\,{}_aI_b^\alpha f(x) + \mu\,{}_aI_b^\alpha g(x),\\
&{}_aI_b^\alpha[(D_x^\alpha f(x))g(x)] = f(x)g(x)\big|_a^b - {}_aI_b^\alpha[f(x)(D_x^\alpha g(x))],\\
&{}_0I_x^\alpha C = \frac{Cx^\alpha}{\Gamma(1+\alpha)},\\
&{}_0I_x^\alpha \frac{x^{k\alpha}}{\Gamma(1+k\alpha)} = \frac{x^{(k+1)\alpha}}{\Gamma(1+(k+1)\alpha)},\\
&{}_0I_x^\alpha E_\alpha(qx^\alpha) = \frac{E_\alpha(qx^\alpha)-1}{q},\\
&{}_0I_x^\alpha \sin_\alpha(x^\alpha) = 1-\cos_\alpha(x^\alpha),\ {}_0I_x^\alpha \cos_\alpha(x^\alpha) = \sin_\alpha(x^\alpha).
\end{aligned}
\tag{9}
$$

3. Local Fractional HPM for the Class of Local Fractional IDEs

In this section, we establish the local fractional HPM for the class of IDEs (2). For convenience, we rewrite Equation (2) as follows:

$$
\begin{aligned}
A_\alpha(u) &= L_\alpha(u) + I_\alpha(u) = 0,\\
L_\alpha(u) &= \frac{d^\alpha u(x)}{dx^\alpha} - f(x),\\
I_\alpha(u) &= -\frac{1}{\Gamma(1+\alpha)}\int_0^1 g(x,t)u(t)(dt)^\alpha,
\end{aligned}
\tag{10}
$$

where A_α represents the local fractional operator.

In view of the local fractional HPM [17], we construct the local fractional homotopy $H_\alpha(u,p^\alpha)$, $u \in R$, and $p \in [0,1]$ by the following:

$$
H_\alpha(u,p^\alpha) = (1-p^\alpha)(L_\alpha(u)-L_\alpha(u_0)) + p^\alpha(L_\alpha(u)+I_\alpha(u)) = 0,
\tag{11}
$$

with the embedded parameter p^α which monotonously changes from 0 to 1 leads to the result that the easy-to-solve equation $L_\alpha(u)-L_\alpha(u_0)=0$ continuously deforms to the original equation $L_\alpha(u)+I_\alpha(u)=0$. Using the constructed homotopy $H_\alpha(u,p^\alpha)$, we can continuously trace a curve which is implicitly defined from a starting point

$$
H_\alpha(u,0) = L_\alpha(u) - L_\alpha(u_0) = 0,
\tag{12}
$$

to a solution function

$$
H_\alpha(u,1) = L_\alpha(u) + I_\alpha(u) = 0.
\tag{13}
$$

From the perspective of topology, the above changing process is called a deformation. In this deformation, $L_\alpha(u) - L_\alpha(u_0)$ and $L_\alpha(u)+I_\alpha(u)$ are homotopic.

Thus, the fractional homotopy $H_\alpha(u,p^\alpha)$ in Equation (11) can be written as below:

$$
\begin{aligned}
H_\alpha(u,p^\alpha) &= (1-p^\alpha)\left[\frac{d^\alpha u(x)}{dx^\alpha} - f(x) - \left(\frac{d^\alpha u_0(x)}{dx^\alpha} - f(x)\right)\right]\\
&\quad + p^\alpha\left[\frac{d^\alpha u(x)}{dx^\alpha} - f(x) - \frac{p^\alpha}{\Gamma(1+\alpha)}\int_0^1 g(x,t)u(t)(\mathrm{d}t)^\alpha\right]\\
&= \frac{\mathrm{d}^\alpha u(x)}{\mathrm{d}x^\alpha} - \frac{d^\alpha u_0(x)}{dx^\alpha} + p^\alpha\left(\frac{d^\alpha u_0(x)}{dx^\alpha} - f(x)\right.\\
&\quad \left. - \frac{1}{\Gamma(1+\alpha)}\int_0^1 g(x,t)u(t)(dt)^\alpha\right) = 0.
\end{aligned}
\tag{14}
$$

Substituting the series u expanded by the fractional homotopy parameter p^α

$$
u = v_0^\alpha + p^\alpha v_1^\alpha + p^{2\alpha}v_2^\alpha + p^{3\alpha}v_3^\alpha + \cdots,
\tag{15}
$$

into Equation (14) and comparing the coefficients of the same power of p^α, we obtain a set of fractional equations:

$$
\begin{aligned}
p^0 &: \frac{d^\alpha v_0^\alpha(x)}{dx^\alpha} - \frac{d^\alpha u_0(x)}{dx^\alpha} = 0,\\
p^\alpha &: \frac{d^\alpha v_1^\alpha(x)}{dx^\alpha} + \frac{d^\alpha u_0(x)}{dx^\alpha} - f(x)\\
&\quad - \frac{1}{\Gamma(1+\alpha)}\int_0^1 g(x,t)v_0^\alpha(t)(dt)^\alpha = 0,\\
p^{2\alpha} &: \frac{d^\alpha v_2^\alpha(x)}{dx^\alpha} - \frac{1}{\Gamma(1+\alpha)}\int_0^1 g(x,t)v_1^\alpha(t)(dt)^\alpha = 0,\\
p^{3\alpha} &: \frac{d^\alpha v_3^\alpha(x)}{dx^\alpha} - \frac{1}{\Gamma(1+\alpha)}\int_0^1 g(x,t)v_2^\alpha(t)(dt)^\alpha = 0, \vdots .
\end{aligned}
\tag{16}
$$

Here u_0 is assumed to be an initial approximate solution of Equation (2). Generally, the initial approximation v_0^α or u_0 can be freely chosen. Solving above set of fractional equations, we can obtain solutions v_0^α, v_1^α, v_2^α, v_3^α, and so on.

Setting $p^\alpha \longrightarrow 1$ and using Equation (15), we finally arrive at an approximate solution of Equation (2).

$$
u = \lim_{p^\alpha \longrightarrow 1}\sum_{k=0}^{\infty} v_k^\alpha(x) = v_0^\alpha + v_1^\alpha + v_2^\alpha + v_3^\alpha + \cdots.
\tag{17}
$$

As pointed by He [18], the series (17) has convergence in most cases and the convergent rate is determined by $L_\alpha(u)$ when $\alpha = 1$. For the case of convergence, the series (17) can reach a closed form solution.

4. A Concrete Example

In this section, we apply the previously established local fractional HPM to the local fractional IDE (4).

Firstly, we construct such a fractional homotopy:

$$H_\alpha(u,p^\alpha)=\frac{d^\alpha u(x)}{dx^\alpha}-\frac{d^\alpha u_0(x)}{dx^\alpha}+p^\alpha\left[\frac{d^\alpha u_0(x)}{dx^\alpha}-3E_\alpha(3x^\alpha)+\left(\frac{E_\alpha(3)}{\Gamma(1+\alpha)}-\frac{E_\alpha(3)-1}{3}\right)x^\alpha-\frac{1}{\Gamma(1+\alpha)}\cdot\int_0^1\frac{3x^\alpha t^\alpha}{\Gamma(1+\alpha)}u(t)(dt)^\alpha\right]=0. \tag{18}$$

Secondly, we substitute Equation (15) into Equation (18), and then, the comparison of the coefficients of $p^{j\alpha}(j=0,1,2,\cdots)$ gives a system of fractional equations:

$$p^0:\frac{d^\alpha v_0^\alpha(x)}{dx^\alpha}-\frac{d^\alpha u_0(x)}{dx^\alpha}=0, \tag{19}$$

$$p^\alpha:\frac{d^\alpha v_1^\alpha(x)}{dx^\alpha}+\frac{d^\alpha u_0(x)}{dx^\alpha}-3E_\alpha(3x^\alpha)+\left(\frac{E_\alpha(3)}{\Gamma(1+\alpha)}-\frac{E_\alpha(3)-1}{3}\right)x^\alpha-\frac{1}{\Gamma(1+\alpha)}\int_0^1\frac{3x^\alpha t^\alpha}{\Gamma(1+\alpha)}v_0^\alpha(t)(dt)^\alpha=0, \tag{20}$$

$$p^{2\alpha}:\frac{d^\alpha v_2^\alpha(x)}{dx^\alpha}-\frac{1}{\Gamma(1+\alpha)}\int_0^1\frac{3x^\alpha t^\alpha}{\Gamma(1+\alpha)}v_1^\alpha(t)(dt)^\alpha=0, \tag{21}$$

$$p^{3\alpha}:\frac{d^\alpha v_3^\alpha(x)}{dx^\alpha}-\frac{1}{\Gamma(1+\alpha)}\int_0^1\frac{3x^\alpha t^\alpha}{\Gamma(1+\alpha)}v_2^\alpha(t)(dt)^\alpha=0,\vdots. \tag{22}$$

In view of the arbitrariness of v_0^α or u_0, here we set

$$\frac{d^\alpha v_0^\alpha(x)}{dx^\alpha}=\frac{d^\alpha u_0(x)}{dx^\alpha}=3E_\alpha(3x^\alpha)-\left(\frac{E_\alpha(3)}{\Gamma(1+\alpha)}-\frac{E_\alpha(3)-1}{3}\right)x^\alpha, \tag{23}$$

and then, from Equations (20)–(23), we have

$$v_0^\alpha=E_\alpha(3x^\alpha)-\left(\frac{E_\alpha(3)}{\Gamma(1+\alpha)}-\frac{E_\alpha(3)-1}{3}\right)\cdot\frac{\Gamma(1+\alpha)}{\Gamma(1+2\alpha)}x^{2\alpha};\frac{d^\alpha v_1^\alpha(x)}{dx^\alpha}-\left(\frac{E_\alpha(3)}{\Gamma(1+\alpha)}-\frac{E_\alpha(3)-1}{3}\right)\cdot\left(1-\frac{3\Gamma(1+3\alpha)}{\Gamma(1+2\alpha)\Gamma(1+4\alpha)}\right)x^\alpha=0, \tag{24}$$

namely,

$$v_1^\alpha=\left(\frac{E_\alpha(3)}{\Gamma(1+\alpha)}-\frac{E_\alpha(3)-1}{3}\right)\left(1-\frac{3\Gamma(1+3\alpha)}{\Gamma(1+2\alpha)\Gamma(1+4\alpha)}\right)\cdot\frac{\Gamma(1+\alpha)}{\Gamma(1+2\alpha)}x^{2\alpha};\frac{d^\alpha v_2^\alpha(x)}{dx^\alpha}-\frac{3\Gamma(1+3\alpha)}{\Gamma(1+2\alpha)\Gamma(1+4\alpha)}\cdot\left(\frac{E_\alpha(3)}{\Gamma(1+\alpha)}-\frac{E_\alpha(3)-1}{3}\right)\left(1-\frac{3\Gamma(1+3\alpha)}{\Gamma(1+2\alpha)\Gamma(1+4\alpha)}\right)x^\alpha=0, \tag{25}$$

namely,

$$v_2^\alpha=\frac{3\Gamma(1+3\alpha)}{\Gamma(1+2\alpha)\Gamma(1+4\alpha)}\left(\frac{E_\alpha(3)}{\Gamma(1+\alpha)}-\frac{E_\alpha(3)-1}{3}\right)\cdot\left(1-\frac{3\Gamma(1+3\alpha)}{\Gamma(1+2\alpha)\Gamma(1+4\alpha)}\right)\frac{\Gamma(1+\alpha)}{\Gamma(1+2\alpha)}x^{2\alpha};\frac{d^\alpha v_3^\alpha(x)}{dx^\alpha}-\frac{3^2\Gamma^2(1+3\alpha)}{\Gamma^2(1+2\alpha)\Gamma^2(1+4\alpha)}\left(\frac{E_\alpha(3)}{\Gamma(1+\alpha)}-\frac{E_\alpha(3)-1}{3}\right)\cdot\left(1-\frac{3\Gamma(1+3\alpha)}{\Gamma(1+2\alpha)\Gamma(1+4\alpha)}\right)x^\alpha=0, \tag{26}$$

namely,

$$v_3^\alpha=\frac{3^2\Gamma^2(1+3\alpha)}{\Gamma^2(1+2\alpha)\Gamma^2(1+4\alpha)}\left(\frac{E_\alpha(3)}{\Gamma(1+\alpha)}-\frac{E_\alpha(3)-1}{3}\right)\cdot\left(1-\frac{3\Gamma(1+3\alpha)}{\Gamma(1+2\alpha)\Gamma(1+4\alpha)}\right)\frac{\Gamma(1+\alpha)}{\Gamma(1+2\alpha)}x^{2\alpha};\frac{d^\alpha v_4^\alpha(x)}{dx^\alpha}-\frac{3^3\Gamma^3(1+3\alpha)}{\Gamma^3(1+2\alpha)\Gamma^3(1+4\alpha)}\left(\frac{E_\alpha(3)}{\Gamma(1+\alpha)}-\frac{E_\alpha(3)-1}{3}\right)\cdot\left(1-\frac{3\Gamma(1+3\alpha)}{\Gamma(1+2\alpha)\Gamma(1+4\alpha)}\right)x^\alpha=0, \tag{27}$$

namely,

$$v_4^\alpha=\frac{3^3\Gamma^3(1+3\alpha)}{\Gamma^3(1+2\alpha)\Gamma^3(1+4\alpha)}\left(\frac{E_\alpha(3)}{\Gamma(1+\alpha)}-\frac{E_\alpha(3)-1}{3}\right)\cdot\left(1-\frac{3\Gamma(1+3\alpha)}{\Gamma(1+2\alpha)\Gamma(1+4\alpha)}\right)\frac{\Gamma(1+\alpha)}{\Gamma(1+2\alpha)}x^{2\alpha};\vdots. \tag{28}$$

Finally, we obtain an approximate solution of Equation (4).

$$u = \lim_{p^{\alpha}\longrightarrow 1}\sum_{k=0}^{\infty} v_k^{\alpha}(x)p^{k\alpha} = E_{\alpha}(3x^{\alpha}) - \left(\frac{E_{\alpha}(3)}{\Gamma(1+\alpha)} - \frac{E_{\alpha}(3)-1}{3}\right)\frac{\Gamma(1+\alpha)}{\Gamma(1+2\alpha)}x^{2\alpha} + \left(1 + \frac{3\Gamma(1+3\alpha)}{\Gamma(1+2\alpha)\Gamma(1+4\alpha)} + \frac{3^2\Gamma^2(1+3\alpha)}{\Gamma^2(1+2\alpha)\Gamma^2(1+4\alpha)} + \frac{3^3\Gamma^3(1+3\alpha)}{\Gamma^3(1+2\alpha)\Gamma^3(1+4\alpha)} + \cdots\right) \times \left(\frac{E_{\alpha}(3)}{\Gamma(1+\alpha)} - \frac{E_{\alpha}(3)-1}{3}\right)\left(1 - \frac{3\Gamma(1+3\alpha)}{\Gamma(1+2\alpha)\Gamma(1+4\alpha)}\right) \cdot \frac{\Gamma(1+\alpha)}{\Gamma(1+2\alpha)}x^{2\alpha}, \tag{29}$$

which can be simplified as follows:

$$u = E_{\alpha}(3x^{\alpha}) - \lim_{m\longrightarrow\infty}\frac{3^{m-1}\Gamma^{m-1}(1+3\alpha)}{\Gamma^{m-1}(1+2\alpha)\Gamma^{m-1}(1+4\alpha)} \cdot \left(\frac{E_{\alpha}(3)}{\Gamma(1+\alpha)} - \frac{E_{\alpha}(3)-1}{3}\right)\frac{\Gamma(1+\alpha)}{\Gamma(1+2\alpha)}x^{2\alpha}. \tag{30}$$

Obviously, the nth-order approximate solution of Equation (4) has the following form:

$$u_n = E_{\alpha}(3x^{\alpha}) - \frac{3^n\Gamma^n(1+3\alpha)}{\Gamma^n(1+2\alpha)\Gamma^n(1+4\alpha)} \cdot \left(\frac{E_{\alpha}(3)}{\Gamma(1+\alpha)} - \frac{E_{\alpha}(3)-1}{3}\right)\frac{\Gamma(1+\alpha)}{\Gamma(1+2\alpha)}x^{2\alpha}, (n = 0, 1, 2, \cdots). \tag{31}$$

When the condition

$$q = \frac{3\Gamma(1+3\alpha)}{\Gamma(1+2\alpha)\Gamma(1+4\alpha)} < 1, \tag{32}$$

holds, the limit of Equation (30) exists. In this case, we obtain

$$u = E_{\alpha}(3x^{\alpha}). \tag{33}$$

In Figure 1, we show the curve of the condition q with fractional order α, where the dashed line represents $q = 1$. We can see from Figure 1 that there exists a unique value $\alpha_0 \in (0.7, 0.75)$ such that $q(\alpha_0) = 1$. At the same time, with the help of Mathematica, we have

$$q(0.73) \approx 1.02522329079942, q(0.74) \approx 0.9916413061494614. \tag{34}$$

Thus, we can more accurately determine the range of α_0 as

$$0.73 < \alpha_0 < 0.74. \tag{35}$$

This tells that $q(\alpha) < q(\alpha_0) = 1$ if and only if $\alpha_0 < \alpha \le 1$.

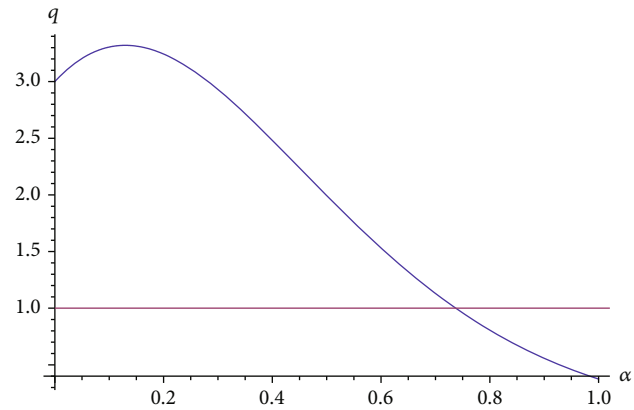

Figure 1: Curve of the condition q with fractional order α.

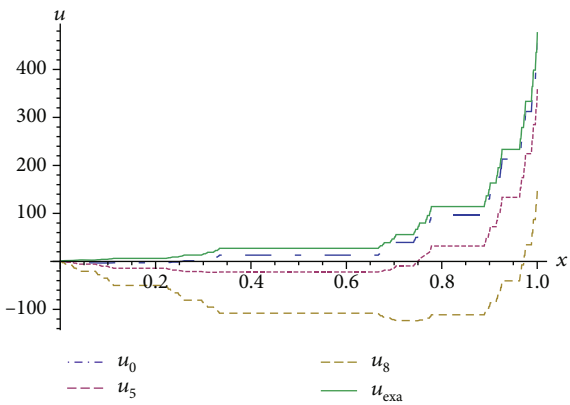

Figure 2: Divergent asymptotic solutions and exact solution in the case $\alpha = \ln 2/\ln 3$.

In Figure 2, the initial solution and 5th-order and 8th-order approximate solutions u_0, u_5, and u_8 and the exact solution u_{exa} are shown by constraining them to a Cantor set with dimension $\alpha = \ln 2/\ln 3 \approx 0.631$ which does not satisfy the convergence condition $\alpha_0 < \alpha \le 1$. In this case, u_{exa}, u_0, u_5, and u_8 form a sequence of divergent approximate solutions.

Since the initial approximation v_0^{α} or u_0 possesses arbitrariness as mentioned earlier, if we set again

$$\frac{d^{\alpha}v_0^{\alpha}(x)}{dx^{\alpha}} = \frac{d^{\alpha}u_0(x)}{dx^{\alpha}} = 3E_{\alpha}(3x^{\alpha}), \tag{36}$$

then the similar process yields

$$v_0^{\alpha} = u_0 = E_{\alpha}(3x^{\alpha}), \tag{37}$$

$$v_1^{\alpha} = v_2^{\alpha} = v_3^{\alpha} = \cdots = 0, \tag{38}$$

from which we finally reach solution (33). So, for any $0 < \alpha \le 1$, the solution (33) is always the exact solution of Equation (4). That is to say, if we chose an appropriate initial approximation v_0^{α} or u_0, then the operation can be

considerably simplified. More importantly, the convergence condition that the sequence of approximate solutions depends on fractional order can be removed.

It should be noted that when $\alpha = 1$ and $u(x)$, $f(x)$, and $g(x,t)$ are all the continuous and differentiable functions, solution (33) reduces to $u = e^{3x}$ which is the known exact solution of the following IDE [19]:

$$\frac{du(x)}{dx} - 3e^{3x} + \frac{1}{3}\left(2e^3 + 1\right)x - \int_0^1 3xtu(t)dt = 0. \tag{39}$$

5. He-Laplace Method and Comparison

As Deng and Ge [21] pointed out, He-Laplace method has a simple and reliable algorithm and it can be coupled with the HPM or the VIM for solving various nonlinear models, shedding a bright light on fractal calculus. A newest typical example of He-Laplace method to illustrate its simplicity, directness, strength, and great prospects can be found in [22]. In what follows, we employ the local fractional version of He-Laplace method [23] to solve the local fractional IDE (4).

Taking the local fractional Laplace transform on Equation (4), we can gain

$$L\left(\frac{d^\alpha u(x)}{dx^\alpha}\right) = L\left[3E_\alpha(3x^\alpha) + \left(\frac{E_\alpha(3)}{\Gamma(1+\alpha)} - \frac{E_\alpha(3)-1}{3}\right)x^\alpha\right] + L\left[\frac{1}{\Gamma(1+\alpha)}\int_0^1 \frac{3x^\alpha t^\alpha}{\Gamma(1+\alpha)}u(t)(dt)^\alpha\right], \tag{40}$$

$$s^\alpha L(u(x)) - u(0) = L\left[3E_\alpha(3x^\alpha) + \left(\frac{E_\alpha(3)}{\Gamma(1+\alpha)} - \frac{E_\alpha(3)-1}{3}\right)x^\alpha\right] + L\left[\frac{1}{\Gamma(1+\alpha)} \cdot \int_0^1 \frac{3x^\alpha t^\alpha}{\Gamma(1+\alpha)}u(t)(dt)^\alpha\right], \tag{41}$$

$$L(u(x)) = \frac{u(0)}{s^\alpha} + \frac{1}{s^\alpha}L\left[3E_\alpha(3x^\alpha) + \left(\frac{E_\alpha(3)}{\Gamma(1+\alpha)} - \frac{E_\alpha(3)-1}{3}\right)x^\alpha\right] + \frac{1}{s^\alpha}L\left[\frac{1}{\Gamma(1+\alpha)} \cdot \int_0^1 \frac{3x^\alpha t^\alpha}{\Gamma(1+\alpha)}u(t)(dt)^\alpha\right]. \tag{42}$$

Then, the inverse local fractional Laplace transform of Equation (42) gives

$$u(x) = E_\alpha(3x^\alpha) - \left(\frac{E_\alpha(3)}{\Gamma(1+\alpha)} - \frac{E_\alpha(3)-1}{3}\right)\frac{\Gamma(1+\alpha)}{\Gamma(1+2\alpha)}x^\alpha + L^{-1}\left\{\frac{1}{s^\alpha}L\left[\frac{1}{\Gamma(1+\alpha)}\int_0^1 \frac{3x^\alpha t^\alpha}{\Gamma(1+\alpha)}u(t)(dt)^\alpha\right]\right\}, \tag{43}$$

where $u(0) = 1$ has been assumed and L and L^{-1} are the local fractional Laplace transform operator and inverse operator [1], respectively.

Dealing Equation (43) with the local fractional HPM, we introduce

$$\sum_{n=0}^{\infty} p^{n\alpha}u_n(x) = E_\alpha(3x^\alpha) - \left(\frac{E_\alpha(3)}{\Gamma(1+\alpha)} - \frac{E_\alpha(3)-1}{3}\right) \cdot \frac{\Gamma(1+\alpha)}{\Gamma(1+2\alpha)}x^\alpha + p^\alpha L^{-1}\left\{\frac{1}{s^\alpha}L\left[\frac{1}{\Gamma(1+\alpha)} \cdot \int_0^1 \frac{3x^\alpha t^\alpha}{\Gamma(1+\alpha)}\sum_{n=0}^{\infty}p^{n\alpha}u_n(x)(dt)^\alpha\right]\right\}, \tag{44}$$

and compare the coefficients of the same powers of p^α; then, He's polynomials can be obtained:

$$\begin{aligned}
p^0 &: u_0(x) = E_\alpha(3x^\alpha) - \left(\frac{E_\alpha(3)}{\Gamma(1+\alpha)} - \frac{E_\alpha(3)-1}{3}\right)\frac{\Gamma(1+\alpha)}{\Gamma(1+2\alpha)}x^{2\alpha},\\
p^\alpha &: u_1(x) = L^{-1}\left\{\frac{1}{s^\alpha}L\left[\frac{1}{\Gamma(1+\alpha)}\int_0^1 \frac{3x^\alpha t^\alpha}{\Gamma(1+\alpha)}u_0(x)(dt)^\alpha\right]\right\}\\
&= \left(1 - \frac{3\Gamma(1+3\alpha)}{\Gamma(1+2\alpha)\Gamma(1+4\alpha)}\right)\left(\frac{E_\alpha(3)}{\Gamma(1+\alpha)} - \frac{E_\alpha(3)-1}{3}\right) \cdot \frac{\Gamma(1+\alpha)}{\Gamma(1+2\alpha)}x^{2\alpha},\\
p^{2\alpha} &: u_2(x) = L^{-1}\left\{\frac{1}{s^\alpha}L\left[\frac{1}{\Gamma(1+\alpha)}\int_0^1 \frac{3x^\alpha t^\alpha}{\Gamma(1+\alpha)}u_1(x)(dt)^\alpha\right]\right\}\\
&= \frac{3\Gamma(1+3\alpha)}{\Gamma(1+2\alpha)\Gamma(1+4\alpha)}\left(1 - \frac{3\Gamma(1+3\alpha)}{\Gamma(1+2\alpha)\Gamma(1+4\alpha)}\right) \cdot \left(\frac{E_\alpha(3)}{\Gamma(1+\alpha)} - \frac{E_\alpha(3)-1}{3}\right)\frac{\Gamma(1+\alpha)}{\Gamma(1+2\alpha)}x^{2\alpha},\\
p^{3\alpha} &: u_3(x) = L^{-1}\left\{\frac{1}{s^\alpha}L\left[\frac{1}{\Gamma(1+\alpha)}\int_0^1 \frac{3x^\alpha t^\alpha}{\Gamma(1+\alpha)}u_2(x)(dt)^\alpha\right]\right\}\\
&= \frac{3^2\Gamma^2(1+3\alpha)}{\Gamma^2(1+2\alpha)\Gamma^2(1+4\alpha)}\left(1 - \frac{3\Gamma(1+3\alpha)}{\Gamma(1+2\alpha)\Gamma(1+4\alpha)}\right) \cdot \left(\frac{E_\alpha(3)}{\Gamma(1+\alpha)} - \frac{E_\alpha(3)-1}{3}\right)\frac{\Gamma(1+\alpha)}{\Gamma(1+2\alpha)}x^{2\alpha},\\
p^{4\alpha} &: u_4(x) = L^{-1}\left\{\frac{1}{s^\alpha}L\left[\frac{1}{\Gamma(1+\alpha)}\int_0^1 \frac{3x^\alpha t^\alpha}{\Gamma(1+\alpha)}u_3(x)(\mathrm{d}t)^\alpha\right]\right\}\\
&= \frac{3^3\Gamma^3(1+3\alpha)}{\Gamma^3(1+2\alpha)\Gamma^3(1+4\alpha)}\left(1 - \frac{3\Gamma(1+3\alpha)}{\Gamma(1+2\alpha)\Gamma(1+4\alpha)}\right) \cdot \left(\frac{E_\alpha(3)}{\Gamma(1+\alpha)} - \frac{E_\alpha(3)-1}{3}\right)\frac{\Gamma(1+\alpha)}{\Gamma(1+2\alpha)}x^{2\alpha}, \vdots .
\end{aligned} \tag{45}$$

We therefore obtain an approximate solution of Equation (4):

$$u = \lim_{p^{\alpha}\longrightarrow 1}\sum_{n=0}^{\infty} p^{n\alpha}u_n^{\alpha}(x) = E_{\alpha}(3x^{\alpha}) - \left(\frac{E_{\alpha}(3)}{\Gamma(1+\alpha)} - \frac{E_{\alpha}(3)-1}{3}\right) \cdot \frac{\Gamma(1+\alpha)}{\Gamma(1+2\alpha)}x^{2\alpha} + \left(1 + \frac{3\Gamma(1+3\alpha)}{\Gamma(1+2\alpha)\Gamma(1+4\alpha)} + \frac{3^2\Gamma^2(1+3\alpha)}{\Gamma^2(1+2\alpha)\Gamma^2(1+4\alpha)} + \frac{3^3\Gamma^3(1+3\alpha)}{\Gamma^3(1+2\alpha)\Gamma^3(1+4\alpha)} + \cdots\right) \times \left(\frac{E_{\alpha}(3)}{\Gamma(1+\alpha)} - \frac{E_{\alpha}(3)-1}{3}\right)\left(1 - \frac{3\Gamma(1+3\alpha)}{\Gamma(1+2\alpha)\Gamma(1+4\alpha)}\right) \cdot \frac{\Gamma(1+\alpha)}{\Gamma(1+2\alpha)}x^{2\alpha}, \tag{46}$$

which is the same as solution (29). It is not difficult to see that solution (46) has the same nth-order approximate solution (31), and when the condition (32) holds, the limit of solution (46) gives the same exact solution (33).

Through comparison, we find that the computational difficulty of solving the local fractional IDE (4) by the above two methods is about the same. When using the local fractional HPM, we need to introduce an appropriate initial approximate solution $v_0(x)$, while the local fractional He-Laplace method uses a known initial value $u(0)$. Generally speaking, it is more difficult to choose an initial approximate solution $v_0(x)$ than to find an initial value $u(0)$. For the latest valuable work on the modified HPM, we suggest to refer to Refs. [24, 25].

6. Conclusion

In summary, we have established the local fractional HPM for the class of local fractional IDEs (1). Based on the established local fractional HPM, an explicit and exact Mittag–Leffler function solution (33) of the local fractional IDE (4) is obtained by selecting two different initial solutions (24) and (37). The comparison shows that the local fractional He-Laplace method [23] can also obtain the same solution (33), but when the initial approximate solution is not easy to choose, the local fractional He-Laplace method [23] has certain advantages over the method used in this paper. The obtained results show that if we choose the approximate solutions appropriately, for example solution (37), then the calculation can be considerably simplified and that the sequence of approximate solutions generated by the local fractional HPM can directly approach the real solution without the influence of fractional order. However, for the selected initial approximate solution (24), we obtained a sequence of approximate solutions converging the real solution (33) in a certain range of the fractional order α, i.e., $\alpha_0 < \alpha \le 1$. At the same time, there is a divergence interval $(0, \alpha_0)$ which depends on the fractional order α. Here, $q(\alpha_0) = 1$, and an approximate range of α_0 is $0.73 < \alpha_0 < 0.74$. That is to say, α_0 is the critical value of convergence and divergence related to fractional order α of the obtained sequence of approximate solutions. This is different from the HPM for integer-order DEs, all the sequences of approximate solutions of which either converge or diverge, and there is no such a critical value of convergence and divergence. When the nth-order approximate solution (31) is constrained to a Cantor set with dimension $\alpha = \ln 2/\ln 3 \approx 0.631$, this paper shows in Figure 2 a sequence of divergent approximate solutions. This paper fails to describe a sequence of convergent approximate solutions of (31), which is due to the complexity of the numerical simulation of fractal set. How to constrain solution (31) to other fractal sets and show some sequences of convergent approximate solutions? This is a question worth exploring. Besides, the research on qualitative behaviors of Equation (4) and other fractional IDEs is worth discussing. Some recent meaningful results of this research can be found in [26–28]. In 2007, Wang and He [29] took three concrete IDEs as examples to illustrate the effectiveness of the VIM for various IDEs. Based on this fact, we conclude that the local fractional version of VIM can also solve the local fractional IDE (4). In fact, the main steps of the local fractional VIM for Equation (4) can be summarized as follows: (i) identifying Lagrange multiplier $\lambda_{\alpha} = -1$, (ii) determining the iterative formula of solution:

$$u_{n+1}(x) = u_n(x) - \frac{1}{\Gamma(1+\alpha)}\int_0^x \left(\frac{d^{\alpha}u_n(\xi)}{d\xi^{\alpha}} + F(u_n(\xi))\right) \cdot (d\xi)^{\alpha}, (n = 0, 1, 2\cdots), \tag{47}$$

with

$$F(u_n(\xi)) = -3E_{\alpha}(3\xi^{\alpha}) + \left(\frac{E_{\alpha}(3)}{\Gamma(1+\alpha)} - \frac{E_{\alpha}(3)-1}{3}\right)\xi^{\alpha} - \frac{1}{\Gamma(1+\alpha)}\int_0^1 \frac{3\xi^{\alpha}t^{\alpha}}{\Gamma(1+\alpha)}u_n(t)(dt)^{\alpha}, \tag{48}$$

and (iii) selecting the initial approximate solution $u_0(x) = E_{\alpha}(3x^{\alpha})$ to obtain the exact solution $u(x) = \lim_{n\longrightarrow\infty} u_n(x) = E_{\alpha}(3x^{\alpha})$ by using the determined iterative formula (47). Nevertheless, it is still worth trying to find an appropriate initial approximate solution and get the approximate solution (29) or (46) by Equation (47).

Data Availability

The data in the manuscript are available from the corresponding author upon reasonable request.

Conflicts of Interest

The authors declare that there is no conflict of interest regarding the publication of this article.

Acknowledgments

The authors B. Xu and S. Zhang are grateful to Professor Xiao-Jun Yang of China University of Mining and Technology for helpful discussion. This work was supported by the Liaoning BaiQianWan Talents Program of China (grant

No. LRS2020[78]), the National Natural Science Foundation of China (grant No. 11547005), the Natural Science Foundation of Education Department of Liaoning Province of China (grant No. LJ2020002), and the Natural Science Foundation of Xinjiang Autonomous Region of China (grant No. 2020D01B01).

References

[1] X. J. Yang, D. Baleanu, and H. M. Srivastava, *Local Fractional Integral Transforms and Their Applications*, Academic Press, London, 2016.

[2] I. Podlubny, *Fractional Differential Equations*, Academic Press, New York, 1998.

[3] Y. Zhao, D. F. Cheng, and X. J. Yang, "Approximation solutions for local fractional Schrödinger equation in the one-dimensional Cantorian system," *Advances in Mathematical Physics*, vol. 2013, Article ID 291386, 5 pages, 2013.

[4] A. M. A. El-Sayed, S. Z. Rida, and A. A. M. Arafa, "Exact solutions of fractional-order biological population model," *Communications in Theoretial Physics*, vol. 52, no. 6, pp. 992–996, 2009.

[5] S. Zhang and H. Q. Zhang, "Fractional sub-equation method and its applications to nonlinear fractional PDEs," *Physics Letters A*, vol. 375, no. 7, pp. 1069–1073, 2011.

[6] S. X. Deng and X. X. Ge, "The variational iteration method for Whitham-Broer-Kaup system with local fractional derivatives," *Thermal Science*, vol. 26, no. 3, pp. 2419–2426, 2022.

[7] S. Zhang, B. Cai, and B. Xu, "Variable separation method for nonlinear time fractional biological population model," *International Journal of Numerical Methods for Heat and Fluid Flow*, vol. 25, no. 7, pp. 1531–1541, 2015.

[8] C. Li and F. Zeng, "The finite difference methods for fractional ordinary differential equations," *Numerical Functional Analysis and Optimization*, vol. 34, no. 2, pp. 149–179, 2013.

[9] M. Nadeem, J. H. He, and A. Islam, "The homotopy perturbation method for fractional differential equations: part 1 Mohand transform," *International Journal of Numerical Methods for Heat and Fluid Flow*, vol. 31, no. 11, pp. 3490–3504, 2021.

[10] S. Habib, A. Batool, A. Islam, M. Nadeem, and J. H. He, "Study of nonlinear hirota-satsuma coupled KdV and coupled mKdV system with time fractional derivative," *Fractals*, vol. 29, article 2150108, no. 5, 2021.

[11] Y. Wang, Y. F. Zhang, J. G. Liu, and M. Iqbal, "A short review on analytical methods for fractional equations with He's fractional derivative," *Thermal Science*, vol. 21, no. 4, pp. 1567–1574, 2022.

[12] B. Xu, Y. F. Zhang, and S. Zhang, "Line soliton interactions for shallow ocean-waves and novel solutions with peakon, ring, conical, columnar and lump structures based on fractional KP equation," *Advances in Mathematical Physics*, vol. 2021, Article ID 6664039, 15 pages, 2021.

[13] K. M. Kolwankar and A. D. Gangal, "Fractional differentiability of nowhere differentiable functions and dimensions," *Chaos*, vol. 6, no. 4, pp. 505–513, 1996.

[14] Y. Wang and Q. G. Deng, "Fractal derivative model for tsunami travelling," *Fractals*, vol. 27, no. 2, article 1950017, 2019.

[15] J. Fan and X. M. Shang, "Fractal heat transfer in wool fiber hierarchy," *Heat Transfer Research*, vol. 44, no. 5, pp. 399–407, 2013.

[16] J. Fan, N. Zhu, L. L. Wang, Z. Liu, C. Y. Wang, and Y. Liu, "Influence of hierarchic structure on the moisture permeability of biomimic woven fabricusing fractal derivative method," *Advances in Mathematical Physics*, vol. 2015, Article ID 817437, 4 pages, 2015.

[17] Y. Zhang, C. Cattani, and X. J. Yang, "Local fractional homotopy perturbation method for solving non-homogeneous heat conduction equations in fractal domains," *Entropy*, vol. 17, no. 12, pp. 6753–6764, 2015.

[18] J. H. He, "Homotopy perturbation technique," *Computer Methods in Applied Mechanics and Engineering*, vol. 178, no. 3-4, pp. 257–262, 1999.

[19] M. Tavassoli Kajani, M. Ghasemi, and E. Babolian, "Comparison between the homotopy perturbation method and the sine-cosine wavelet method for solving linear integro-differential equations," *Computers & Mathematics with Applications*, vol. 54, no. 7-8, pp. 1162–1168, 2007.

[20] G. Jumarie, "On the representation of fractional Brownian motion as an integral with respect to (dt) a," *Applied Mathematics Letters*, vol. 18, no. 7, pp. 739–748, 2005.

[21] S. X. Deng and X. X. Ge, "Approximate analytical solution for Phi-four equation with He's fractal derivative," *Thermal Science*, vol. 25, no. 3 Part B, pp. 2369–2375, 2021.

[22] J. H. He, G. M. Moatimid, and M. H. Zekry, "Forced nonlinear oscillator in a fractal space," *Facta Universitatis-Series: Mechanical Engineering*, vol. 20, no. 1, pp. 001–020, 2022.

[23] H. Y. Zhang, M. Nadeem, A. Rauf, and Z. G. Hui, "A novel approach for the analytical solution of nonlinear time-fractional differential equations," *International Journal of Numerical Methods for Heat and Fluid Flow*, vol. 31, no. 4, pp. 1069–1084, 2021.

[24] X. X. Li and C. H. He, "Homotopy perturbation method coupled with the enhanced perturbation method," *Journal of Low Frequency Noise, Vibration & Active Control*, vol. 38, no. 3-4, pp. 1399–1403, 2019.

[25] C. H. He and Y. O. El-Dib, "A heuristic review on the homotopy perturbation method for non-conservative oscillators," *Journal of Low Frequency Noise, Vibration & Active Control*, vol. 41, no. 2, pp. 572–603, 2022.

[26] M. Bohner, O. Tunç, and C. Tunç, "Qualitative analysis of Caputo fractional integro-differential equations with constant delays," *Computational and Applied Mathematics*, vol. 40, no. 6, 2021.

[27] C. Tunç and O. Tunç, "On the stability, integrability and boundedness analyses of systems of integro-differential equations with time-delay retardation," *Revista de la Real Academia de Ciencias Exactas, Físicas y Naturales. Serie A. Matemáticas*, vol. 115, no. 3, article 115, 2021.

[28] C. Tunç, Y. H. Yang, O. Tunç, and J. C. Yao, "New and improved criteria on fundamental properties of solutions of integro—delay differential equations with constant delay," *Mathematics*, vol. 9, no. 24, article 3317, 2021.

[29] S. Q. Wang and J. H. He, "Variational iteration method for solving integro-differential equations," *Physics Letters A*, vol. 367, no. 3, pp. 188–191, 2007.

Hindawi
Advances in Mathematical Physics
Volume 2022, Article ID 1638571, 9 pages
https://doi.org/10.1155/2022/1638571

Research Article

A Numerical and Analytical Study of a Stochastic Epidemic SIR Model in the Light of White Noise

Shah Hussain,[1] **Elissa Nadia Madi**,[1] **Hasib Khan**,[2] **and Mohammed S. Abdo**[3]

[1]*Faculty of Informatics and Computing, Universiti Sultan Zainal Abidin (UniSZA), Besut Campus, Terengganu, Malaysia*
[2]*Department of Mathematics, Shaheed Benazir Bhutto University, Sheringal, Dir Upper, Khyber Pakhtunkhwa, Pakistan*
[3]*Department of Mathematics, Hodeidah University, Al-Hodeidah, Yemen*

Correspondence should be addressed to Mohammed S. Abdo; msabdo@hoduniv.net.ye

Received 11 June 2022; Revised 18 July 2022; Accepted 26 July 2022; Published 27 August 2022

Academic Editor: Qura tul Ain

This study examines a novel SIR epidemic model that takes into account the impact of environmental white noise. According to the study, white noise has a significant impact on the disease. First, we establish the solution's existence and uniqueness. Following that, we explain that the stochastic basic production $\mathfrak{R}_0$ is a threshold that determines the extinction or persistence of the disease. When noise levels are high, we acquire $\mathfrak{R}_0 < 1$, which causes the sickness to disappear. A sufficient condition for the existence of a stationary distribution is archived when the noise intensity is high, which suggests the infection is prevalent when $\mathfrak{R}_0 > 1$. Finally, numerical simulations are used to explain the key findings.

1. Introduction

The goal of this research is to show how challenging SIR models are for understanding the epidemic and to offer a useful model for establishing proposal insights into its spread. The traditional susceptible-infected-removed SIR model of Kermack and McKendrick is the progenitor of nearly all mathematical models for the transmission of infectious illnesses. Numerous researchers have thoroughly studied the dynamic behavior of various epidemic models and many of their expansions. The presence of the threshold values that determine whether a disease dies out, the stability of the disease-free and endemic equilibria, permanence, and extinction are the fundamental and essential study topics for contemporary studies.

For many years, the spread and transmission of illnesses have been questioned and examined. In reality, Graunt was the first scientist to attempt to scientifically quantify causes of mortality [1], and his investigation of causes of death resulted in a hypothesis that is now widely accepted among current epidemiologists. Bernoulli was the first mathematician to propose an infectious disease mathematical model. He modeled the transmission of smallpox [2], which was widespread at the time, and advocated for the benefits of variolation [3] in 1760. In 1927, McKendrick and Kermack proposed a basic deterministic (compartmental) model for forecasting the behavior of epidemic outbreaks [4]. SIR models are an extremely versatile modeling approach developed by the researchers. They are often used in the modeling of infectious illnesses using mathematics. People are divided into groups with the letters S, I, and R (susceptible, infectious, and recovered). ODE, which are deterministic, are most often applied to run the models, but they may also be used with a stochastic (random) framework, which is more realistic but trickier to evaluate.

According to John M. Last, epidemiology is the study of the spread and determinants of disease or well-being status in a population, or it is the outlet of medicine that deals with the occurrence, distribution, possible mechanism of malady, and other factors related to health. It is the foundation of common safety and nature's tactic varieties, as well as evidence-based preparation by distinct risk factors for illness and emphases on protective curative amenities. Syndrome diffusion experts assist by deliberating on proposals, variety,

and measurable investigation of evidence, altering understanding and spread of outcomes (calculating viscount inspection and periodic proficient review). As a result, epidemiology has generated techniques in scientific analysis, common safety education, and, less suggestively, fundamental surveys in the biological disciplines [5]. Disease causality, diffusion, epidemic analysis, disease observation, environmental epidemiology, forensic epidemiology, occupational epidemiology, screening, biomonitoring, and comparisons of cure effects, such as in clinical trials, are all important areas of epidemiological study. Further scientific castigations are used by epidemiologists, such as biology to better understand disease progressions, statistics to make actual use of data and advance appropriate outcomes, social sciences to better understand local and terminal grounds, and engineering to increase revelation.

The word "epidemiology" is usually used to describe and illuminate not only epidemics and infectious diseases, but disease in general, as well as associated circumstances. High blood pressure, mental disease, and obesity are objective insufficient of the concerns studied by epidemiology. As a consequence, this epidemiology is based on how the pattern of disease produces a change in human function. Mathematical research has generated great improvements in practical and theoretical fields [6–8].

To investigate the influence of environmental conditions on the epidemic model and make the results more realistic, we first developed a stochastic mathematical SIR model. Recent scientific advances with a focus on the transmission of numerous infectious illnesses (SDE) and (ODE) have been front and center. An SDE is a differential equation in which one or more of the terms are stochastic processes, with the solution likewise being a stochastic process. SDEs often include a variable that is calculated as the Wiener process or Brownian motion derivative and represents random white noise. Other kinds of random behavior, including jump processes, are indeed feasible. Stochastic differential equations and random differential equations are conjugate [9], while differential equation having one or more functions of one independent variable and their derivatives is known as an ordinary differential equation (ODE) in mathematics. Ordinary differential equations are applied in contrast to partial differential equations, which may refer to more than one independent variable [10].

The current paper will investigate the persistence and extinction of the epidemic, provide the system's threshold value, and be affected by motion brought on by white noise. Even though stochastic system perturbations have many more varied features, we still took into account how this system's threshold compares to those of other models that include the same motion [11]. Finally, we visualize the numerical simulations using MATLAB.

2. Stochastic Epidemic Model Description

In this section, we provide our new stochastic model in the form of differential equations.

(i) The total inhabitant $\mathfrak{N}_t$ is distributed in three compartments: $\mathcal{S}_t$, $\mathcal{I}_t$, and $\mathcal{R}_t$ represent the susceptible, infected peoples, and recovered people, respectively

(ii) The indicated stochastic model's variables and parameters are both nonnegative

(iii) We perturbed β and γ, i.e., $\beta \longrightarrow \beta + \sigma_1 \mathfrak{B}_1$ and $\gamma \longrightarrow \gamma + \sigma_2 \mathfrak{B}_2$. Where $\mathfrak{B}_1, \mathfrak{B}_2$ are the Brownian motion with the property $\mathfrak{B}_{1_0} = 0 = \mathfrak{B}_{2_0}$ and the intensity σ_1^2, σ_2^2 are positive

Remark 1. The deterministic general epidemic study estimates that if $\mathfrak{R}_0 < 1$, a small outburst will aries, and if $\mathfrak{R}_0 > 1$, a large outbreak will occur, infecting a large chunk of the population. The results are based on the assumption that the community is homogeneous and that individuals mingle evenly. However, if the hypothesis of an evenly mixed society is accepted, the model may not be appropriate in particular situations. When contemplating a tiny population, such as an epidemic outbreak in a daycare center or school, it appears logical to presume that the eventual number of infected will be unpredictable or random. Also, even if $\mathfrak{R}_0 > 1$ and the society is huge, if the outbreak is started by only one (or a few) early invective's, the plagues may never take off by accident. The formulation of a related stochastic epidemic model is motivated by these two aspects. It allows parameter estimation from disease outbreak data to include standard error, and the subject of the disease extinction is better suited for the stochastic model for researching epidemic diseases.

In the light of above speculations, we established the below new stochastic SIR epidemic model.

$$\begin{aligned} &d(S_t) = (\Lambda - \beta S_t I_t - dS_t)dt - \sigma_1 S_t I_t d\mathfrak{B}_1(t), \\ &, d(I_t) = (\beta S_t I_t - (d+\gamma)dI_t - \mathfrak{h}(I))dt + \sigma_1 S_t I_t d\mathfrak{B}_1(t) - \sigma_2 I_t d\mathfrak{B}_2(t), \\ &d(R_t) = (\gamma I + \mathfrak{h}(I) - dR)dt + \sigma_2 I_t d\mathfrak{B}_2(t). \end{aligned} \tag{1}$$

The above Table 1 represents the parameters and their values, while Table 2 represents the compartments and their values. Note that $h(I)$ is the elimination of the transferable entities due to the cure of the form:

$$h(I) = \begin{cases} \mathfrak{M} > 0 & \text{for} \quad I > 0\,; \\ \mathfrak{M} = 0 & I = 0. \end{cases} \tag{2}$$

The authors [12] have the following deterministic.

$$\begin{aligned} \frac{d(S_t)}{dt} &= \Lambda - \beta S_t I_t - dS_t, \\ \frac{d(I_t)}{dt} &= \beta S_t I_t - (d+\gamma)dI_t - \mathfrak{h}(I), \\ \frac{d(R_t)}{dt} &= \gamma I + \mathfrak{h}(I) - dR, \end{aligned} \tag{3}$$

Table 1: Parametric description of the model.

Symbol	Description	Value
Λ	Constitute the recruitment rate in the susceptible inhabitant	0.1
β	Is the diffusion rate	0.01
d	Is the usual passing away rate	0.006
γ	Is the impulsive salvage amount of the virulent entities	0.03

Table 2: Compartments and description.

Symbol	Description	Value
$\mathcal{S}$	Susceptible	20
I	Infected peoples	6
$\mathcal{R}$	Recovered peoples	1

and

$$d(\mathfrak{N}) = \Lambda - d\mathfrak{N}, \tag{4}$$

where $\mathfrak{N}_t = S_t + I_t + R_t$ indicates the entire constant residents for $\Lambda \approx \mu\mathfrak{N}$ and $\mathfrak{N}_0 = \mathcal{S}_0 + \mathcal{I}_0 + \mathcal{R}_0$. Equation (4) has the exact solution

$$\mathfrak{N}_t = e^{-dt}\left[\mathfrak{N}_0 + \frac{\Lambda}{d}e^{dt}\right]. \tag{5}$$

Also, we have

$$0 \geq \mathcal{S}_0, 0 \geq \mathcal{I}_0, \mathcal{R}_0 \geq 0 \Rightarrow S_t \geq 0, I_t \geq 0, 0 \leq R_t. \tag{6}$$

So that the result has positivity property. For the stability analysis of the model (3), we have the reproduction number, which is

$$\mathfrak{R}_0 = \frac{\beta\Lambda}{(d+\gamma)d}. \tag{7}$$

If $\mathfrak{R}_0 < 1$, the system (3) will be locally steady and will be unsteady if $\mathfrak{R}_0 \geq 1$ asymptotically stable. Further, the system (3) will be globally asymptotic if $\Lambda = 0$.

3. Preliminaries

Throughout this paper, we formulated the necessary assumptions. Suppose Rd_+ is the d-dimensional Euclidean space. $R_+^d = \{j \in R^d : 0 < j_i, d > 1\}$.

Let $(\mho, F, \mathfrak{P})$ a whole probability space that has been filtered by $\{F\}_{\mathfrak{t}\geq 0}$ and $\{\mathfrak{B}_\mathfrak{t}\}_{\mathfrak{t}\geq 0}$ is a 1-dimensional Brownian motion defined on it. Usually, we consider a SDE of n-dimension as

$$d\omega(\mathfrak{t}) = \mathfrak{F}(\mathfrak{y}(\mathfrak{t}), \mathfrak{t})d\mathfrak{t} + \mathfrak{G}(\mathfrak{y}(\mathfrak{t}), \mathfrak{t})d\mathfrak{B}(\mathfrak{t})), \quad \text{for} \quad \mathfrak{t} \geq \mathfrak{t}_0, \tag{8}$$

with initial value $\mathfrak{y}(\mathfrak{t}_0) = \mathfrak{y}_0 \varepsilon \mathfrak{R}^d$. By defining the dimensional operator £ with equation (8)

$$£ = \frac{\partial}{\partial\mathfrak{t}} + \sum_{i=1}^{d}\mathfrak{F}_i(\mathfrak{y}, \mathfrak{t})\frac{\partial}{\partial\mathfrak{y}_i} + \frac{1}{2}\sum_{i,j=1}^{d}\left[\mathfrak{G}^T(\mathfrak{y}, \mathfrak{t})\mathfrak{G}(\mathfrak{y}, \mathfrak{t})\right]_{ij}\frac{\partial^2}{\partial\mathfrak{y}_i\partial\mathfrak{y}_j}. \tag{9}$$

If the operator £ acts on the a function $\mathfrak{V} = (\mathbb{R}^d \times \mathbb{R}_+ ; \mathbb{R}_+)$ then

$$£\mathfrak{V} = \mathfrak{V}_t(\mathfrak{y}, \mathfrak{t}) + \mathfrak{V}_\mathfrak{y}(\mathfrak{y}, \mathfrak{t})\mathfrak{F}(\mathfrak{y}, \mathfrak{t}) + \frac{1}{2}\text{trace}\left[\mathfrak{G}^T(\mathfrak{y}, \mathfrak{t})\mathfrak{V}_{\mathfrak{y}\mathfrak{y}}\mathfrak{G}(\mathfrak{y}, \mathfrak{t})\right]. \tag{10}$$

4. Existence and Uniqueness

By utilizing the technique in [13–15], the following theorem can be proof with ease.

Theorem 2. *(S_t, I_t, R_t) is a unique positive solution of system (1)for $t \geq 0$ with $(\mathcal{S}_0, \mathcal{I}_0, \mathcal{R}_0) \in R_+^3$, and result will be left in R_+^3, with probability equals to one.*

We outline a $\mathfrak{C}^2$-function $\mathfrak{U} : \mathbb{R}_+^3 \longrightarrow \mathbb{R}_+$, by the resulting formulation

$$\mathfrak{U}(\mathcal{S}_t, \mathcal{I}_t, R_t) = (S_t - 1 - \ln S_t) + \left(I_t - \left(\frac{2}{3} + \frac{1}{3}\right) - \ln I_t\right) + \left(R_t - \left(\frac{2}{3} + \frac{1}{3}\right) - \ln R_t\right). \tag{11}$$

By applying Ito formula, we have

$$d\mathfrak{U}(S_t, I_t, R_t) = \left(1 - \frac{1}{S_t}\right)dS_t + \frac{1}{2S_t^2}(dS_t)^2 + \left(1 - \frac{1}{I_t}\right) \cdot dI_t + \frac{1}{2I_t^2}(dI_t)^2 + \left(1 - \frac{1}{R_t}\right)dR_t + \frac{1}{2R_t^2}(dR_t)^2, \tag{12}$$

$$= \mathfrak{L}^*\mathfrak{U}dt + \sigma_1(\mathcal{I}_t - \mathcal{S}_t)d\mathfrak{B}_1(t) + \sigma_2(\mathcal{I}_t - \mathcal{S})d\mathfrak{B}_2(t), \tag{13}$$

where $\mathfrak{L}^*\mathfrak{U} : \mathbb{R}_+^3 \longrightarrow \mathbb{R}_+$ is defined by

$$\begin{aligned}\mathfrak{L}^*\mathfrak{U} &= \left(1-\frac{1}{S_t}\right)(\Lambda-\beta S_t I_t - dS_t) + \frac{1}{2}\sigma_1^2 I^2 \\ &+ \left(1-\frac{1}{I_t}\right)(\beta S_t I_t - d(d+\gamma)I_t) + \frac{1}{2}\sigma_1^2 S^2 + \frac{1}{2}\sigma_2^2 I^2 \\ &+ \left(1-\frac{1}{R_t}\right)(\gamma I_t - dR) + \sigma_2^2, = \Lambda - \beta S_t I_t - dS_t - dS_t \\ &- \frac{\Lambda}{\mathcal{S}_t} + \beta I_t + d + \beta S_t I_t - (d+\gamma)d - \beta S_t + (d+\gamma)d \\ &+ \gamma I - dR_t - \gamma\frac{I_t}{R_t} + d + \frac{1}{2}\sigma_1^2 S^2 + \frac{1}{2}\sigma_2^2 I_+^2 \sigma_2^2. \leq \Lambda + d \\ &+ d^2 + \gamma d + d + + \frac{1}{2}\sigma_1^2 S^2 + \frac{1}{2}\sigma_2^2 I_+^2 \sigma_2^2 \coloneqq A.\end{aligned} \tag{14}$$

The rest of the proof can be followed from [16–18].

5. Extinction of the Disease

In this part, we will figure out when the sickness will wipe out, as well as when it will resurface. As a result, system's (1) basic reproduction number is provided. We may deduce the following lemmas from the proof in [19].

Lemma 3 (see [20]). *Let (S_t, I_t, R_t) be the solution of system (1) with initial value $(S_0, I_0, R_0) \in \mathbb{R}_+^3$. Then*

$$Lim_{t\longrightarrow\infty}\frac{S_t + I_t + R_t}{t} = 0 \quad a.s. \tag{15}$$

6. Remark

In fact, combine with solution positivity and equation (15), we have by [20]

$$\mathrm{Lim}_{t\longrightarrow\infty}\left(\frac{\mathcal{S}_t}{t}\right) = 0, \mathrm{Lim}_{t\longrightarrow\infty}\left(\frac{I_t}{t}\right) = 0, \mathrm{Lim}_{t\longrightarrow\infty}\left(\frac{R_t}{\mathfrak{t}}\right) = 0\ a.s., \tag{16}$$

and according to lemma 2.2 of [20], we have

Lemma 4. *Assume $d > 1/2(\sigma_1^2 \vee \sigma_2^2)$. Let (S_t, I_t, R_t) be the solution of system (1) with initial value $(S_0, I_0, R_0) \in \mathbb{R}_+^3$, then*

$$\begin{aligned}Lim_{t\longrightarrow\infty}\frac{\int_0^t S(r)}{t} &= 0, \\ Lim_{t\longrightarrow\infty}\frac{\int_0^t S(r)}{t} &= 0, \\ Lim_{t\longrightarrow\infty}\frac{\int_0^t S(r)}{t} &= 0.\end{aligned} \tag{17}$$

$\mathfrak{R}_0 = \beta\Lambda/d(d+\gamma)$ is the basic reproduction of the system (3) in [12].

and

$$\mathfrak{R}_0^{\bullet} = \frac{\beta\Lambda}{d\left(d+\gamma+(1/2)\sigma_2^2\right)} = \mathfrak{R}_0 - \frac{\beta\Lambda}{2d(d+\gamma)\left(d+\gamma+(1/2)\sigma_2^2\right)}\sigma_2^2. \tag{18}$$

We will study the results in the next part based on Lemma 3 and 4.

Theorem 5. *Suppose $d > 1/2(\sigma_1^2 \vee \sigma_2^2)$. Let (S_t, I_t, R_t) be the solution of the system (1) with any initial value $(S_0, I_0, R_0) \in \mathbb{R}_+^3$. If $1 > \mathfrak{R}_0^{\bullet}$, then*

$$Lim_{t\longrightarrow\infty}\ \sup\ \frac{\log I_t}{t} \leq \left(d+\gamma+\frac{1}{2}\sigma_2^2\right)(\mathfrak{R}_0^{\bullet} - 1) < 0\ a.s. \tag{19}$$

I_t approaches to 0 exponentially almost sure. In other words, the illness will most likely die out.

Proof. From system (1), we have

$$\begin{aligned}\frac{-S_0 + S_t}{t} &= -(-\Lambda) - \frac{d}{t}\int_0^t S(s)ds - \frac{\beta}{t}\int_0^t I(s)S(s) \\ &\cdot ds - \frac{\sigma_1}{t}\int_0^t S(s)I(s)d\mathfrak{B}_1(s), \\ \frac{-I_0 + I_t}{t} &= \beta\frac{\int_0^t S(s)I(s)ds}{t} - d(d+\gamma)\frac{\int_0^t I(s)ds}{t} \\ &- \frac{\int_0^t h(I)ds}{t} + \sigma_1\frac{\int_0^t S(s)I(s)}{t}d\mathfrak{B}_1(s) \\ &- \sigma_2\frac{\int_0^t I(s)d\mathfrak{B}_2(s)}{t}, \\ \frac{-R_0 + R_t}{t} &= \gamma\frac{\int_0^t I(s)ds}{t} + \frac{\int_0^t h(I)ds}{t} - d\frac{\int_0^t R(s)ds}{t} + \sigma_2\frac{\int_0^t I(s)d}{t}\mathfrak{B}_2(s),\end{aligned} \tag{20}$$

then

$$\begin{aligned}d\frac{\int_0^t S(s)ds}{t} + d(d+\gamma)\frac{\int_0^t I(s)ds}{t} &= \Lambda - \frac{I_t - S_t}{t} + \frac{I_0 - S_0}{t} \\ &- \frac{\int_0^t h(I)ds}{t} - \sigma_2\frac{\int_0^t I(s)d\mathfrak{B}_2(s)}{t} = \Lambda + \xi(t),\end{aligned} \tag{21}$$

where $\xi(t)$ possesses the property that

$$\mathrm{Lim}_{t\longrightarrow\infty}\xi(t) = 0. \tag{22}$$

According to (15) and (17), we have

$$\mathrm{Lim}_{t\longrightarrow\infty}\frac{d\int_0^t S(s)ds + d(d+\gamma)\int_0^t I(s)ds}{t} = \Lambda. \tag{23}$$

Furthermore

$$\begin{aligned}\log \mathrm{I}_t - \log I_0 &= \beta\int_0^t \mathrm{S}(s)ds - \left(d+\gamma+\frac{1}{2}\sigma_2^2\right)\\ &\quad\cdot t + \sigma_1 \mathrm{S}(s)\mathfrak{B}_1(t) - \sigma_2\mathfrak{B}_2(t),\\ \log \mathrm{I}_t &= \log I_0 + \beta\frac{\Lambda}{d}t - \beta(d+\gamma)\int_0^t I(s)ds + \frac{\beta}{d}t\xi(t)\\ &\quad - \left(d+\gamma+\frac{1}{2}\sigma_2^2\right)t + \sigma_1\mathrm{S}(s)\mathfrak{B}_1(t) - \sigma_2\mathfrak{B}_2(t),\\ &= \left[t\beta\frac{\Lambda}{d} - \left(\gamma+\frac{1}{2}\sigma_2^2+d\right)\right]t - \beta(d+\gamma)\int_0^t I(s)ds\\ &\quad + \log I_0 + \frac{\beta}{d}t\xi(t) + \sigma_1\mathrm{S}(s)\mathfrak{B}_1(t) - \sigma_2\mathfrak{B}_2(t).\\ &\le \left[\beta\frac{\Lambda}{d}t - \left(d+\gamma+\frac{1}{2}\sigma_2^2\right)\right]t + \log I_0\\ &\quad + \frac{\beta}{d}t\xi(t) - \sigma_2\mathfrak{B}_2(t),\end{aligned} \tag{24}$$

and

$$\mathrm{Lim}_{t\longrightarrow\infty}\frac{1}{t}\left[\log I_0 + \frac{\beta}{d}t\xi(t) - \sigma_2\mathfrak{B}_2(t)\right] = 0 \quad a.s. \tag{25}$$

By (22) and the property of Brownian motion. If $1 > \mathfrak{R}_0^{\bullet}$, then, from (24), we have

$$\begin{aligned}\mathrm{Lim}_{t\longrightarrow\infty} \quad \sup\ \frac{\log I_t}{t} &\le \frac{\beta\Lambda}{d} - \left(d+\gamma+\frac{1}{2}\sigma_2^2\right)\\ &= \left(d+\gamma+\frac{1}{2}\sigma_2^2\right)(\mathfrak{R}_0^{\bullet}-1) < 0,\end{aligned} \tag{26}$$

as required. □

7. Persistence of the Disease

In this section, we will look at the infection's persistence in the pandemic context (1), with the following theorem introducing our main result.

Theorem 6. *Suppose $d > 1/2(\sigma_1^2 \vee \sigma_2^2)$. Let (S_t, I_t, R_t) be the solution of the system (1) with any initial value $(S_0, I_0, R_0) \in \mathbb{R}_+^3$. If $1 < \mathfrak{R}_0^{\bullet}$, then*

$$\begin{aligned}&Lim_{t\longrightarrow\infty}\frac{1}{t}\int_0^t S(s)ds = \frac{\Lambda}{d\mathfrak{R}_0^{\bullet}},\\ &Lim_{t\longrightarrow\infty}\frac{1}{t}\int_0^t \mathscr{I}(s)ds = \frac{d\left(\gamma+(1/2)\sigma_2^2+d\right)}{(d\beta+\gamma\beta)}(\mathfrak{R}_0^{\bullet}-1),\\ &Lim_{t\longrightarrow\infty}\frac{1}{t}\int_0^t \mathscr{R}(s)ds = \frac{\gamma\left(d+\gamma+(1/2)\sigma_2^2\right)}{\beta(d+\gamma)}(\mathfrak{R}_0^{\bullet}-1).\end{aligned} \tag{27}$$

Proof. If $\mathfrak{R}_0^{\bullet} > 1$, then, by (24) and by Lemma 3 and 5.2 in [21].

$$\begin{aligned}\mathrm{Lim}_{t\longrightarrow\infty}\frac{1}{t}\int_0^t I(s)ds &= \frac{(1/d)(\beta\Lambda) - \left(d+(1/2)\sigma_2^2+\gamma\right)}{(d\beta+\gamma\beta)/d},\\ &= \frac{\gamma\left(d+\gamma+(1/2)\sigma_2^2\right)}{\beta(d+\gamma)}(\mathfrak{R}_0^{\bullet}-1).\end{aligned} \tag{28}$$

Along with (23)

$$\mathrm{Lim}_{t\longrightarrow\infty}\frac{1}{t}\int_0^t S(s)ds = \frac{\Lambda}{d} - \left(\frac{\gamma+d+(1/2)\sigma_2^2}{\beta}\right)(\mathfrak{R}_0^{\bullet}-1), = \frac{\Lambda}{d\mathfrak{R}_0^{\bullet}}. \tag{29}$$

Further, integrating from 0 to t the last equation of system (1), we get

$$\frac{R_t - R_0}{t} = \frac{\gamma}{t}\int_0^t I(s)ds + \int_0^t h(I)ds - \frac{d}{t}\int_0^t R(s)ds + \frac{\sigma_2^2}{t}\int_0^t R(s)d\mathfrak{B}_2(s), \tag{30}$$

now (17) and (28) ⇒

$$\mathrm{Lim}_{t\longrightarrow\infty}\frac{1}{t}\int_0^t \mathscr{R}(s)ds = \frac{\left(\gamma+d+(1/2)\sigma_2^2\right)\gamma}{\beta(d+\gamma)}(\mathfrak{R}_0^{\bullet}-1). \tag{31}$$

□

Remark 7. Theorems 5 and 6 reveal that the illness's ability to die out or endure is highly influenced by the strength of white noise disturbances, with tiny white noise disturbances promoting long-term disease prevalence and big white noise disturbances causing the epidemic disease to die out.

8. Numerical Scheme and Results

Our study of disease extinction and persistence has now concluded. We will now perform some numerical simulations of (1) to illustrate the applicability of our findings. The Milstein technique [22] is used to generate numerical simulations. Consider the model's discretization equation:

$$\begin{aligned}S_{k+1} &= S_k + (\Lambda - \beta S_k I_k - dS_k)\Delta t - \sigma_1 S_k I_k\sqrt{\Delta t}\tau_k - \frac{\sigma_1^2}{2}S_k I_k\left(\tau_k^2-1\right)\Delta t,\\ I_{k+1} &= I_k + (\beta S_k I_k - d(d+\gamma)I_k - \mathfrak{M})\Delta t + \sigma_1 S_k I_k\sqrt{\Delta t}\tau_k\\ &\quad + \frac{\sigma_1^2}{2}S_k I_k\left(\tau_k^2-1\right)\Delta t - \sigma_2 I_k\sqrt{\Delta t}\tau_k - \frac{\sigma_2^2}{2}I_k\left(\tau_k^2-1\right)\Delta t,\\ R_{k+1} &= R_k + (\gamma I_k + \mathfrak{M} - dR_k)\Delta t + \sigma_2 I_k\sqrt{\Delta t}\tau_k + \frac{\sigma_2^2}{2}I_k\left(\tau_k^2-1\right)\Delta t.\end{aligned} \tag{32}$$

8.1. Numerical Data. Here, we highlight the numerical data for the stochastic model (1). For the parametric and initial values, we refer to [12].

Figures 1(a) and 1(b) are the comparison of S class in the deterministic system and in the stochastic system, with

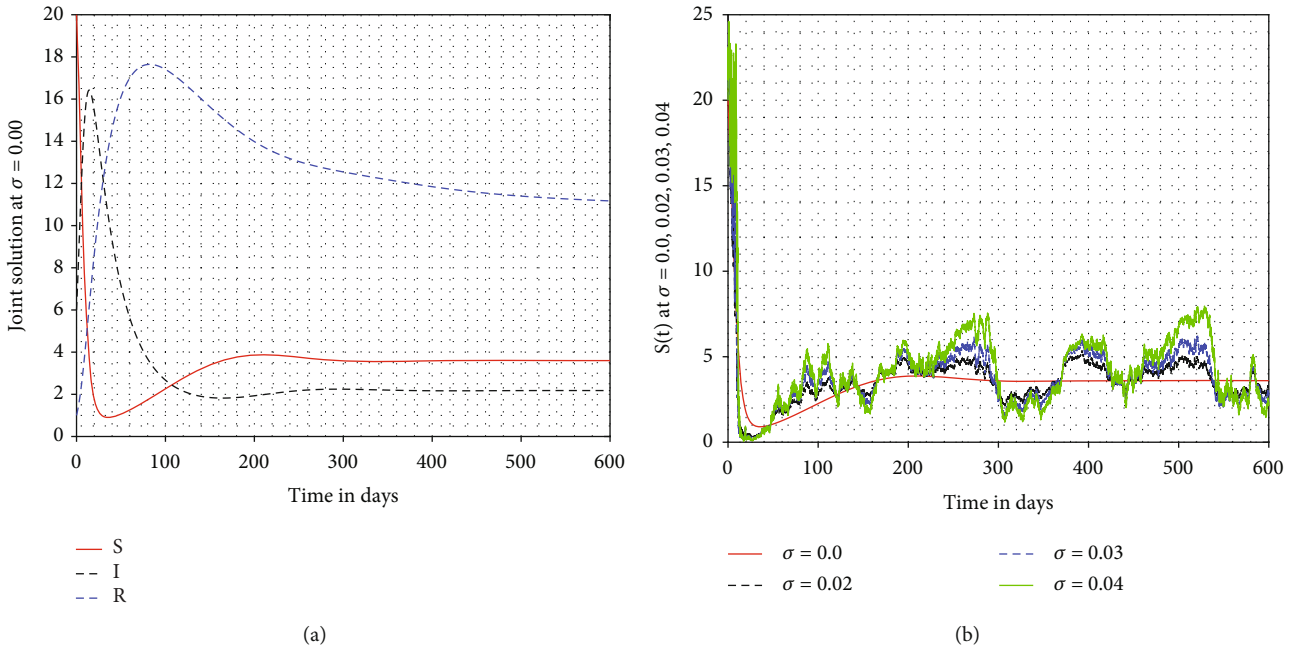

Figure 1: (a, b) Joint solution of (1) at $\sigma = 0.0$ and $S(t)$.

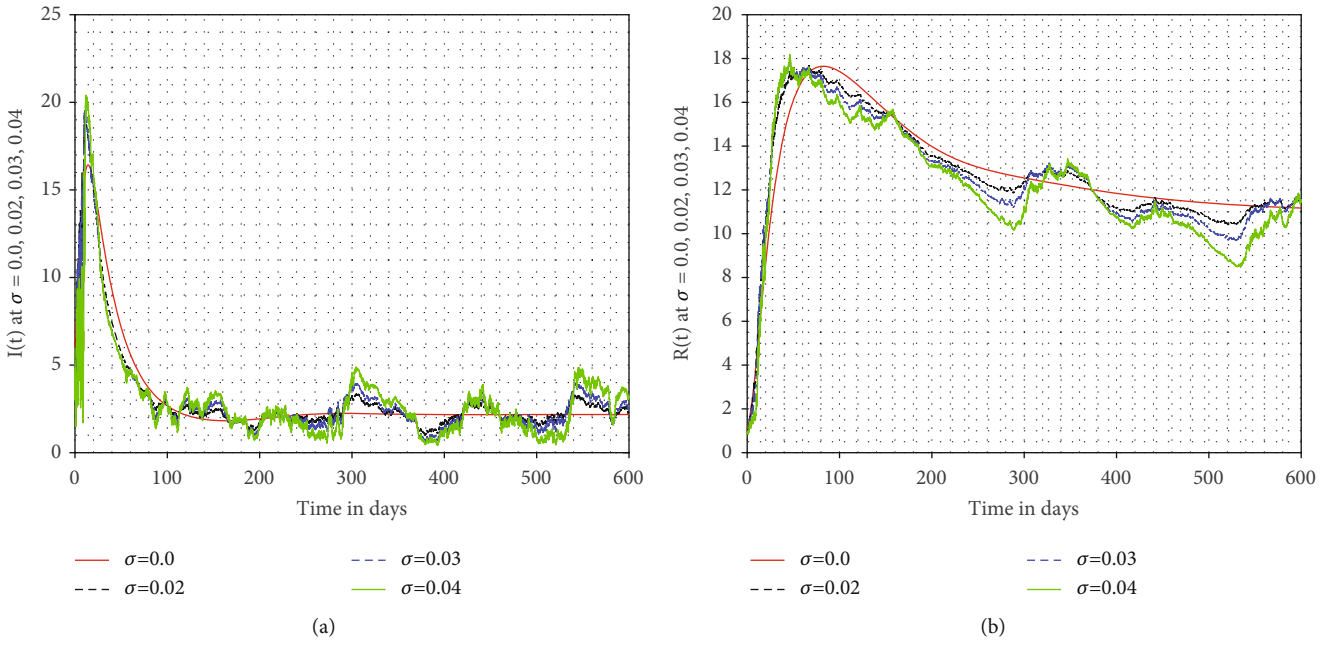

Figure 2: (a, b) $I(t)$ and $R(t)$ for different values of σ.

$\Lambda = 0.1, d = 0.006, m = 0.00001, \beta = 0.01, \gamma = 0.03$ and initial values $S(0) = 20, I(0) = 6, R(0) = 1$. In Figures 1(a) and 1(b), we have presented the joint solution of the model (1) for $\sigma = 0.0$, S, and different values of σ. Comparing the first figure, the noise getting smaller, the fluctuation of the system of model (1) is getting weaker. If we increase the value of $\sigma = 0.02, 0.03, 0.04$, respectively, the amplitude of fluctuation becomes stronger. That is to say, noise intensities have great effect on the solution of S.

Figures 2(a) and 2(b) are the comparison of I, R classes in the deterministic system and in the stochastic system, with $\Lambda = 0.1, d = 0.006, m = 0.00001, \beta = 0.01, \gamma = 0.03$ and initial values $S(0) = 20, I(0) = 6, R(0) = 1$. In Figure 2, we presented the dynamics of I and R of the model (1) for $\sigma = 0.0$, S, and different values of σ. Then, I will tend to zero exponentially with probability one. That is to say, an event distinct from its corresponding deterministic model might cause the illness to become extinct when there are enormous noises (3). The role of parameters on the stochastic model (1) has an importance. For observing this, we have modified the parametric values and observed a change in the dynamics of all the classes. Even, there is a change in the dynamics as a whole

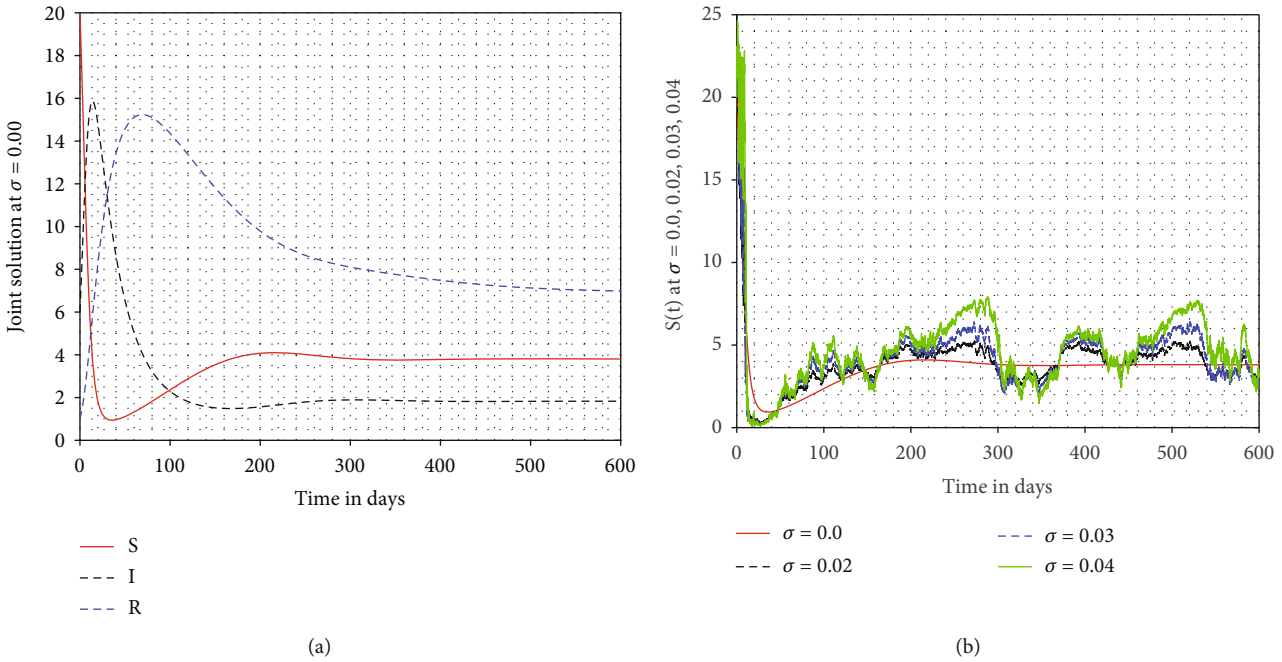

FIGURE 3: (a, b) Joint solution of (1) at $\sigma = 0.0$ and $S(t)$.

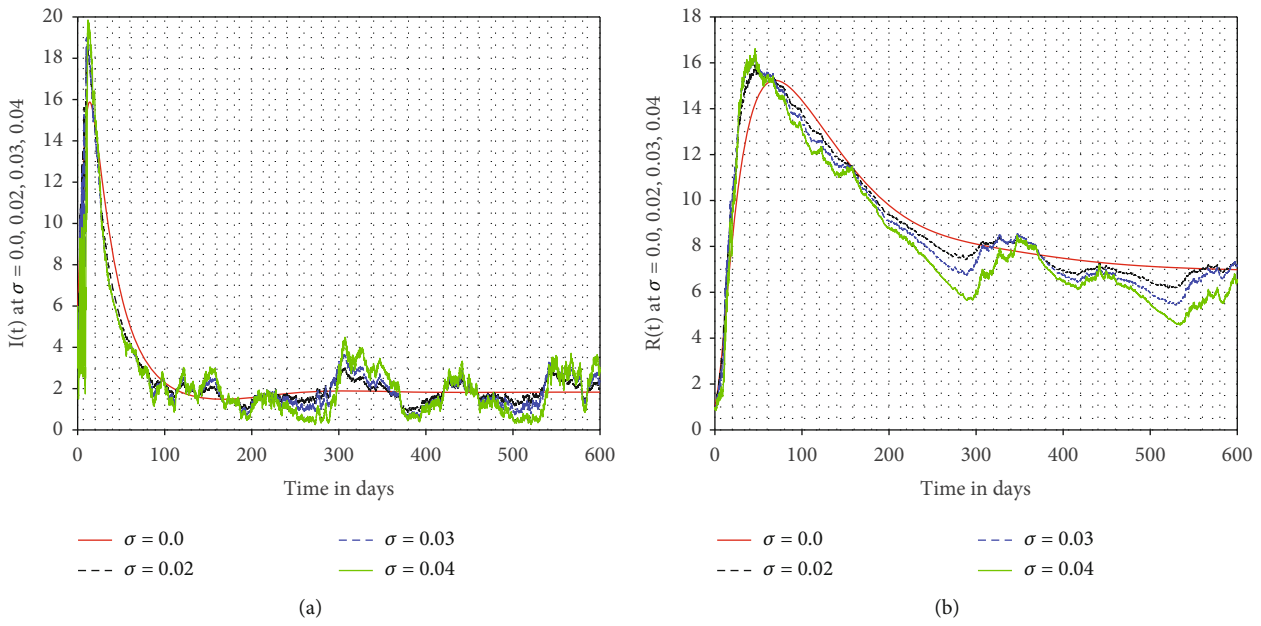

FIGURE 4: (a, b) $I(t)$ and $R(t)$ for different values of σ.

which can be observed in Figure 3(a). In Figures 3 and 4, the considered parametric values are $\Lambda = 0.1, d = 0.008, r = 0.1, m = 0.0001, \beta = 0.01, \gamma = 0.03$ and while keeping the initial values unchanged and σ is changed as mentioned in the graphs.

9. Conclusions

In this research, we explored the dynamic behavior of a novel SIR epidemic model that takes into account the impact of information intervention and environmental noise. Information intervention and white noise have been demonstrated to have significant effects on the condition.

The following are the key findings:

(i) We have thought about how white noise in the environment affects the condition

We have proven that the $\mathfrak{R}_0^{\bullet} = \mathfrak{R}_0 - \beta\Lambda/2d(d+\gamma)(d+\gamma+(1/2)\sigma_2^2)\sigma_2^2$ is a model (1) threshold for the illness to die out or endure, and noise intensities can modify the value of the stochastic reproduction number $\mathfrak{R}_0^{\bullet}$.

(ii) If $\mathfrak{R}_0^{\bullet} < 1$, the illness will be eradicated with a strong probability

(iii) If $\mathfrak{R}_0^{\bullet} > 1$, on the other hand, model (2) has a stationary distribution, indicating that the illness will dominate

(iv) Additionally, we have examined the numerical simulation of both deterministic and stochastic models that give a reasonable level of support for our examined technique

10. Remark

Comparing with the results in [23, 24], we observed that stochastic dynamics of fractional order are commonly demonstrated as nonrandom differential equation driven by fractional Brownian motion. On the other hand, our stochastic models are likely to provide various outcomes each time they are performed. Using random variables, our stochastic system indicates the probability of various outcomes under various circumstances. Our stochastic model offers information and forecasts results that take into account various degrees of randomness or inconsistency, and an abrupt change can be observed in (1).

There are still a number of intriguing aspects that we will discuss later. For instance, rapid climate change, weather warming or cooling, and wetness or evaporation may all have an impact on disease propagation. As a result, when a discontinuous random process, like variational noise, is added to model (1), how does it affect disease spread? This is something we will look into later.

Data Availability

No data were used to support this study.

Additional Points

Preprint Statement. This manuscript is not reposited on any preprint server.

Conflicts of Interest

The authors have no conflicts of interest regarding the publication of this paper.

Authors' Contributions

All the authors have equal contributions in this article.

References

[1] J. Graunt, "Natural and political observations mentioned in a following index, and made upon the bills of mortality," in *Mathematical Demography*Springer, Berlin Heidelberg.

[2] D. Bernoulli, *Essai d une nouvelle analyse de la mortalite causee par la petite verole, et des avantages de l inoculation pour la prevenir*, Histoire de l Acad., Roy. Sci.(Paris) avec Mem, 1760.

[3] D. Bernoulli, *Reflexions sur les avantages de l inoculation, Mercure de France 1760 173.190*, R. Pulskamp, Ed., Department of Mathematics and Computer Science, Xavier University, Cincinnati, 2009.

[4] W. O. Kermack and A. G. McKendrick, "A contribution to the mathematical theory of epidemics," *Proceedings of the royal society of london. Series A, Containing papers of a mathematical and physical character*, vol. 115, no. 772, pp. 700–721, 1927.

[5] M. Porta, Ed., *A Dictionary of Epidemiology*, Oxford University Press, 2014.

[6] R. M. May and R. M. Anderson, "Population biology of infectious diseases: part II," *Nature*, vol. 280, no. 5722, pp. 455–461, 1979.

[7] E. Beretta and Y. Takeuchi, "Convergence results in _SIR_ epidemic models with varying population sizes," *Nonlinear Analysis: Theory, Methods & Applications*, vol. 28, no. 12, pp. 1909–1921, 1997.

[8] E. Beretta, T. Hara, W. Ma, and Y. Takeuchi, "Global asymptotic stability of an _SIR_ epidemic model with distributed time delay," *Nonlinear analysis, theory, methods and applications*, vol. 47, no. 6, pp. 4107–4115, 2001.

[9] P. Imkeller and B. Schmalfuss, "The conjugacy of stochastic and random differential equations and the existence of global attractors," *Journal of Dynamics and Differential Equations*, vol. 13, no. 2, pp. 215–249, 2001.

[10] I. Newton, J. Fourier, G. Leibniz et al., "Ordinary differential equation".

[11] Y. Lin, D. Jiang, and P. Xia, "Long-time behavior of a stochastic SIR model," *Applied Mathematics and Computation*, vol. 236, pp. 1–9, 2014.

[12] H. Cao, H. Wu, and X. Wang, "Bifurcation analysis of a discrete SIR epidemic model with constant recovery," *Advances in Difference Equations*, vol. 2020, 20 pages, 2020.

[13] Y. Song, A. Miao, T. Zhang, X. Wang, and J. Liu, "Extinction and persistence of a stochastic SIRS epidemic model with saturated incidence rate and transfer from infectious to susceptible," *Advances in Difference Equations*, vol. 2018, no. 1, 2018.

[14] X. Mao, *Stochastic Differential Equations and Applications*, Elsevier, 2007.

[15] A. Lahrouz and L. Omari, "Extinction and stationary distribution of a stochastic SIRS epidemic model with non-linear incidence," *Statistics and Probability Letters*, vol. 83, no. 4, pp. 960–968, 2013.

[16] L. Zhu and H. Hu, "A stochastic SIR epidemic model with density dependent birth rate," *Advances in Difference Equations*, vol. 2015, no. 1, Article ID 330, 2015.

[17] S. Hussain, E. N. Madi, H. Khan et al., "Investigation of the stochastic modeling of COVID-19 with environmental noise from the analytical and numerical point of view," *Mathematics*, vol. 9, no. 23, p. 3122, 2021.

[18] S. Hussain, E. N. Madi, H. Khan et al., "On the stochastic modeling of COVID-19 under the environmental white noise," *Journal of Function Spaces*, vol. 2022, 9 pages, 2022.

[19] Y. N. Zhao and D. Q. Jiang, "The threshold of a stochastic SIS epidemic model with vaccination," *Applied Mathematics and Computation*, vol. 243, pp. 718–727, 2014.

[20] C. Ji and D. Jiang, "The extinction and persistence of a stochastic SIR model," *Advances in Difference Equations*, vol. 2017, 8 pages, 2017.

[21] C. Ji and D. Jiang, "Threshold behaviour of a stochastic SIR model," *Applied Mathematical Modelling*, vol. 38, no. 21-22, pp. 5067–5079, 2014.

[22] D. J. Higham, "An algorithmic introduction to numerical simulation of stochastic differential equations," *SIAM review*, vol. 43, no. 3, pp. 525–546, 2001.

[23] T. Sathiyaraj and P. Balasubramaniam, "Controllability of Hilfer fractional stochastic system with multiple delays and Poisson jumps," *The European Physical Journal Special Topics*, vol. 228, no. 1, pp. 245–260, 2019.

[24] T. Sathiyaraj and P. Balasubramaniam, "Controllability of fractional order stochastic differential inclusions with fractional Brownian motion in finite dimensional space," *IEEE/CAA Journal of Automatica Sinica*, vol. 3, no. 4, pp. 400–410, 2016.

Hindawi
Advances in Mathematical Physics
Volume 2022, Article ID 1333109, 17 pages
https://doi.org/10.1155/2022/1333109

Research Article

Analysis of Fractional Differential Equations with the Help of Different Operators

Naveed Iqbal,[1] **Moteb Fheed Saad Al Harbi**,[1] **Saleh Alshammari**,[1] **and Shamsullah Zaland**[2]

[1]*Department of Mathematics, College of Science, University of Ha'il, Ha'il 2440, Saudi Arabia*
[2]*Faculty of Mathematics, Kabul Polytechnic University, Afghanistan*

Correspondence should be addressed to Shamsullah Zaland; shamszaland@kpu.edu.af

Received 12 June 2022; Revised 26 July 2022; Accepted 29 July 2022; Published 19 August 2022

Academic Editor: Muhammad Nadeem

This study uses an Elzaki decomposition method with two fractional derivatives to solve a fractional nonlinear coupled system of Whitham-Broer-Kaup equations. For the fractional derivatives, we used Caputo and Atangana-Baleanu derivatives in the Caputo manner. Furthermore, the proposed techniques are compared to the solutions of other renowned analytical methods, including the Adomian decomposition technique, variation iteration technique, and homotopy perturbation technique. We used two nonlinear problems to illustrate the accuracy and validity of the proposed approaches. The results of numerical simulations were used to verify that the proposed methods are accurate and efficient, and the results are displayed in graphs and tables. The obtained results demonstrate that the algorithm is very real, simple to apply, and effective in investigating the nature of complicated nonlinear models in science and engineering.

1. Introduction

In 1695, Leibniz presented fractional calculus (FC), one of the advancements of standard calculus [1]. In recent decades, the FC theory has played a significant role in physics, entropy, fluid mechanics, and engineering [2–5]. Using fractional calculus, specific physical models and engineering processes can be explained more precisely and practically. For instance, entropies based on fractional calculus may be applied more generally than Shannon entropy [6]. Due to its vast application, fractional entropy has been a popular subject of study [7]. Furthermore, fractional differential equations are effective for modelling several events [8]. This is because the next state of a system is decided not just by its current form, but also by all of its prior conditions. Such equations may mimic physical reality more closely than integer-order differential equations. It is important to note that the theory and applications of fractional calculus have been thoroughly studied in the literature [9–13].

Due to the accurate description of complicated events in system identification, non-Brownian motion, control problems, viscoelastic materials, polymers, and signal processing, fractional differential equations (FDEs) have garnered considerable attention in recent decades [14]. FDEs are nonlocal, which means that the next state of a system is determined not just by its current state but also by all of its prior states [15]. Using fractional derivatives, the fluid-dynamic traffic model, for instance, can overcome the weakness caused by the assumption of continuous traffic flow [15, 16]. Recent research has focused on fractional functional analysis [17, 18]. The characteristics and theorems of Yang-Fourier and Yang-Laplace transform, as well as their applications to fractional ordinary differential equations, fractional ordinary differential systems, and fractional partial differential equations, have been investigated.

The logical question is "How can we find the exact solutions to FDEs?" To comprehend the mechanics of complex nonlinear physical phenomena and implement them in daily

life, nonlinear fractional differential equations (FDEs) have an important role in studying various areas of engineering, physics, and applied mathematics. In order to obtain numerical and analytical solutions of PDEs, a number of potent techniques, such as the Elzaki transform decomposition method [19, 20], the Iterative Laplace transform method [21], the variational iteration method [22], the Laplace transform decomposition method [23], the differential transform method [24], and the homotopy perturbation method [25], have been numerous scholars that have researched and solved numerous FDEs, including impulsive fractional differential equations [26], space and time-fractional advection-dispersion equation [27], and fractional generalised Burgers fluid [28].

Many well-known integral models, such as the KdV equation, Boussinesq equation, K-P equation, and WBK equation, are used to represent the propagation of shallow water. Whitham, Broer, and Kaup [29–31] developed nonlinear WBK equations using the Boussinesq approximation:

$$\begin{aligned} \mathbb{J}_{\rho} + \mathbb{J}\mathbb{J}_{\zeta} + \mathbb{K}_{\zeta} + q\mathbb{J}_{\zeta\zeta} = 0, \\ \mathbb{K}_{\rho} + \mathbb{K}\mathbb{J}_{\zeta} + \mathbb{J}\mathbb{K}_{\zeta} - q\mathbb{K}_{\zeta\zeta} + p\mathbb{J}_{\zeta\zeta\zeta} = 0, \end{aligned} \tag{1}$$

where $\mathbb{J} = \mathbb{J}(\zeta, \rho), \mathbb{K} = \mathbb{K}(\zeta, \rho)$ denotes the horizontal velocity and height of the fluids, which fluctuate substantially from equilibrium, and q, p are constants made up of various diffusion powers. Wang and Zheng [32] employed an extended fractional Riccati subequation approach to get approximate solutions for the coupled system of (WBK) equations for fractional order (2). El-Borai et al. [33] used the exponential function method to solve coupled system (2). Author [34] employed the coupled fractional reduced differential transform method (CFRDTM) to get approximate analytical solutions to the model as mentioned earlier (2). The authors of [2] investigated numerical solutions to the specified coupled system using the residual power series method (RPSM) (2). Also employed to obtain numerical solutions to the coupled system (2) are the finite element method [36], the finite difference approach [35], the exponential-function method [37], variation iteration method (VIM), homotopy perturbation method (HPM), homotopy analysis method (HAM), and others [38–40].

Adomian introduced the Adomian decomposition methodology (ADM) in 1980, which is a method for locating numerical and explicit solutions to various differential equations that represent physical conditions. This method is applicable to initial value problems, boundary value problems, partial and ordinary differential equations, including linear and nonlinear equations, and stochastic systems. Combining the Adomian decomposition method and the Elzaki transform method yields the Elzaki transform decomposition method (ETDM). The ETDM has also been utilized in several studies to solve fractional-order nonlinear partial differential equations numerically [41, 42].

In 1998, He was the first to introduce the homotopy perturbation method (HPM) [43, 44]. Later on, the solutions of some nonlinear nonhomogeneous partial differential equations are obtained through this semianalytical method [45, 46]. The solution that they get is in the form of an infinite sequence that converges rapidly to the exact solutions. Due to its quick results, the method was further used for solving linear and nonlinear equations. In the present work, we used an approximate analytical technique that combines the Elzaki transform and HPM, known as the HPTM. The proposed methods and solutions are in good agreement with the exact solution of the targeted problems. The fractional view analysis of the problems is also shown using the suggested techniques. It is noticed that the proposed methods can be modified to solve other fractional PDEs and their systems [47, 48]. In this study, we apply ETDM with two different derivatives to investigate the general and numerical solution of the coupled system of fractional-order Whitham-Broer-Kaup equations, as suggested by the studies mentioned above. ETDM is a straightforward and effective technique that requires no disturbance. We compare the outcomes of our proposed method to those of well-known methodologies such as VIM, ADM, and OHAM. We may observe that the provided strategy for finding solutions to nonlinear fractional-order partial differential equations is superior to the previously discussed method. We execute the calculations with Maple. The convergence of the proposed method is also ensured by extending the concept described in [49, 50].

2. Basic Definitions

This section introduces the essential ideas of fractional derivatives, fractional integrals, and the Elzaki transform with and without a singular kernel.

Definition 1. The fractional Caputo derivative (CFD) is given as follows:

$$D_{\wp}^{\delta}(\ell(\wp)) = \begin{cases} \dfrac{1}{\Gamma(m-\delta)} \displaystyle\int_0^{\wp} \frac{\ell^m(\eta)}{(\wp-\eta)^{\delta+1-m}} d\eta, & m-1 < \delta < m, \\ \dfrac{d^m}{d\wp^m}\ell(\wp), & \delta = m. \end{cases} \tag{2}$$

Definition 2. The derivative in terms of the Atangana-Baleanu Caputo manner (ABC) is given as follows:

$$D_{\wp}^{\delta}(\ell(\wp)) = \frac{N(\delta)}{1-\delta} \int_m^{\wp} \ell'(\eta) E_{\delta}\left[-\frac{\delta(\wp-\eta)^{\delta}}{1-\delta}\right] d\eta, \tag{3}$$

where $\ell \in H^1(\alpha, \beta), \beta > \alpha, \delta \in [0, 1]$. A normalisation function equal to 1 when $\delta = 0$ and $\delta = 1$ is represented by $N(\delta)$ in equation (11).

Definition 3. The ABC fractional integral operator is as follows:

$$I_{\wp}^{\delta}(\ell(\wp)) = \frac{1-\delta}{N(\delta)}\ell(\wp) + \frac{\delta}{\Gamma(\delta)N(\delta)} \int_m^{\wp} \ell(\eta)(\wp-\eta)^{\delta-1} d\eta. \tag{4}$$

Definition 4. The Elzaki transform's exponential function is given as in set A:

$$A = \left\{ \ell(\wp) : \exists G, p_1, p_2 > 0, |\ell(\wp)| < Ge^{|\wp|/p_j}, \quad \text{if} \wp \in (-1)^j \times [0,\infty) \right\}. \tag{5}$$

For a certain function in the set, G is a finite number but p_1, p_2 can be finite or infinite.

Definition 5. For the function $\ell(\wp)$, the transformation in terms of Elzaki is as follows:

$$\mathscr{E}\{\ell(\wp)\}(\varpi) = \tilde{U}(\varpi) = \varpi \int_0^\infty e^{-(\wp/\varpi)} \ell(\wp) d\wp, \tag{6}$$

where $\wp \geq 0, p_1 \leq \varpi \leq p_2$.

Theorem 6 (Elzaki transformation convolution theorem). *The following equality holds:*

$$\mathscr{E}\{\ell * v\} = \frac{1}{\varpi} \mathscr{E}(\ell) \mathscr{E}(v), \tag{7}$$

where Elzaki transform is indicated by $\mathscr{E}\{.\}$.

Definition 7. The Elzaki transform of the CFD operator $D_\wp^\delta(\ell(\wp))$ is given by

$$\mathscr{E}\left\{ D_\wp^\delta(\ell(\wp)) \right\}(\varpi) = \varpi^{-\delta} \tilde{U}(\varpi) - \sum_{k=0}^{m-1} \varpi^{2-\delta+k} \ell^k(0), \tag{8}$$

where $m - 1 < \delta < m$.

Theorem 8. *The ABC fractional derivative* $D_\wp^\delta(\ell(\wp))$ *Elzaki transform is defined as follows:*

$$\mathscr{E}\left\{ D_\wp^\delta(\ell(\wp)) \right\}(\varpi) = \frac{N(\delta)\varpi}{\delta\varpi^\delta + 1 - \delta} \left(\frac{\tilde{U}(\varpi)}{\varpi} - \varpi\ell(0) \right), \tag{9}$$

where $\mathscr{E}\{\ell(\wp)\}\varpi = \tilde{U}(\varpi)$.

Proof. From Definition 2, we have the following:

$$\mathscr{E}\left\{ D_\wp^\delta(\ell(\wp)) \right\}(\varpi) = \mathscr{E}\left\{ \frac{N(\delta)}{1-\delta} \int_0^\wp \ell'(\eta) E_\delta \left[-\frac{\delta(\wp-\eta)^\delta}{1-\delta} \right] d\eta \right\}(\varpi). \tag{10}$$

□

Then, taking into account the definition and convolution of the Elzaki transform, we get the following:

$$\begin{aligned} &\mathscr{E}\left\{ D_\wp^\delta(\ell(\wp)) \right\}(\varpi) \\ &= \mathscr{E}\left\{ \frac{N(\delta)}{1-\delta} \int_0^\wp \ell'(\eta) E_\delta \left[-\frac{\delta(\wp-\eta)^\delta}{1-\delta} \right] d\eta \right\} \\ &= \frac{N(\delta)}{1-\delta} \frac{1}{\varpi} \mathscr{E}\left\{ \ell'(\eta) \right\} \mathscr{E}\left\{ E_\delta \left[-\frac{\delta\wp^\delta}{1-\delta} \right] d\eta \right\} \\ &= \frac{N(\delta)}{1-\delta} \left[\frac{\tilde{U}(\varpi)}{\varpi} - \varpi\ell(0) \right] \left[\int_0^\infty e^{-(1/\varpi)} E_\delta \left[-\frac{\delta\wp^\delta}{1-\delta} \right] d\wp \right] \\ &= \frac{N(\delta)\varpi}{\delta\varpi^\delta + 1 - \delta} \left[\frac{\tilde{U}(\varpi)}{\varpi} - \varpi\ell(0) \right]. \end{aligned} \tag{11}$$

3. Methodology

Here, we give the general methodology of the proposed technique to solve the given equation.

$$D_\rho^\delta \mathbb{J}(\zeta, \rho) = \mathscr{L}(\mathbb{J}(\zeta, \rho)) + N(\mathbb{J}(\zeta, \rho)) + h(\zeta, \rho) = M(\zeta, \rho), \tag{12}$$

with initial condition

$$\mathbb{J}(\zeta, 0) = \phi(\zeta), \tag{13}$$

having $\mathscr{L}$, N linear and nonlinear terms and $h(\zeta, \rho)$ is the source term.

3.1. Case I ($ETDM_C$). By means of Caputo fractional derivative and Elzaki transform, equation (12) can be stated as follows:

$$\frac{1}{p(\delta, \ell, \kappa)} \left(\mathbf{E}[\mathbb{J}(\zeta, \rho)] - \kappa^2 \phi(\zeta) \right) = \mathbf{E}[M(\zeta, \rho)], \tag{14}$$

with

$$p(\delta, \ell, \kappa) = \kappa^\delta. \tag{15}$$

On employing the Elzaki inverse transform, we have

$$\mathbb{J}(\zeta, \rho) = \mathbf{E}^{-1}\left(\kappa^2 \phi(\zeta) + p(\delta, \ell, \kappa) \mathbf{E}[M(\zeta, \rho)] \right). \tag{16}$$

Thus, for $\mathbb{J}(\zeta, \rho)$, the solution in the series form is stated as follows:

$$\mathbb{J}(\zeta, \rho) = \sum_{i=0}^\infty \mathbb{J}_i(\zeta, \rho). \tag{17}$$

And $N(\mathbb{J}(\zeta,\rho))$ can be decomposed as follows:

$$N(\mathbb{J}(\zeta,\rho)) = \sum_{i=0}^{\infty} A_i(\mathbb{J}_0, \cdots, \mathbb{J}_i), \tag{18}$$

having A_i as the Adomian polynomials and can be calculated as

$$A_n = \frac{1}{n!}\frac{d^n}{d\varepsilon^n} N\rho, \quad \Sigma_{k=0}^{n}\varepsilon^k \mathbb{J}_k\Big|_{\varepsilon=0}. \tag{19}$$

Putting equations (18) and (17) into (16), we obtain

$$\sum_{i=0}^{\infty} \mathbb{J}_i(\zeta,\rho) = \mathbf{E}^{-1}\left(\kappa^2\phi(\zeta) + p(\delta,\ell,\kappa)\mathbf{E}[h(\zeta,\rho)]\right) + \mathbf{E}^{-1}\left(p(\delta,\ell,\kappa)\mathbf{E}\left[\sum_{i=0}^{\infty}\mathscr{L}(\mathbb{J}_i(\zeta,\rho)) + A_\rho\right]\right). \tag{20}$$

From (20), we get

$$\begin{aligned}
\mathbb{J}_0^C(\zeta,\rho) &= \mathbf{E}^{-1}\left(\frac{\phi(\zeta)}{\kappa} + p(\delta,\ell,\kappa)\mathbf{E}[h(\zeta,\rho)]\right),\\
\mathbb{J}_1^C(\zeta,\rho) &= \mathbf{E}^{-1}(p(\delta,\ell,\kappa)\mathbf{E}[\mathscr{L}(\mathbb{J}_0(\zeta,\rho)) + A_0]),\\
&\vdots\\
\mathbb{J}_{l+1}^C(\zeta,\rho) &= \mathbf{E}^{-1}(p(\delta,\ell,\kappa)\mathbf{E}[\mathscr{L}(\mathbb{J}_l(\zeta,\rho)) + A_l]), \quad l = 1, 2, 3\cdots.
\end{aligned} \tag{21}$$

Thus, we get the solution of (12) by substituting (21) into (17) using $ETDM_C$:

$$\mathbb{J}^C(\zeta,\rho) = \mathbb{J}_0^C(\zeta,\rho) + \mathbb{J}_1^C(\zeta,\rho) + \mathbb{J}_2^C(\zeta,\rho)+\cdots. \tag{22}$$

3.2. Case II ($ETDM_{ABC}$). By means of ABC fractional derivative and Elzaki transform, equation (12) can be stated as follows:

$$\frac{1}{q(\delta,\ell,\kappa)}\left(\mathbf{E}[\mathbb{J}(\zeta,\rho)] - \frac{\phi(\zeta)}{\kappa}\right) = \mathbf{E}[M(\zeta,\rho)], \tag{23}$$

with

$$q(\delta,\ell,\kappa) = \frac{1-\delta+\delta(\ell/\kappa)^\delta}{B(\delta)}. \tag{24}$$

On employing the Elzaki inverse transform, we have

$$\mathbb{J}(\zeta,\rho) = \mathbf{E}^{-1}\left(\frac{\phi(\zeta)}{\kappa} + q(\delta,\ell,\kappa)\mathbf{E}[M(\zeta,\rho)]\right). \tag{25}$$

By means of Adomian decomposition, we get

$$\sum_{i=0}^{\infty} \mathbb{J}_i(\zeta,\rho) = \mathbf{E}^{-1}\left(\frac{\phi(\zeta)}{\kappa} + q(\delta,\ell,\kappa)\mathbf{E}[h(\zeta,\rho)]\right) + \mathbf{E}^{-1}\left(q(\delta,\ell,\kappa)\mathbf{E}\left[\sum_{i=0}^{\infty}\mathscr{L}(\mathbb{J}_i(\zeta,\rho)) + A_\rho\right]\right). \tag{26}$$

From (20), we get

$$\begin{aligned}
\mathbb{J}_0^{ABC}(\zeta,\rho) &= \mathbf{E}^{-1}\left(\frac{\phi(\zeta)}{\kappa} + q(\delta,\ell,\kappa)\mathbf{E}[h(\zeta,\rho)]\right),\\
\mathbb{J}_1^{ABC}(\zeta,\rho) &= \mathbf{E}^{-1}(q(\delta,\ell,\kappa)\mathbf{E}[\mathscr{L}(\mathbb{J}_0(\zeta,\rho)) + A_0]),\\
&\vdots\\
\mathbb{J}_{l+1}^{ABC}(\zeta,\rho) &= \mathbf{E}^{-1}(q(\delta,\ell,\kappa)\mathbf{E}[\mathscr{L}(\mathbb{J}_l(\zeta,\rho)) + A_l]), l = 1, 2, 3\cdots.
\end{aligned} \tag{27}$$

Thus, we get the solution of (12), by using $ETDM_{ABC}$

$$\mathbb{J}^{ABC}(\zeta,\rho) = \mathbb{J}_0^{ABC}(\zeta,\rho) + \mathbb{J}_1^{ABC}(\zeta,\rho) + \mathbb{J}_2^{ABC}(\zeta,\rho)+\cdots. \tag{28}$$

4. Applications

In this part, we implemented the proposed technique to solve nonlinear systems of Whitham-Broer-Kaup equations having order fraction.

Example 9. Let us consider the fractional WBKEs system:

$$\begin{aligned}
&D_\rho^\delta \mathbb{J}(\zeta,\rho) + \mathbb{J}(\zeta,\rho)\frac{\partial \mathbb{J}(\zeta,\rho)}{\partial\zeta} + \frac{\partial \mathbb{J}(\zeta,\rho)}{\partial\zeta} + \frac{\partial \mathbb{K}(\zeta,\rho)}{\partial\zeta} = 0,\\
&D_\rho^\delta \mathbb{K}(\zeta,\rho) + \mathbb{J}(\zeta,\rho)\frac{\partial \mathbb{K}(\zeta,\rho)}{\partial\zeta} + \mathbb{K}(\zeta,\rho)\frac{\partial \mathbb{J}(\zeta,\rho)}{\partial\zeta} + 3\frac{\partial^3 \mathbb{J}(\zeta,\rho)}{\partial\zeta^3} - \frac{\partial^2 \mathbb{K}(\zeta,\rho)}{\partial\zeta^2} = 0,\\
&0 < \delta \le 1, -1 < \rho \le 1, \quad -10 \le \zeta \le 10,
\end{aligned} \tag{29}$$

having initial condition

$$\begin{aligned}
\mathbb{J}(\zeta,0) &= \frac{1}{2} - 8\tan h(-2\zeta),\\
\mathbb{K}(\zeta,0) &= 16 - 16\tan h^2(-2\zeta).
\end{aligned} \tag{30}$$

On employing the Elzaki transform, we have

$$\begin{aligned}\mathbf{E}\left[D_\rho^\delta \mathbb{J}(\zeta,\rho)\right] &= -\mathbf{E}\left[\mathbb{J}(\zeta,\rho)\frac{\partial \mathbb{J}(\zeta,\rho)}{\partial\zeta} + \frac{\partial \mathbb{J}(\zeta,\rho)}{\partial\zeta} + \frac{\partial \mathbb{K}(\zeta,\rho)}{\partial\zeta}\right],\\ \mathbf{E}\left[D_\rho^\delta \mathbb{K}(\zeta,\rho)\right] &= -\mathbf{E}\left[\mathbb{J}(\zeta,\rho)\frac{\partial \mathbb{K}(\zeta,\rho)}{\partial\zeta} + \mathbb{K}(\zeta,\rho)\frac{\partial \mathbb{J}(\zeta,\rho)}{\partial\zeta} + 3\frac{\partial^3 \mathbb{J}(\zeta,\rho)}{\partial\zeta^3} - \frac{\partial^2 \mathbb{K}(\zeta,\rho)}{\partial\zeta^2}\right],\end{aligned} \tag{31}$$

Thus, we have

$$\begin{aligned}\frac{1}{\kappa^\delta}\mathbf{E}[\mathbb{J}(\zeta,\rho)] - \kappa^{2-\delta}\mathbb{J}(\zeta,0) &= -\mathbf{E}\left[\mathbb{J}(\zeta,\rho)\frac{\partial \mathbb{J}(\zeta,\rho)}{\partial\zeta} + \frac{\partial \mathbb{J}(\zeta,\rho)}{\partial\zeta} + \frac{\partial \mathbb{K}(\zeta,\rho)}{\partial\zeta}\right],\\ \frac{1}{\kappa^\delta}\mathbf{E}[\mathbb{K}(\zeta,\rho)] - \kappa^{2-\delta}\mathbb{J}(\zeta,0) &= -\mathbf{E}\left[\mathbb{J}(\zeta,\rho)\frac{\partial \mathbb{K}(\zeta,\rho)}{\partial\zeta} + \mathbb{K}(\zeta,\rho)\frac{\partial \mathbb{J}(\zeta,\rho)}{\partial\zeta} + 3\frac{\partial^3 \mathbb{J}(\zeta,\rho)}{\partial\zeta^3} - \frac{\partial^2 \mathbb{K}(\zeta,\rho)}{\partial\zeta^2}\right].\end{aligned} \tag{32}$$

On simplification, we have

$$\begin{aligned}\mathbf{E}[\mathbb{J}(\zeta,\rho)] &= \kappa^2\left[\frac{1}{2} - 8\tan h(-2\zeta)\right] - \kappa^\delta\mathbf{E}\left[\mathbb{J}(\zeta,\rho)\frac{\partial \mathbb{J}(\zeta,\rho)}{\partial\zeta} + \frac{\partial \mathbb{J}(\zeta,\rho)}{\partial\zeta} + \frac{\partial \mathbb{K}(\zeta,\rho)}{\partial\zeta}\right],\\ \mathbf{E}[\mathbb{K}(\zeta,\rho)] &= \kappa^2\left[16 - 16\tan h^2(-2\zeta)\right] - \kappa^\delta\mathbf{E}\left[\mathbb{J}(\zeta,\rho)\frac{\partial \mathbb{K}(\zeta,\rho)}{\partial\zeta} + \mathbb{K}(\zeta,\rho)\frac{\partial \mathbb{J}(\zeta,\rho)}{\partial\zeta} + 3\frac{\partial^3 \mathbb{J}(\zeta,\rho)}{\partial\zeta^3} - \frac{\partial^2 \mathbb{K}(\zeta,\rho)}{\partial\zeta^2}\right].\end{aligned} \tag{33}$$

On applying the inverse ET, we get

$$\begin{aligned}\mathbb{J}(\zeta,\rho) &= \left[\frac{1}{2} - 8\tan h(-2\zeta)\right] - \mathbf{E}^{-1}\left[\kappa^\delta\mathbf{E}\left\{\mathbb{J}(\zeta,\rho)\frac{\partial \mathbb{J}(\zeta,\rho)}{\partial\zeta} + \frac{\partial \mathbb{J}(\zeta,\rho)}{\partial\zeta} + \frac{\partial \mathbb{K}(\zeta,\rho)}{\partial\zeta}\right\}\right],\\ \mathbb{K}(\zeta,\rho) &= \left[16 - 16\tan h^2(-2\zeta)\right] - \mathbf{E}^{-1}\left[\kappa^\delta\mathbf{E}\left\{\mathbb{J}(\zeta,\rho)\frac{\partial \mathbb{K}(\zeta,\rho)}{\partial\zeta} + \mathbb{K}(\zeta,\rho)\frac{\partial \mathbb{J}(\zeta,\rho)}{\partial\zeta} + 3\frac{\partial^3 \mathbb{J}(\zeta,\rho)}{\partial\zeta^3} - \frac{\partial^2 \mathbb{K}(\zeta,\rho)}{\partial\zeta^2}\right\}\right].\end{aligned} \tag{34}$$

4.1. Solution by Means of EDM$_C$. The solutions in the series form for the unknown function $\mathbb{J}(\zeta,\rho)$ and $\mathbb{K}(\zeta,\rho)$ are stated as follows:

$$\mathbb{J}(\zeta,\rho) = \sum_{l=0}^{\infty}\mathbb{J}_l(\zeta,\rho),$$

$$\mathbb{K}(\zeta,\rho) = \sum_{l=0}^{\infty}\mathbb{J}_l(\zeta,\rho). \tag{35}$$

The nonlinear terms by means of Adomian polynomials are stated as $\mathbb{J}\mathbb{J}_\zeta = \sum_{m=0}^{\infty}\mathscr{A}_m$, $\mathbb{J}\mathbb{K}_\zeta = \sum_{m=0}^{\infty}\mathscr{B}_m$ and $\mathbb{K}\mathbb{J}_\zeta = \sum_{m=0}^{\infty}\mathscr{C}_m$; thus, by means of these terms, equation (34) can be determined as follows:

$$\begin{aligned}\sum_{l=0}^{\infty}\mathbb{J}_{l+1}(\zeta,\rho) &= \frac{1}{2} - 8\tan h(-2\zeta) - \mathbf{E}^{-1}\left[\kappa^\delta\mathbf{E}\left\{\sum_{l=0}^{\infty}\mathscr{A}_l + \frac{\partial \mathbb{J}(\zeta,\rho)}{\partial\zeta} + \frac{\partial \mathbb{K}(\zeta,\rho)}{\partial\zeta}\right\}\right],\\ \sum_{l=0}^{\infty}\mathbb{K}_{l+1}(\zeta,\rho) &= 16 - 16\tan h^2(-2\zeta) - \mathbf{E}^{-1}\left[\kappa^\delta\mathbf{E}\left\{\sum_{l=0}^{\infty}\mathscr{B}_l + \sum_{l=0}^{\infty}\mathscr{C}_l + 3\frac{\partial^3 \mathbb{J}(\zeta,\rho)}{\partial\zeta^3} - \frac{\partial^2 \mathbb{K}(\zeta,\rho)}{\partial\zeta^2}\right\}\right].\end{aligned} \tag{36}$$

By the comparison of both sides of equation (36), we obtain

$$\begin{aligned}
\mathbb{J}_0(\zeta,\rho) &= \frac{1}{2} - 8\tan h(-2\zeta),\\
\mathbb{K}_0(\zeta,\rho) &= 16 - 16\tan h^2(-2\zeta),\\
\mathbb{J}_1(\zeta,\rho) &= -8\sec h^2(-2\zeta)\frac{\rho^{\delta}}{\Gamma(\delta+1)},\\
\mathbb{K}_1(\zeta,\rho) &= -32\sec h^2(-2\zeta)\tan h(-2\zeta)\frac{\rho^{\delta}}{\Gamma(\delta+1)},\\
\mathbb{J}_2(\zeta,\rho) &= -16\sec h^2(-2\zeta)\big(4\sec h^2(-2\zeta) - 8\tan h^2(-2\zeta)\\
&\quad + 3\tan h(-2\zeta)\big)\frac{\rho^{2\delta}}{\Gamma(2\delta+1)},\\
\mathbb{K}_2(\zeta,\rho) &= -32\sec h^2 2(-2\zeta)\big\{40\sec h^2(-2\zeta)\tan h(-2\zeta)\\
&\quad + 96\tan h(-2\zeta) - 2\tan h^2(-2\zeta)\\
&\quad - 32\tan h^3(-2\zeta) - 25\sec h^2(-2\zeta)\big\}\frac{\rho^{2\delta}}{\Gamma(2\delta+1)}.
\end{aligned} \tag{37}$$

Thus, for $\mathbb{J}_l$ and $\mathbb{K}_l$ with $(l \geq 3)$, the remaining components are easily computable. So, the solution in series form is as follows:

$$\begin{aligned}
\mathbb{J}(\zeta,\rho) &= \sum_{l=0}^{\infty}\mathbb{J}_l(\zeta,\rho) = \mathbb{J}_0(\zeta,\rho) + \mathbb{J}_1(\zeta,\rho) + \mathbb{J}_2(\zeta,\rho)+\cdots,\\
\mathbb{J}(\zeta,\rho) &= \frac{1}{2} - 8\tan h(-2\zeta) - 8\sec h^2(-2\zeta)\frac{\rho^{\delta}}{\Gamma(\delta+1)}\\
&\quad - 16\sec h^2(-2\zeta)\big(4\sec h^2(-2\zeta) - 8\tan h^2(-2\zeta)\\
&\quad + 3\tan h(-2\zeta)\big)\frac{\rho^{2\delta}}{\Gamma(2\delta+1)}+\cdots.\\
\mathbb{K}(\zeta,\rho) &= \sum_{l=0}^{\infty}\mathbb{K}_l(\zeta,\rho) = \mathbb{K}_0(\zeta,\rho) + \mathbb{K}_1(\zeta,\rho) + \mathbb{K}_2(\zeta,\rho)+\cdots,\\
\mathbb{K}(\zeta,\rho) &= 16 - 16\tan h^2(-2\zeta) - 32\sec h^2(-2\zeta)\tan h(-2\zeta)\\
&\quad \cdot\frac{\rho^{\delta}}{\Gamma(\delta+1)} - 32\sec h^2(-2\zeta)\big\{40\sec h^2(-2\zeta)\tan h(-2\zeta)\\
&\quad + 96\tan h(-2\zeta) - 2\tan h^2(-2\zeta) - 32\tan h^3(-2\zeta)\\
&\quad - 25\sec h^2(-2\zeta)\big\}\frac{\rho^{2\delta}}{\Gamma(2\delta+1)}+\cdots.
\end{aligned} \tag{38}$$

4.2. Solution by Means of EDM_{ABC}. The solutions in the series form for the unknown function $\mathbb{J}(\zeta,\rho)$ and $\mathbb{K}(\zeta,\rho)$ are stated as follows:

$$\begin{aligned}
\mathbb{J}(\zeta,\rho) &= \sum_{l=0}^{\infty}\mathbb{J}_l(\zeta,\rho),\\
\mathbb{K}(\zeta,\rho) &= \sum_{l=0}^{\infty}\mathbb{J}_l(\zeta,\rho).
\end{aligned} \tag{39}$$

The nonlinear terms by means of Adomian polynomials are stated as $\mathbb{J}\mathbb{J}_{\zeta} = \sum_{l=0}^{\infty}\mathscr{A}_l$ and $\mathbb{J}^2\mathbb{J}_{\zeta} = \sum_{l=0}^{\infty}\mathscr{B}_l$; thus, by means of these terms, equation (34) can be determined as follows:

$$\sum_{l=0}^{\infty}\mathbb{J}_{l+1}(\zeta,\rho) = \frac{1}{2} - 8\tan h(-2\zeta) - \mathbf{E}^{-1}\left[\frac{\ell^{\delta}\big(\kappa^{\delta}+\delta\big(\ell^{\delta}-\kappa^{\delta}\big)\big)}{\kappa^{2\delta}}\mathbf{E}\left\{\sum_{l=0}^{\infty}\mathscr{A}_l + \frac{\partial\mathbb{J}(\zeta,\rho)}{\partial\zeta} + \frac{\partial\mathbb{K}(\zeta,\rho)}{\partial\zeta}\right\}\right], \tag{40}$$

$$\sum_{l=0}^{\infty}\mathbb{K}_{l+1}(\zeta,\rho) = 16 - 16\tan h^2(-2\zeta) - \mathbf{E}^{-1}\left[\frac{\ell^{\delta}\big(\kappa^{\delta}+\delta\big(\ell^{\delta}-\kappa^{\delta}\big)\big)}{\kappa^{2\delta}}\mathbf{E}\left\{\sum_{l=0}^{\infty}\mathscr{B}_l + \sum_{l=0}^{\infty}\mathscr{C}_l + 3\frac{\partial^3\mathbb{J}(\zeta,\rho)}{\partial\zeta^3} - \frac{\partial^2\mathbb{K}(\zeta,\rho)}{\partial\zeta^2}\right\}\right]. \tag{41}$$

By the comparison of both sides of equation (41), we obtain

$$\begin{aligned}
\mathbb{J}_0(\zeta,\rho) &= \frac{1}{2} - 8\tan h(-2\zeta),\\
\mathbb{K}_0(\zeta,\rho) &= 16 - 16\tan h^2(-2\zeta),\\
\mathbb{J}_1(\zeta,\rho) &= -8\sec h^2(-2\zeta)\left(1-\delta+\frac{\delta\rho^{\delta}}{\Gamma(\delta+1)}\right),\\
\mathbb{K}_1(\zeta,\rho) &= -32\sec h^2(-2\zeta)\tan h(-2\zeta)\left(1-\delta+\frac{\delta\rho^{\delta}}{\Gamma(\delta+1)}\right),\\
\mathbb{J}_2(\zeta,\rho) &= -16\sec h^2(-2\zeta)\big(4\sec h^2(-2\zeta)\\
&\quad - 8\tan h^2(-2\zeta) + 3\tan h(-2\zeta)\big)\\
&\quad \cdot\left[\frac{\delta^2\rho^{2\delta}}{\Gamma(2\delta+1)} + 2\delta(1-\delta)\frac{\rho^{\delta}}{\Gamma(\delta+1)} + (1-\delta)^2\right],\\
\mathbb{K}_2(\zeta,\rho) &= -32\sec h^2(-2\zeta)\big\{40\sec h^2(-2\zeta)\tan h(-2\zeta)\\
&\quad + 96\tan h(-2\zeta) - 2\tan h^2(-2\zeta)
\end{aligned}$$

$$- 32 \tan h^3(-2\zeta) - 25 \sec h^2(-2\zeta)\}\cdot\left[\frac{\delta^2\rho^{2\delta}}{\Gamma(2\delta+1)} + 2\delta(1-\delta)\frac{\rho^{\delta}}{\Gamma(\delta+1)} + (1-\delta)^2\right]. \tag{42}$$

Thus, for $\mathbb{J}_l$ with $(l \geq 3)$, the remaining components are easily computable. So, the solution in the series form is as follows:

$$\mathbb{J}(\zeta,\rho) = \sum_{l=0}^{\infty}\mathbb{J}_l(\zeta,\rho) = \mathbb{J}_0(\zeta,\rho) + \mathbb{J}_1(\zeta,\rho) + \mathbb{J}_2(\zeta,\rho)+\cdots,$$

$$\begin{aligned}\mathbb{J}(\zeta,\rho) = {} & \frac{1}{2} - 8\tan h(-2\zeta) - 8\sec h^2(-2\zeta)\left(1-\delta+\frac{\delta\rho^{\delta}}{\Gamma(\delta+1)}\right)\\ & - 16\sec h^2(-2\zeta)\left(4\sec h^2(-2\zeta)\right.\\ & \left. - 8\tan h^2(-2\zeta) + 3\tan h(-2\zeta)\right)\\ & \cdot\left[\frac{\delta^2\rho^{2\delta}}{\Gamma(2\delta+1)} + 2\delta(1-\delta)\frac{\rho^{\delta}}{\Gamma(\delta+1)} + (1-\delta)^2\right]+\cdots,\end{aligned}$$

$$\mathbb{K}(\zeta,\rho) = \sum_{l=0}^{\infty}\mathbb{K}_l(\zeta,\rho) = \mathbb{K}_0(\zeta,\rho) + \mathbb{K}_1(\zeta,\rho) + \mathbb{K}_2(\zeta,\rho)+\cdots,$$

$$\begin{aligned}\mathbb{K}(\zeta,\rho) = {} & 16 - 16\tan h^2(-2\zeta) - 32\sec h^2(-2\zeta)\tan h(-2\zeta)\\ & \cdot\left(1-\delta+\frac{\delta\rho^{\delta}}{\Gamma(\delta+1)}\right) - 32\sec h^2(-2\zeta)\\ & \cdot\{40\sec h^2(-2\zeta)\tan h(-2\zeta) + 96\tan h(-2\zeta)\\ & - 2\tan h^2(-2\zeta) - 32\tan h^3(-2\zeta) - 25\sec h^2(-2\zeta)\}\\ & \cdot\left[\frac{\delta^2\rho^{2\delta}}{\Gamma(2\delta+1)} + 2\delta(1-\delta)\frac{\rho^{\delta}}{\Gamma(\delta+1)} + (1-\delta)^2\right]+\cdots.\end{aligned} \tag{43}$$

On taking $\delta = 1$, we obtain the exact solution as follows:

$$\mathbb{J}(\zeta,\rho) = \frac{1}{2} - 8\tan h\left\{-2\left(\zeta-\frac{\rho}{2}\right)\right\},$$

$$\mathbb{K}(\zeta,\rho) = 16 - 16\tan h^2\left\{-2\left(\zeta-\frac{\rho}{2}\right)\right\}. \tag{44}$$

Figure 1 shows a graphical view of the exact and analytical solution for $\mathbb{J}(\zeta,\rho)$ at $\delta = 1$ of system 1. Figure 2 shows a graphical view of the analytical solution for $\mathbb{J}(\zeta,\rho)$ at $\delta =$ 0.8,0.6 of system 1, and Figure 3 shows that of the analytical solution at various values of δ for $\mathbb{J}(\zeta,\rho)$ of system 1. Figure 4 shows the absolute error graph of $\mathbb{J}(\zeta,\rho)$ of system 1. Similarly, Figures 5–7 show that the exact and analytical solution for $\mathbb{K}(\zeta,\rho)$ at $\delta = 1$ of system 1 and $\mathbb{K}(\zeta,\rho)$ at the different fractional order of $\delta = 0.8,0.6$ of system 1. Tables 1 and 2 show that the different fractional order of δ of system 1.

Example 10. Let us consider the fractional WBKE system:

$$\begin{aligned}& D_{\rho}^{\delta}\mathbb{J}(\zeta,\rho) + \mathbb{J}(\zeta,\rho)\frac{\partial\mathbb{J}(\zeta,\rho)}{\partial\zeta} + \frac{1}{2}\frac{\partial\mathbb{J}(\zeta,\rho)}{\partial\zeta} + \frac{\partial\mathbb{K}(\zeta,\rho)}{\partial\zeta} = 0,\\ & D_{\rho}^{\delta}\mathbb{K}(\zeta,\rho) + \mathbb{J}(\zeta,\rho)\frac{\partial\mathbb{K}(\zeta,\rho)}{\partial\zeta} + \mathbb{K}(\zeta,\rho)\frac{\partial\mathbb{J}(\zeta,\rho)}{\partial\zeta} - \frac{1}{2}\frac{\partial^2\mathbb{K}(\zeta,\rho)}{\partial\zeta^2} = 0,\\ & 0 < \delta \leq 1, \quad -1 < \rho \leq 1, -10 \leq \zeta \leq 10,\end{aligned} \tag{45}$$

having the initial condition

$$\begin{aligned}\mathbb{J}(\zeta,0) &= \lambda - \kappa\cot h[\kappa(\zeta+\theta)],\\ \mathbb{K}(\zeta,0) &= -\kappa^2\,\mathrm{cosec}\,h^2[\kappa(\zeta+\theta)].\end{aligned} \tag{46}$$

On employing the Elzaki transform, we have

$$\begin{aligned}\mathbf{E}\left[D_{\rho}^{\delta}\mathbb{J}(\zeta,\rho)\right] &= -\mathbf{E}\left[\mathbb{J}(\zeta,\rho)\frac{\partial\mathbb{J}(\zeta,\rho)}{\partial\zeta} + \frac{1}{2}\frac{\partial\mathbb{J}(\zeta,\rho)}{\partial\zeta} + \frac{\partial\mathbb{K}(\zeta,\rho)}{\partial\zeta}\right],\\ \mathbf{E}\left[D_{\rho}^{\delta}\mathbb{K}(\zeta,\rho)\right] &= -\mathbf{E}\left[\mathbb{J}(\zeta,\rho)\frac{\partial\mathbb{K}(\zeta,\rho)}{\partial\zeta} + \mathbb{K}(\zeta,\rho)\frac{\partial\mathbb{J}(\zeta,\rho)}{\partial\zeta} - \frac{1}{2}\frac{\partial^2\mathbb{K}(\zeta,\rho)}{\partial\zeta^2}\right].\end{aligned} \tag{47}$$

Thus, we have

$$\begin{aligned}\frac{1}{\kappa^{\delta}}\mathbf{E}[\mathbb{J}(\zeta,\rho)] - \kappa^{2-\delta}\mathbb{J}(\zeta,0) &= -\mathbf{E}\left[\mathbb{J}(\zeta,\rho)\frac{\partial\mathbb{J}(\zeta,\rho)}{\partial\zeta} + \frac{1}{2}\frac{\partial\mathbb{J}(\zeta,\rho)}{\partial\zeta} + \frac{\partial\mathbb{K}(\zeta,\rho)}{\partial\zeta}\right],\\ \frac{1}{\kappa^{\delta}}\mathbf{E}[\mathbb{K}(\zeta,\rho)] - \kappa^{2-\delta}\mathbb{J}(\zeta,0) &= -\mathbf{E}\left[\mathbb{J}(\zeta,\rho)\frac{\partial\mathbb{K}(\zeta,\rho)}{\partial\zeta} + \mathbb{K}(\zeta,\rho)\frac{\partial\mathbb{J}(\zeta,\rho)}{\partial\zeta} - \frac{1}{2}\frac{\partial^2\mathbb{K}(\zeta,\rho)}{\partial\zeta^2}\right].\end{aligned} \tag{48}$$

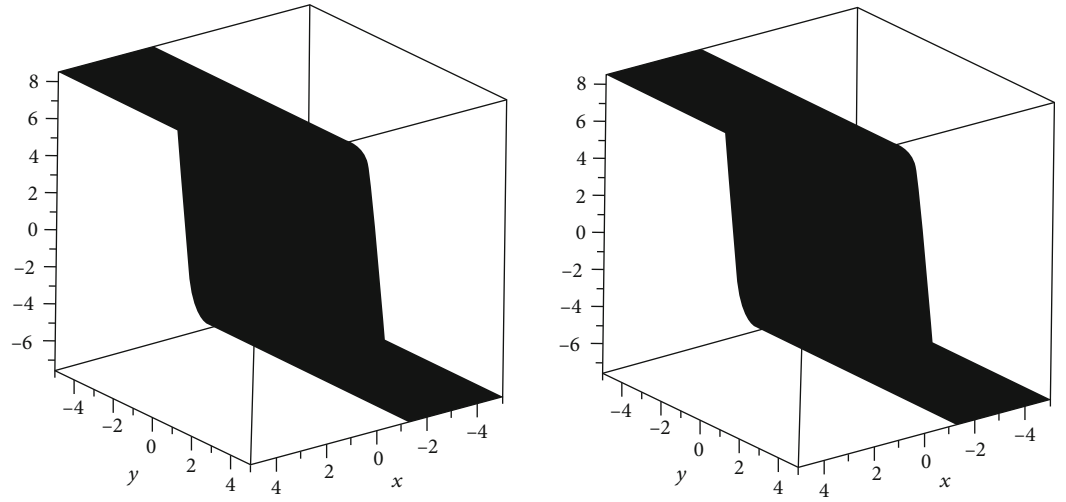

Figure 1: Graphical view of the exact and analytical solution for $\mathbb{J}(\zeta, \rho)$ at $\delta = 1$ of system 1.

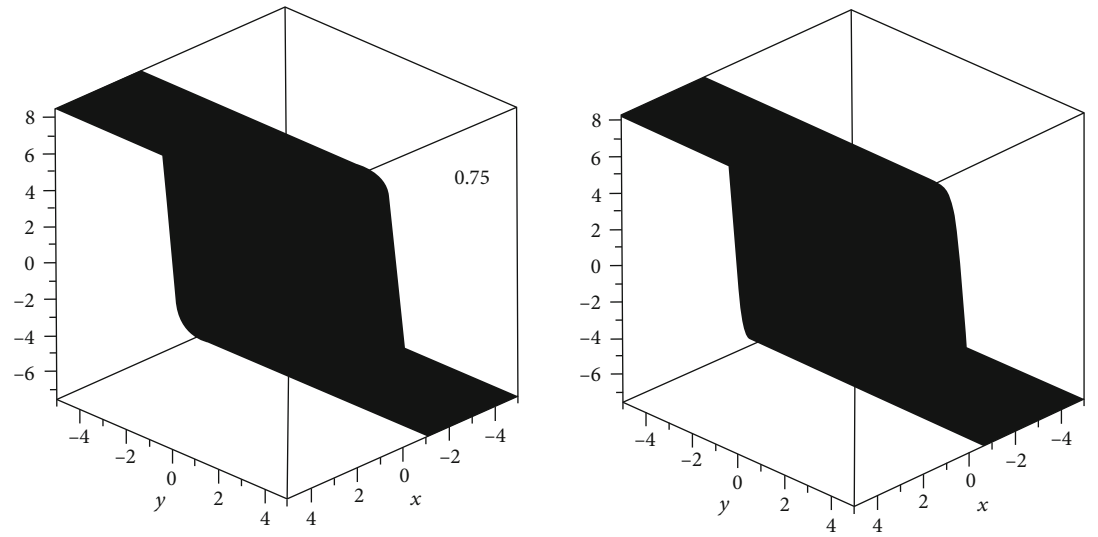

Figure 2: Graphical view of the analytical solution for $\mathbb{J}(\zeta, \rho)$ at $\delta = 0.8,0.6$ of system 1.

On simplification, we have

$$\mathbf{E}[\mathbb{J}(\zeta,\rho)] = \kappa^2[\lambda - \kappa \cot h[\kappa(\zeta+\theta)]] - \kappa^{\delta}\mathbf{E} \cdot \left[\mathbb{J}(\zeta,\rho)\frac{\partial \mathbb{J}(\zeta,\rho)}{\partial\zeta} + \frac{1}{2}\frac{\partial \mathbb{J}(\zeta,\rho)}{\partial\zeta} + \frac{\partial \mathbb{K}(\zeta,\rho)}{\partial\zeta}\right],$$

$$\mathbf{E}[\mathbb{K}(\zeta,\rho)] = \kappa^2\left[-\kappa^2 \operatorname{cosec} h^2[\kappa(\zeta+\theta)]\right] - \kappa^{\delta}\mathbf{E} \cdot \left[\mathbb{J}(\zeta,\rho)\frac{\partial \mathbb{K}(\zeta,\rho)}{\partial\zeta} + \mathbb{K}(\zeta,\rho)\frac{\partial \mathbb{J}(\zeta,\rho)}{\partial\zeta} - \frac{1}{2}\frac{\partial^2 \mathbb{K}(\zeta,\rho)}{\partial\zeta^2}\right]. \tag{49}$$

On applying the inverse NT, we get

$$\mathbb{J}(\zeta,\rho) = \left[\frac{1}{2} - 8\tan h(-2\zeta)\right] - \mathbf{E}^{-1} \cdot \left[\kappa^{\delta}\mathbf{E}\left\{\mathbb{J}(\zeta,\rho)\frac{\partial \mathbb{J}(\zeta,\rho)}{\partial\zeta} + \frac{1}{2}\frac{\partial \mathbb{J}(\zeta,\rho)}{\partial\zeta} + \frac{\partial \mathbb{K}(\zeta,\rho)}{\partial\zeta}\right\}\right],$$

$$\mathbb{K}(\zeta,\rho) = \left[16 - 16\tan h^2(-2\zeta)\right] - \mathbf{E}^{-1} \cdot \left[\kappa^{\delta}\mathbf{E}\left\{\mathbb{J}(\zeta,\rho)\frac{\partial \mathbb{K}(\zeta,\rho)}{\partial\zeta} + \mathbb{K}(\zeta,\rho)\frac{\partial \mathbb{J}(\zeta,\rho)}{\partial\zeta} - \frac{1}{2}\frac{\partial^2 \mathbb{K}(\zeta,\rho)}{\partial\zeta^2}\right\}\right]. \tag{50}$$

4.3. Solution by Means of NDM_C. The solutions in series form for the unknown function $\mathbb{J}(\zeta, \rho)$ and $\mathbb{K}(\zeta, \rho)$ are stated as follows:

$$\mathbb{J}(\zeta,\rho) = \sum_{l=0}^{\infty}\mathbb{J}_l(\zeta,\rho) \text{ and } \mathbb{K}(\zeta,\rho) = \sum_{l=0}^{\infty}\mathbb{J}_l(\zeta,\rho). \tag{51}$$

The nonlinear terms by means of Adomian polynomials are stated as $\mathbb{J}\mathbb{J}_{\zeta} = \sum_{m=0}^{\infty}\mathscr{A}_m$, $\mathbb{J}\mathbb{K}_{\zeta} = \sum_{m=0}^{\infty}\mathscr{B}_m$ and $\mathbb{K}\mathbb{J}_{\zeta} = \sum_{m=0}^{\infty}\mathscr{C}_m$; thus, by means of these terms, equation (50) can be determined as follows:

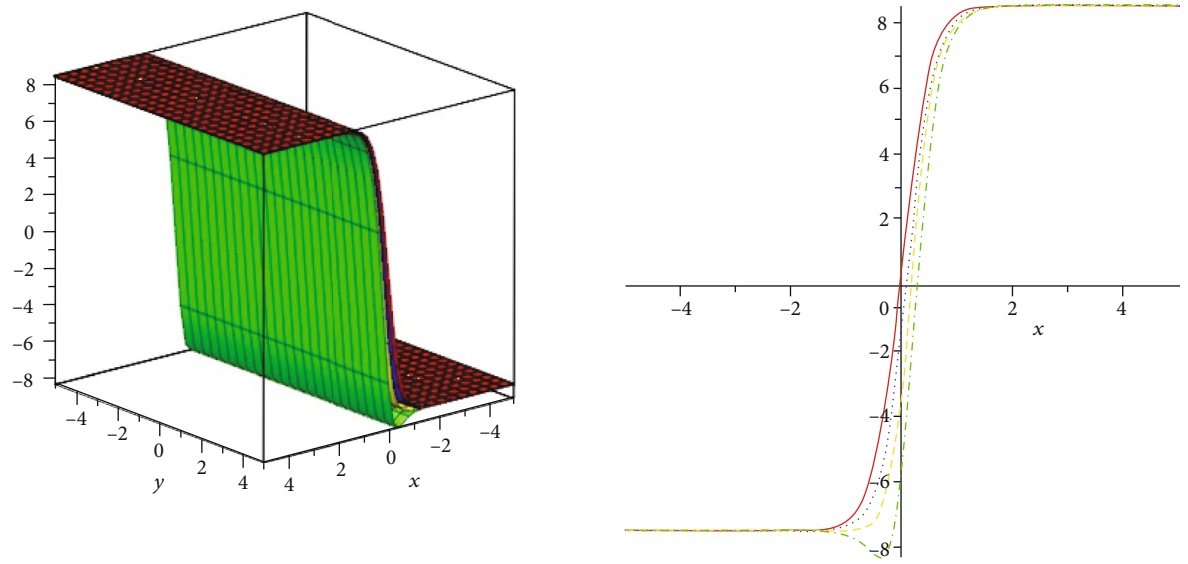

FIGURE 3: Graphical view of the analytical solution at various values of δ for $\mathbb{J}(\zeta, \rho)$ of system 1.

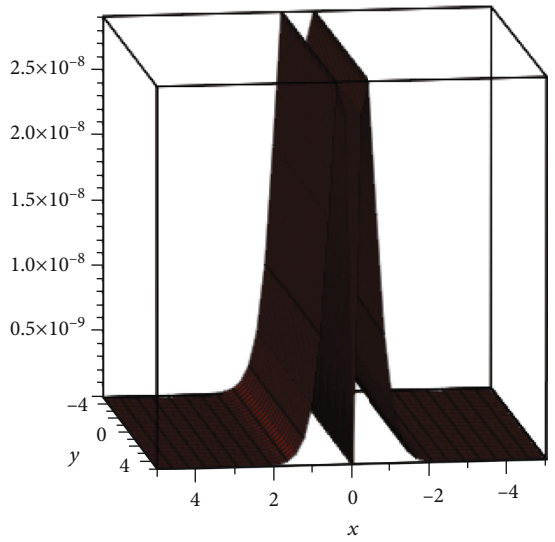

FIGURE 4: Graphical view of the absolute error for $\mathbb{J}(\zeta, \rho)$ of system 1.

$$\sum_{l=0}^{\infty} \mathbb{J}_{l+1}(\zeta,\rho) = \lambda - \kappa \cot h[\kappa(\zeta+\theta)] - \mathbf{E}^{-1} \cdot \left[\kappa^{\delta}\mathbf{E}\left\{\sum_{l=0}^{\infty} \mathscr{A}_l + \frac{1}{2}\frac{\partial \mathbb{J}(\zeta,\rho)}{\partial\zeta} + \frac{\partial \mathbb{K}(\zeta,\rho)}{\partial\zeta}\right\}\right],$$

$$\sum_{l=0}^{\infty} \mathbb{K}_{l+1}(\zeta,\rho) = -\kappa^2 \operatorname{cosec} h^2[\kappa(\zeta+\theta)] - \mathbf{E}^{-1} \cdot \left[\kappa^{\delta}\mathbf{E}\left\{\sum_{l=0}^{\infty} \mathscr{B}_l + \sum_{l=0}^{\infty} \mathscr{C}_l - \frac{1}{2}\frac{\partial^2 \mathbb{K}(\zeta,\rho)}{\partial\zeta^2}\right\}\right]. \tag{52}$$

By the comparison of both sides of equation (52), we obtain

$$\begin{aligned}
\mathbb{J}_0(\zeta,\rho) &= \lambda - \kappa \cot h[\kappa(\zeta+\theta)],\\
\mathbb{K}_0(\zeta,\rho) &= -\kappa^2 \operatorname{cosec} h^2[\kappa(\zeta+\theta)],\\
\mathbb{J}_1(\zeta,\rho) &= -\lambda\kappa^2 \operatorname{cosec} h^2[\kappa(\zeta+\theta)]\frac{\rho^{\delta}}{\Gamma(\delta+1)},\\
\mathbb{K}_1(\zeta,\rho) &= -\lambda\kappa^2 \operatorname{cosec} h^2[\kappa(\zeta+\theta)] \cot h[\kappa(\zeta+\theta)]\frac{\rho^{\delta}}{\Gamma(\delta+1)},\\
\mathbb{J}_2(\zeta,\rho) &= \lambda\kappa^4 \operatorname{cosec} h^2[\kappa(\zeta+\theta)] \cdot \left\{2\lambda\kappa\frac{\rho^{3\delta}}{\Gamma(3\delta+1)} - \left(3\cot h^2([\kappa(\zeta+\theta)]-1)\right)\frac{\rho^{2\delta}}{\Gamma(2\delta+1)}\right\},\\
\mathbb{K}_2(\zeta,\rho) &= \left[2\lambda\kappa^5 \operatorname{cosec} h^2[\kappa(\zeta+\theta)]\right] \cdot \left[\lambda\kappa \operatorname{cosec} h^2\left(3\cot h^2([\kappa(\zeta+\theta)]-1)\right)\frac{\rho^{2\delta}}{\Gamma(2\delta+1)}\right.\\
&\quad + \frac{2\lambda\kappa \operatorname{cosec} h^2 \cot h^2([\kappa(\zeta+\theta)])\rho^{3\delta}}{\Gamma(\delta+1)\Gamma(3\delta+1)}\\
&\quad \left. - 2\lambda \coth\left(3\operatorname{cosec} h^2([\kappa(\zeta+\theta)]-1)\right)\frac{\rho^{2\delta}}{\Gamma(2\delta+1)}\right].
\end{aligned} \tag{53}$$

Thus, for $\mathbb{J}_l$ and $\mathbb{K}_l$ with $(l \geq 3)$, the remaining components are easily computable. So, the solution in series form is as follows:

$$\begin{aligned}
\mathbb{J}(\zeta,\rho) &= \sum_{l=0}^{\infty} \mathbb{J}_l(\zeta,\rho) = \mathbb{J}_0(\zeta,\rho) + \mathbb{J}_1(\zeta,\rho) + \mathbb{J}_2(\zeta,\rho) + \cdots,\\
\mathbb{J}(\zeta,\rho) &= \lambda - \kappa \cot h[\kappa(\zeta+\theta)] - \lambda\kappa^2 \operatorname{cosec} h^2[\kappa(\zeta+\theta)] \cdot \frac{\rho^{\delta}}{\Gamma(\delta+1)} + \lambda\kappa^4 \operatorname{cosec} h^2[\kappa(\zeta+\theta)]\\
&\quad \cdot \left\{2\lambda\kappa\left\{(1-\delta)^2 3\delta\rho + (1-\delta)^3 + \frac{3\delta^2(1-\delta)\rho^2}{2} + \frac{\delta^3\rho^3}{3!}\right\}\right.\\
&\quad \left. - \left(3\cot h^2([\kappa(\zeta+\theta)]-1)\right)\frac{\rho^{2\delta}}{\Gamma(2\delta+1)}\right\} + \cdots.
\end{aligned}$$

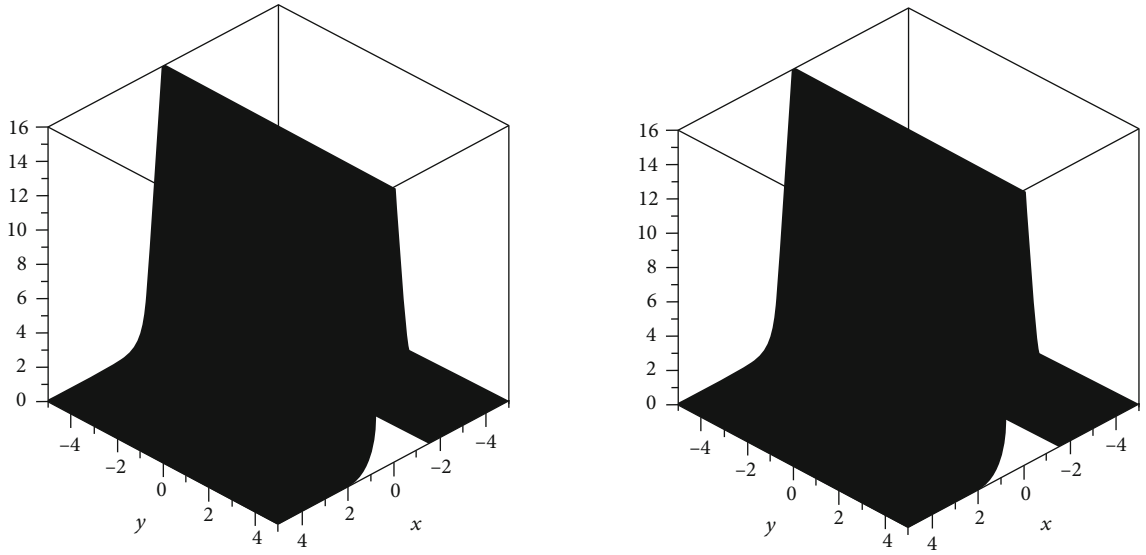

Figure 5: Graphical view of the exact and analytical solution for $\mathbb{K}(\zeta,\rho)$ at $\delta=1$ of system 1.

$$\begin{aligned}
\mathbb{K}(\zeta,\rho)&=\sum_{l=0}^{\infty}\mathbb{K}_l(\zeta,\rho)=\mathbb{K}_0(\zeta,\rho)+\mathbb{K}_1(\zeta,\rho)+\mathbb{K}_2(\zeta,\rho)+\cdots,\\
\mathbb{K}(\zeta,\rho)&=-\kappa^2\ \mathrm{cosec}\,h^2[\kappa(\zeta+\theta)]-\lambda\kappa^2\ \mathrm{cosec}\,h^2[\kappa(\zeta+\theta)]\cot h\\
&\quad\cdot[\kappa(\zeta+\theta)]\frac{\rho^{\delta}}{\Gamma(\delta+1)}+\left[2\lambda\kappa^5\ \mathrm{cosec}\,h^2[\kappa(\zeta+\theta)]\right]\\
&\quad\cdot\left[\lambda\kappa\ \mathrm{cosec}\,h^2\left(3\cot h^2([\kappa(\zeta+\theta)]-1)\right)\frac{\rho^{2\delta}}{\Gamma(2\delta+1)}\right.\\
&\quad+\frac{2\lambda\kappa\ \mathrm{cosec}\,h^2\ \cot h^2([\kappa(\zeta+\theta)])\rho^{3\delta}}{\Gamma(\delta+1)\Gamma(3\delta+1)}\\
&\quad-2\lambda\ \cot h\left(3\ \mathrm{cosec}\,h^2([\kappa(\zeta+\theta)]-1)\right)\\
&\quad\cdot\left.\left((1-\delta)^2+2\delta(1-\delta)\rho+\frac{\delta^2\rho^2}{2}\right)\right]+\cdots.
\end{aligned}\tag{54}$$

4.4. Solution by Means of EDM_{ABC}. The solutions in series form for the unknown function $\mathbb{J}(\zeta,\rho)$ and $\mathbb{K}(\zeta,\rho)$ are stated as follows:

$$\begin{aligned}
\mathbb{J}(\zeta,\rho)&=\sum_{l=0}^{\infty}\mathbb{J}_l(\zeta,\rho),\\
\mathbb{K}(\zeta,\rho)&=\sum_{l=0}^{\infty}\mathbb{J}_l(\zeta,\rho).
\end{aligned}\tag{55}$$

The nonlinear terms by means of Adomian polynomials are stated as $\mathbb{J}\mathbb{J}_{\zeta}=\sum_{l=0}^{\infty}\mathscr{A}_l$ and $\mathbb{J}^2\mathbb{J}_{\zeta}=\sum_{l=0}^{\infty}\mathscr{B}_l$; thus, by means of these terms, equation (50) can be determined as follows:

$$\begin{aligned}
\sum_{l=0}^{\infty}\mathbb{J}_{l+1}(\zeta,\rho)&=\lambda-\kappa\cot h[\kappa(\zeta+\theta)]+\mathbf{E}^{-1}\left[\frac{\ell^{\delta}\left(\kappa^{\delta}+\delta\left(\ell^{\delta}-\kappa^{\delta}\right)\right)}{\kappa^{2\delta}}\mathbf{E}\left\{\sum_{l=0}^{\infty}\mathscr{A}_l+\frac{1}{2}\frac{\partial\mathbb{J}(\zeta,\rho)}{\partial\zeta}+\frac{\partial\mathbb{K}(\zeta,\rho)}{\partial\zeta}\right\}\right],\\
\sum_{l=0}^{\infty}\mathbb{K}_{l+1}(\zeta,\rho)&=-\kappa^2\ \mathrm{cosec}\,h^2[\kappa(\zeta+\theta)]+\mathbf{E}^{-1}\left[\frac{\ell^{\delta}\left(\kappa^{\delta}+\delta\left(\ell^{\delta}-\kappa^{\delta}\right)\right)}{\kappa^{2\delta}}\mathbf{E}\left\{\sum_{l=0}^{\infty}\mathscr{B}_l+\sum_{l=0}^{\infty}\mathscr{C}_l-\frac{1}{2}\frac{\partial^2\mathbb{K}(\zeta,\rho)}{\partial\zeta^2}\right\}\right].
\end{aligned}\tag{56}$$

By the comparison of both sides of equation (56), we obtain

$$\begin{aligned}
\mathbb{J}_0(\zeta,\rho)&=\lambda-\kappa\cot h[\kappa(\zeta+\theta)],\\
\mathbb{K}_0(\zeta,\rho)&=-\kappa^2\ \mathrm{cosec}\,h^2[\kappa(\zeta+\theta)],\\
\mathbb{J}_1(\zeta,\rho)&=-\lambda\kappa^2\ \mathrm{cosec}\,h^2[\kappa(\zeta+\theta)]\left(1-\delta+\frac{\delta\rho^{\delta}}{\Gamma(\delta+1)}\right),\\
\mathbb{K}_1(\zeta,\rho)&=-\lambda\kappa^2\ \mathrm{cosec}\,h^2[\kappa(\zeta+\theta)]\cot h[\kappa(\zeta+\theta)]\\
&\quad\cdot\left(1-\delta+\frac{\delta\rho^{\delta}}{\Gamma(\delta+1)}\right),\\
\mathbb{J}_2(\zeta,\rho)&=\lambda\kappa^4\ \mathrm{cosec}\,h^2[\kappa(\zeta+\theta)]\\
&\quad\cdot\left\{2\lambda\kappa\frac{\rho^{3\delta}}{\Gamma(3\delta+1)}-\left(3\cot h^2([\kappa(\zeta+\theta)]-1)\right)\right.\\
&\quad\cdot\left.\left[\frac{\delta^2\rho^{2\delta}}{\Gamma(2\delta+1)}+2\delta(1-\delta)\frac{\rho^{\delta}}{\Gamma(\delta+1)}+(1-\delta)^2\right]\right\},
\end{aligned}$$

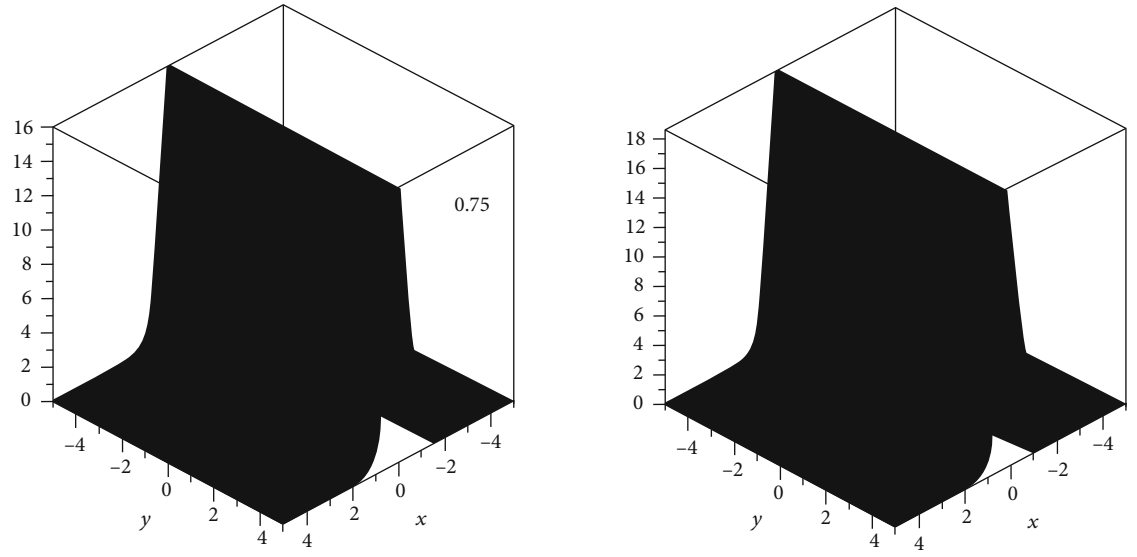

Figure 6: Graphical view of the analytical solution for $\mathbb{K}(\zeta, \rho)$ at $\delta = 0.8,0.6$ of system 1.

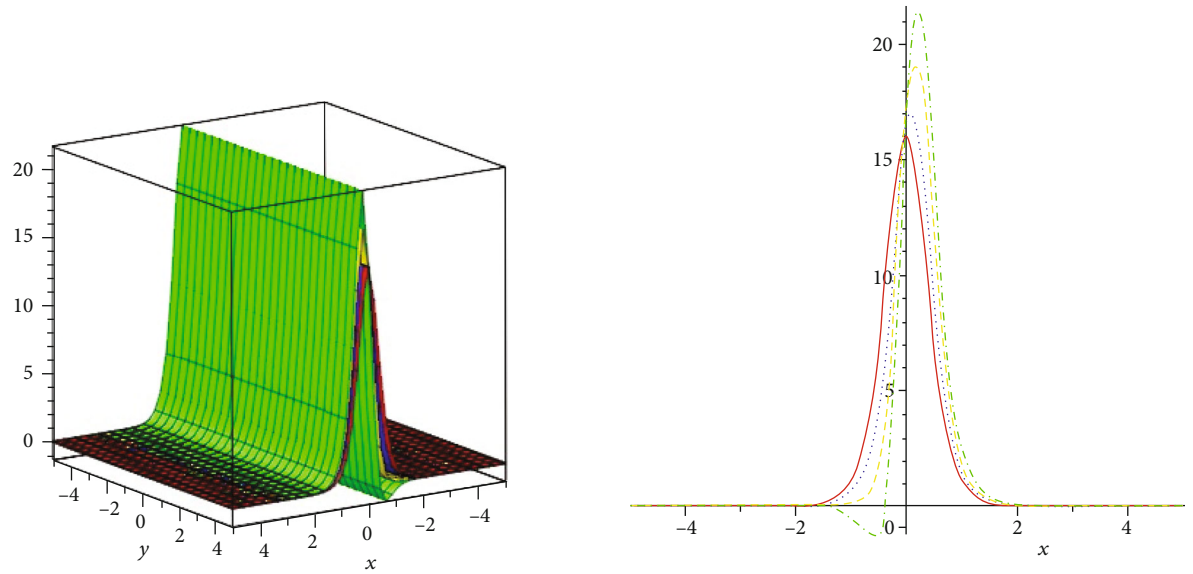

Figure 7: Graphical view of analytical solution at various values of δ for $\mathbb{K}(\zeta, \rho)$ of system 1.

Table 1: Proposed method solution for $\mathbb{J}(\zeta, \rho)$ at different fractional orders of problem 1.

(ζ, ρ)	$\mathbb{J}(\zeta, \rho)$ at $\delta = 0.5$	$\mathbb{J}(\zeta, \rho)$ at $\delta = 0.75$	$(ETDM_{ABC})$ at $\delta = 1$	$(ETDM_{C})$ at $\delta = 1$	Exact result
(0.2,0.01)	2.427701	2.427745	2.427806	2.427806	2.427806
(0.4,0.02)	4.701611	4.711644	4.711736	4.711736	4.711736
(0.6,0.03)	6.057710	6.057766	6.157882	6.157882	6.157882
(0.2,0.01)	2.414601	2.415654	2.414781	2.414781	2.414781
(0.4,0.02)	4.602065	4.702334	4.702226	4.702226	4.702226
(0.6,0.03)	6.053106	6.153617	6.153237	6.153237	6.153237
(0.2,0.01)	2.426313	2.426388	2.426426	2.426426	2.426426
(0.4,0.02)	4.700712	4.700746	4.710841	4.710841	4.710841
(0.6,0.03)	6.057423	6.057369	6.157403	6.157403	6.157403
(0.2,0.01)	2.324601	2.425646	2.425742	2.425742	2.425742
(0.4,0.02)	4.710311	4.710355	4.710403	4.710403	4.710403
(0.6,0.03)	6.058112	6.157050	6.157150	6.157150	6.157150
(0.2,0.01)	2.426076	2.425223	2.425158	3.536168	3.536168
(0.4,0.02)	4.700002	4.710010	4.810046	4.810046	4.810046
(0.6,0.03)	6.058000	6.057002	6.057015	6.057015	6.057015

Table 2: Proposed method solution for $\mathbb{K}(\zeta, \rho)$ at different fractional orders of problem 1.

(ζ, ρ)	$\mathbb{K}(\zeta, \rho)$ at δ =0.5	$\mathbb{K}(\zeta, \rho)$ at δ =0.75	$(ETDM_{ABC})$ at $\delta = 1$	$(ETDM_{C})$ at $\delta = 1$	Exact result
(0.2,0.01)	12.58221	12.571167	12.581150	12.581150	12.581150
(0.4,0.02)	7.835001	7.835012	7.835060	7.835060	7.835060
(0.6,0.03)	3.771048	3.772101	3.771122	3.771122	3.771122
(0.2,0.01)	12.61072	12.630787	12.610884	12.610884	12.610884
(0.4,0.02)	7.857405	8.857468	7.857542	7.857542	7.857542
(0.6,0.03)	3.785415	3.785477	3.785514	3.785514	3.785514
(0.2,0.01)	12.58215	12.582201	12.585430	12.585430	12.585430
(0.4,0.02)	8.837267	7.837311	7.838556	7.838556	7.838556
(0.6,0.03)	3.771568	3.771604	3.772651	3.772651	3.772651
(0.2,0.01)	12.58320	12.58321	12.583270	12.583270	12.583270
(0.4,0.02)	7.838476	8.838511	7.838463	7.838463	7.838463
(0.6,0.03)	3.772401	4.772434	4.772464	4.772464	4.772464
(0.2,0.01)	12.58427	12.584301	12.584310	12.584310	12.584310
(0.4,0.02)	7.840625	7.840667	8.840713	8.840713	8.840713
(0.6,0.03)	3.773177	3.773215	4.773278	4.773278	4.773278

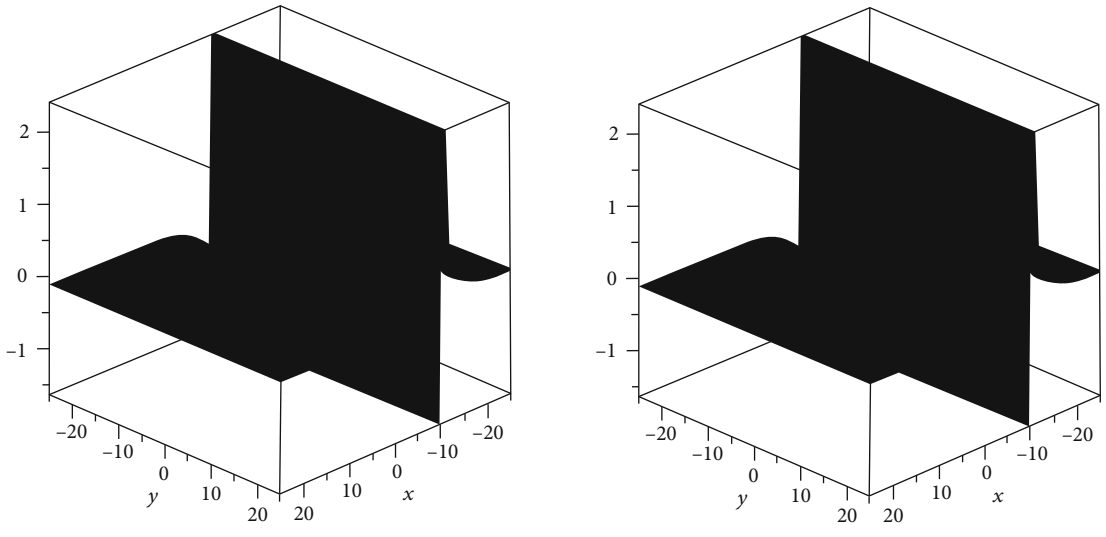

Figure 8: Graphical view of the exact and analytical solution for $\mathbb{J}(\zeta, \rho)$ at $\delta = 1$ of system 2.

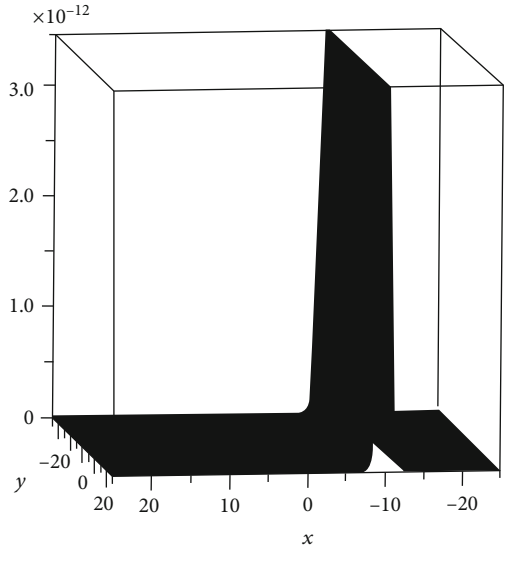

Figure 9: Graphical view of the absolute error for $\mathbb{J}(\zeta, \rho)$ of system 2.

$$\begin{aligned}\mathbb{K}_2(\zeta,\rho) = {} & \left[2\lambda\kappa^5 \operatorname{cosec} h^2[\kappa(\zeta+\theta)]\right] \\ & \cdot \left[\lambda\kappa \operatorname{cosec} h^2\left(3\cot h^2([\kappa(\zeta+\theta)]-1)\right)\frac{\rho^{2\delta}}{\Gamma(2\delta+1)}\right. \\ & + \frac{2\lambda\kappa \operatorname{cosec} h^2 \cot h^2([\kappa(\zeta+\theta)])\rho^{3\delta}}{\Gamma(\delta+1)\Gamma(3\delta+1)} \\ & - 2\lambda \cot h\left(3 \operatorname{cosec} h^2([\kappa(\zeta+\theta)]-1)\right) \\ & \left.\cdot \left[\frac{\delta^2\rho^{2\delta}}{\Gamma(2\delta+1)} + 2\delta(1-\delta)\frac{\rho^{\delta}}{\Gamma(\delta+1)} + (1-\delta)^2\right]\right].\end{aligned} \tag{57}$$

Thus, for $\mathbb{J}_l$ and $\mathbb{K}_l$ with $(l \geq 3)$, the remaining components are easily computable. So, the solution in series form is as follows:

$$\mathbb{J}(\zeta,\rho) = \sum_{l=0}^{\infty} \mathbb{J}_l(\zeta,\rho) = \mathbb{J}_0(\zeta,\rho) + \mathbb{J}_1(\zeta,\rho) + \mathbb{J}_2(\zeta,\rho) + \cdots,$$

$$\begin{aligned}\mathbb{J}(\zeta,\rho) = {} & \lambda - \kappa \cot h[\kappa(\zeta+\theta)] - \lambda\kappa^2 \operatorname{cosec} h^2[\kappa(\zeta+\theta)] \\ & \cdot \left(1 - \delta + \frac{\delta\rho^{\delta}}{\Gamma(\delta+1)}\right) + \lambda\kappa^4 \operatorname{cosec} h^2[\kappa(\zeta+\theta)] \\ & \cdot \left\{2\lambda\kappa\left\{(1-\delta)^2 3\delta\rho + (1-\delta)^3 + \frac{3\delta^2(1-\delta)\rho^2}{2} + \frac{\delta^3\rho^3}{3!}\right\}\right. \\ & - \left(3\cot h^2([\kappa(\zeta+\theta)]-1)\right) \\ & \left.\cdot \left[\frac{\delta^2\rho^{2\delta}}{\Gamma(2\delta+1)} + 2\delta(1-\delta)\frac{\rho^{\delta}}{\Gamma(\delta+1)} + (1-\delta)^2\right]\right\} + \cdots.\end{aligned}$$

$$\mathbb{K}(\zeta,\rho) = \sum_{l=0}^{\infty} \mathbb{K}_l(\zeta,\rho) = \mathbb{K}_0(\zeta,\rho) + \mathbb{K}_1(\zeta,\rho) + \mathbb{K}_2(\zeta,\rho) + \cdots,$$

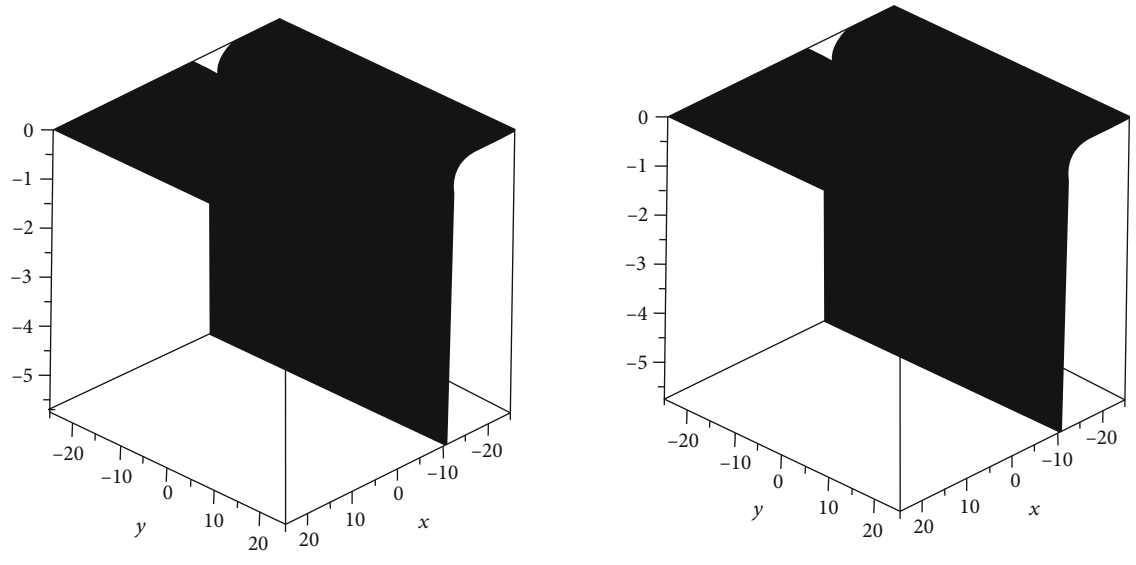

Figure 10: Graphical view of the exact and analytical solution for $\mathbb{K}(\zeta,\rho)$ at $\delta=1$ of system 2.

$$\begin{aligned}\mathbb{K}(\zeta,\rho) &= -\kappa^2\,\mathrm{cosec}\,h^2[\kappa(\zeta+\theta)] - \lambda\kappa^2\,\mathrm{cosec}\,h^2[\kappa(\zeta+\theta)]\,\cot h[\kappa(\zeta+\theta)]\\ &\cdot\left(1-\delta+\frac{\delta\rho^{\delta}}{\Gamma(\delta+1)}\right)+\left[2\lambda\kappa^5\,\mathrm{cosec}\,h^2[\kappa(\zeta+\theta)]\right]\\ &\cdot\left[\lambda\kappa\,\mathrm{cosec}\,h^2\left(3\cot h^2([\kappa(\zeta+\theta)]-1)\right)\frac{\rho^{3\delta}}{\Gamma(3\delta+1)}\right.\\ &+\frac{2\lambda\kappa\,\mathrm{cosec}\,h^2\cot h^2([\kappa(\zeta+\theta)])\rho^{3\delta}}{\Gamma(\delta+1)\Gamma(3\delta+1)}\\ &-2\lambda\cot h\left(3\,\mathrm{cosec}\,h^2([\kappa(\zeta+\theta)]-1)\right)\\ &\cdot\left.\left[\frac{\delta^2\rho^{2\delta}}{\Gamma(2\delta+1)}+2\delta(1-\delta)\frac{\rho^{\delta}}{\Gamma(\delta+1)}+(1-\delta)^2\right]\right]+\cdots.\end{aligned} \tag{58}$$

We obtain the below series form solution at integer order $\delta=1$, $\kappa=0.1$, $\lambda=0.005$, $\theta=10$, as follows:

$$\begin{aligned}\mathbb{J}(\zeta,\rho) &= 0.005-0.1\cot h(0.1\zeta+10)\\ &-0.0005\,\mathrm{cosec}\,h^2(0.1\zeta+10)\rho+5\\ &\times10^{-7}\,\mathrm{cosec}\,h^2(0.1\zeta+10)0.003\rho^3\\ &-0.5\left(3\cot h^2(0.1\zeta+10)-1.\right)\rho^2,\end{aligned}$$

$$\begin{aligned}\mathbb{K}(\zeta,\rho) &= -0.01\,\mathrm{cosec}\,h^2(0.1\zeta+10)\\ &-0.000010\,\mathrm{cosec}\,h^2(0.1\zeta+10)\\ &\times\cot h(0.1\zeta+10)\rho+1.0\\ &\times10^{-7}\,\mathrm{cosec}\,h^2(0.1\zeta+10)\\ &\times\left[8.3\times10^{-5}\rho^3\,\mathrm{cosec}\,h^2(0.1\zeta+10)\right.\\ &\cdot\left(3\cot h(0.1\zeta+10)-1\right)-\rho^2\cot h(0.1\zeta+10)\\ &\cdot\left.\left(3\,\mathrm{cosec}\,h^2(0.1\zeta+10)-1\right)+1.6\right.\\ &\times10^{-4}\rho^3\,\mathrm{cosec}\,h^2(0.1\zeta+10)\cot h(0.1\zeta+10)].\end{aligned} \tag{59}$$

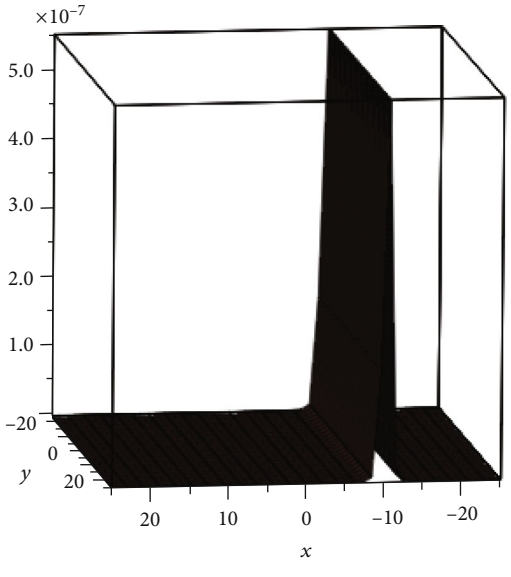

Figure 11: Graphical view of the absolute error for $\mathbb{K}(\zeta,\rho)$ of system 2.

The exact solution of equation (45) at $\delta=1$ and taking $\kappa=0.1$, $\lambda=0.005$, $\theta=10$,

$$\begin{aligned}\mathbb{J}(\zeta,\rho) &== \lambda-\kappa\cot h[\kappa(\zeta+\theta-\lambda\rho)],\\ \mathbb{K}(\zeta,\rho) &= -\kappa^2\,\mathrm{cosec}\,h^2[\kappa(\zeta+\theta-\lambda\rho)].\end{aligned} \tag{60}$$

Figure 8 shows the graphical view of the exact and analytical solution for $\mathbb{J}(\zeta,\rho)$ at $\delta=1$ of system 2, and Figure 9 shows the absolute error for $\mathbb{J}(\zeta,\rho)$ of system 2. Similarly, Figure 10 represents the exact and analytical solution for $\mathbb{K}(\zeta,\rho)$ at $\delta=1$ of system 2 and Figure 11 of the

Table 3: Proposed method solution for $\mathbb{J}(\zeta, \rho)$ at different fractional orders of problem 2.

(ζ, ρ)	$\mathbb{J}(\zeta, \rho)$ at $\delta = 0.5$	$\mathbb{J}(\zeta, \rho)$ at $\delta = 0.75$	$(ETDM_{ABC})$ at $\delta = 1$	$(ETDM_{C})$ at $\delta = 1$	Exact result
(0.2,0.01)	−0.134802	−0.132796	−0.134882	−0.134882	−0.134882
(0.4,0.01)	−0.133485	−0.132568	−0.133543	−0.123553	−0.123553
(0.6,0.01)	−0.132287	−0.133292	−0.132380	−0.132380	−0.132380
(0.2,0.02)	−0.133907	−0.142898	−0.134992	−0.134992	−0.134992
(0.4,0.02)	−0.132497	−0.132578	−0.133453	−0.133453	−0.133453
(0.6,0.02)	−0.123499	−0.133293	−0.132380	−0.132380	−0.132380
(0.2,0.03)	−0.124909	−0.145899	−0.134792	−0.134792	−0.134792
(0.4,0.03)	−0.124586	−0.132568	−0.133453	−0.133453	−0.133453
(0.6,0.03)	−0.111299	−0.133289	−0.132380	−0.132380	−0.132380
(0.2,0.04)	−0.134808	−0.142896	−0.134792	−0.134792	−0.134792
(0.4,0.04)	−0.132489	−0.132576	−0.133453	−0.133453	−0.133453
(0.6,0.04)	−0.144496	−0.135288	−0.132380	−0.132380	−0.132380
(0.2,0.05)	−0.145905	−0.135897	−0.134792	−0.134792	−0.134792
(0.4,0.05)	−0.187578	−0.132564	−0.133453	−0.133453	−0.133453
(0.6,0.05)	−0.133298	−0.133290	−0.132480	−0.132480	−0.132480

Table 4: Proposed method solution for $\mathbb{K}(\zeta, \rho)$ at different fractional orders of problem 2.

(ζ, ρ)	$\mathbb{K}(\zeta, \rho)$ at $\delta = 0.5$	$\mathbb{K}(\zeta, \rho)$ at $\delta = 0.75$	$(ETDM_{ABC})$ at $\delta = 1$	$(ETDM_{C})$ at $\delta = 1$	Exact result
(0.2,0.01)	−0.005794	−0.005784	−0.006771	−0.006771	−0.006872
(0.4,0.01)	−0.005446	−0.005436	−0.006424	−0.006424	−0.006525
(0.6,0.01)	−0.005319	−0.005313	−0.006100	−0.006100	−0.006200
(0.2,0.02)	−0.005794	−0.005684	−0.006773	−0.006773	−0.006773
(0.4,0.02)	−0.005442	−0.005433	−0.006424	−0.006424	−0.006424
(0.6,0.02)	−0.005319	−0.005314	−0.006301	−0.006301	−0.006301
(0.2,0.03)	−0.005789	−0.005783	−0.006871	−0.006871	−0.006871
(0.4,0.03)	−0.005443	−0.005437	−0.006424	−0.006424	−0.006424
(0.6,0.03)	−0.005316	−0.005306	−0.006100	−0.006100	−0.006100
(0.2,0.04)	−0.005789	−0.005782	−0.006773	−0.006773	−0.006773
(0.4,0.04)	−0.005441	−0.005431	−0.006421	−0.006421	−0.006421
(0.6,0.04)	−0.005118	−0.005306	−0.006301	−0.006301	−0.006301
(0.2,0.05)	−0.005789	−0.005782	−0.006572	−0.006572	−0.006572
(0.4,0.05)	−0.005446	−0.005437	−0.006424	−0.006424	−0.006424
(0.6,0.05)	−0.005323	−0.005112	−0.006201	−0.006201	−0.006201

absolute error for $\mathbb{K}(\zeta, \rho)$ of system 2. Tables 3 and 4 show that the different fractional order of δ of system 2.

5. Conclusion

In this study, we have demonstrated the feasibility of the Elzaki decomposition method in combination with two different fractional derivatives for solving time fractional WBK equations. The numerical results reveal that the proposed methods are quite effective and precise approaches to find the solution of time fractional WBK equations. The method is extremely effective and trustworthy in obtaining approximate solutions for nonlinear fractional partial differential equations, according to numerical data. The proposed technique is an efficient and easy tool for investigating numerical solution of nonlinear coupled systems of fractional partial differential equations when compared to previous analytical techniques. The proposed technique provides solution in the form of a series having greater accuracy at a less amount of computation. Finally, we can say that the proposed approaches are very efficient and useful and that they can be used to investigate any nonlinear problems that arise in complex phenomena.

Data Availability

The numerical data used to support the findings of this study are included within the article.

Conflicts of Interest

The authors declare that there are no conflicts of interest regarding the publication of this article.

Acknowledgments

This research has been funded by the scientific research deanship at University of Ha'il, Saudi Arabia, through project number GR-22 037.

References

[1] K. B. Oldham and J. Spanier, *The Fractional Calculus*, Academic Press, New York, NY, USA, 1974.

[2] H. Beyer and S. Kempfle, "Definition of physically consistent damping laws with fractional derivatives," *Zeitschrift für Angewandte Mathematik und Mechanik*, vol. 75, no. 8, pp. 623–635, 1995.

[3] J. H. He, "Some applications of nonlinear fractional differential equations and their approximations," *Science and Technology Studies*, vol. 15, pp. 86–90, 1999.

[4] M. Caputo, "Linear models of dissipation whose Q is almost frequency independent-II," *Geophysical Journal International*, vol. 13, no. 5, pp. 529–539, 1967.

[5] A. M. Lopes, J. A. T. Machado, C. M. A. Pinto, and A. M. S. F. Galhano, "Fractional dynamics and MDS visualization of earthquake phenomena," *Computers & Mathematcs with Applications*, vol. 66, no. 5, pp. 647–658, 2013.

[6] M. R. Ubriaco, "Entropies based on fractional calculus," *Physics Letters A*, vol. 373, no. 30, pp. 2516–2519, 2009.

[7] J. Prehl, F. Boldt, C. Essex, and K. H. Hoffmann, "Time evolution of relative entropies for anomalous diffusion," *Entropy*, vol. 15, no. 12, pp. 2989–3006, 2013.

[8] K. S. Miller and B. Ross, *An Introduction to the Fractional Calculus and Fractional Differential Equations*, John Willy and Sons, Inc., New York, NY, USA, 1993.

[9] J. A. T. Machado, "Optimal tuning of fractional controllers using genetic algorithms," *Nonlinear Dynamics*, vol. 62, no. 1-2, pp. 447–452, 2010.

[10] R. Alyusof, S. Alyusof, N. Iqbal, and M. A. Arefin, "Novel evaluation of the fractional acoustic wave model with the exponential-decay kernel," *Complexity*, vol. 2022, article 9712388, pp. 1–4, 2022.

[11] J. A. T. Machado, "Entropy analysis of integer and fractional dynamical systems," *Nonlinear Dynamics*, vol. 62, no. 1-2, pp. 371–378, 2010.

[12] J. Prehl, C. Essex, and K. H. Hoffmann, "Tsallis relative entropy and anomalous diffusion," *Entropy*, vol. 14, no. 4, pp. 701–716, 2012.

[13] L. Sommacal, P. Melchior, A. Dossat, J. M. Cabelguen, A. Oustaloup, and A. J. Ijspeert, "Improvement of the muscle fractional multimodel for low-rate stimulation," *Biomedical Signal Processing and Control*, vol. 2, no. 3, pp. 226–233, 2007.

[14] N. Iqbal, T. Botmart, W. W. Mohammed, and A. Ali, "Numerical investigation of fractional-order Kersten-Krasil'shchik coupled KdV-mKdV system with Atangana-Baleanu derivative," *Advances in Continuous and Discrete Models*, vol. 2022, no. 1, pp. 1–20, 2022.

[15] Z. Odibat and S. Momani, "The variational iteration method: an efficient scheme for handling fractional partial differential equations in fluid mechanics," *Computers & Mathematics with Applications*, vol. 58, no. 11-12, pp. 2199–2208, 2009.

[16] N. H. Aljahdaly, A. Akgul, I. Mahariq, and J. Kafle, "A comparative analysis of the fractional-order coupled Korteweg–De Vries equations with the Mittag–Leffler law," *Journal of Mathematics*, vol. 2022, Article ID 8876149, 30 pages, 2022.

[17] H. Yasmin and N. Iqbal, "A comparative study of the fractional-order nonlinear system of physical models via analytical methods," *Mathematical Problems in Engineering*, vol. 2022, Article ID 7488996, 23 pages, 2022.

[18] I. Podlubny, *Fractional Differential Equations*, Academic Press, San Diego, California, USA, 1999.

[19] E. M. Elsayed and K. Nonlaopon, "The analysis of the fractional-order Navier-Stokes equations by a novel approach," *Journal of Function Spaces*, vol. 2022, Article ID 8979447, 18 pages, 2022.

[20] P. Sunthrayuth, N. H. Aljahdaly, A. Ali, I. Mahariq, and A. M. Tchalla, "Φ-Haar wavelet operational matrix method for fractional relaxation-oscillation equations containing -Caputo fractional derivative," *Journal of Function Spaces*, vol. 2021, Article ID 7117064, 14 pages, 2021.

[21] M. Areshi, R. Shah, and K. Nonlaopon, "Analytical investigation of fractional-order Newell-whitehead-Segel equations via a novel transform," *AIMS Mathematics*, vol. 7, no. 4, pp. 6936–6958, 2022.

[22] S. A. Bhanotar and M. K. Kaabar, "Analytical solutions for the nonlinear partial differential equations using the conformable triple Laplace transform decomposition method," *International Journal of Differential Equations*, vol. 2021, Article ID 9988160, 18 pages, 2021.

[23] H. Yasmin and N. Iqbal, "A comparative study of the fractional coupled burgers and Hirota-Satsuma KdV equations via analytical techniques," *Symmetry*, vol. 14, no. 7, p. 1364, 2022.

[24] Y. Qin, A. Khan, I. Ali et al., "An efficient analytical approach for the solution of certain fractional-order dynamical systems," *Energies*, vol. 13, no. 11, p. 2725, 2020.

[25] G. M. Mophou, "Weighted pseudo almost automorphic mild solutions to semilinear fractional differential equations," *Applied Mathematics and Computation*, vol. 217, no. 19, pp. 7579–7587, 2011.

[26] R. K. Pandey, O. P. Singh, and V. K. Baranwal, "An analytic algorithm for the space-time fractional advection-dispersion equation," *Computer Physics Communications*, vol. 182, no. 5, pp. 1134–1144, 2011.

[27] C. Xue, J. Nie, and W. Tan, "An exact solution of start-up flow for the fractional generalized Burgers' fluid in a porous half-space," *Nonlinear Analysis: Theory, Methods & Applications*, vol. 69, no. 7, pp. 2086–2094, 2008.

[28] R. Y. Molliq, M. S. M. Noorani, I. Hashim, and R. R. Ahmad, "Approximate solutions of fractional Zakharov-Kuznetsov equations by VIM," *Journal of Computational and Applied Mathematics*, vol. 233, no. 2, pp. 103–108, 2009.

[29] G. B. Whitham, "Variational methods and applications to water waves. Proceedings of the Royal Society of London," *Series A. Mathematical and Physical Sciences*, vol. 299, no. 1456, pp. 6–25, 1967.

[30] F. Xie, Z. Yan, and H. Zhang, "Explicit and exact traveling wave solutions of Whitham-Broer-Kaup shallow water equations," *Physics Letters A*, vol. 285, no. 1-2, pp. 76–80, 2001.

[31] D. Kaup, "A higher-order water-wave equation and the method for solving it," *Progress of Theoretical Physics*, vol. 54, no. 2, pp. 396–408, 1975.

[32] M. Alshammari, N. Iqbal, W. W. Mohammed, and T. Botmart, "The solution of fractional-order system of KdV equations with exponential-decay kernel," *Results in Physics*, vol. 38, article 105615, p. 14, 2022.

[33] M. M. El-Borai, W. G. El-Sayed, and R. M. Al-Masroub, "Exact solution for time fractional coupled Whitham-Broer-Kaup equations via exp-function method," *International Research Journal of Engineering and Technology*, vol. 2, no. 6, pp. 307–315, 2015.

[34] S. S. Ray, "A novel method for travelling wave solutions of fractional Whitham–Broer–Kaup, fractional modified Boussinesq and fractional approximate long wave equations in shallow water," *Mathematicsl Methods in the Applied Sciences*, vol. 38, no. 7, pp. 1352–1368, 2015.

[35] Q. Huang, G. Huang, and H. Zhan, "A finite element solution for the fractional advection-dispersion equation," *Advances in Water Resources*, vol. 31, no. 12, pp. 1578–1589, 2008.

[36] M. Cui, "Compact finite difference method for the fractional diffusion equation," *Journal of Computational Physics*, vol. 228, no. 20, pp. 7792–7804, 2009.

[37] B. Zheng, "Exp-function method for solving fractional partial differential equations," *Scientific World Journal*, vol. 2013, article 465723, 8 pages, 2013.

[38] H. Yasmin and N. Iqbal, "Analysis of fractional-order system of one-dimensional Keller-Segel equations: a modified analytical method," *Symmetry*, vol. 14, no. 7, p. 1321, 2022.

[39] H. N. Hassan and M. A. El-Tawil, "A new technique of using homotopy analysis method for solving high-order nonlinear differential equations," *Mathematical Methods in the Applied Sciences*, vol. 34, no. 6, pp. 728–742, 2011.

[40] Z. Zhang, X. Yong, and Y. Chen, "Symmetry analysis for Whitham-Broer-Kaup equations," *Journal of Nonlinear Mathematical Physics*, vol. 15, no. 4, pp. 383–397, 2008.

[41] N. A. Shah, Y. S. Hamed, K. M. Abualnaja, J. D. Chung, R. Shah, and A. Khan, "A comparative analysis of fractional-order Kaup-Kupershmidt equation within different operators," *Symmetry*, vol. 14, no. 5, p. 986, 2022.

[42] H. Eltayeb, Y. T. Abdalla, I. Bachar, and M. H. Khabir, "Fractional telegraph equation and its solution by natural transform decomposition method," *Symmetry*, vol. 11, no. 3, p. 334, 2019.

[43] J. H. He, "Homotopy perturbation technique," *Computer Methods in Applied Mechanics and Engineering*, vol. 178, no. 3-4, pp. 257–262, 1999.

[44] J. H. He, "A coupling method of a homotopy technique and a perturbation technique for non-linear problems," *International Journal of Non-Linear Mechanics*, vol. 35, no. 1, pp. 37–43, 2000.

[45] S. Rashid, A. Khalid, S. Sultana, Z. Hammouch, and A. M. Alsharif, "A novel analytical view of time-fractional Korteweg-De Vries equations via a new integral transform," *Symmetry*, vol. 13, no. 7, p. 1254, 2021.

[46] H. Khan, D. Baleanu, P. Kumam, and M. Arif, "The analytical investigation of time-fractional multi-dimensional Navier-Stokes equation," *Alexandria Engineering Journal*, vol. 59, no. 5, pp. 2941–2956, 2020.

[47] H. Khan, U. Farooq, D. Baleanu, P. Kumam, and M. Arif, "Analytical solutions of (2+ time fractional order) dimensional physical models, using modified decomposition method," *Applied Sciences*, vol. 10, no. 1, p. 122, 2020.

[48] R. Shah, H. Khan, P. Kumam, and M. Arif, "An analytical technique to solve the system of nonlinear fractional partial differential equations," *Mathematics*, vol. 7, no. 6, p. 505, 2019.

[49] M. Kbiri Alaoui, K. Nonlaopon, A. M. Zidan, A. Khan, and R. Shah, "Analytical investigation of fractional-order Cahn-Hilliard and Gardner equations using two novel techniques," *Mathematics*, vol. 10, no. 10, p. 1643, 2022.

[50] T. Botmart, R. P. Agarwal, M. Naeem, A. Khan, and R. Shah, "On the solution of fractional modified Boussinesq and approximate long wave equations with non-singular kernel operators," *AIMS Mathematics*, vol. 7, no. 7, pp. 12483–12513, 2022.

Hindawi
Advances in Mathematical Physics
Volume 2022, Article ID 1534067, 8 pages
https://doi.org/10.1155/2022/1534067

Research Article

The Analytical Solutions of the Stochastic Fractional RKL Equation via Jacobi Elliptic Function Method

Farah M. Al-Askar[1] **and Wael W. Mohammed**[2,3]

[1]*Department of Mathematical Science, College of Science, Princess Nourah Bint Abdulrahman University, P.O. Box 84428, Riyadh 11671, Saudi Arabia*
[2]*Department of Mathematics, College of Science, University of Ha'il, Ha'il 2440, Saudi Arabia*
[3]*Department of Mathematics, Faculty of Science, Mansoura University, Mansoura 35516, Egypt*

Correspondence should be addressed to Wael W. Mohammed; wael.mohammed@mans.edu.eg

Received 21 June 2022; Revised 13 July 2022; Accepted 30 July 2022; Published 15 August 2022

Academic Editor: Qura tul Ain

This article considers the stochastic fractional Radhakrishnan-Kundu-Lakshmanan equation (SFRKLE), which is a higher order nonlinear Schrödinger equation with cubic nonlinear terms in Kerr law. To find novel elliptic, trigonometric, rational, and stochastic fractional solutions, the Jacobi elliptic function technique is applied. Due to the Radhakrishnan-Kundu-Lakshmanan equation's importance in modeling the propagation of solitons along an optical fiber, the derived solutions are vital for characterizing a number of key physical processes. Additionally, to show the impact of multiplicative noise on these solutions, we employ MATLAB tools to present some of the collected solutions in 2D and 3D graphs. Finally, we demonstrate that multiplicative noise stabilizes the analytical solutions of SFRKLE at zero.

1. Introduction

Deterministic partial differential equations (DPDEs) are utilized to explain the dynamic behavior of the phenomena in physics and other scientific areas including nonlinear optics, biology, elastic media, fluid dynamics, molecular biology, hydrodynamics, surface of water waves, quantum mechanics, and plasma physics. As a result, solving nonlinear problems is crucial in nonlinear sciences. Some of these methods, such as Darboux transformation [1], sine-cosine [2, 3], $\exp(-\phi(\varsigma))$-expansion [4], (G'/G)-expansion [5, 6], Hirota's function [7], perturbation [8, 9], Jacobi elliptic function [10, 11], trial function [12], tanh-sech [13], fractal semi-inverse method [14, 15], F-expansion method [16], and homotopy perturbation method [17], have been recently developed. However, it is completely obvious that the phenomena that happen in the environment are not always deterministic. Recently, fluctuations/noise has been demonstrated to play an important role in a wide range in describing different phenomena that appear in oceanography, environmental sciences, finance, meteorology, information systems, biology, physics, and other fields [18–24]. Therefore, partial differential equations with noise or random effects are ideal mathematical problems for modeling complex systems.

On the other hand, fractional partial differential equations (FPDEs) have been used to explain many physical phenomena in biology, physics, finance, engineering applications, electromagnetic theory, mathematical, signal processing, and different scientific studies; see, for example, [25–35]. These new fractional-order models are better equipped than the previously utilized integer-order models because fractional-order integrals and derivatives allow for the representation of memory and hereditary qualities of different substances [36]. Compared to integer-order models, where such effects are ignored, fractional-order models have the most significant advantage.

It appears that studying stochastic equations with fractional derivative is more essential. As a result, the next stochastic fractional Radhakrishnan-Kundu-Lakshmanan equation (SFRKLE) [37–39] perturbed by multiplicative noise in the Stratonovich sense is treated:

$$id\Psi + \left[\ell_1 \mathbb{D}_{xx}^{\alpha}\Psi_{xx} - i\ell_2 \mathbb{D}_x^{\alpha}\Psi + \ell_3|\Psi|^2\Psi - i\ell_4\Psi\mathbb{D}_x^{\alpha}\left(|\Psi|^2\right) - -i\ell_5\mathbb{D}_x^{\alpha}\left(|\Psi|^2\Psi\right) + i\ell_6\mathbb{D}_{xxx}^{\alpha}\Psi\right]dt + i\sigma\Psi \circ d\mathscr{W} = 0, \tag{1}$$

where $\Psi \in \mathbb{C}$, $\mathbb{D}_x^{\alpha}$ is the conformable fractional derivative (CFD) [40], ℓ_1 is the group-velocity dispersion, ℓ_2 is the intermodal dispersion, ℓ_3 is the coefficient of nonlinearity, ℓ_4 is the higher-order dispersion coefficient, ℓ_5 is the coefficient of self-steepening for short pulses, and ℓ_6 is the third-order dispersion term. While σ denotes the noise intensity, $\mathscr{W}(t)$ is a standard Wiener process (SWP).

Many researchers have recently developed exact solutions of SFRKLE (1), with $\sigma = 0$, using a variety of methods including trial equation method [41], Lie group analysis [42], sine-cosine method [43], first integral method [44], extended simple equation method [45], the modified Khater method [46], and improved tan $(\phi(\varsigma)/2)$-expansion method [47], while the analytical solutions of SFRKLE (1) have not yet been investigated.

Our motivation of this article is to achieve exact stochastic-fractional solutions for SFRKLE (1). This is the first study to attain the exact solutions of SFRKLE (1) in the existence of a stochastic term and fractional derivative. To get a wide variety of solutions such as trigonometric, hyperbolic, elliptic, and rational functions, we apply the Jacobi elliptic function method. Due to the significance of the RKL in modeling the propagation of solitons through an optical fiber, the solutions obtained are useful for describing some important physical phenomena. In addition, we investigate the impact of BM on the acquired solutions of SFRKLE (1) by generating 3D and 2D diagrams for these solutions.

The outline of this article is as follows. In Section 2, we use a proper wave transformation to deduce the SFRKLE's wave equation (1). While in Section 3, we utilize Jacobi elliptic function method to create the analytic solutions of SFRKLE (1). In Section 4, the influence of the SWP on the obtained solutions is investigated. The conclusion of the document is displayed last.

2. Wave Equation for SFRKLE

The next wave transformation is used to get the wave equation of SFRKLE (1):

$$\Psi(x,t) = \Phi(\eta)e^{\left(i\theta(x,t)-\sigma\mathscr{W}(t)-\sigma^2t\right)}, \quad \eta = \frac{x^{\alpha}}{\alpha} - \nu t, \qquad \theta(x,t) = -\frac{k}{\alpha}x^{\alpha} + \omega t, \tag{2}$$

where Φ is deterministic function that describes the profile of the pulse, $\theta(x,t)$ is the phase component of the soliton, and ν,k, and ω are nonzero constants. Plugging equation (2) into equation (1) and using

$$\begin{aligned} d\Psi &= \left[\left(-\nu\Phi' + i\omega\Phi + \frac{1}{2}\sigma^2\Phi - \sigma^2\Phi\right)dt - \sigma\Phi d\mathscr{W}\right]e^{\left(i\theta(x,t)-\sigma\mathscr{W}(t)-\sigma^2t\right)} \\ &= \left[\left(-\nu\Phi' + i\omega\Phi\right)dt - \sigma\Phi \circ d\mathscr{W}\right]e^{\left(i\theta(x,t)-\sigma\mathscr{W}(t)-\sigma^2t\right)}, \end{aligned} \tag{3}$$

where $(1/2)\sigma^2\Phi$ is the Itô correction term, and

$$\begin{aligned} \mathbb{D}_x^{\alpha}\Psi &= \left(\Phi' - ik\Phi\right)e^{\left(i\theta(x,t)-\sigma\mathscr{W}(t)-\sigma^2t\right)}, \\ \mathbb{D}_{xx}^{\alpha}\Psi &= \left[\Phi'' - 2ik\Phi' - k^2\Phi\right]e^{\left(i\theta(x,t)-\sigma\mathscr{W}(t)-\sigma^2t\right)}, \\ \mathbb{D}_{xxx}^{\alpha}\Psi &= \left[\Phi''' - 3ik\Phi'' - 3k^2\Phi' + ik^3\Phi\right]e^{\left(i\theta(x,t)-\sigma\mathscr{W}(t)-\sigma^2t\right)}, \\ \Psi\mathbb{D}_x^{\alpha}\left(|\Psi|^2\right) &= 2\Phi^2\Phi' e^{\left(i\theta(x,t)-3\sigma\mathscr{W}(t)-3\sigma^2t\right)}, \\ \mathbb{D}_x^{\alpha}\left(|\Psi|^2\Psi\right) &= \left(3\Phi^2\Phi' - ik\Phi^3\right)e^{\left(i\theta(x,t)-3\sigma\mathscr{W}(t)-3\sigma^2t\right)}, \end{aligned} \tag{4}$$

we get for imaginary part

$$\ell_6k^3\Phi''' - \left(3\ell_6k^2 + \ell_2 + 2k\ell_1 + \nu\right)\Phi' - \left(3\ell_5 + 2\ell_4\right)\Phi^2\Phi' e^{\left(-2\sigma\mathscr{W}(t)-2\sigma^2t\right)} = 0, \tag{5}$$

and for real part,

$$\left(\ell_1 + 3k\ell_6\right)\Phi'' - \left(k^2\ell_1 + k\ell_2 - k^3\ell_6\right)\Phi + \left(\ell_3 - k\ell_5\right)\Phi^3 e^{\left(-2\sigma\mathscr{W}(t)-2\sigma^2t\right)} = 0. \tag{6}$$

Taking expectation $\mathbb{E}(\cdot)$ on both sides for equations (5) and (6) and using

$$\mathbb{E}\left(e^{\sigma\mathscr{W}(t)}\right) = e^{\left(\sigma^2/2\right)t}, \tag{7}$$

we have

$$\ell_6k^3\Phi''' - \left(3\ell_6k^2 + \ell_2 + 2k\ell_1 + \nu\right)\Phi' - \left(3\ell_5 + 2\ell_4\right)\Phi^2\Phi' = 0, \tag{8}$$

$$\left(\ell_1 + 3k\ell_6\right)\Phi'' - \left(\omega + k^2\ell_1 + k\ell_2 + k^3\ell_6\right)\Phi - \left(k\ell_5 - \ell_3\right)\Phi^3 = 0, \tag{9}$$

where Φ is deterministic functions. Integrating equation (8) and setting the integration constant to zero, we get

$$\ell_6k^3\Phi'' - \left(3\ell_6k^2 + \ell_2 + 2k\ell_1 + \nu\right)\Phi - \left(\ell_5 + \frac{2}{3}\ell_4\right)\Phi^3 = 0. \tag{10}$$

Since the same function Φ fulfills both equations (9) and (10), we get the next constraint conditions:

$$\frac{\ell_1 + 3k\ell_6}{\ell_6 k^3} = \frac{\omega + k^2\ell_1 + k\ell_2 + k^3\ell_6}{3\ell_6 k^2 + \ell_2 + 2k\ell_1 + \nu} = \frac{3(k\ell_5 - \ell_3)}{3\ell_5 + 2\ell_4}, \tag{11}$$

whenever

$$\ell_3 = -\frac{3\ell_5\ell_1 + \ell_1\ell_4 + 6k\ell_6\ell_5 + 3k\ell_6\ell_4}{3\ell_6}, \tag{12}$$

$$\omega = \frac{8k^3\ell_6^2 + 8k^2\ell_1\ell_6 + 2k\ell_1^2 + 2k\ell_2\ell_6 + \ell_1\ell_2 + \nu(3k\ell_6 + \ell_1)}{\ell_6}. \tag{13}$$

Plugging equation (13) into equation (9), we have the wave equation as follows:

$$\Phi'' - \hbar_1\Phi^3 - \hbar_2\Phi = 0, \tag{14}$$

where

$$\hbar_1 = \frac{3\ell_5\ell_1 + \ell_1\ell_4 + 9k\ell_6\ell_5 + 3k\ell_6\ell_4}{3\ell_6(\ell_1 + 3k\ell_6)},$$
$$\hbar_2 = \frac{9k^3\ell_6^2 + 9k^2\ell_1\ell_6 + 2k\ell_1^2 + 3k\ell_2\ell_6 + \ell_1\ell_2 + \nu(3k\ell_6 + \ell_1)}{\ell_6(\ell_1 + 3k\ell_6)}. \tag{15}$$

3. Analytical Solutions of SFRKLE

To determine the solutions to equation (14), we employ the Jacobi elliptic function method [48]. As a result, we are able to acquire the exact solutions of SFRKLE (1).

3.1. Jacobi Elliptic Function Method. Initially, let the solutions of equation (14) have the form

$$\Phi(\eta) = \sum_{i=1}^{M} a_i\varphi^i(\eta), \tag{16}$$

where φ solves

$$\varphi' = \sqrt{\frac{1}{2}p\varphi^4 + q\varphi^2 + r}, \tag{17}$$

where p, q, and r are real parameters and M is a positive integer number and will be defined later in (19).

We note that equation (17) has different kind of solutions depending on p, q, and r.

$sn(\eta) = sn(\eta, m), cn(\eta) = cn(\eta, m), dn(\eta, m) = dn(\eta, m)$ are the Jacobi elliptic functions (JEFs) for $0 < m < 1$. When $m \longrightarrow 1$, the JEFs are transformed into the following hyperbolic functions:

$$cn(\eta) \longrightarrow \operatorname{sech}(\eta), sn(\eta) \longrightarrow \tanh(\eta), cs(\eta) \longrightarrow \operatorname{csch}(\eta),$$
$$ds \longrightarrow \operatorname{csch}(\eta), dn(\eta) \longrightarrow \operatorname{sech}(\eta). \tag{18}$$

3.2. Solutions of SFRKLE. Now, let us determine the parameter M by balancing Φ'' with Φ^3 in equation (14) as

$$M + 2 = 3M \Rightarrow M = 1. \tag{19}$$

Rewriting equation (16) with $M = 1$ as

$$\Phi = a_0 + a_1\varphi. \tag{20}$$

Differentiating equation (20) twice, we have, by using (17),

$$\Phi'' = a_1 q\varphi + a_1 p\varphi^3. \tag{21}$$

Substituting equations (20) and (21) into equation (14), we obtain

$$\left(a_1 p - \hbar_1 a_1^3\right)\varphi^3 - 3a_0 a_1^2\hbar_1\varphi^2 + \left(a_1 q - 3\hbar_1 a_0^2 a_1 - \hbar_2 a_1\right)\varphi - \left(\hbar_1 a_0^3 + \hbar_2 a_0\right) = 0. \tag{22}$$

Putting each coefficient of φ^k equal zero, we get for $k = 0, 1, 2, 3$

$$\begin{aligned} a_1 p - \hbar_1 a_1^3 &= 0, \\ 3a_0 a_1^2\hbar_1 &= 0, \\ a_1 q - 3\hbar_1 a_0^2 a_1 - \hbar_2 a_1 &= 0, \\ \hbar_1 a_0^3 + \hbar_2 a_0 &= 0. \end{aligned} \tag{23}$$

Solving these equations, we obtain

$$a_0 = 0, a_1 = \pm\sqrt{\frac{p}{\hbar_1}}, q = \hbar_2. \tag{24}$$

Hence, the solution of equation (14) is

$$\Phi(\eta) = \pm\sqrt{\frac{p}{\hbar_1}}\varphi(\eta), \tag{25}$$

for $p/\hbar_1 > 0$. There are two sets depending only on p and $\hbar_1$ as follows.

First set: if $p > 0$ and $\hbar_1 > 0$, then the solutions $\varphi(\eta)$ of equation (17) corresponding to Table 1 are as follows.

If $m \longrightarrow 1$, then the above table degenerates to the following.

Table 1: All solutions of equation (17).

Case	p	q	r	φ
1	$2m^2$	$-(1+m^2)$	1	$sn(\eta)$
2	2	$2m^2-1$	$-m^2(1-m^2)$	$ds(\eta)$
3	2	$2-m^2$	$(1-m^2)$	$cs(\eta)$
4	$-2m^2$	$2m^2-1$	$(1-m^2)$	$cn(\eta)$
5	-2	$2-m^2$	(m^2-1)	$dn(\eta)$
6	$\frac{m^2}{2}$	$\frac{(m^2-2)}{2}$	$\frac{1}{4}$	$\frac{sn(\eta)}{1\pm dn(\eta)}$
7	$\frac{m^2}{2}$	$\frac{(m^2-2)}{2}$	$\frac{m^2}{4}$	$\frac{sn(\eta)}{1\pm dn(\eta)}$
8	$\frac{-1}{2}$	$\frac{(m^2+1)}{2}$	$\frac{-(1-m^2)^2}{4}$	$mcn(\eta)\pm dn(\eta)$
9	$\frac{m^2-1}{2}$	$\frac{(m^2+1)}{2}$	$\frac{(m^2-1)}{4}$	$\frac{dn(\eta)}{1\pm sn(\eta)}$
10	$\frac{1-m^2}{2}$	$\frac{(1-m^2)}{2}$	$\frac{(1-m^2)}{4}$	$\frac{cn(\eta)}{1\pm sn(\eta)}$
11	$\frac{(1-m^2)^2}{2}$	$\frac{(1-m^2)^2}{2}$	$\frac{1}{4}$	$\frac{sn(\eta)}{dn\pm cn(\eta)}$
12	2	0	0	$\frac{c}{\eta}$
13	0	1	0	ce^{η}

Table 2: All solutions $\varphi(\eta)$ of equation (17) for $p>0$ and $\hbar_1>0$.

Case	p	q	r	$\varphi(\eta)$
1	$2m^2$	$-(1+m^2)$	1	$sn(\eta)$
2	2	$2m^2-1$	$-m^2(1-m^2)$	$ds(\eta)$
3	2	$2-m^2$	$(1-m^2)$	$cs(\eta)$
4	$\frac{m^2}{2}$	$\frac{(m^2-2)}{2}$	1/4 or $m^2/4$	$\frac{sn(\eta)}{1\pm dn(\eta)}$
5	$\frac{1-m^2}{2}$	$\frac{(1-m^2)}{2}$	$\frac{(1-m^2)}{4}$	$\frac{cn(\eta)}{1\pm sn(\eta)}$
6	$\frac{(1-m^2)^2}{2}$	$\frac{(1-m^2)^2}{2}$	$\frac{1}{4}$	$\frac{sn(\eta)}{dn\pm cn(\eta)}$
7	2	0	0	$\frac{c}{\eta}$

Table 3: All solutions of equation (17) when $m\longrightarrow 1$.

Case	p	q	r	$\varphi(\eta)$
1	2	-2	1	$\tanh(\eta)$
2	2	1	0	$\operatorname{csch}(\eta)$
3	$\frac{1}{2}$	$\frac{-1}{2}$	$\frac{1}{4}$	$\frac{\tanh(\eta)}{1\pm \operatorname{sech}(\eta)}$
4	2	0	0	$\frac{c}{\eta}$

Table 4: All solutions $\varphi(\eta)$ of equation (17) when $p<0$.

Case	p	q	r	φ
1	$-2m^2$	$2m^2-1$	$(1-m^2)$	$cn(\eta)$
2	-2	$2-m^2$	(m^2-1)	$dn(\eta)$
3	$\frac{-1}{2}$	$\frac{(m^2+1)}{2}$	$\frac{-(1-m^2)^2}{4}$	$mcn(\eta)\pm dn(\eta)$
4	$\frac{m^2-1}{2}$	$\frac{(m^2+1)}{2}$	$\frac{(m^2-1)}{4}$	$\frac{dn(\eta)}{1\pm sn(\eta)}$

Table 5: All solutions $\varphi(\eta)$ of equation (17) when $m\longrightarrow 1$ and $p<0$.

Case	p	q	r	φ
1	-2	1	0	$\operatorname{sech}(\eta)$
2	$\frac{-1}{2}$	2	0	$2\operatorname{sech}(\eta)$

Now, using Table 2 (or Table 3) and equations (2) and (25), we get the solutions of SFRKLE (1) as follows:

$$\Psi(x,t)=\sqrt{\frac{p}{\hbar_1}}\varphi(\eta)e^{\left(i\theta(x,t)-\sigma\mathscr{W}(t)-\sigma^2t\right)}\ \text{for}\ \frac{p}{\hbar_1}>0, \tag{26}$$

where $\eta=(x^\alpha/\alpha)-\nu t$.

Second set: if $p<0$ and $\hbar_1<0$, then the solutions $\varphi(\eta)$ of equation (17) corresponding to Table 1 are as follows.

If $m\longrightarrow 1$, then Table 3 degenerates to the following.

In this case, using Table 4 (or Table 5), we obtain the analytical solutions of SFRKLE (1) as stated in equation (26).

4. The Impact of SWP on the Solutions of SFRKLE

The effect of SWP on the analytical solutions of SFRKLE (1) is discussed here. Fix the parameters $\ell_1=\ell_2=\ell_4=\ell_5=\ell_6=1, k=-1, \nu=-11/3$, and $m=\sqrt{2/3}$. Hence, $\ell_3=5/3$, $\hbar_1=4/3$, and $\hbar_2=-5/3$. Now, we offer some graphs for distinct value of σ (noise strength) and α (fractional order) for $t,x\in[0,6]$. We utilize the MATLAB tools to create some graphs for the following solutions:

$$\Psi(x,t)=sn\left(\frac{x^\alpha}{\alpha}+\frac{11}{3}t\right)e^{\left(i\theta(x,t)-\sigma\mathscr{W}(t)-\sigma^2t\right)}, \tag{27}$$

$$\Psi(x,t)=\sqrt{\frac{3}{2}}ds\left(\frac{x^\alpha}{\alpha}+\frac{11}{3}t\right)e^{\left(i\theta(x,t)-\sigma\mathscr{W}(t)-\sigma^2t\right)}. \tag{28}$$

If $\sigma=0$, we can see how the surface oscillates (periodic solutions) in Figure 1 and the surface expands as the fractional order increases $\alpha=0.3,0.5,0.7,1$.

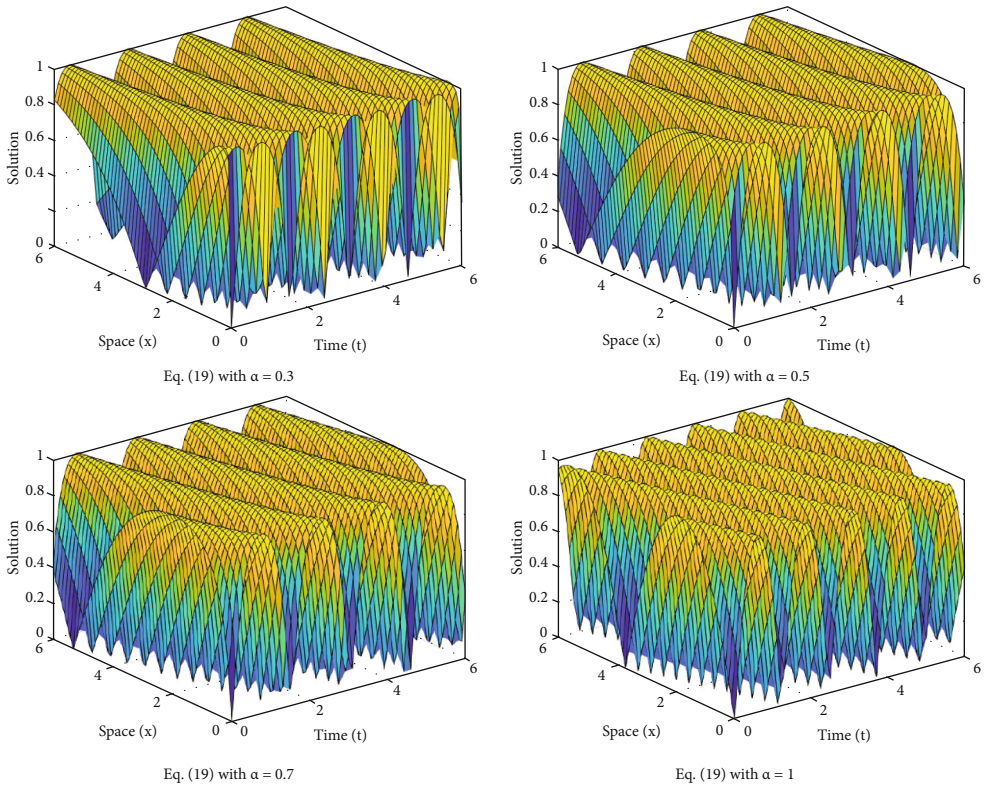

FIGURE 1: 3D graphs of equation (27) with $\sigma = 0$ and for different values of α.

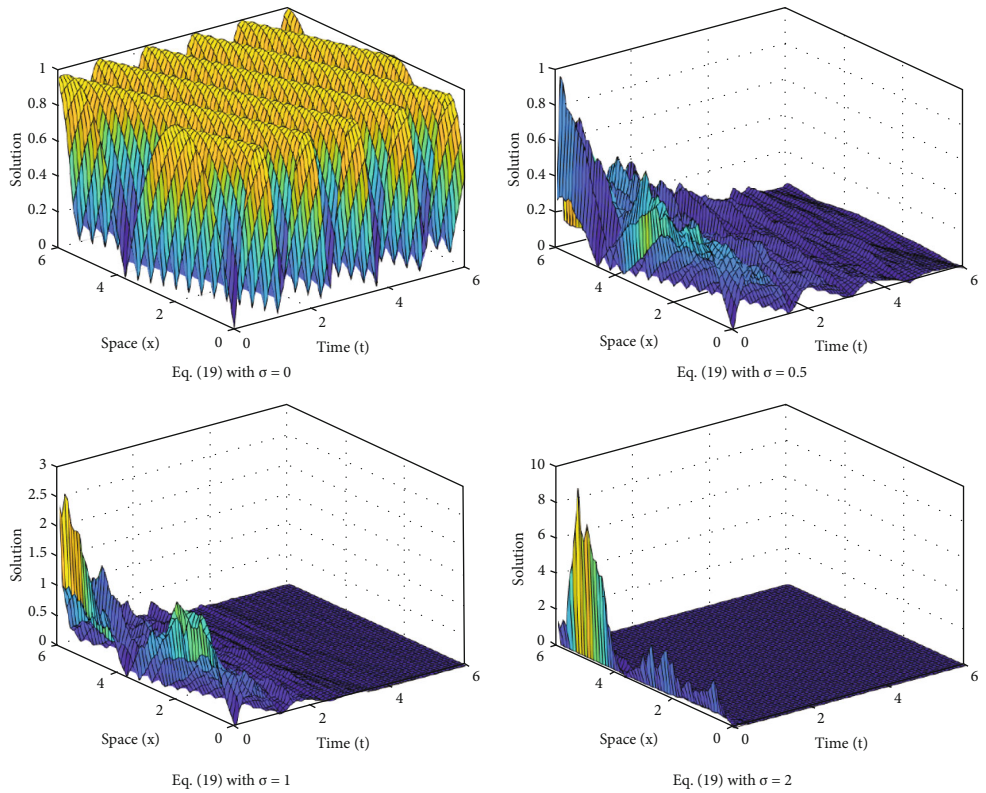

FIGURE 2: 3D shape of equation (27) with $\alpha = 1$ and for different values of σ.

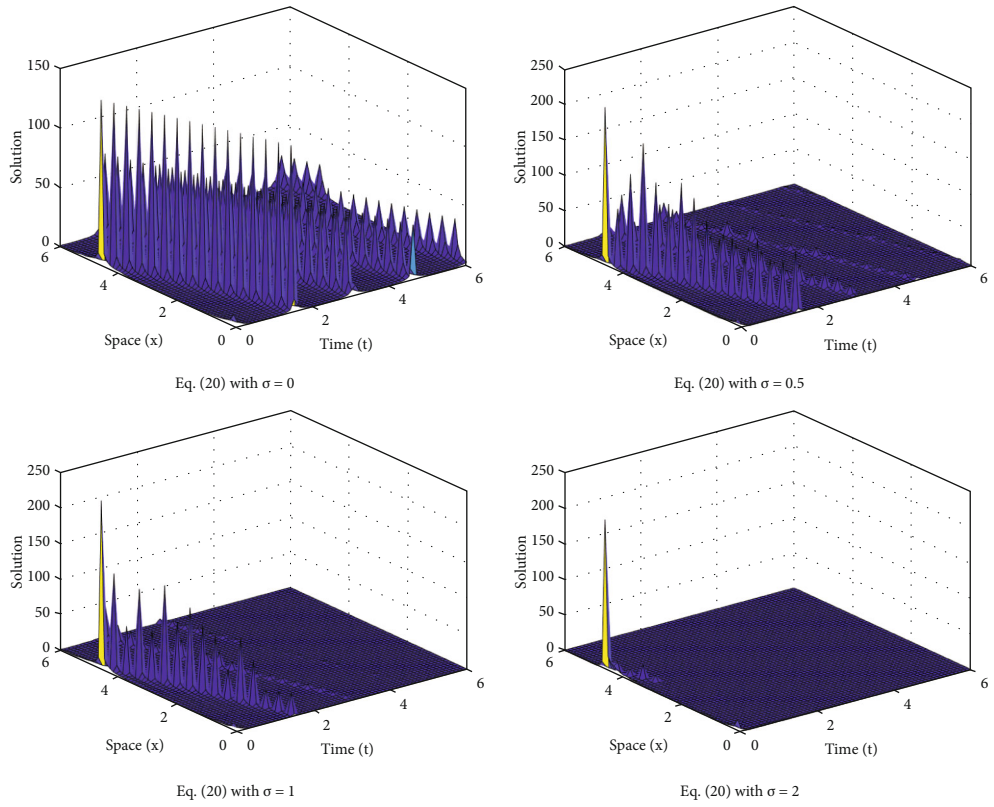

Figure 3: 3D shape of equation (28) with $\sigma = 0,0.5,1,2$.

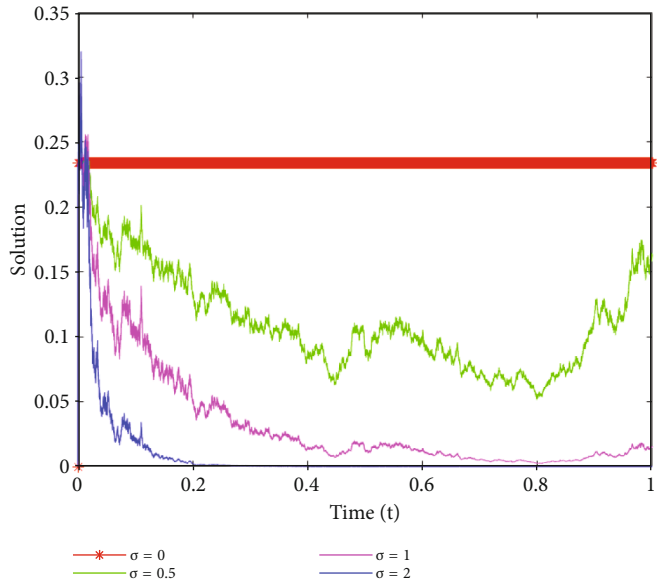

Figure 4: 2D shape of equation (27) with $\sigma = 0,0.5,1,2$.

In Figures 2 and 3, we can see that when noise is introduced after small transit patterns, the surface starts to be flat as the noise intensity increases $\sigma = 0.5,1,2$.

Figure 4 shows the 2D shape of equation (27) with $\sigma = 0,0.5,1,2$ which highlight the above results.

We can deduce from Figures 1–4 that

(1) the solutions of SFRKLE (1) are stabilized around zero by the SWP

(2) as the fractional order α decreases, the surface shrinks

5. Conclusions

We considered here the stochastic fractional Radhakrishnan-Kundu-Lakshmanan equation (1) which has never been considered before with fractional derivative and stochastic term. To get hyperbolic, rational, and elliptic stochastic fractional solutions, we used the Jacobi elliptic function method. Because of the importance of SFRKLE in representing the propagation of solitons via an optical fiber, the derived solutions may be utilized to represent a wide range of exciting physical phenomena. Finally, we achieved by plotting the derived solutions to show how multiplicative noise and fractional derivative influence these solutions. We deduced that the SWP stabilizes the solutions around zero when the noise strength increases. In future work, we can try to get the exact solutions of SFRKLE (1) with additive noise or multiplicative color noise.

Data Availability

All data are available in this paper.

Conflicts of Interest

The authors declare that they have no competing interests.

Authors' Contributions

All authors contributed equally to the writing of this paper. All authors read and approved the final manuscript.

Acknowledgments

The study was supported by the Princess Nourah Bint Abdulrahman University Researchers Supporting Project number PNURSP2022R273, Princess Nourah Bint Abdulrahman University, Riyadh, Saudi Arabia.

References

[1] M. Wen-Xiu and B. Sumayah, "A binary Darboux transformation for multicomponent NLS equations and their reductions," *Analysis and Mathematical Physics*, vol. 11, no. 2, p. 44, 2021.

[2] A. M. Wazwaz, "A sine-cosine method for handlingnonlinear wave equations," *Mathematical and Computer Modelling*, vol. 40, no. 5-6, pp. 499–508, 2004.

[3] C. Yan, "A simple transformation for nonlinear waves," *Physics Letters A*, vol. 224, no. 1-2, pp. 77–84, 1996.

[4] K. Khan and M. A. Akbar, "The exp(−$\Phi(\xi)$)-expansion method for finding travelling wave solutions of Vakhnenko-Parkes equation," *International Journal of Dynamical Systems and Differential Equations*, vol. 5, no. 1, pp. 72–83, 2014.

[5] M. L. Wang, X. Z. Li, and J. L. Zhang, "The (G'/G)-expansion method and travelling wave solutions of nonlinear evolution equations in mathematical physics," *Physics Letters A*, vol. 372, pp. 417–423, 2008.

[6] H. Zhang, "New application of the (G'/G)-expansion method," *Communications in Nonlinear Science and Numerical Simulation*, vol. 14, pp. 3220–3225, 2009.

[7] R. Hirota, "Exact solution of the Korteweg-de Vries equation for multiple collisions of solitons," *Physical Review Letters*, vol. 27, no. 18, pp. 1192–1194, 1971.

[8] W. W. Mohammed, "Fast-diffusion limit for reaction–diffusion equations with degenerate multiplicative and additive noise," *Journal of Dynamics and Differential Equations*, vol. 33, no. 1, pp. 577–592, 2021.

[9] W. W. Mohammed and D. Blömker, "Fast-diffusion limit for reaction-diffusion equations with multiplicative noise," *Journal of Mathematical Analysis and Applications*, vol. 496, no. 2, article 124808, 2021.

[10] Z. L. Yan, "Abundant families of Jacobi elliptic function solutions of the (2+1)-dimensional integrable Davey-Stewartson-type equation via a new method," *Chaos, Solitons and Fractals*, vol. 18, no. 2, pp. 299–309, 2003.

[11] E. Fan and J. Zhang, "Applications of the Jacobi elliptic function method to special-type nonlinear equations," *Physics Letters A*, vol. 305, no. 6, pp. 383–392, 2002.

[12] A. M. Wazwaz, "An analytic study of compactons structures in a class of nonlinear dispersive equations," *Mathematics and Computers in Simulation*, vol. 63, no. 1, pp. 35–44, 2003.

[13] W. Malfliet and W. Hereman, "The tanh method. I. Exact solutions of nonlinear evolution and wave equations," *Physica Scripta*, vol. 54, no. 6, pp. 563–568, 1996.

[14] K. Wang, "Fractal solitary wave solutions for fractal nonlinear dispersive Boussinesq-like models," *Fractals*, vol. 30, no. 4, p. 2250083, 2022.

[15] F. M. Al-Askar, W. W. Mohammed, A. M. Albalahi, and M. El-Morshedy, "The impact of the Wiener process on the analytical solutions of the stochastic $(2+1)$-dimensional breaking soliton equation by using tanh–coth method," *Mathematics*, vol. 10, no. 5, p. 817, 2022.

[16] A. Filiz, M. Ekici, and A. Sonmezoglu, "F-expansion method and new exact solutions of the Schrödinger-KdV equation," *Scientific World Journal*, vol. 2014, p. 14, 2014.

[17] G. Rehman, S. Qin, Q. T. Ain et al., "A study of moisture content in unsaturated porous medium by using homotopy perturbation method (HPM) and variational iteration method," *GEM - International Journal on Geomathematics*, vol. 13, no. 3, 2022.

[18] E. J. Allen, "Derivation of stochastic partial differential equations," *Stochastic Analysis and Applications*, vol. 26, no. 2, pp. 357–378, 2008.

[19] V. Capasso and D. Morale, "Stochastic modelling of tumour-induced angiogenesis," *Journal of Mathematical Biology*, vol. 58, no. 1-2, pp. 219–233, 2009.

[20] W. W. Mohammed, A. M. Albalahi, S. Albadrani, E. S. Aly, R. Sidaoui, and A. E. Matouk, "The analytical solutions of the stochastic fractional Kuramoto–Sivashinsky equation by using the Riccati equation method," *Mathematical Problems in Engineering*, vol. 2022, 8 pages, 2022.

[21] B. Guo and D. Huang, "3D stochastic primitive equations of the large-scale ocean: global well-posedness and attractors," *Communications in Mathematical Physics*, vol. 286, pp. 697–723, 2009.

[22] A. Din and Y. Li, "Lévy noise impact on a stochastic hepatitis B epidemic model under real statistical data and its

fractal–fractional Atangana–Baleanu order model," *Physica Scripta*, vol. 96, no. 12, article 124008, 2021.

[23] T. Sathiyaraj, M. Feckan, and J. R. Wang, "Null controllability results for stochastic delay systems with delayed perturbation of matrices," *Chaos, Solitons & Fractals*, vol. 138, p. 109927, 2020.

[24] A. Din and Q. T. Ain, "Stochastic optimal control analysis of a mathematical model: theory and application to non-singular kernels," *Fractal and Fractional*, vol. 6, p. 279, 2022.

[25] S. B. Yuste, L. Acedo, and K. Lindenberg, "Reaction front in anA+B→Creaction-subdiffusion process," *Physical Review E*, vol. 69, no. 3, article 036126, 2004.

[26] W. W. Mohammed, N. Iqbal, and T. Botmart, "Additive noise effects on the stabilization of fractional-space diffusion equation solutions," *Mathematics*, vol. 10, no. 1, p. 130, 2022.

[27] D. A. Benson, S. W. Wheatcraft, and M. M. Meerschaert, "The fractional-order governing equation of Lévy motion," *Water Resources Research*, vol. 36, pp. 1413–1423, 2000.

[28] F. M. Al-Askar, W. W. Mohammed, M. Alshammari, and M. El-Morshedy, "Effects of the Wiener Process on the Solutions of the Stochastic Fractional Zakharov System," *Mathematics*, vol. 10, no. 7, p. 1194, 2022.

[29] F. M. Al-Askar, W. W. Mohammed, and M. Alshammari, "Impact of Brownian motion on the analytical solutions of the space-fractional stochastic approximate long water wave equation," *Symmetry*, vol. 14, no. 4, p. 740, 2022.

[30] E. Barkai, R. Metzler, and J. Klafter, "From continuous time random walks to the fractional Fokker-Planck equation," *Physical Review*, vol. 61, no. 1, pp. 132–138, 2000.

[31] A. Khan, T. Abdeljawad, J. F. Gómez-Aguilar, and H. Khan, "Dynamical study of fractional order mutualism parasitism food web module," *Chaos, Solitons & Fractals*, vol. 134, article 109685, 2020.

[32] A. Khan, H. M. Alshehri, J. F. Gómez-Aguilar, A. Khan, and G. Fernández-Anaya, "A predator–prey model involving variable-order fractional differential equations with Mittag-Leffler kernel," *Advances in Difference Equations*, vol. 183, 18 pages, 2021.

[33] A. Din, Y. Li, F. M. Khan, Z. U. Khan, and P. Liu, "On analysis of fractional order mathematical model of hepatitis B using Atangana-Baleanu Caputo (ABC) derivative," *Fractals*, vol. 30, no. 1, p. 2240017, 2022.

[34] Q. T. Ain, T. Sathiyaraj, S. Karim, M. Nadeem, and P. K. Mwanakatwe, "ABC fractional derivative for the alcohol drinking model using two-scale fractal dimension," *Complexity*, vol. 2022, Article ID 8531858, 2022.

[35] Q. T. Ain, A. Khan, M. I. Ullah, M. A. Alqudahd, and T. Abdeljawad, "On fractional impulsive system for methanol detoxification in human body," *Chaos, Solitons & Fractals*, vol. 160, article 112235, 2022.

[36] I. Podlubny, *Fractional Differential Equations*, Academic Press, New York, 1999.

[37] D. D. Ganji, A. Asgari, and Z. Z. Ganji, "Exp-function based solution of nonlinear Radhakrishnan, Kundu and Laskshmanan (RKL) equation," *Acta Applicandae Mathematicae*, vol. 104, no. 2, article 201209, 2008.

[38] A. Biswas, "1-soliton solution of the generalized Radhakrishnan, Kundu, Lakshmanan equation," *Physics Letters A*, vol. 373, no. 30, pp. 2546–2548, 2009.

[39] B. Sturdevant, D. A. Lott, and A. Biswas, "Topological 1-soliton solution of the generalized Radhakrishnan, Kundu, Lakshmanan equation with nonlinear dispersion," *Modern Physics Letters B*, vol. 24, no. 16, pp. 1825–1831, 2010.

[40] R. Khalil, M. Al Horani, A. Yousef, and M. Sababheh, "A new definition of fractional derivative," *Journal of Computational and Applied Mathematics*, vol. 264, pp. 65–70, 2014.

[41] A. Biswas, Y. Yildirim, E. Yasar et al., "Optical soliton perturbation for Radhakrishnan-Kundu-Lakshmanan equation with a couple of integration schemes," *Optik*, vol. 163, pp. 126–136, 2018.

[42] A. Bansal, A. Biswas, M. F. Mahmood et al., "Optical soliton perturbation with Radhakrishnan-Kundu-Lakshmanan equation by Lie group analysis," *Optik*, vol. 163, pp. 137–141, 2018.

[43] J.-L. Zhang and M.-L. Wang, "Various exact solutions for two special type RKL models," *Chaos, Solitons & Fractals*, vol. 37, no. 1, article 215226, pp. 215–226, 2008.

[44] S. S. Singh, "Solutions of Kudryashov-Sinelshchikov equation and generalized Radhakrishnan-Kundu-Lakshmanan equation by the first integral method," *International Journal of Physical Research*, vol. 4, no. 2, pp. 37–42, 2016.

[45] D. Lu, A. R. Seadawy, and M. M. Khater, "Dispersive optical soliton solutions of the generalized Radhakrishnan-Kundu-Lakshmanan dynamical equation with power law nonlinearity and its applications," *Optik*, vol. 164, pp. 54–64, 2018.

[46] A. Tripathy and S. Sahoo, "New optical behaviours of the time-fractional Radhakrishnan-Kundu-Lakshmanan model with Kerr law nonlinearity arise in optical fibers," *Optical and Quantum Electronics*, vol. 54, no. 4, p. 232, 2022.

[47] G. Akram, M. Sadaf, and M. Dawood, "Abundant soliton solutions for Radhakrishnan-Kundu-Laksmananequation with Kerr law non-linearity by improved tan $(\phi(\varsigma)/2)$-expansion technique," *Optik*, vol. 247, article 167787, 2021.

[48] Y. Z. Peng, "Exact solutions for some nonlinear partial differential equations," *Physics Letters A*, vol. 314, no. 5-6, pp. 401–408, 2003.